UNIVERSITÄT BAYREUTH

Characterization of Sorption and Desorption of Organic Pollutants onto Microplastics, and Investigations into Chemical Leaching

Dissertation

Submitted to obtain the academic degree Doctor rerum naturalium (Dr. rer. nat.)

At the faculty of Biology, Chemistry & Earth Sciences,

University of Bayreuth

Submitted by

Emeka Ephraim Emecheta

Born in Nigeria

Bayreuth, 2024

This thesis was carried out at the German Federal Institute for Risk Assessment (BfR) in Berlin from October 2019 to July 2023. The work in this dissertation was part of a larger project Innovative materials and production processes: safety in the life cycle and industrial value chains (InnoMat.Life) funded by the German Federal Ministry of Education and Research (BMBF), with the project number: 03XP0216A. The thesis was supervised by PD Dr. Andrea Haase and Prof. Dr. Eva Lehndorff.

This is a full reprint of the thesis submitted to obtain the academic degree of Doctor of Natural Sciences (Dr. rer. Nat.) and approved by the Faculty of Biology, Chemistry and Geosciences of the University of Bayreuth.

Form of thesis: Cumulative thesis
Date of submission: 16.08.2023
Admission by the doctoral committee: 27.09.2023
Date of defence: 27.02.2024

Acting Dean: Prof. Dr. Cyrus Samimi

Doctoral committee:
Prof. Dr. Eva Lehndorff (Reviewer)
PD Dr. Andrea Haase (Reviewer)
Jprof. Dr. Anke Nölscher (Reviewer)
Prof. Dr. Andreas Römpp (Chair)
Prof. Dr. Christian Laforsch

TABLE OF CONTENTS

ABBREVIATIONS AND NOMENCLATURE

MP: Microplastic

OECD: Organization for economic co-operation and development

ECHA: European chemicals agency

PTFE: polytetrafluoroethylene

PVC: polyvinyl chloride

ABS: acrylonitrile-butadiene styrene

PE: Polyethylene

PP: Polypropylene

PET: Poly(ethylene-terephthalate)

PA-6: polyamide-6 (PA-6)

PU: polyurethane

SBR: Styrene-butadiene rubber

TPE: thermoplastic elastomers

AM: Additive manufacturing

3D: Three-dimensional

SLS: Selective laser sintering

EBM: Electron beam melting

SLM: Selective metal building

UNEP: United Nations Environment Programme

POP: Persistent organic pollutant

PAE: Phthalic acid esters

BHT: Butylated hydroxytoluene

UV: Ultraviolet

BPA: Bisphenol A

PAH: Polycyclic aromatic hydrocarbon

PCB: Polychlorinated biphenyl

TPP: Third-phase partition

IAS: Intentionally added substances

NIAS: Non-intentionally-added substances

GI: Gastrointestinal

GIT: Gastrointestinal tract

WHO: World Health Organization

FAO: Food Agriculture Organization

TD-GC-MS: Thermal desorption gas chromatography mass spectrometry

PMMA: Polymethyl methacrylate

TPU: Thermoplastic polyurethane

CRM: Cumulative relative desorption

LDPE: Low-density polyethylene

ICP-MS: Inductively coupled plasma-mass spectrometry

AOP: Adverse outcome pathways

AhR: Aryl hydrocarbon receptors

PLC: Polymers of low concern

Dub-Rad*:* Dubinin-Radushkevich

BET: Brunauer-Emmett-Teller

PA-12: Polyamide-12

TR: Tyre Rubber

Anth: Anthracene

B[*a*]P: Benzo[*a*]pyrene

DB[*a,l*]P: Dibenzo[*a,l*]pyrene

$K_{MP/W}$: Sorption distribution coefficient (L/kg)

C_{MP}: Concentrations of PAH in MP phase at equilibrium

C_W: Concentrations of PAH in water at equilibrium

C_{PDMS}: Concentrations of PAH in PDMS at equilibrium

T_g: Glass transition temperature

T_m: melting point

K_L: Langmuir adsorption coefficient

q_t: sorption capacity at t

k_{id}: Intraparticle diffusion rate constant.

θ: Intercept

t: time (h)

k_2: Pseudo-second kinetic rate constant

k_1: Pseudo-first kinetic rate constant

n: exponent

K_{SIP}: SIP isotherm constant

q_e: calculated equilibrium sorption capacity

α_s: SIP isotherm constant (L/μg)

α_R: Redlich-Peterson isotherm constant (L/μg)

α_L: Langmuir isotherm constant (L/μg)

q_m: BET monolayer adsorption capacity (μg/g)

q_s: Dubinin-Radushkevich maximum sorption capacity

k_l: BET the isotherm coefficient at upper layer (L/μg)

k_s: BET the isotherm coefficient at monolayer (L/μg)

k_{ad}: Dubinin-Radushkevich isotherm constant (mol^2/ kJ^2)

ε: Dubinin-Radushkevich isotherm coefficient

K_R: Redlich-Peterson isotherm coefficient

K_F: Freundlich isotherm coefficient

K_H: Henry isotherm coefficient

A_T: Tempkin adsorption constant (L/kg)

b_t: Tempkin factor

R: Ideal gas constant (J / mol·K)

T: Temperature (k)

LIST OF FIGURES

LIST OF TABLES

1. SUMMARY

The ubiquity of microplastics (MPs) has raised safety concerns regarding human exposure. While there has been a deluge of studies focusing on MPs recently, polydisperse MPs used as raw materials for additive manufacturing (AM) applications have received comparatively less attention and are not covered by existing EU chemicals regulations. Consequently, our understanding of their sorption and desorption of ubiquitous persistent organic pollutants (POPs) is inadequate. Certain POPs, including specific polycyclic aromatic hydrocarbons (PAHs) and polychlorinated biphenyls (PCBs), are known for their chronic toxicity. Thus, exposure to humans via MPs could induce adverse effects. Similarly, the leaching behavior and human health implications of chemical additives and monomer residues from MPs are not well understood. This thesis aims to fill part of these knowledge gaps by systematically investigating the extent to which MPs could act as carriers of toxic chemicals to humans. To achieve this overarching aim, three individual studies were conducted, one addressing the sorption of PAHs, another one on the desorption of POPs, and a final one investigating the leaching of chemicals from the MPs in simulated gastrointestinal fluids.

In general, the sorption of PAHs by MPs has already been widely studied, mainly using the batch-equilibrium method; yet uncertainties persist. For instance, the sorption of highly hydrophobic pollutants is still understudied due to the analytical challenges they pose. Also, separation of submicron- and nanoplastics from aqueous phase remain challenging. To circumvent these challenges, a novel third-phase partition (TPP) method utilizing a re-usable polydimethylsiloxane stir-bar as third phase, and a thermal desorption-mass spectrometry-gas chromatography system for online extraction and analysis was developed (study 1). The TPP-method eliminated the necessity for filtration and solvent-extraction steps.

Applying the TPP-method, the sorption of benzo[a]pyrene (B[a]P, a representative PAH) to seventeen MP variants was investigated. Sorption affinity to the MPs were generally strong (> log 5), differing by over 100-fold, being mainly dependent on the polymer types in the order of polyamides (PA) > polyethylenes (PE) > tyre rubber (TR) > thermoplastic polyurethanes ~ polyurethanes > polymethyl methacrylate. Within polymer classes, particle size, polarity, and polymer backbones influenced sorption. When comparing three PAHs, their sorption to selected MPs increased over five-orders of magnitude with hydrophobicity: anthracene < B[a]P < dibenzo[a,l]pyrene. Photo-aging of three MPs via an ISO-standardized protocol decreased their sorption of B[a]P. Sorption of anthracene and B[a]P to selected MPs using the TPP-method showed comparable results with the batch-equilibrium method, thus validating the TPP-method as a rapid and reliable alternative to existing methods.

Study two investigated desorption of sorbed pollutants. The strong affinity of ubiquitous MPs to widespread PAHs have sparked concerns about human exposure. Ingestion and inhalation may serve as plausible pathways for exposure to MP-sorbed PAHs. To mimic the conditions relevant to human exposure, a physiology-based in-vitro digestion model was utilized to sequentially investigate the release of MP-sorbed pollutants in saliva, gastric, and intestinal fluid simulants.

The cumulative relative desorption (CRD) of B[a]P was negligible in saliva fluid simulant but increased from gastric (4%) to large intestinal fluid simulants (29%) across the three selected MPs evaluated consecutively across all gastrointestinal compartments. Eleven MP variants were investigated for their desorption of B[a]P in the small intestinal fluid simulants, their CRD were moderate, ranging from 4% to 19%. Only PA-6_7 µm showed an exceptionally high CRD of 51%. For the same material, 100% desorption of PCB-153 was observed in the sequential intestinal fluid simulants. The observed high sorption and desorption in PA-6 was attributed to its reversible high water-absorption capacity which presumably enhanced transport of solubilized pollutants to and from the particle's bulk. Assessment of human POPs exposure via MPs indicated that the contribution of MP-sorbed pollutants relative to exposure via other sources was rather minimal (≤ 0.1%).

In addition to sorbed pollutants, MPs contain chemical additives and monomer residues. Human exposure to these chemicals could induce adverse effects. Therefore, study three focused on the leaching and toxicity assessments of the MP-chemicals released during in-vitro gastrointestinal digestion.

Among the three classes of MPs studied, TR particles released more chemicals compared to PA-6 and TPU MPs. Notable high concentrations leachates include benzothiazole, 2(3H)-Benzothiazolone, and zinc quantified respectively at 112 µg/g, 83 µg/g, and 1147 µg/g in the small intestine fluid simulants. For PA-6, monomer and dimer residues were identified in the gastrointestinal fluid simulants, with caprolactam (PA-6_7 µm monomer) quantified at a concentration of 1549 µg/g. Photo-aging of the particles facilitated the leaching of new compounds. Leaching of chemicals were modulated by the composition of the medium and incubation time. Twenty leached compounds were linked to different adverse outcome pathways (AOPs). Prominent AOPs involved Aryl hydrocarbon receptor (AhR) activation, nuclear receptor activation, among others. These findings raise further concern about human exposure to toxic chemicals through MPs, particularly tyre particles.

The results of this thesis provide a focus for human health hazard characterization of the MPs and also support grouping as an efficient approach for risk assessment.

2. ZUSAMMENFASSUNG

Das ubiquitäre Vorkommen von Mikroplastik (MP) hat Bedenken hinsichtlich möglicher Gesundheitsrisiken für Menschen aufgeworfen. Viele kürzlich erschiene Studien konzentrierten sich auf wenige Arten von monodispersen Mikroplastik, während polydisperses Mikroplastik, das u.a als Rohmaterial für die additiven Fertigung (AM) verwendet wird, vergleichsweise weniger untersucht wurde. Außerdem ist es derzeit nicht Gegenstand bestehender EU-Chemikalienregulationen. Folglich ist unser Verständnis ihrer Sorption und Desorption von allgegenwärtigen persistenten organischen Schadstoffen (POPs) unzureichend. Bestimmte POPs, darunter bestimmte polyzyklische aromatische Kohlenwasserstoffe (PAHs) und polychlorierte Biphenyle (PCBs), sind für ihre chronische Toxizität bekannt. Daher könnte eine Exposition des Menschen über MP schädliche Auswirkungen haben. Auch das Auslaugverhalten und die Auswirkungen auf die menschliche Gesundheit von chemischen Zusatzstoffen und Monomerrückständen aus MPs sind nicht gut bekannt. In dieser Arbeit soll ein Teil dieser Wissenslücken geschlossen werden, indem systematisch untersucht wird, inwieweit MPs als Träger von toxischen Chemikalien für den Menschen fungieren könnten. Um dieses übergeordnete Ziel zu erreichen, wurden drei Einzelstudien durchgeführt: eine zur Sorption von PAK, eine weitere zur Desorption von POP und eine letzte zur Auswaschung von Chemikalien aus den MP in simulierten Magen-Darm-Flüssigkeiten.

Im Allgemeinen wurde die Sorption von PAK durch MPs bereits umfassend untersucht, wobei hauptsächlich die Batch-Gleichgewichtsmethode verwendet wurde; dennoch bestehen weiterhin Unsicherheiten. So ist beispielsweise die Sorption von stark hydrophoben Schadstoffen aufgrund der analytischen Herausforderungen, die sie mit sich bringen, noch nicht ausreichend untersucht. Auch die Abtrennung von Submikron- und Nanokunststoffen aus der wässrigen Phase bleibt eine Herausforderung. Um diese Herausforderungen zu umgehen, wurde eine neuartige Third-Phase-Partition (TPP)-Methode entwickelt, die einen wiederverwendbaren Polydimethylsiloxan-Rührstab als dritte Phase und ein thermisches Desorptions-Massenspektrometrie-Gaschromatographie-System für die Online-Extraktion und -Analyse verwendet (Studie 1). Mit der TPP-Methode entfielen die Schritte Filtration und Lösungsmittelextraktion.

Unter Anwendung der TPP-Methode wurde die Sorption von Benzo[a]pyren (B[a]P, ein repräsentativer PAH) an siebzehn MP-Varianten untersucht. Die Sorptionsaffinität für die MPs war im Allgemeinen stark (> log 5) und unterschied sich um mehr als das 100-fache, wobei sie hauptsächlich von den Polymertypen in der Reihenfolge Polyamide (PA) > Polyethylene (PE)

> Reifengummi (TR) > thermoplastische Polyurethane ~ Polyurethane > Polymethylmethacrylat abhing. Innerhalb der Polymerklassen beeinflussten die Partikelgröße, die Polarität und die Polymerrückgrate die Sorption. Beim Vergleich von drei PAHs stieg ihre Sorption an ausgewählten MPs über fünf Größenordnungen mit der Hydrophobizität: Anthracen < B[a]P < Dibenzo[a,l]pyren. Die Photoalterung von drei MPs über ein ISO-standardisiertes Protokoll verringerte ihre Sorption von B[a]P. Die Sorption von Anthracen und B[a]P an ausgewählte MPs unter Verwendung der TPP-Methode zeigte vergleichbare Ergebnisse wie die Batch-Gleichgewichtsmethode, wodurch die TPP-Methode als schnelle und zuverlässige Alternative zu bestehenden Methoden validiert wurde.

Studie zwei untersuchte die Desorption von sorbierten Schadstoffen. Die starke Affinität der ubiquitären MPs zu weit verbreiteten PAHs hat Bedenken hinsichtlich der Exposition des Menschen geweckt. Verschlucken und Einatmen können plausible Wege für die Exposition gegenüber MP-sorbierten PAHs sein. Um die für die Exposition des Menschen relevanten Bedingungen zu imitieren, wurde ein auf der Physiologie basierendes In-vitro-Verdauungsmodell verwendet, um die Freisetzung von MP-gebundenen Schadstoffen in Speichel-, Magen- und Darmflüssigkeitssimulantien zu untersuchen.

Die kumulative relative Desorption (CRD) von B[a]P war in der Speichelflüssigkeitssimulanz vernachlässigbar, stieg jedoch von der Magenflüssigkeitssimulanz (4 %) bis zur Dickdarmflüssigkeitssimulanz (29 %) bei den drei ausgewählten MP an, die nacheinander in allen gastrointestinalen Kompartimenten untersucht wurden. Elf MP-Varianten wurden auf ihre Desorption von B[a]P in den Dünndarmsimulanzien untersucht. Ihre CRD war moderat und reichte von 4% bis 19%. Nur PA-6_7 µm zeigte eine außergewöhnlich hohe CRD von 51%. Für dasselbe Material wurde eine 100%ige Desorption von PCB-153 in den sequenziellen Darmflüssigkeitssimulanzien beobachtet. Die beobachtete hohe Sorption und Desorption von PA-6 wurde auf seine reversible, hohe Wasseraufnahmekapazität zurückgeführt, die vermutlich den Transport von gelösten Schadstoffen in und aus dem Partikelvolumen verbesserte. Die Bewertung der Exposition des Menschen gegenüber POPs über MPs ergab, dass der Beitrag von MP-sorbierten Schadstoffen im Vergleich zur Exposition über andere Quellen eher minimal war (≤ 0,1%).

Zusätzlich zu den sorbierten Schadstoffen enthalten MPs chemische Zusatzstoffe und Monomerrückstände. Die Exposition des Menschen gegenüber diesen Chemikalien könnte zu schädlichen Auswirkungen führen. Daher konzentrierte sich Studie drei auf die Auslaugung und die Bewertung der Toxizität der MP-Chemikalien, die bei der in-vitro-Verdauung im Magen-Darm-Trakt freigesetzt werden.

Von den drei untersuchten MP-Klassen setzten TR-Partikel im Vergleich zu PA-6 und TPU MP mehr Chemikalien frei. Zu den bemerkenswerten hohen Konzentrationen, die ausgelaugt wurden, gehören Benzothiazol, 2(3H)-Benzothiazolon und Zink, die mit 112 µg/g, 83 µg/g bzw. 1147 µg/g in den Dünndarmflüssigkeitssimulantien quantifiziert wurden. Für PA-6 wurden Monomer- und Dimerrückstände in den Simulanzien der Magen-Darm-Flüssigkeit identifiziert, wobei Caprolactam (PA-6_7µm Monomer) in einer Konzentration von 1549 µg/g quantifiziert wurde. Die UV-Alterung der Partikel erleichterte die Auslaugung neuer Verbindungen. Die Auslaugung von Chemikalien wurde durch die Zusammensetzung des Mediums und die Inkubationszeit moduliert. Zwanzig ausgewaschene Verbindungen wurden mit verschiedenen unerwünschten Wirkungspfaden (englisch: Adverse Outcome Pathways, AOPs) in Verbindung gebracht. Zu den wichtigsten AOPs gehörten die Aktivierung von Aryl-Kohlenwasserstoff-Rezeptoren (AhR), die Aktivierung von Nuclear Rezeptors und andere. Diese Ergebnisse geben Anlass zu weiterer Besorgnis über die Exposition des Menschen gegenüber toxischen Chemikalien durch MP, insbesondere Reifenpartikel.

Die Ergebnisse dieser Arbeit bieten einen Schwerpunkt für die Charakterisierung der Gesundheitsrisiken von MP und unterstützen auch die Gruppierung als effizienten Ansatz für die Risikobewertung.

3. INTRODUCTION

3.1. PLASTICS IN OUR ENVIRONMENT – COMPOSITIONS, USES, AND POLLUTION

Plastics are defined as materials which contain a high relative molecular mass of polymer as its main ingredient, and which can during its processing be shaped by flow into finished products [1]. Although the commercial production of plastic has been known for nearly 80 years [2], compared to other ancient and traditional materials such as glass, clay, wood, and metal, it can be referred to as fairly modern material. Plastics have since evolved and have displaced the traditional materials thanks to their ductility, versatility, cheap cost and ease of production.

Plastic composition and classification

Plastics are typically composed of polymers and additives which impact specific properties onto the plastics. The polymers are high molecular weight molecules, which are comprised of multiple repetition units of low molecular mass molecules called monomers [3]. Chemical additives of different kind are usually added to polymers at varying concentrations, according to their functions [4].

Polymers can be classified according to their origin, or characteristics such as structure, molecular force, or mode of polymerization (**Figure 1**). Most plastics are produced from synthetic polymers. That is, their starting materials (monomers) are traditionally obtained from crude oil and gas. It is suggested that the growing demand of these monomers from non-renewable and climate-unfriendly fossil fuel is a catalyst boosting the oil and gas industry [5, 6].

Recently, biodegradable plastics, which are made from either naturally occurring or artificial biodegradable polymers are gradually becoming popular as sustainable alternatives to fossil based plastics [7]. These materials which include polylactic acid, polyhydroxy butyrate, and polyhydroxyalkonoate, among others, are able to degrade from the attacks of microorganism under aerobic, or anaerobic conditions [8]. However, the ecological and in-vitro toxicity of these bioplastics are similar to those of conventional plastics [9-12].

It is noteworthy that there is no consensus regarding what is classed as plastics and what is not [13-15]. Some synthetic thermosets, elastomers and fibres are sometimes excluded as plastics, as they cannot be recycled [15]. However, these plastics consist of polymers and additives, and therefore are plastics by definition.

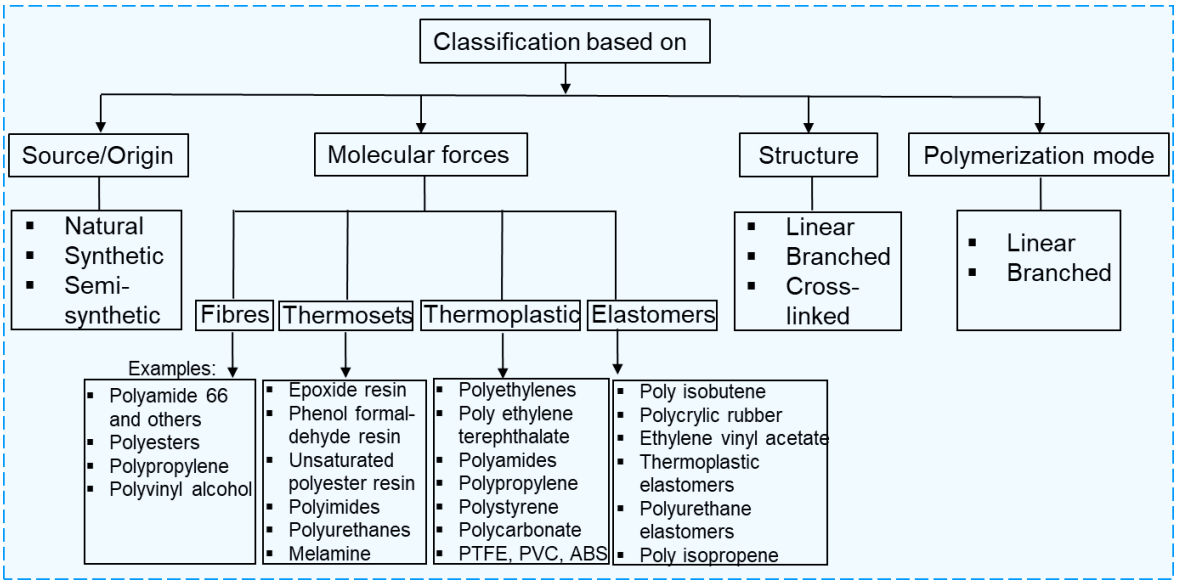

Figure 1: Classification of plastic materials: PTFE: polytetrafluoroethylene, PVC: polyvinyl chloride, ABS: acrylonitrile-butadiene styrene. Graphic modified from WHO [16] and Andrady A.L [17]

Evolution and uses of plastics

Since the mid-1940s, global plastic production has sustained a continuous growth. This growth is paralleled with increase in human population and world economy. Between 1960 to 2021, human population have grown form 3 billion to 7.9 billion people (**Figure 2**), within the same period, plastic production has increased by over two orders of magnitude to 391 million metric tons (Mt) in 2021 (**Figure 2**). Therefore, this growth in production is a direct consequence of increasing demand by a growing population. Based on projection, world population is forecasted to reach 9.7 billion by 2050 [18]. By the same time, plastic population is forecasted to reach 589 Mt [19].

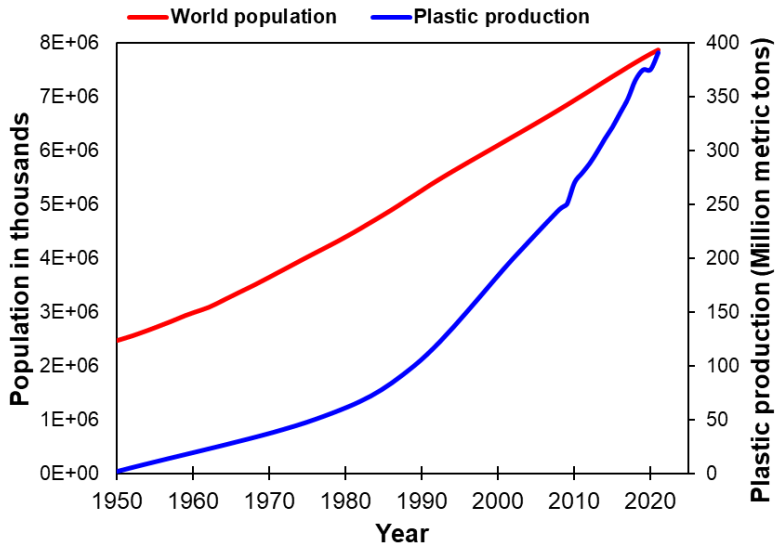

Figure 2: Growths in human population (1950-2021) and plastic production (1950-2021). Created with data from Plastics Europe [19] and United Nations [18].

Plastic has become an integral and indispensable part of our everyday life. Its affordability, versatility [14], and durability [20] have endeared it to us, and our creativity have expanded its applications over the years. They are now part of the clothing we wear, our shoes and bags, our food and water packaging, our furniture and gadgets, automobiles, and even our care and beauty products, to name a few. In 2021, plastics used in packaging and construction/building accounted for 62% of the global plastic use (**Figure 3**). However, while plastics have unarguably made human lives easy, accumulated effects of poor waste-management practices and policies [2] have created an enormous plastic pollution which has become a serious threat to human and animal health [21-23] and biodiversity of the ecosystem [24].

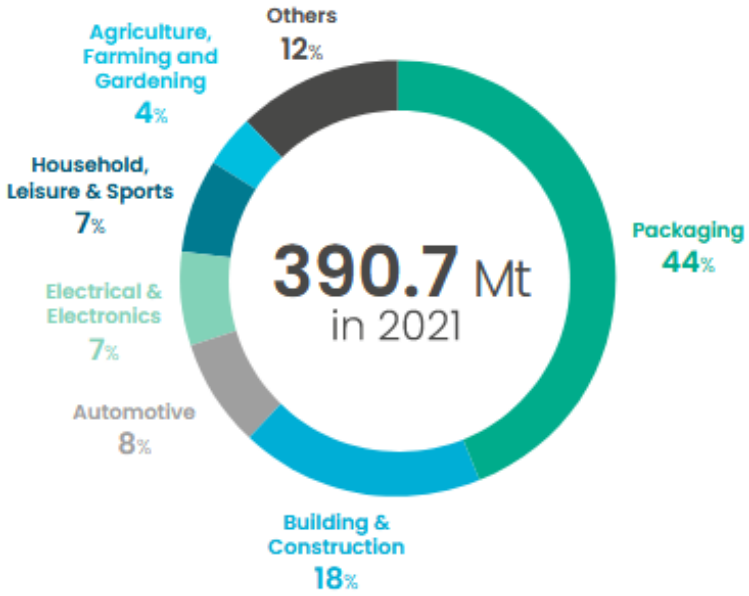

Figure 3: Distribution of global plastic use by applications. Plastic-thermosets and fibres used as synthetic textiles, adhesives, sealants, and coatings are not included, source: Plastics Europe [15]

Plastic pollution

Plastic pollution in the different strata of the environment is a direct consequence of uncoordinated disposal and management of plastic wastes. It is widely agreed that plastics are already ubiquitous [25-27]. According to the organization for economic co-operation and development (OECD), of the 353 Mt of plastic wastes generated globally in 2019, only about 6% was recycled, while 82% was inadequately disposed of, and the rest ended as litters in the aquatic and marine environment [28]. In developed nations however, the recycling rate have increased consistently since the last two decades; for the European Union nations as example, plastic wastes (from packaging only) reached 46% in 2020 [15]. Remarkably, the amount of waste generated is related to lifespan of the plastics, average lifespan of plastics differ according to their applications [29]. Packaging plastics have an average lifespan of 0.5 years, while plastics in constructions have an average lifespan of 35 years [28]. It is therefore logical that waste from packaging plastics dominate the total annual plastic wastes generated. This further imply that a significantly improved recycling effort on the global scale will improve the circularity of plastics use as well as mitigate microplastics (MP) pollution.

3.2. MICROPLASTICS AND LEAKAGE SOURCES

MPs are loosely defined as plastic particles less than 5 mm in diameter [30], or plastic particles within the range of 1000 µm to 1µm [31]. Thompson *et al*. [32] was first to utilize the term 'microplastics' in 2004 to describe particles around 20 µm in size. As research progressed, the definition was expanded to include plastic particles less than 5 mm [33, 34]. Accordingly, other plastic particles with different size ranges are defined. Mesoplastics and macroplastics are respectively described as particles between 5 to 25 mm, and particles greater than or equal to 25 mm [35], while nanoplastics are defined as plastic particles less than 1 µm [16], or more strictly, particles less than 100 nm [36].

Officially, the European chemicals agency (ECHA), defines MPs as a heterogeneous and water-insoluble solid polymer-containing particles, to which additives or other substances may have been added, and in which greater than or equal to 1% w/w of particles have (i) all dimensions 1 nm ≤ x ≤ 5 mm, or (ii), a length of 3 nm ≤ *x* ≤ 15 mm and a length to diameter ratio of > 3 [37]. Based on their source and origin, MPs in the environment are categorized as primary or secondary MPs [30].

3.2.1. PRIMARY MICROPLASTICS

Primary MPs are plastic particles originally manufactured in a size range within 5 mm, typically between 3 – 5 mm [38]. They include microbeads used in hygiene and personal care products such as shampoos, shower gels, toothpaste, soaps and facial cleansers [31, 39-41]. Other examples include microbeads which are added into cosmetic and detergent products to act as exfoliating and abrasive agents, or simply as emulsifier, or suspending agents [42-44]. According to Gouin *et al* estimate in 2015, microbeads used in personal care products are primarily made from polyethylene (PE), polypropylene (PP), and poly(ethylene-terephthalate) (PET) [45]. Recently, engineering and innovative polymers have been increasingly utilized [46, 47]. However, due to consumer safety and environmental concerns, a restriction of intentional primary MPs on care products have been proposed [48].

The definition of primary MPs has been expanded to include particles released directly as MPs during use of a product [49-51]. The classification of MPs based on their stepwise degradation after end of their life, or based on their formation during use is still equivocal and subject to debate. Nonetheless, MPs released continuously from a product during its use are widely regarded to as primary [52, 53].

Examples include MP fibres released from clothing during use [54, 55]. It is estimated that during the lifetime of a clothing, 2% of its polymers are released as MPs via washing [53]. Other examples are MPs from abrasions of shoe soles, protective coatings of ship and vehicles, and

exterior paints [56]; as well as polymer particles emitting from road stripes [53, 57]. This category of primary MPs also includes wears from tyres during their use. Results from mapping studies suggests that about 20% of rubber is lost from an average tyre during its lifetime [53, 58]. Global annual tyre rubber production was estimated at 2.35 billion in 2021 [59], and is projected to increase to 2.80 billion tyres by 2026 [59]. Consequently, MPs from tyre abrasions will also increase. Although the release rate will also depend on other factors as driving style, weather, and nature of road [58]. It is therefore unsurprising that MPs from tyres are the highest contributor of MP pollution.

Another source of primary MPs is the artificial turf used in sporting facilities such as tennis courts, golf courses, or football fields. Artificial turf are made of polymers such as polyamide-6 (PA-6), polyurethanes (PU), PE, and PP [49]. Styrene-butadiene rubber (SBR) and thermoplastic elastomers (TPE) are widely reported as fillers for artificial turf. As the turf ages, the particles wear and leach to the environment [60]. TPE particles stick to shoe soles and are transported into the environment [49, 61, 62].

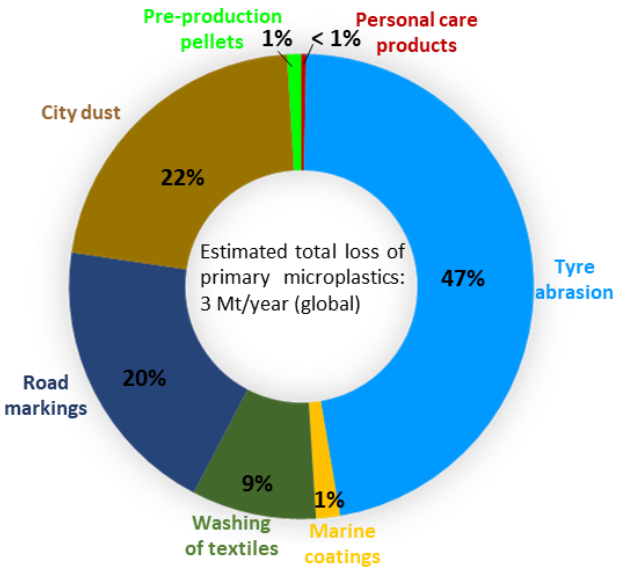

Figure 4: Estimated main sources of annual loss of primary MPs to the environment. Graphic created with data from UNEP [56]. Other minor sources of MP loss are not included due to inadequate knowledge.

Another category of primary MPs often overlooked are the polymer powders used for additive manufacturing (AM) or three-dimensional (3D) printing. Over the last decade, 3D-printing technology have grown rapidly [63], including the aspects utilizing polymer powders as base materials such as selective laser sintering (SLS), electron beam melting (EBM), and selective

metal building (SLM), among others [61]. Pre- and post-production waste, spillages during transportations or accidents have been identified as hotspots for losses to the environment [64].

3.2.2. SECONDARY MICROPLASTICS

Secondary MPs are formed by the gradual degradation of larger plastic debris under the actions of chemical, biological, and physical processes such as photo-irradiation, microbial activities, and mechanical grinding [49]. MP pollution in the aquatic and terrestrial environment are dominated by secondary MPs [49, 65].

Sources of secondary MPs are believed to originate from the fragmentation of macroplastics [56]. Hotspot sources of macroplastics include mismanaged plastic waste such as plastic bags, plastic bottles, single use plastics, and plastic packaging [28, 38, 56]. Loss due to indiscriminate littering, as well as loss of fishing nets and other marine activities also contribute to the formation of secondary MPs (**Figure 5**).

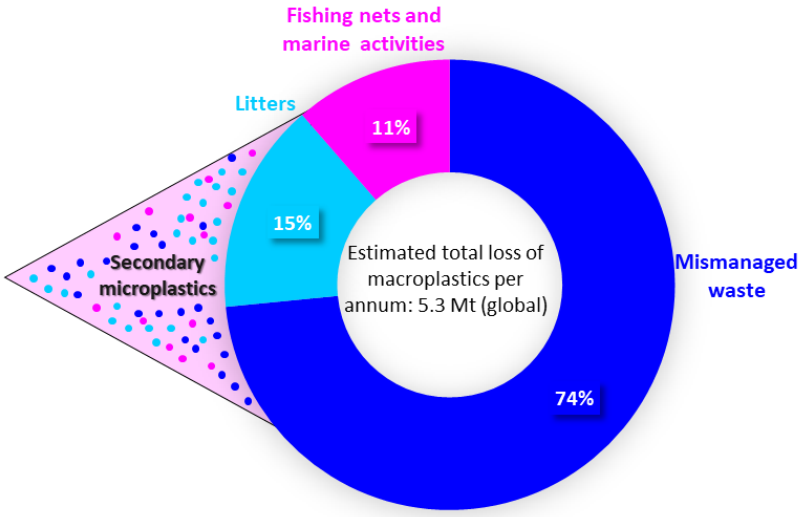

Figure 5: Estimated main sources of annual macroplastics loss to the environment. Graphic created with data from UNEP [56]. Other minor sources of plastic loss are not included due to inadequate knowledge.

It is noteworthy that while there is a consensus on the dominance of secondary MPs in the environment, estimate of secondary MPs originating from macroplastics is unknown. Estimation is particularly challenged by the uncertainty in the modelling estimates of macroplastics. Due to differences in the scope and methodology of the different studies, available results are difficult to compare [28]. For example, in 2019, an estimated 19 Mt of macroplastics waste was released to the environment according to OECD report [2], while the

United Nations Environment Programme (UNEP) reported presented an average annual waste of 5.3 Mt of macroplastics [56].

3.3. INTERACTIONS OF MICROPLASTICS WITH ORGANIC POLLUTANTS

MPs in terrestrial and aquatic environment contain organic chemicals that can be categorized into two. Group one consists of chemical additives, monomers, and oligomers originally present in the plastics. These chemicals are intentionally added to polymers during production to impart specific properties to the plastics. The second group consists of the contaminants, including persistent organic pollutants (POPs) which are either absorbed or adsorbed onto the MPs from the surrounding environment via different mechanisms.

Under favourable physico-chemical conditions, the chemicals associated with environmental MPs can be desorbed into air, water, or gastrointestinal fluids.

Moreover, both MP and the associated chemicals have been severally detected in marine organisms, from where they can contaminate human food chains. Notably, most of the MP-associated chemicals are hazardous to both human and animals. Also, different cellular effects observed in animal studies have been linked to exposure to MPs [30]. The interaction of MPs and associated chemicals with the ecosystem is illustrated in **Figure 6**.

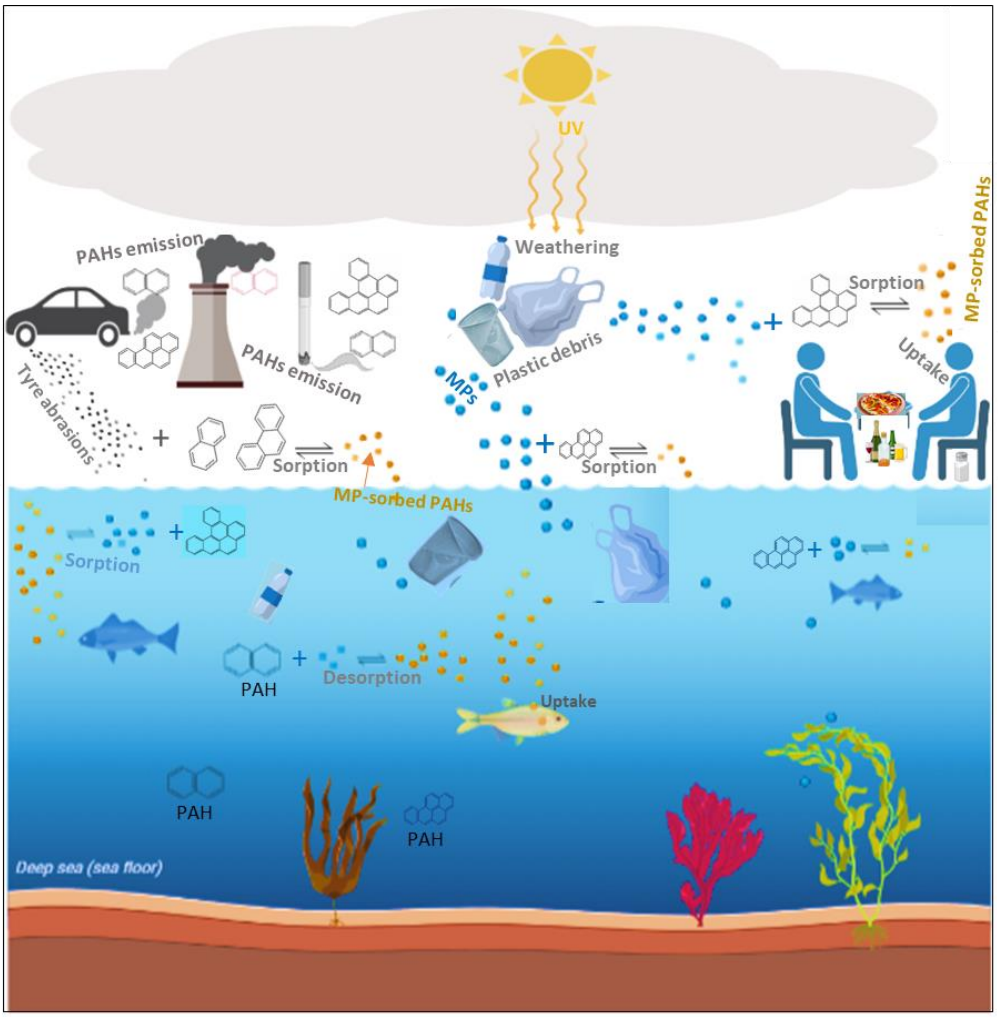

Figure 6: Interactions of MPs with pops in the ecosystem, Ubiquitous PAHs can be sorbed to MPs formed from plastic debris, or from vehicle Tyres as abrasives, among other sources. MP-sorbed PAHs can be taken up by marine organisms and humans. Under favourable conditions, depending on concentration gradient, sorbed PAHs can be desorbed.

3.3.1. CHEMICAL ADDITIVES FROM PLASTICS

Plastic additives are commonly grouped into four categories according to their functions [66-68]. They include (1) fillers such as calcium carbonate, barium sulphate, aluminium oxide, magnesium oxide, among others. (2) Functional additives such as plasticizers, stabilizers, flame retardants, antistatic agents, lubricants, foaming agents and others. (3) Colorants such as soluble azo colorants, and pigments. (4) Reinforcement agents such as glass fibres, and carbon fibres. The functions and concentration ranges of the additives are well documented [66-68].

The leaching of additives from plastics during their use, and during different stages of their transformations to MPs is well researched [69-71]. However, most additives are retained at

varying concentrations in MPs [72]. Moreover, particles intentionally produced as MPs also contain different additives [73]. Many of the additives, as well as residues of monomers and oligomers are not chemical bound to plastics [74], and therefore are susceptible to leaching. Some of these additives are toxic to both humans and animals [75]. Their toxicities, including endocrine disruption are well characterized [76, 77].

Within MPs collected from the environment, different additives such as phthalic acid esters (PAEs), Ultraviolet (UV)-stabilizers, Bisphenol A (BPA), octylphenol, nonylphenol, Butylated hydroxytoluene (BHT), among others, have been detected. Under favourable conditions, they can be leached from the plastic particles. For example, an estimated mass of 190 Mt of chemical additives entered the oceans in 2015 via common plastic debris [78].

3.3.2. PERSISTENT ORGANIC POLLUTANTS (POPs)

Some organic pollutants are termed 'persistent' due to their inability to degrade under environmental stress conditions [79]. They are usually lipophilic, semi- or non-volatile, and have low-water solubility and inherent toxicity [79, 80]. They are subject to long range transportations via air, or accumulation in soil, sediment, and water bodies; from where they enter human and ecological food chains [81, 82].

Polycyclic aromatic hydrocarbons (PAHs), and polychlorinated biphenyls (PCBs) are common examples as POPs [83], among others [79]. PAHs, originating mainly from incomplete combustion of fossil fuel are ubiquitous in the environment [84]. Though PCB production have ceased [85], its emission into the environment have continued via many pathways; including reservoirs, use and discard of PCB-containing products [86].

Many POPs are hydrophobic, and thus have strong affinity for hydrophobic MP particles. Sorption of different POPs to environmental MPs have been confirmed in numerous field [87], and laboratory studies [88-90]. MP-sorbed POPs can contribute to human and animal chemical toxicity [91].

3.3.3. SORPTION AND DESORPTION OF POPS ON MICROPLASTICS

Types of sorption

Sorption is generally used to refer to both adsorption and absorption, or when both phenomena occur simultaneously, or when the operative mechanism is unclear [92]. In adsorption, the compound or POP (sorbate) are confined at the interface between the sorbate and solid or MP

(sorbent) phases. In absorption, the sorbate penetrates inside the matrix of the sorbent (**Figure 7**). Partitioning and absorption are sometimes used interchangeably [93].

Sorption is also classified into physisorption (physical sorption), or chemisorption (chemical sorption). The former involves non-covalent interaction and reversible reaction, while the latter describes a non-reversible formation of covalent bond between the sorbate and sorbent [92, 94].

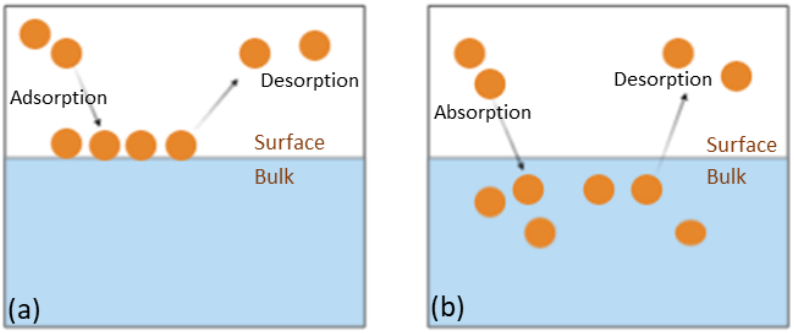

Figure 7: Types of sorption in a liquid-solid system. (a) – adsorption, and (b) – absorption. Adsorption and absorption can be physical or chemical. At sorption equilibrium, ab- and ad-sorption can become reversible (desorption).

Sorption mechanisms

Affinity of sorption depends strongly on the mechanism(s) governing the interactions of the sorbate with the MPs and water phases. Six mechanisms are mainly used to describe sorption process (**Figure 8a)**. Van der Waals interactions occurs between any types of molecules [89]. Hydrogen bonding occurs between H-bond acceptor and donor molecules in liquid and solid phases [95]. Similarly, π-interaction may occur between the liquid and aromatic sorbents [96]. Cavity formation (hydrophobicity effect) is the process of creating a cavity in each phase to accommodate the molecule to be sorbed. Sorption affinity is high in the direction where it is energetically favourable to form more cavities [92, 97]. Charged molecules between phases have led to attractive or repulsive electrostatic interactions. Lastly, pore-filling whereby sorbate molecules enter pores of the MP particles and become trapped have been attributed to several sorption processes [98-100].

The occurrence of one or more mechanisms depends on the properties of the sorbent and the sorbate; in addition to the condition and composition of the liquid phase (**Figure 8b**).

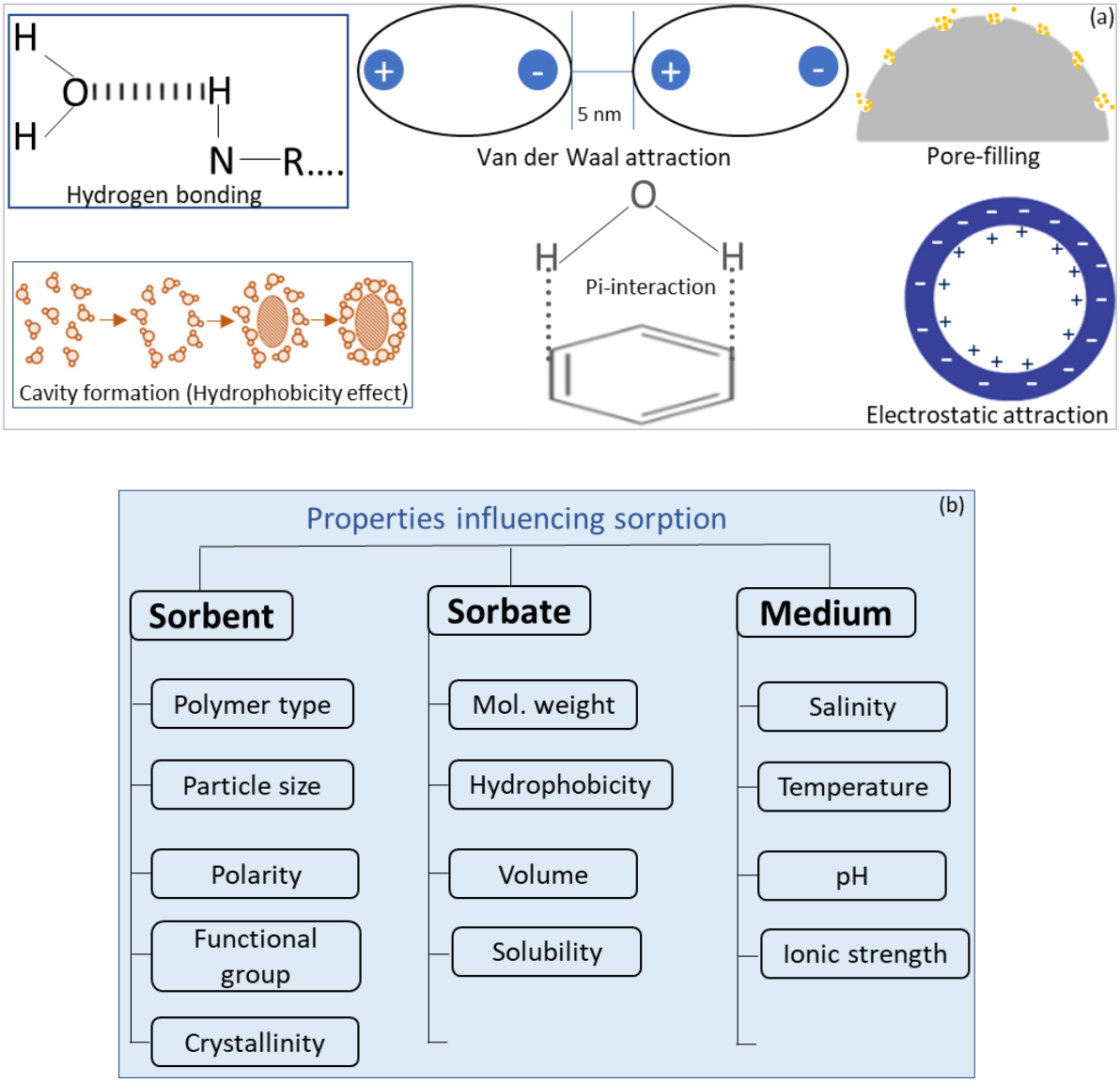

Figure 8: Mechanisms and properties influencing MP sorption. Activation of one or more mechanisms (a) depends on the properties of the sorbent, sorbate and the medium (b).

Sorption and desorption quantification methods

Sorption and desorption processes are usually quantified by the direct measurement of $K_{MP/W}$, which is defined as the equilibrium sorbate concentration in the sorbent or MP C_{MP}, divided by the sorbate concentration in the aqueous phase C_W. Sorption kinetics and isotherms are also used to quantify sorption.

$K_{MP/W}$ is usually determined by the batch-equilibrium method. However, in addition to its labour and time consumption, this method is unsuitable for compounds that have low solubility, or that significantly bind to the test apparatus. These shortfalls have motivated the development of other sorption characterization methods [101-106], including the third-phase partition (TPP)

method utilized in this study. The principle, pros and cons of the methods are summarized in **Table 1**.

Method	Principle	Note
Batch-equilibrium method [107]	Equilibrium distribution of sorbate between the sorbent and aqueous phase.	Easy mathematical treatment of results. Can be challenging for sorbates with low water solubility.
Third-phase partition (old) [101]	Passive sampling of sorbate onto the third-phase polymer: POM, mass balance of sorbate between sorbent, water and POM	Limited to the linear range of log K_{POM} vs K_{OW} (3.5 - 7.3). Soxhlet-extraction and clean-up steps can be labour/time consuming.
Co-solvent method [102]	Partition of sorbate between sorbent- and liquid-phase in mixed solvents	Compensates for sorption to glass or DOM. Requires large quantity of solvents.
Inverse gas-chromatography method [105]	Interactions of the injected sorbate with particles packed into GC-column	Can yield various parameters, including sorption energy. Limited to very volatile sorbates and sorbents with high melting points (>200 °C).
High performance liquid-chromatography method [106]	Interactions of the sorbates between the loaded polymer particles and mobile phase.	Expertise required in loading. Uncertainty due to dead volume. Difficulty in accurate determination of dead volume.
New Third-phase partition (This study)	Passive sampling of sorbate onto a re-usable PDMS stir-bar (third-phase polymer), & mass balance of sorbate between sorbent, water and PDMS.	Applicable within the linear range of log K_{PDMS} vs K_{OW} (4.0 - 7.5). Soxhlet-extraction and clean-up steps can be labour/time consuming.

Table 1: Overview of different sorption quantification methods.

Kinetic models (**Table 2**) are also utilized for sorption and desorption quantification. However, unlike isotherms, kinetic studies are mostly conducted using a fixed concentration, and therefore prone to larger uncertainties.

Desorption of sorbed compounds depends on many factors such as strength of sorption, sorption type, and properties of the medium or the environment such as salinity, pH, ionic strength, and temperature [108]. Depending on study conditions, one or more factors may dominate. For instance, absorbed compounds desorb easily compared to adsorbed

compounds which are slow in desorbing or even resistant to desorption [109, 110]. Also, plastic additives typically dissolved within the polymer matrix are widely reported to desorb substantially from the polymers.

Sorption isotherms and sorption models

If $K_{MP/W}$ is constant across the whole concentration range of the sorbate, such sorption is called 'linear' [92]. Non-linear sorption results when $K_{MP/W}$ depends on C_W [111]. A plot of C_{MP} vs C_w across the observed concentration range is called 'isotherm' [111], and valid only at a constant temperature. For linear sorption, linear isotherm is referred, while non-linear sorption are described by non-linear isotherms (**Figure 9**). Different models have been utilized to describe the non-linear isotherms. An overview descriptions and limitations of the models are illustrated in **Table 2**.

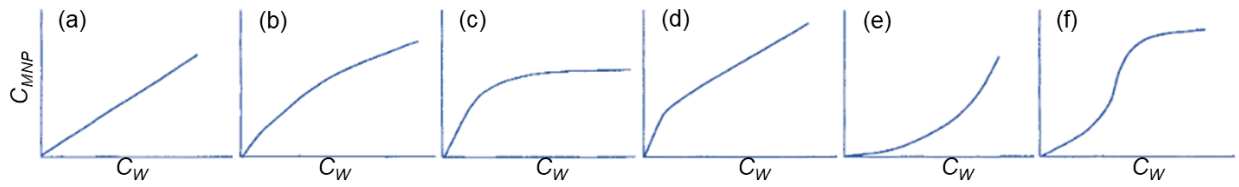

Figure 9: types of isotherms. Shapes differ depending on the equilibrium concentration of the sorbate in the liquid and solid phases within the isotherm – (a): affinity of sorbate for the sorbent remains constant across the enTyre concentration range. (b-c): affinity decreases at higher sorbate concentrations, binding sites less attractive or saturated. (d): combination of isotherm a & c. (e): previously sorbed sorbates triggers sorbent modification, favouring more sorption. (f): sorption-promoting effects becomes triggered after a certain loading of the sorbent. Isotherm shapes provides supportive validations but are insufficient to prove the prevalence of a mechanism, for which isotherm models are utilized.

.

Table 2: Overview of commonly used sorption kinetics and isotherm models, their assumptions, applications, and limitations. Over 100 isotherm models have been developed, in an attempt to describe the six isotherm shapes [112]. Commonly used models are shown. BET: Brunauer-Emmett-Teller, Dub-Rad: *Dubinin-Radushkevich. See nomenclatures for definition of model equations.*

Model	Equation	Principles / Assumptions	Limitations
Henry [113]	$C_{MP} = K_H C_W$	Describes the adsorption at low adsorbate concentration onto the adsorbent. Assumes that all adsorbate molecules are secluded from their neighbours.	Fails at medium to high concentration of adsorbate loading.

Temkin [114]	$C_{MP} = \frac{RT}{b_T} \ln A_T C_W$	Assumes that the heat of adsorption decreases linearly rather than logarithmically with an increase in surface coverage.	Ignores extremely low and large concentration values.
Freundlich [115]	$C_{MP} = K_F C_W{}^n$	Describes sorption on heterogeneous surface of adsorbent. Applicable to mono- and multilayer adsorption.	Assumes infinite active adsorption sites. i.e., amount of adsorbate adsorbed increases indefinitely
Langmuir [99]	$C_{MNP} = \frac{K_L * C_w}{1 + \alpha_L * C_w}$	Describes monolayer adsorption. Sorption to definite localized sites. No lateral interactions / steric hindrance. Characterized graphically by a plateau.	Assumes uniform site energy and homogenous surface.
Dub-Rad [113]	$C_{MP} = (q_s) \exp(-\text{Kad}\ \varepsilon^2)$	Empirical model - sorption follows pore filling mechanism. Can distinguish chemical and physical adsorption using its mean free energy.	Does not predict Henry's law at low concentration. Maximum adsorption prediction incomparable with Langmuir's
BET [116]	$C_{MNP} = q_m \frac{Ks * C_w}{(1 - K_l * C_w)(1 - K_l * C_w + Ks * Cw)}$	Multilayer adsorption behaviour-monolayer adsorption capacity. Adsorbent's surface area and pore size distribution can be extrapolated	Applies to systems of multilayer adsorption (high concentration), suitable for gas-solid systems
Redlich-Peterson [113]	$C_{MP} = \frac{\text{K}_R C_W}{1 + \alpha_\text{R} C_W{}^n}$	Applies to both homogenous and heterogeneous systems. Approaches Freundlich and Langmuir model at high and low sorbate concentration respectively	High Standard errors of parameters - (suitable for large isotherm points)
SIPS [117]	$C_{MP} = \frac{\text{K}_\text{sip} C_W{}^n}{1 + \alpha_\text{s} C_W{}^n}$	Combined form of Langmuir and Freundlich isotherm - applies to heterogenous sorption. Circumvent Freundlich isotherm's limitation - infinite sorbate concentration	High Standard errors of parameters - (suitable for large isotherm points)
Pseudo-first order [118]	$q_t = q_e(1 - e^{-k_1 t})$	Typically describes diffusion (physiosorption). Diffusion is the rate controlling step	Assumes that the concentration of one reactant is very high and the other is small and negligible - first order

Pseudo-second order [118]	$q_t = \frac{q_e^2 k_2 t}{(1 + k_2 q_e t)}$	Adsorption (chemisorption) on active sites may be the rate limiting process. Assumes sorbate sorb onto active sorbent site rather than diffuse around the sorbent.	Cannot predict how adsorption kinetics will change as a function of initial concentration and concentration at time *t*
Intra-particle diffusion [119]	$q_t = k_{\mathrm{id}} \cdot t^{1/2} + \theta$	External diffusion is the rate limiting step.	Several other factors influences sorption. Model equation not yet unified.

3.4. HUMAN EXPOSURE TO MICROPLASTICS-ASSOCIATED CHEMICALS

As described above, MPs contain intentionally added substances (IAS) such as chemical additives and residual monomers (**Section 3.3.1**), as well as non-intentionally added substances (NIAS) such as degradation products, but also sorbed pollutants such as PAHs, metals, PCBs, (**Section 3.3.2**). These chemicals are either adsorbed or absorbed to the MPs and can be released under favourable conditions (**Section 3.3.3**). Following the emerging evidence of MPs in food products [120, 121], as well as the detection of MPs in human lungs [122], and faeces [123], it is conceivable that MPs exposed to humans contains NIAS and IAS that can be potentially released in gastrointestinal (GI) or lung fluids where they can contribute to the body's chemical burden.

3.4.1. SOURCES AND ROUTES OF HUMAN EXPOSURE TO MICROPLASTICS

A potential source of human exposure to MPs is via ingestion of seafood and fish; especially those wholly consumed without removing the gastrointestinal tract (GIT). Examples include bivalves, small fish, and crustaceans [124-126]. Possibilities of exposure via the tissues of edible larger fish has been suggested [127]. A review of MPs found in other food types, including alcoholic and non-alcoholic beverages have been recently summarized, covering a wide range of 1 – 2400 particles/kg food [16]. Another major source of MP ingestion by humans is via tap and bottled water. A broad range of 0.1 – 5 x 10^7 particles/L across several studies has been summarized [128, 129].

Beside ingestion via food, concerns about inadvertent inhalation of MP particles are growing. Occurrences of respirable and inhalable (< 1 – 10 µm) MP particles, predominantly from synthetic fibres and Tyre wear particles have been characterized in indoor and outdoor air [130-132]. Indoor particles can be deposited on prepared meals [126] or inhaled directly [122, 133]. While ingestion and inhalation are the major routes of MP exposure to humans, penetration of nanoplastics across dermal barriers have been reported by a few studies [134-136].

3.4.2. MICROPLASTICS AS CHEMICAL CARRIERS: CURRENT KNOWLEDGE

Currently, there appear to be a consensus about the possibility of chemical transfer to organisms, including humans. However, the 'importance' or significance of such contributions relative to the overall chemical exposure not well-known and subject to debate [24, 38]. Current state of evidence from laboratory, field, and modelling studies suggests that the contribution of ingested MPs to marine animals is likely small (< 5 – 10%), relative to uptake from other sources [91, 137-140]. For humans, such contribution is probably even smaller [91]. This claim was corroborated by World Health Organization (WHO) [129] and the Food Agriculture Organization (FAO) [14] studies, where contributions of 1% and 0.1% were respectively reported.

Remarkably, MP-mediated exposure could be high in remote areas where background pollution is low, but small in areas of high background pollution, e.g. industrial areas [141]. Furthermore, if an animal has a greater burden of chemical than the ingested MP particles, the MPs will act as a 'cleaner' as the chemical will move in the direction of equilibrium based on the fugacity gradient [142]. The reverse is also true [143]. Hence, in this thesis, contributions of MPs to PAHs exposures was evaluated under sorption equilibrium relative to the optimal dietary concentrations of PAHs in the human body.

Summarily, MPs can act both as a source and sink of chemicals to marine animals, and possibly humans depending on the properties of the microplastics, concentration gradient, and spatial variations.

4. RESEARCH GOALS AND STRATEGIES

4.1. RESEARCH GOALS

The overarching aim of this research was to investigate to which extent MPs could act as carriers of toxic pollutants and thereby have an impact on human exposure. The carrier hypothesis postulates that the MPs act as transport vehicles for toxic pollutants such as PAHs. That is, the particles can *sorb* toxic contaminants such as POPs from the surrounding environment or at exposure hotspots, and under changed conditions such as medium, or pH as examples, the sorbed pollutants will be desorbed. Also, the opposite might be true, meaning that particles bind the POPs but rather serve a sink, thereby decreasing human burden of the POPs (scavenger effect). Similarly, chemical additives introduced to the plastics during production can be released along with the sorbed contaminants. For humans, the contributions and relevance of these chemicals to the body's chemical burden is ascertained.

To achieve the overarching aim, three specific aims were addressed in three different studies. Study one was aimed to evaluate the sorption kinetics and isotherms of three PAHs on seventeen MP variants. To this end, certain hypotheses were formulated and subsequently investigated: One, similar particle sizes and particle size distributions means similar sorption of organic pollutants. Two, If the chemical composition of the MPs is the same, the materials behave in a similar way regarding their sorption of organic pollutants. Three, sorption affinity of PAHs onto MPs increases with increasing hydrophobicity of the PAHs and vice versa.

Study two was aimed at the investigation of the desorption of MP-sorbed PAHs in human GI fluid simulants. Here, it was hypothesized that the desorption of MP-sorbed PAHs will increase along the GIT, from saliva to large intestine fluid simulants. secondly, if the chemical composition of the MPs is the same, the MPs exhibit similar desorption behaviours for PAHs. Thirdly, relative to the overall dietary sources, the contribution of MPs to the total PAHs intake by humans will be small.

The specific aim of study three was to identify the chemicals leaching from tyres and AM-MPs during in-vitro digestion in human GI fluid simulants, as well as to identify potential adverse outcomes of human exposure to the MP-associated leached compounds. For these, it was hypothesized that the leaching of chemical additives and monomer/dimer residues from the MPs will increase with longer incubation time in GI fluid simulants. Secondly, Aging of the MPs via photo-irradiation will facilitate the leaching of additional chemicals. Thirdly, compared to

distilled water, the composition of the GI fluid simulants will modulate the leaching of the chemicals from the MPs.

4.2. RESEARCH STRATEGY

To investigate the sorption of organic pollutants to different MPs, three PAHs of varying ring size and toxicity, anthracene (Anth), benzo[*a*]pyrene (B[*a*]P), and dibenzo[*a,l*]pyrene (DB[*a,l*]P) were chosen as model POPs, with B[*a*]P serving as lead sorbate.

Similarly, the above-stated goals were largely studied using plastic particles for innovative applications, specifically AM or 3D-printing application. These polymer classes are seldom studied. Examples of AM plastics chosen for investigations include PA-6, PA-12, TPU, and PU particles. These particles are also (primary) MPs because they contain realistic polymer compositions, polydisperse distributions (less than 5mm), wide-ranging chemical structures, and non-spheroidal morphology. For comparison, different variants of conventional MPs such as PE, polymethyl methacrylate (PMMA), and recycled end-of-life TR particles were studied.

Sorption experiments are usually performed using the batch-equilibrium method. though reliable, this method is associated with certain limitations unlike the TPP method. For instance, when dealing with super-hydrophobic sorbates that have low water solubility, the resulting sorption coefficient may be underestimated, and the equilibrium aqueous concentration may be too small to accurately measure. Additionally, when working with nano-sized and low-density sorbents, separating them from the mixture through filtration or centrifugation can be difficult and expensive. Another issue is the extraction of sorbate concentration from either the aqueous solution or the sorbent phase, which demands large amounts of organic solvent, time, and labour-intensive efforts.

To circumvent these challenges, a novel third-phase partition (TPP) method was developed, validated, and utilized for the sorption isotherms experiment. The TPP method involves the partitioning of the sorbate in a three-phase system comprised of the medium (water), the sorbent, and a re-usable polydimethylsiloxane (PDMS) coated stir-bar, otherwise referred to as the third-phase (**Figure 10**). In brief, the plastic particles are incubated in a containing PAH aqueous solution, and a characterized thermo-extractable PDMS-coated stir-bar until a pre-determined equilibrium is reached. The stir bar is removed, spiked with an internal standard and the concentration of PAH adsorbed to the PDMS coating C_{PDMS} is determined via thermal desorption gas chromatography mass spectrometry (TD-GC-MS). Subsequently, the

coefficient of PAH distributions between the plastic and water phases was determined via C_{PDMS} and the system characteristics. For selected MPs/PAHs pairs, the sorption coefficients and the corresponding isotherms obtained with the TPP method was validated using the batch-equilibrium method. See manuscript 1 and supplementary manuscript 1 for details.

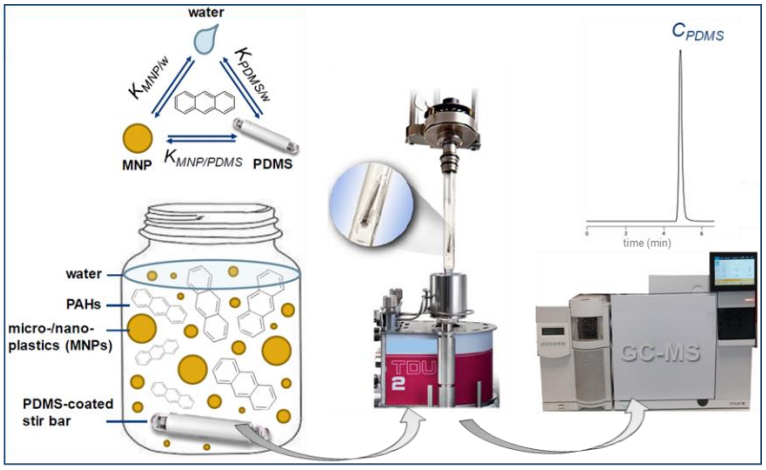

Figure 10: Illustrative workflow of third-phase partition method

With knowledge of the sorption capacities and coefficients of the MPs, study 2 focused on the second stage of the carrier hypothesis, desorption of sorbed pollutants. For relevance to human exposure, scenarios of human intake of MPs contaminated with PAHs was simulated in vitro. After physical-chemical characterization of the MPs, and photo-irradiation of selected variants, the particles were incubated in water containing low PAHs concentration range (ng/L) until equilibrium was reached. Subsequently, the PAH concentrations sorbed to the MPs were within the same range with those collected from the open environment.

The PAH-loaded MPs were sequentially digested in fluid simulants of the saliva, gastric, the small -, and large intestines. The released PAHs were then analysed by GC-MS, and the contributions of the released PAHs to the total PAHs intake was investigated. See manuscript 2 and supplementary manuscript 2 for details.

In study 3, the leaching of chemical additives and metals from the selected MPs was similarly simulated in the human GIT in vitro. In this case, MPs without POPs contaminations was sequentially digested in human saliva, gastric, and intestinal fluid simulants. For this study, two variants of micronized end-of-life Tyre rubber (TR) was studied as these materials are rich in additives. Also, TR particles are the major contributor of MP pollution and exposure.

In addition to TR MPs, aged and non-aged TPU and PA-6 materials were also studied for their leaching of additives. These material classes popularly used in 3D-printing are less studied compared with other conventional MPs such as PET, PP, PVC and others.

The additives and the non-intentionally added substances (NIAS) released following the digestion was analysed by GC-MS, and ICP-MS for the metal contents. Lastly, the toxicity and adverse outcomes associated with leached chemicals were assessed. Details are shown in manuscript 3 and supplementary manuscript.

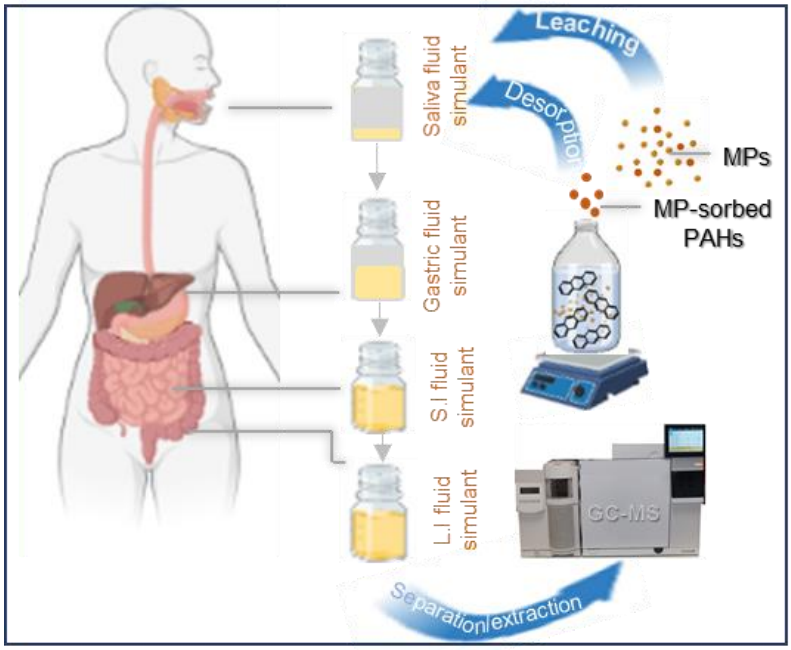

Figure 11: Simplified workflow of desorption and leaching experiments.

5. SYNOPSIS OF THE MANUSCRIPTS

Over the past two decades, research focussing on MP particles have grown progressively. A number of these studies focused on the possibility for MPs-induced adverse effects to humans. A concern which has grown, and justifiably due to the detection of environmental media with direct relevance for human exposure, including in water, air, dust, food, vegetables, and fruits. The presence of MPs in human lungs, blood, and stool confirms human exposure to these particles. Field evidence indicates that ingestion and inhalation are the main exposure routes to humans. Most of the respirable and inhalable MPs may be subject to mucociliary clearance.

Though research on the direct toxic effects of MPs remains ongoing and inconclusive, suggestions of adverse effects like those of other micro- and nanoparticles have been made for MPs, due to the similarity of their mode of actions. However, MPs can potentially induce health-hazards via many pathways. For example, by acting as carriers of toxic chemicals, or vectors of biofilms which may host pathogens.

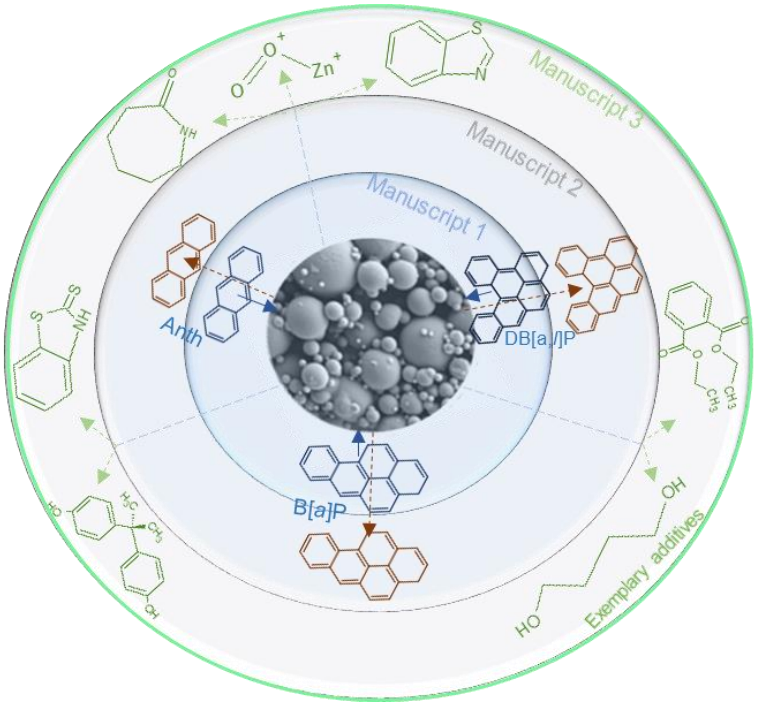

Figure 12: Graphical synopsis of the thesis. In manuscript 1, sorption of three PAHs to different polydisperse MPs was studied using a novel method. In manuscript 2, desorption of PAHs from different MPs was simulated in human gastrointestinal fluids. In manuscript 3, the leaching of chemical additives and monomer residues from the MPs was simulated. Selected additives are shown for illustration.

However, as depicted in **Figure 12**, this thesis focused on chemical carrier effects of the MPs, in support of a comprehensive risk assessment of human exposure. Accordingly, the sorption of PAHs as a model for POPs was investigated for seventeen MP variants using a novel

analytical method (Manuscript 1). Following, desorption of MP-sorbed POPs was studied using a physiology-based in vitro model comprised of digestions in simulated gastrointestinal fluids (Manuscript 2). Beside sorbed chemicals, MPs also contains additives, unreacted monomers and NIAS that could also be released either in food products or in the human GIT upon exposure. Therefore, the chemical profile of selected MPs was characterized via leaching experiments in GI fluid simulants, and the toxicity of leached compounds were assessed (Manuscript 3). The key findings and conclusions of the three studies are summarized as follows:

5.1. MANUSCRIPT 1: A COMPARATIVE INVESTIGATION OF THE SORPTION OF POLYCYCLIC AROMATIC HYDROCARBONS TO VARIOUS POLYDISPERSE MICRO- AND NANOPLASTICS USING A NOVEL THIRD-PHASE PARTITION METHOD

Initially, the novel TPP-method for sorption quantification was developed. This entailed the determination of the partition coefficients of the PAHs onto the PDMS third-phase polymer, coupled with the identification of the requisite equilibrium durations for effective partitioning of PAHs onto the PDMS polymer substrate. Furthermore, the TD-GC-MS system was developed for the purpose of extracting and analysing sorbed PAHs, with a meticulous delineation of optimal parameters.

Following, the sorption of B[*a*]P to seventeen MP variants were determined using the TPP-method which enabled the quantification of sorption, including those with poor water-solubility without the need for filtrations and solvent-extractions typical for the batch-equilibrium method. Prior, kinetic experiments which established the equilibrium times showed that the two most common kinetic models, the pseudo-first and pseudo-second-order models were both suitable to describe the kinetic process. This inferred that diffusion-driven mass transfer of the sorbate to the sorbent or sorption onto the active sites of the sorbent or both phenomena may be the rate limiting steps of the sorption process.

Generally, B[*a*]P sorption across the different MPs were generally strong, with their log of sorption coefficients $K_{MP/W}$ greater than 5.2 but differed by over two-orders of magnitude (**Figure 13a**). After comparing the experimental sorption isotherms in different isotherm models for their goodness of fit and the plausibility of their parameters, the Langmuir model was found most suitable for comparison of the PAHs sorption to the MPs. Using the Langmuir adsorption

coefficients K_L, a ranking of the MPs revealed clustering according to their chemical composition, irrespective of their size distributions, following the order of PA > PE > TR > TPU ~ PU > PMMA (**Figure 13b**). Notably, PA-6, a polymer used for example in AM applications, was observed to show exceptionally high sorption of B[*a*]P despite its relatively high polarity, which might be due to the transport of dissolved B[*a*]P to the bulk of the polymer.

However, within polymer types, particle size significantly influenced B[*a*]P sorption, with increased K_L was observed with decreasing mean particle size. Similarly, polymer backbones and chain segments of copolymers also influenced sorption. For example, K_L of TPU polymers with equal proportions of hard (aromatic isocyanate) and soft (polyester) segments was slightly lower compared with their counterpart formulated mainly with polyester soft segments.

Selected MP particles aged by prolonged UV light irradiation for 1000–2000 h which is supposed to simulate roughly one year of exposure to sunlight in Europe decreased their sorption of B[*a*]P. This effect was presumably due to the functionalization of the surfaces of the aged MPs, making them more hydrophilic. Unlike B[*a*]P, hydrophilic pollutants may sorb more strongly. In addition, hydrophobicity of the PAH sorbates strongly influenced their sorption to MPs. The K_L for the three selected MPs: PA-6_42µm, LDPE_215µm, and TPU_est_arom followed the order of DB[*a,l*]P > B[*a*]P > Anth and differed by more than five orders of magnitude. Furthermore, the coefficients of the PAHs sorption to the respective MPs were observed to correlate strongly with the molecular weights and octanol-water coefficients of the PAHs. This highlights the potential for a reliable prediction of the sorption coefficients of MPs and organic pollutants within a substance class.

Moreso, the sorption of PAHs to the MPs in tri-sorbate systems revealed competitive sorption. Compared with mono-sorbate systems, the sorption of Anth to selected MPs decreased significantly in the presence of other more hydrophobic PAHs. The effect was less pronounced for B[*a*]P, while the sorption of DB[*a,l*]P was unaffected in mono- and tri-sorbate systems.

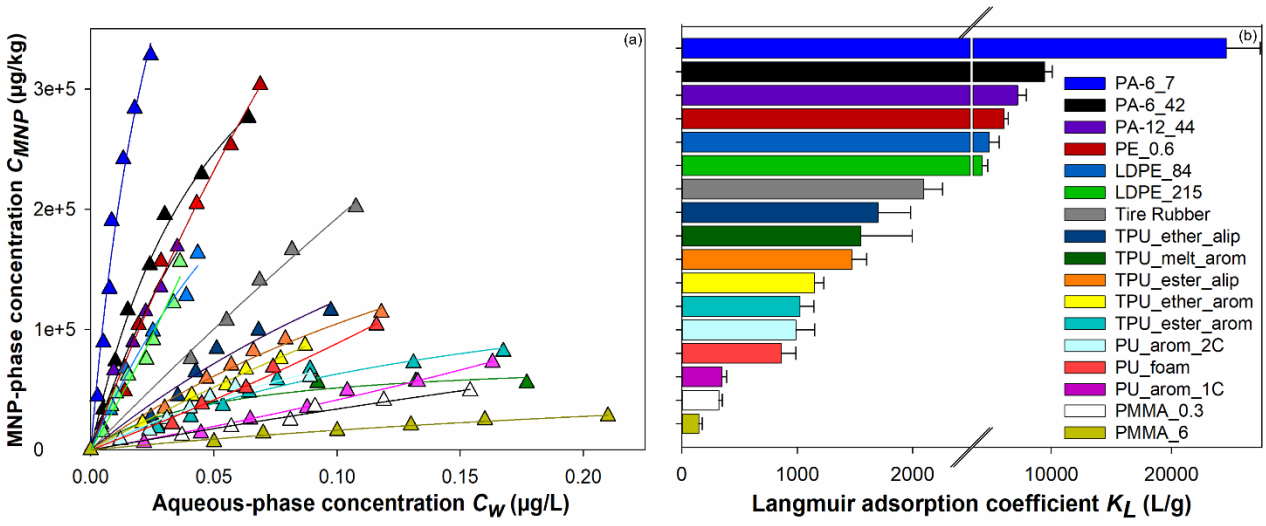

Figure 13 (a): Experimental sorption isotherms for B[a]P and MPs fitted to the Langmuir model. (b): Ranking of B[a]P sorption to MPs according to the Langmuir adsorption coefficients K_L (error bars represent standard errors of K_L).

5.2. MANUSCRIPT 2: DESORPTION OF POLYCYCLIC AROMATIC HYDROCARBONS FROM MPS IN HUMAN GASTROINTESTINAL FLUID SIMULANTS – IMPLICATIONS FOR EXPOSURE ASSESSMENT

The strong sorption of MPs confirms their potential to act as carriers for PAHs. MPs and PAHs are ubiquitous in the environment, their interaction in the open and aquatic environment have been demonstrated in field studies. However, of growing concern is the inevitability of human exposure to plastic particles, either via ingestion through food products, or via inhalation.

In addition to the potential for direct toxic effect by the MP particles, MP-sorbed pollutants may be released in the human GIT upon exposure and could contribute to human chemical load. Currently, the assessment of MPs contribution to human chemical intake remains speculative due to paucity of data. This knowledge gap prompted a systematic investigation for the release of MP-sorbed PAHs utilizing a physiology-based model comprising digestion in simulated saliva, gastric, small, and large intestinal fluids.

For three MPs: low density (LD)PE, TPU and PA-6 evaluated consecutively in all four GI fluid simulants for their release of B[*a*]P, the cumulative relative desorption (CRD) was negligible in

saliva simulant but increased from gastric (4 ± 1 %) to large intestinal fluid simulants (29 ± 6 %) across the three MPs.

Similarly, in a sub-study not included in the above-referenced manuscript, the release of PCB-153 from PA-$6_{7\mu m}$ was investigated by the sequential digestion of PCB153-loaded particles in the GI fluid simulants. As shown in **Figure 14a**, the CRD of PCB-153 increased from 6 ± 1 % and 18 ± 1 % respectively for the saliva and gastric simulants, to absolute release in the intestinal fluid simulants. Of note, 0.3 %w/w of PCB-153 was artificially loaded to the PA-$6_{7\mu m}$ particles by incubation in acetone for 7 days. The effect of this loading procedure in contrast with the PAHs where MPs were incubated in water until equilibrium was not evaluated.

Considering that the digestion and absorption of ingested food occurs predominantly in the small intestine in-vivo, the CRD of the eleven MP variants were compared in the sequential small intestine fluid simulant. Owing to a presumable kinetic effect, the CRD values for most of the MPs were rather moderate, ranging from 4 % (PU_arom_1C) to 19 % (PA-$6_{42\mu m}$). Only PA-$6_{7\mu m}$ showed an exceptionally high CRD of 51 % (**Figure 14b)**. Photo-aging of TPU and PA-6 MP variants had negligible effect on their release of B[*a*]P in the small intestine fluid simulant. This implies that the observed functionalization of the aged MP surfaces had no significant effect on desorption, pointing to bulk-diffusion being the rate-limiting step for desorption.

Beside B[*a*]P, the sequential desorption of Anth and DB[*a,l*]P into the small intestinal fluid simulant was studied for PA-6 and LDPE MPs The degree of desorption varied based on both the type of PAH and MP material employed. DB[*a,l*]P, for example, exhibited the strongest desorption (46 – 61 %) from both MPs, presumably due to predominant surface adsorption to the particles given its larger molar volume and very low water solubility. Desorption of Anth from the MPs were less, 6% and 36% respectively for LDPE and PA-6 materials. This is possibly due to different modes of transport from the bulk to the particle surfaces of the two polymers.

To provide insight to the potential health risk posed by human exposure to MPs, an exposure assessment was performed. This revealed a daily PAHs intake range of 0.2–2.4 pg/kg bw/day across all studied MPs, and 4.7 pg/kg bw/day for PCB-153 from PA-$6_{7\mu m}$. The contribution of MP-sorbed POPs to total POP dietary intake was calculated at ≤ 0.1 %.

It was further observed that depending on the assumed values of MP intake, and concentrations of associated PAHs, the calculated contribution of MPs as PAH carriers can exceed those from other dietary sources. A conservative MP ingestion rate of 4.1 µg/capita/day, and an environmentally-relevant PAH load were utilized herein. However, MP

ingestion rate greater than 4-orders of magnitude than our estimate have been suggested. Moreover, significantly higher MP exposure have been reported at local hotspots.

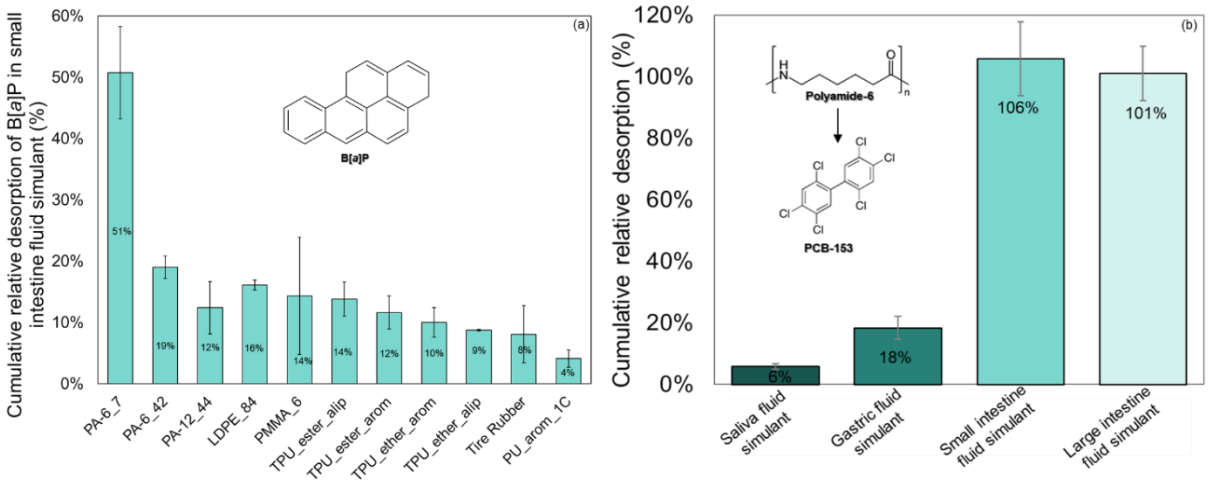

Figure 14 (a): Cumulative relative desorption (CRD) of B[a]P from different MPs in small intestine fluid simulant which contains the preceding saliva and gastric simulant (n = ≥3 ± SD). (b): CRD of PCB-153 from PA-6_7µm following sequential digestion in the human GI fluid simulants (n = ≥3 ± SD).

5.3. LEACHING OF CHEMICAL ADDITIVES FROM MICROPLASTICS DURING *IN VITRO* GASTROINTESTINAL DIGESTION AND TOXICITY ASSESSMENT OF LEACHED COMPOUNDS

The release of chemical additives from aged- and non-aged variants of TR, PA-6, and TPU particles in human GI fluids was simulated in vitro by the sequential digestion of the particles in intestinal fluids, following physiological conditions. Prior, the leachable chemicals as well as the signature monomers and oligomers associated with the particles were characterized via the online-coupled thermal desorption (TD)- and pyrolysis (Pyr)-GC-MS respectively. Also, the metal contents were characterized by microwave-assisted extraction, followed by inductively coupled plasma-mass spectrometry (ICP-MS) analysis.

GC-MS analyses of the leachates revealed that TR particles released more chemicals compared to other MPs. Among selected chemicals quantified via the method- and matrix matched calibrations, caprolactam (monomer of PA-6 polymer) and benzothiazole from TR_{LKW} particles leached at the highest concentrations of 1549 µg/g and 112 µg/g respectively. Leaching of the chemicals were promoted by the composition of the medium and the incubation

time. New chemicals were leached from the particles after UV-irradiation of the particles. For PA-6 MP, decreasing particle size enhanced the leaching of selected quantified chemicals.

Regarding the metal leachates, a total of 24 isotopic elements were quantified leaching from the TR MPs in the sequential small intestine fluid simulants at varying concentrations: including arsenic, silver, lead, aluminium, and copper. Zinc from TR_{infill} particles leached at the highest concentrations of 1147µg/g. Assessment of human metal intake via TR exposure ranged from 9.14E-11 µg/kg/day for mercury to 1.07E-05 µg/kg/day for zinc. However, the estimated daily intake of all leached metals is below the calculated tolerable daily intake.

Regarding the leached additives, 58 chemicals were identified via non-target screening with a NIST match-score of ≥ 80%, including residues of PA-6 monomer and dimer: caprolactam and 1,8-diazocyclotetradecane-2,9-dione. 54 out of the 58 compounds were found in the ToxCast database, and 20 of them were linked to several adverse outcome pathways (AOPs) with taxonomic applicability to humans, and moderate to high evidence of a connection between molecular initiating events, key events, and adverse outcomes. Notable AOPs include those associated with the activation of Aryl hydrocarbon receptors (AhR): AOP 41, 57, 131, and 150; estrogen receptors (AOP 167, 200); cyclooxygenase inhibition (AOP 63, 102, 103); and nuclear receptors (AOP 63, 102, 103). Of all released chemicals, 2-mercaptobenzothiazole was associated with the highest number of potential adverse outcomes.

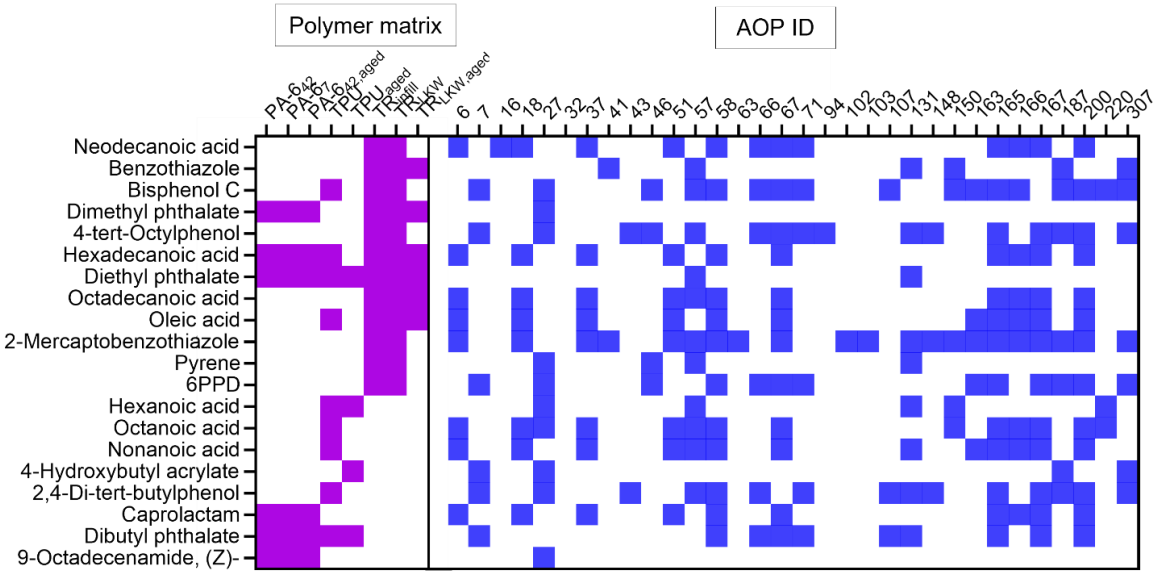

Figure 15: Outline of potential AOPs of chemicals released from MPs in human GI fluid simulants

To confirm the AOPs, a key event leading to AhR activations (AOP 57, 131), upregulation of CYP1A1 was experimentally investigated as an example using the MP particles and the supernatants resulting from the in vitro digestion of the particles. Only tyre particles induced CYP 1A1. Photo irradiation of the tyre particles significantly decreased the CYP 1A1 expression. Interestingly, the concentrations of benzothiazole and derivatives leaching from photo-aged TR particles decreased in comparison with non-aged particles. Thus, signalling a benzothiazole- and derivatives-mediated induction.

This study highlights the potential for human exposure to toxic chemical additives via MP particles. However, comprehensive risk characterization will entail assessment of the exposure in addition to the hazard. A thorough assessment of human exposure to chemical additives from MPs is challenged by huge uncertainties related to the mass of MP intake by humans. Besides, human exposure to respirable and inhalable submicron- and nano-plastics is largely uncharacterized. Secondly, the extent of the bioavailability of leached chemicals are usually assumed. Factors influencing chemical bioavailability remains unknown. Thirdly, the contributions of the bioavailable chemical additives to the body's chemical burden are elusive; unlike POPs for which a minimal contribution have been suggested. If MPs are generally confirmed as a significant source of human exposure to these chemical additives, then MPs could represent a potent health hazard to humans, especially for scenarios of routine exposures.

6. CONCLUSIONS AND OUTLOOK

6.1. GENERAL CONCLUSIONS AND DISCUSSIONS

In this dissertation, utilizing B[*a*]P as a model pollutant for sorption and desorption study, we observed that chemical composition (polymer type) of the plastic particles was the most important determinant for B[*a*]P sorption in water, modulating its uptake by over 100-fold across 17 MP variants. Regarding desorption, which was performed under physiology rather than equilibrium conditions, the effect of polymer type was less prominent. However, quantified desorption of B[*a*]P differed by over 10-fold across 11 MP variants, although their relevance to total human dietary POP exposure was observed to be very small under current MP-sorbed PAHs pollution level.

Other factors such as particle size, polarity, and chain segments were relevant within specific polymer types. In particular, hydrophobicity of the PAHs strongly influenced their sorption to MPs; implying that pollutants of similar hydrophobicity could exhibit similar sorption affinity onto specific sorbents.

Regarding grouping, our sorption study supports OECD classification of chemical composition or polymer chemistry as a relevant grouping criterion for the MPs [144]. However, considering the complex composition of plastics, including their polydisperse molecular weight, additive contents and residual monomer, other criteria in addition to the polymer chemistry need to considered to formulate a grouping framework. Remarkably, the plastic particles studied in this thesis, including variants of polyamides; polyurethanes; polyesters; polyethers; and others such as polyethylene and tyre rubber particles have been generally classified by OECD as polymers of low concern (PLC) or potential concern.

However, subject to further hazard characterization, PA-6 particles may be a polymer of low health concern rather than potential health concern. This is predicated on the high content and subsequent leaching of the residual monomer: caprolactam; in addition to the leaching of the dimer, metals and other chemical additives from the polymer. A cumulative intestinal leached concentration of 1800 ng/mg caprolactam was quantified from PA-$6_{7\mu m}$. Also, compared with other polymers, PA-6 particles exhibited the highest sorption and desorption capacities for pollutants (PAHs, PCB) in a size-dependent manner.

Similarly, tyre rubber particles might represent an MP of ‘concern’; owing to the cocktail of chemical additives, degradation products, and contaminants characterized from this material. Volatile toxic additives could be released from tyre wear particles in the open environment, or in food products, or in human GIT upon direct exposure. Exposure of the particles in European sunlight for one year, which was simulated via an ISO-standardized aging process revealed significant decrease of benzothiazole, 2(3H)-Benzothiazolone, phthalimide, and other additives in tyre rubber particles. Also, more chemicals, including sorbed pollutants were leached from tyre particles in the GI fluid simulants. Strikingly, in comparison with other MPs, only tyre particles induced CYP 1A1 enzyme, a key event leading to the activation of AhR adverse outcome. Some of the released chemicals were associated with other adverse outcomes in human. This is particularly concerning considering the widespread sources of human exposure to tyre wear particles, including from dust, tracks, playfields, and recycling vicinities. This thesis once again highlights the need for stricter regulation of the uses and disposal methods of end-of-life tyres, particularly in developing countries where these regulations seem lacking.

Nevertheless, the concentration of leached chemicals is key to the attribution of adverse effects to the MPs. The toxicity of MP-associated chemicals may not necessarily pose a health risk if the exposure is well below a defined margin of exposure limit; or if the leached concentration is negligible compared with exposure from other sources. In this study, efforts were made to quantify selected leached chemicals. Across investigated MPs, the cumulative intestinal leached concentrations ranged from 4µg/g for dibutyl phthalates from tyre particles to 1800µg/g for caprolactam from PA-$6_{7\mu m}$ particles. Beside leached chemicals, information on the initial concentrations of the chemical additives and monomers in the particles is paramount for exposure assessment, as different additives are present in different concentrations according to their uses in the plastics. In this thesis, the initial and leached concentrations of metals in the MPs were quantified. Hence, assessment of human exposure to metals via MPs was feasible. However, the calculated tolerable daily intakes of the metals were above the estimated daily intakes from MPs.

6.2. OUTLOOK

In this thesis, a re-usable PDMS stir-bar was used as third-phase polymer for the development of the novel TPP method for quantifying sorption of pollutants to MPs. In a further study, a method utilizing characterized PDMS and online-coupled TD-GC-MS to measure desorption rates of pollutants from MPs can be developed. This will among other advantages, eliminate the need for centrifugation/filtration of the supernatant, as well as the labour-intensive solvent-extractions of the filtrate. Similarly, the TPP-method can be utilized to quantify the sorption affinity of POPs other than PAHs to MPs, if the PDMS-water partition coefficients of the POPs are known from literature or pre-determined experimentally.

The plastic particles studied in this thesis were polydisperse MPs of <1 mm to 20 µm in size. For two polymer classes, inhalable fractions (1 – 10 µm) were studied. The sorption of pollutants generally increased with decreasing particle sizes within specific polymer classes. For PA-6, desorption of pollutants and leaching of chemical additives from submicron inhalable particles significantly increased with decreasing particle size. Therefore, further studies focussing on the sorption and desorption behaviours of nanoplastics is needed for better understanding of the scale and effect of human exposure to nanoplastics.

A strong correlation between sorption affinity and hydrophobicity of three PAHs was observed within this thesis. An expanded additional study involving more than the three PAHs will confirm the practicability of modelling the sorption of a broad selection of pollutants to specific polymer types. Furthermore, human exposure assessment of sorbed pollutants were performed in this thesis. However, determination of risk will involve the characterization of possible hazard associated with the plastic particles, including cytotoxicity, reactivity, oxidative stress, genotoxicity, and others. This can be tailored towards sub-micron and nano-sized particles for which the potential for risk was established in this thesis.

Lastly, this work focused on the carrier effect of real-life tyre particles and AM-applicable MPs, a similar study utilizing other MPs collected from the open and marine environment will broaden the current knowledge of the chemical risks associated with MP-exposures.

LITERATURE

1. International organization for standard, *ISO 472:2013 Plastics — Vocabulary*. 2013, Geneva.
2. OECD, *Global Plastics Outlook: Economic Drivers, Environmental Impacts and Policy Options,* . 2022.
3. IUPAC., *Compendium of polymer terminology and nomenclature: IUPAC recommendations 2008*. 2008: Cambridge.
4. MP, S., *Polymer additives: Part 1. Mechanical property modifiers. .* J Chem Educ., 1993. **70**(6): p. 444-8.
5. GERVET, B., *The use of crude oil in plastic making contributes to global warming*. 2007, Luleå University of Technology: Sweden.
6. Baheti, P. *How Is Plastic Made? A Simple Step-By-Step Explanation*. British plastic federation [cited 2023 June].
7. Ghosh, K. and B.H. Jones, *Roadmap to Biodegradable Plastics—Current State and Research Needs.* ACS Sustainable Chemistry & Engineering, 2021. **9**(18): p. 6170-6187.
8. Tokiwa, Y., et al., *Biodegradability of plastics.* Int J Mol Sci, 2009. **10**(9): p. 3722-3742.
9. Zimmermann, L., et al., *Are bioplastics and plant-based materials safer than conventional plastics? In vitro toxicity and chemical composition.* Environ Int, 2020. **145**: p. 106066.
10. Qin, M., et al., *A review of biodegradable plastics to biodegradable microplastics: Another ecological threat to soil environments?* Journal of Cleaner Production, 2021. **312**.
11. Ribba, L., et al., *Biodegradable plastics in aquatic ecosystems: latest findings, research gaps, and recommendations.* Environmental Research Letters, 2022. **17**(3).
12. Fan, P., et al., *A review on the occurrence and influence of biodegradable microplastics in soil ecosystems: Are biodegradable plastics substitute or threat?* Environ Int, 2022. **163**: p. 107244.
13. AJ, V., *Towards a definition of microplastics: considerations for the specification of physico-chemical properties.* Bilthoven: National Institute for Pubic Health and the Environment, 2015.
14. (FAO), Food agricultural organization of the united nations, *Microplastics in fisheries and aquaculture. Status of knowledge on their occurrence and implications for aquatic organisms and food safety*. 2017.
15. PlasticsEurope, *Plastics - the facts*. 2022: Brussels, Belgium.

16. W.H.O, *Dietary and inhalation exposure to nano- and microplastic particles and potential implications for human health*. 2022: Geneva.
17. Andrady, A.L., *Biodegradability of Polymers* in *Physical Properties of Polymers Handbook*, J.E. Mark, Editor. 2007, Springer Material: USA.
18. United Nations, Department of Economic and Social Affairs Population Division , *World Population Prospects 2022.* Online Edition, 2022.
19. PlasticsEurope (PEMRG), *Annual production of plastics worldwide from 1950 to 2021*. 2022.
20. Pritchard, G., *Reinforced plastics durability*. 1999, Germany: CRC press.
21. Wright, S.L. and F.J. Kelly, *Plastic and Human Health: A Micro Issue?* Environ Sci Technol, 2017. **51**(12): p. 6634-6647.
22. Vethaak, A.D. and H.A. Leslie, *Plastic Debris Is a Human Health Issue.* Environ Sci Technol, 2016. **50**(13): p. 6825-6.
23. Thompson, R.C., et al., *Plastics, the environment and human health: current consensus and future trends.* Philos Trans R Soc Lond B Biol Sci, 2009. **364**(1526): p. 2153-66.
24. Mine B. Tekman, B.A.W., Corina Peter, , *Impacts of plastic pollution in the oceans on marine species, biodiversity and ecosystems,*, J. Bentley, Editor. 2022: Berlin, Germany. p. 221.
25. Moyo, S., *An enigma: A meta-analysis reveals the effect of ubiquitous microplastics on different taxa in aquatic systems.* Frontiers in Environmental Science, 2022. **10**.
26. Lim, X., *Microplastics are everywhere - but are they harmful?* Nature, 2021. **593**(7857): p. 22-25.
27. Farady, S.E., *Microplastics as a new, ubiquitous pollutant: Strategies to anticipate management and advise seafood consumers.* Marine Policy, 2019. **104**: p. 103-107.
28. OCED, *Global Plastics Outlook: Economic Drivers, Environmental Impacts and Policy Options*. 2022: Paris.
29. PlasticsEurope, *Plastics – the Facts 2019: An analysis of European plastics production, demand and waste data*. 2019: Brussels, Belgium. p. 42.
30. Ramasamy, E.V. and A.K. Harit, *Microplastics in Human Consumption*. 2023, USA: CRC Press.
31. E.C.D.E, *Intentionally added microplastics in products*. 2017: Brussels.
32. Thompson, R.C., et al., *Lost at sea: where is all the plastic?* Science, 2004. **304**(5672): p. 838.

33. Arthur, C., J. Baker and H. Bamford (eds). *Proceedings of the International Research Workshop on the Occurrence, Effects and Fate of Microplastic Marine Debris.* in *NOAA Technical Memorandum NOS-OR&R-30*. 2009. USA: NOAA.
34. Betts, K., *Why small plastic particles may pose a big problem in the oceans.* Environ Sci Technol, 2008. **42**(24): p. 8995.
35. Christopher Blair Crawford, B.Q., *Microplastic Pollutants*. 2016: Elsevier publications.
36. Gigault, J., et al., *Nanoplastics are neither microplastics nor engineered nanoparticles.* Nat Nanotechnol, 2021. **16**(5): p. 501-507.
37. ECHA, *ANNEX XV RESTRICTION REPORT – MICROPLASTICS*. 2019: Finland.
38. GESAMP, *"Sources, fate and effects of microplastics in the marine environment: part two of a global assessment*, P.J. Kershaw, and Rochman, C.M., eds. (IMO/FAO/UNESCO-IOC/UNIDO/WMO/IAEA/UN/UNEP/UNDP Joint Group of Experts on the Scientific Aspects of Marine Environmental Protection, Editor. 2016, IMO/FAO/UNESCO-IOC/UNIDO/WMO/IAEA/UN/UNEP/UNDP Joint Group of Experts on the Scientific Aspects of Marine Environmental Protection: London. p. 220.
39. Peng, J., J. Wang, and L. Cai, *Current understanding of microplastics in the environment: Occurrence, fate, risks, and what we should do.* Integr Environ Assess Manag, 2017. **13**(3): p. 476-482.
40. Lei, K., et al., *Microplastics releasing from personal care and cosmetic products in China.* Mar Pollut Bull, 2017. **123**(1-2): p. 122-126.
41. Patil, A. and M.S. Ferritto, *Polymers for Personal Care and Cosmetics: Overview*, in *Polymers for Personal Care and Cosmetics*. 2013. p. 3-11.
42. Cole, M., et al., *Microplastics as contaminants in the marine environment: a review.* Mar Pollut Bull, 2011. **62**(12): p. 2588-97.
43. Fendall, L.S. and M.A. Sewell, *Contributing to marine pollution by washing your face: microplastics in facial cleansers.* Mar Pollut Bull, 2009. **58**(8): p. 1225-1228.
44. Siegfried, M., et al., *Export of microplastics from land to sea. A modelling approach.* Water Res, 2017. **127**: p. 249-257.
45. T. Gouin, J.A., I. Brunning, et al., *Use of Micro-Plastic Beads in Cosmetic Products in Europe and Their Estimated Emissions to the North Sea Environment.* International Journal for Applied Science, 2015(3): p. 40-46.
46. Cubas, A.L.V., et al., *Plastics and Microplastic in the Cosmetic Industry: Aggregating Sustainable Actions Aimed at Alignment and Interaction with UN Sustainable Development Goals.* Polymers (Basel), 2022. **14**(21).

47. Bashari, A., A. Rouhani Shirvan, and M. Shakeri, *Cellulose-based hydrogels for personal care products.* Polymers for Advanced Technologies, 2018. **29**(12): p. 2853-2867.
48. Directorate-General for Internal Market, I., Entrepreneurship and SMEs, *REACH committee votes to restrict intentional microplastics.* European commission news article, 2023.
49. L. An, Q.L., Y. Deng, W. Wu, Y. Gao, and W. Ling. , *Sources of microplastic in the environment*, in *Microplastics in Terrestrial Environments,*, Y.L. Defu He, Editor. 2020, Springer.
50. Jürgen bertling, r.b., leandra hamann, *Kunststoffe in der umwelt: Mikro- und Makro-plastik.* fraunhofer-institut für umwelt-, sicherheits- und energietechnik UMSICHT, 2018.
51. ETC experts: Saskia Manshoven (VITO), Anse Smeets (VITO), Christian Malarciuc (CSCP), Anna Tenhunen (VTT), *Microplastic pollution from textile consumption in Europe*. 2022.
52. Meides, N., *Mechanisms for the Formation and Degradation of Microplastic: Results from Accelerated Weathering Studies*. 2023, University of Bayreuth.
53. Julien Boucher, D.F., *Primary Microplastics in the Oceans: a Global Evaluation of Sources*, in *INTERNATIONAL UNION FOR CONSERVATION OF NATURE*. 2017: Gland, Switzerland.
54. Sol, D., et al., *Contribution of household dishwashing to microplastic pollution.* Environ Sci Pollut Res Int, 2023. **30**(15): p. 45140-45150.
55. Periyasamy, A.P. and A. Tehrani-Bagha, *A review on microplastic emission from textile materials and its reduction techniques.* Polymer Degradation and Stability, 2022. **199**.
56. U.N.E.P, *Mapping of global plastics value chain and plastics losses to the environment (with a particular focus on marine environment)*, M. Ryberg, Laurent, A., Hauschild, M, Editor. 2018, United Nations Environment Programme Nairobi, Kenya.
57. Peter Sundt, P.-E.S., Frode Syversen, *Sources of microplastics-pollution to the marine environmnet.* Norwegian Environment Agency Miljødirektoaret, 2014: p. 84.
58. Wik, A. and G. Dave, *Occurrence and effects of tire wear particles in the environment--a critical review and an initial risk assessment.* Environ Pollut, 2009. **157**(1): p. 1-11.
59. Smithers. *The Future of Global Tires to 2026*. 2021.
60. Kerstin Magnusson, K.E., Anna Fråne, Kalle Haikonen, Johan Hultén, Mikael Olshammar, Johanna Stadmark, Anais Voisin, *Swedish sources and pathways for microplastics to the marine environment*. 2017, Swedish Environmental Research Institute Stockholm, Sweden.

61. Saleh Alghamdi, S., et al., *Additive Manufacturing of Polymer Materials: Progress, Promise and Challenges.* Polymers (Basel), 2021. **13**(5).
62. Faludi, J., et al., *Comparing environmental impacts of additive manufacturing vs traditional machining via life-cycle assessment.* Rapid Prototyping Journal, 2015. **21**(1): p. 14-33.
63. Coherent market insights. *Polymers for additive manufacturing market analysis*. 2021; Available from: https://www.coherentmarketinsights.com/market-insight/polymers-for-additive-manufacturing-market-4496.
64. Rodriguez-Hernandez, A.G., et al., *3D printer waste, a new source of nanoplastic pollutants.* Environ Pollut, 2020. **267**: p. 115609.
65. Andrady, A.L., *The plastic in microplastics: A review.* Mar Pollut Bull, 2017. **119**(1): p. 12-22.
66. (ECHA), E.C.A. *Mapping exercise – Plastic additives initiative*. 2023 May 2023]; Available from: https://echa.europa.eu/mapping-exercise-plastic-additives-initiative.
67. Bridson, J.H., et al., *Release of additives and non-intentionally added substances from microplastics under environmentally relevant conditions.* Environmental Advances, 2023. **12**.
68. Hahladakis, J.N., et al., *An overview of chemical additives present in plastics: Migration, release, fate and environmental impact during their use, disposal and recycling.* J Hazard Mater, 2018. **344**: p. 179-199.
69. Hamilton, B.M., et al., *Plastics as a carrier of chemical additives to the Arctic: possibilities for strategic monitoring across the circumpolar North.* Arctic Science, 2023. **9**(2): p. 284-296.
70. Luo, H., et al., *Effects of aging on environmental behavior of plastic additives: Migration, leaching, and ecotoxicity.* Sci Total Environ, 2022. **849**: p. 157951.
71. Bridson, J.H., et al., *Leaching and extraction of additives from plastic pollution to inform environmental risk: A multidisciplinary review of analytical approaches.* J Hazard Mater, 2021. **414**: p. 125571.
72. Chen, Y., et al., *An Overview of Chemical Additives on (Micro)Plastic Fibers: Occurrence, Release, and Health Risks.* Reviews of Environmental Contamination and Toxicology, 2022. **260**(1).
73. Amec Foste Wheeler Environment & Infrastructure, *Intentionally added microplastics in products. Final report.* October 2017: London, United Kingdom.
74. Lewis, A., L. Ferguson, J. Sipe, M. Wiesner, A. Williams, AND C. Lowe, *Additive release from plastics in environmental and biological fluids*. 2022, Microplastics, Ascona: Switzerland.

75. Hermabessiere, L., et al., *Occurrence and effects of plastic additives on marine environments and organisms: A review.* Chemosphere, 2017. **182**: p. 781-793.
76. ECHA. *Endocrine disruptor assessment list*. 2023 [cited May 2023; Available from: https://echa.europa.eu/ed-assessment.
77. Lahimer, M.A., N; Horriche, J; Belgaied, S *Characterization of plastic packaging additives: Food contact, stability and toxicity* Arabian Journal of Chemistry, 2017 **10**.
78. De Frond, H.L., et al., *Estimating the Mass of Chemicals Associated with Ocean Plastic Pollution to Inform Mitigation Efforts.* Integr Environ Assess Manag, 2019. **15**(4): p. 596-606.
79. Heidelore Fiedler, V.B.-A., *The Handbook of Environmental Chemistry*. Vol. 3. 2003, Berlin Heidelberg: Springer-Verlag.
80. Eduljee, G.H., *Persistent Organic Pollutants - Environmental Behavior and Pathways of Human Exposure*, ed. S. Harrad. 2001, New York: Springer Science+Business Media.
81. Li, Q.Q., et al., *Persistent organic pollutants and adverse health effects in humans.* J Toxicol Environ Health A, 2006. **69**(21): p. 1987-2005.
82. Guo, W., et al., *Persistent Organic Pollutants in Food: Contamination Sources, Health Effects and Detection Methods.* Int J Environ Res Public Health, 2019. **16**(22).
83. Pawlak, F., et al., *Persistent organic pollutants (POPs) as an indicator of surface water quality in the vicinity of the Polish Polar Station, Horsund.* Monatshefte für Chemie - Chemical Monthly, 2019. **150**(9): p. 1573-1578.
84. Lee, B.-K., *Sources, Distribution and Toxicity of Polyaromatic Hydrocarbons (PAHs) in Particulate Matter*. Air Pollution, ed. V. Villanyi. 2010, United Kingdom: IntechOpen.
85. Collection, U.N.T., *Stockholm Convention on Persistent Organic Pollutants* 2001.
86. Montano, L., et al., *Polychlorinated Biphenyls (PCBs) in the Environment: Occupational and Exposure Events, Effects on Human Health and Fertility.* Toxics, 2022. **10**(7).
87. Ogata, Y., et al., *International Pellet Watch: global monitoring of persistent organic pollutants (POPs) in coastal waters. 1. Initial phase data on PCBs, DDTs, and HCHs.* Mar Pollut Bull, 2009. **58**(10): p. 1437-46.
88. Kinigopoulou, V., et al., *Microplastics as carriers of inorganic and organic contaminants in the environment: A review of recent progress.* Journal of Molecular Liquids, 2022. **350**.
89. Torres, F.G., et al., *Sorption of chemical contaminants on degradable and non-degradable microplastics: Recent progress and research trends.* Sci Total Environ, 2021. **757**: p. 143875.

90. Emecheta, E.E., et al., *A comparative investigation of the sorption of polycyclic aromatic hydrocarbons to various polydisperse micro- and nanoplastics using a novel third-phase partition method.* Microplastics and Nanoplastics, 2022. **2**(1).
91. Koelmans, A.A., et al., *Microplastic as a Vector for Chemicals in the Aquatic Environment: Critical Review and Model-Supported Reinterpretation of Empirical Studies.* Environ Sci Technol, 2016. **50**(7): p. 3315-26.
92. Satshi Endo, A.K., *Sorption of Hydrophobic Organic Compounds to Plastics in the Marine Environment: Equilibrium*, in *Hazardous Chemicals Associated with Plastics in the Marine Environment,*, H.K.K. H. Takada, Editor. 2016, Springer International Publishing: Switzerland.
93. Mayer, P., W.H. Vaes, and J.L. Hermens, *Absorption of hydrophobic compounds into the poly(dimethylsiloxane) coating of solid-phase microextraction fibers: high partition coefficients and fluorescence microscopy images.* Anal Chem, 2000. **72**(3): p. 459-64.
94. Karapanagioti, H.K., Werner, D., *Sorption of Hydrophobic Organic Compounds to Plastics in the Marine Environment: Sorption and Desorption Kinetics*, in *Hazardous Chemicals Associated with Plastics in the Marine Environment. The Handbook of Environmental Chemistry*, H. Takada, Karapanagioti, H., Editor. 2018, Springer: Switzerland.
95. Tourinho, P.S., et al., *Partitioning of chemical contaminants to microplastics: Sorption mechanisms, environmental distribution and effects on toxicity and bioaccumulation.* Environ Pollut, 2019. **252**(Pt B): p. 1246-1256.
96. Huffer, T., A.K. Weniger, and T. Hofmann, *Sorption of organic compounds by aged polystyrene microplastic particles.* Environ Pollut, 2018. **236**: p. 218-225.
97. Goss, K.-U. and R.P. Schwarzenbach, *Rules of Thumb for Assessing Equilibrium Partitioning of Organic Compounds: Successes and Pitfalls.* Journal of Chemical Education, 2003. **80**(4).
98. Wang, Q., et al., *The adsorption behavior of metals in aqueous solution by microplastics effected by UV radiation.* J Environ Sci (China), 2020. **87**: p. 272-280.
99. Wang, F., et al., *Sorption Behavior and Mechanisms of Organic Contaminants to Nano and Microplastics.* Molecules, 2020. **25**(8).
100. Wu, P., et al., *Adsorption mechanisms of five bisphenol analogues on PVC microplastics.* Sci Total Environ, 2019. **650**(Pt 1): p. 671-678.
101. Jonker, M.T.O. and A.A. Koelmans, *Polyoxymethylene solid phase extraction as a partitioning method for hydrophobic organic chemicals in sediment and soot.* Environmental Science & Technology, 2001. **35**(18): p. 3742-3748.

102. Hegeman, W.J., C.H. Van Der Weijden, and J.P. Loch, *Sorption of Benzo[a]pyrene and Phenanthrene on Suspended Harbor Sediment as a Function of Suspended Sediment Concentration and Salinity: A Laboratory Study Using the Cosolvent Partition Coefficient.* Environ Sci Technol, 1995. **29**(2): p. 363-71.
103. Garbarini, D.R. and L.W. Lion, *Evaluation of sorptive partitioning of nonionic pollutants in closed systems by headspace analysis.* Environ Sci Technol, 1985. **19**(11): p. 1122-8.
104. Allen-King, R.M., H. Groenevelt, and D.M. Mackay, *Analytical method for the sorption of hydrophobic organic pollutants in clay-rich materials.* Environ Sci Technol, 1995. **29**(1): p. 148-53.
105. Davydova, M.B. and Y.P. Yampolskii, *An inverse gas chromatography study of sorption in polyphenylene oxide.* Polymer Science U.S.S.R., 1991. **33**(3): p. 495-501.
106. Marchetti, N., et al., *Determination of adsorption isotherms by means of HPLC: adsorption mechanism elucidation and separation optimization.* J Sep Sci, 2009. **32**(5-6): p. 727-41.
107. OECD, *Guideline for the testing of chemicals: Adsorption - Desorption Using a Batch Equilibrium Method*. 2000.
108. Hartmann, N.B., et al., *Microplastics as vectors for environmental contaminants: Exploring sorption, desorption, and transfer to biota.* Integr Environ Assess Manag, 2017. **13**(3): p. 488-493.
109. Cornelissen, G., et al., *Extensive sorption of organic compounds to black carbon, coal, and kerogen in sediments and soils: mechanisms and consequences for distribution, bioaccumulation, and biodegradation.* Environ Sci Technol, 2005. **39**(18): p. 6881-95.
110. Mayer, P., et al., *A contaminant trap as a tool for isolating and measuring the desorption resistant fraction of soil pollutants.* Environ Sci Technol, 2011. **45**(7): p. 2932-7.
111. Rene P. Schwarzenbach, P.M.G., Dieter M. Imboden, *Sorption I: General Introduction and Sorption Processes Involving Organic Matter*, in *Environmental organic chemistry*. 2002, Wiley & Sons Inc.
112. Shimizu, S. and N. Matubayasi, *Understanding Sorption Mechanisms Directly from Isotherms.* Langmuir, 2023. **39**(17): p. 6113-6125.
113. Foo, K.Y. and B.H. Hameed, *Insights into the modeling of adsorption isotherm systems.* Chemical Engineering Journal, 2010. **156**(1): p. 2-10.
114. Eriksson, M., I. Lundström, and L.G. Ekedahl, *A model of the Temkin isotherm behavior for hydrogen adsorption at Pd–SiO2 interfaces.* Journal of Applied Physics, 1997. **82**(6): p. 3143-3146.

115. Al-Ghouti, M.A. and D.A. Da'ana, *Guidelines for the use and interpretation of adsorption isotherm models: A review.* J Hazard Mater, 2020. **393**: p. 122383.
116. Ebadi, A., J.S. Soltan Mohammadzadeh, and A. Khudiev, *What is the correct form of BET isotherm for modeling liquid phase adsorption?* Adsorption, 2009. **15**(1): p. 65-73.
117. Sips, R., *On the Structure of a Catalyst Surface.* The Journal of Chemical Physics, 1948. **16**(5): p. 490-495.
118. Simonin, J.-P., *On the comparison of pseudo-first order and pseudo-second order rate laws in the modeling of adsorption kinetics.* Chemical Engineering Journal, 2016. **300**: p. 254-263.
119. Wang, J. and X. Guo, *Rethinking of the intraparticle diffusion adsorption kinetics model: Interpretation, solving methods and applications.* Chemosphere, 2022. **309**(Pt 2): p. 136732.
120. Toussaint, B., et al., *Review of micro- and nanoplastic contamination in the food chain.* Food Addit Contam Part A Chem Anal Control Expo Risk Assess, 2019. **36**(5): p. 639-673.
121. Jin, M., et al., *Microplastics contamination in food and beverages: Direct exposure to humans.* J Food Sci, 2021. **86**(7): p. 2816-2837.
122. Jenner, L.C., et al., *Detection of microplastics in human lung tissue using muFTIR spectroscopy.* Sci Total Environ, 2022. **831**: p. 154907.
123. Luqman, A., et al., *Microplastic Contamination in Human Stools, Foods, and Drinking Water Associated with Indonesian Coastal Population.* Environments, 2021. **8**(12).
124. Cox, K.D., et al., *Human Consumption of Microplastics.* Environ Sci Technol, 2019. **53**(12): p. 7068-7074.
125. Van Cauwenberghe, L. and C.R. Janssen, *Microplastics in bivalves cultured for human consumption.* Environ Pollut, 2014. **193**: p. 65-70.
126. Catarino, A.I., et al., *Low levels of microplastics (MP) in wild mussels indicate that MP ingestion by humans is minimal compared to exposure via household fibres fallout during a meal.* Environ Pollut, 2018. **237**: p. 675-684.
127. Daniel, D.B., et al., *Microplastics in the edible tissues of shellfishes sold for human consumption.* Chemosphere, 2021. **264**(Pt 2): p. 128554.
128. Koelmans, A.A., et al., *Microplastics in freshwaters and drinking water: Critical review and assessment of data quality.* Water Res, 2019. **155**: p. 410-422.
129. W.H.O, *Microplastics in drinking-water*. 2019.
130. Dris, R., et al., *Microplastic contamination in an urban area: a case study in Greater Paris.* Environmental Chemistry, 2015. **12**(5).

131. Dris, R., et al., *A first overview of textile fibers, including microplastics, in indoor and outdoor environments.* Environ Pollut, 2017. **221**: p. 453-458.
132. Sommer, F., et al., *Tire Abrasion as a Major Source of Microplastics in the Environment.* Aerosol and Air Quality Research, 2018. **18**(8): p. 2014-2028.
133. Luis Fernando Amato-Lourenco, R.C.O., Gabriel Ribeiro Junior, Luciana Dos Santos Galvao, Romulo Augusto Ando, Thais Mauad, *Microplastics inhalation: evidence in human lung tissue.* European Respiratory Journal 2021.
134. Vogt, A., et al., *40 nm, but not 750 or 1,500 nm, nanoparticles enter epidermal CD1a+ cells after transcutaneous application on human skin.* J Invest Dermatol, 2006. **126**(6): p. 1316-22.
135. Mahe, B., et al., *Nanoparticle-based targeting of vaccine compounds to skin antigen-presenting cells by hair follicles and their transport in mice.* J Invest Dermatol, 2009. **129**(5): p. 1156-64.
136. Hernandez, L.M., N. Yousefi, and N. Tufenkji, *Are There Nanoplastics in Your Personal Care Products?* Environmental Science & Technology Letters, 2017. **4**(7): p. 280-285.
137. Koelmans, A.A., *Modeling the Role of Microplastics in Bioaccumulation of Organic Chemicals to Marine Aquatic Organisms. A Critical Review*, in *Marine Anthropogenic Litter*. 2015. p. 309-324.
138. Ziccardi, L.M., et al., *Microplastics as vectors for bioaccumulation of hydrophobic organic chemicals in the marine environment: A state-of-the-science review.* Environ Toxicol Chem, 2016. **35**(7): p. 1667-76.
139. Rochman, C.M., et al., *Polystyrene plastic: a source and sink for polycyclic aromatic hydrocarbons in the marine environment.* Environ Sci Technol, 2013. **47**(24): p. 13976-84.
140. Bakir, A., et al., *Relative importance of microplastics as a pathway for the transfer of hydrophobic organic chemicals to marine life.* Environ Pollut, 2016. **219**: p. 56-65.
141. Tanaka, K., et al., *Facilitated Leaching of Additive-Derived PBDEs from Plastic by Seabirds' Stomach Oil and Accumulation in Tissues.* Environ Sci Technol, 2015. **49**(19): p. 11799-807.
142. Koelmans, A.A., et al., *Plastic as a carrier of POPs to aquatic organisms: a model analysis.* Environ Sci Technol, 2013. **47**(14): p. 7812-20.
143. Mohamed Nor, N.H. and A.A. Koelmans, *Transfer of PCBs from Microplastics under Simulated Gut Fluid Conditions Is Biphasic and Reversible.* Environ Sci Technol, 2019. **53**(4): p. 1874-1883.
144. OECD, *Data Analysis Of The Identification Of Correlations Between Polymer Characteristics And Potential For Health Or Ecotoxicological Concern*. 2009.

7 MANUSCRIPTS

7.1 LIST OF PUBLICATIONS AND MANUSCRIPTS

This thesis is written as a cumulative dissertation of three research manuscripts.

1. **A comparative investigation of the sorption of polycyclic aromatic hydrocarbons to various polydisperse micro- and nanoplastics using a novel third-phase partition method.**

Emecheta E.E, Borda D.B, Pfohl P.M, Wohlleben W., Hutzler C., Haase A., Roloff A.

MPs and Nanoplastics (2022) 2:29. *https://doi.org/10.1186/s43591-022-00049-9*

2. **Desorption of Polycyclic Aromatic Hydrocarbons from MPs in Human Gastrointestinal Fluid Simulants – Implications for Exposure Assessment**

Emecheta E.E, Pfohl P.M, Wohlleben W., Haase A., Roloff A. *ACS Omega 2024, 9, 23, 24281–24290. https://doi.org/10.1021/acsomega.3c09380*

3. **Leaching of Chemical Additives from Microplastics during *in vitro* Gastrointestinal Digestion and Toxicity Assessment of leached compounds**

Emecheta E.E, Vogel A., Begert A., Schmidt R., Wohlleben W., Haase A., Roloff A.

Manuscript ready for submission.

6.2. CONTRIBUTIONS TO THE JOINT PUBLICATIONS

Manuscript 1

The study was conceived by Alexander Roloff (AR) and Christoph Hutzler (CH), with contributions from Andrea Haase (AH). Emeka Ephraim Emecheta (EEE) designed and carried out the study under the supervision of AR, with contributions from AH and CH. Patrizia Marie Pfohl (MP aging and FT-IR spectroscopy) and Diana Borda (batch-method experiments) contributed to the experimental study. WW and PMP characterized the MPs. EEE performed the data analysis, prepared the figures and tables as well as wrote the manuscript (original draft). AR supported the writing of the manuscript by reviews, rephrasing, and editing. AH and

WW gave valuable feedbacks and recommendations to the manuscript. EEE and AR revised the manuscript after peer-review.

Manuscript 2

AR and AH conceptualized the study. EEE designed and carried out the study under the supervisions of AR and AH. Characterization of the particles was performed by EEE (DLS, FT-IR) and PMP (SEM, Mastersizer). EEE performed the data analysis, prepared the figures and tables as well as wrote the manuscript (original draft). AR and AH supported the writing of the manuscript by reviews, rephrasing, and editing. WW gave valuable feedback and recommendations to the manuscript. EEE and AR revised the manuscript after peer-review.

Manuscript 3

EEE conceptualized the study, with contributions from AR and AH. EEE and Amelie Vogel (AV) designed the study. In addition to the toxicity assessment in Figure 4, EEE preformed all analytical experiments of this study, including characterization of contents of the MPs by microwave-assisted extractions, TD-GC-MS, Pyrolysis-GC-MS and in-vitro digestions. Roman Schmidt (RS) and EEE performed the ICP-MS measurements. AV and Antje Begert (AB) performed the Cell culture, viability, and PCR experiments. Data analysis and preparation of tables/figures were performed by EEE (GC- and ICP-MS data of in-vitro digestion, Pyrolysis-GC-MS data of polymer signatures, TD-GC-MS data of additive characterization, and AOP screening of leachates) and AV (viability and CYP 1A1 induction of the MPs). EEE and AV wrote the manuscript. AR and AH supervised the study. AR and AH, and WW supported the writing of the manuscript by reviews, rephrasing, and editing. WW also gave valuable feedback to the manuscript.

6.3. MANUSCRIPT 1

A Comparative Investigation of the Sorption of Polycyclic Aromatic Hydrocarbons to Various Polydisperse Micro- and Nanoplastics using a Novel Third-Phase Partition Method

Emeka Ephraim Emecheta[1,2], Diana Borda Borda[1], Patrizia Marie Pfohl[3], Wendel Wohlleben[3], Christoph Hutzler[1], Andrea Haase[1*], Alexander Roloff[1*]

Corresponding authors:

Alexander Roloff, alexander.roloff@bfr.bund.de

Andrea Haase, andrea.haase@bfr.bund.de

Abstract Art

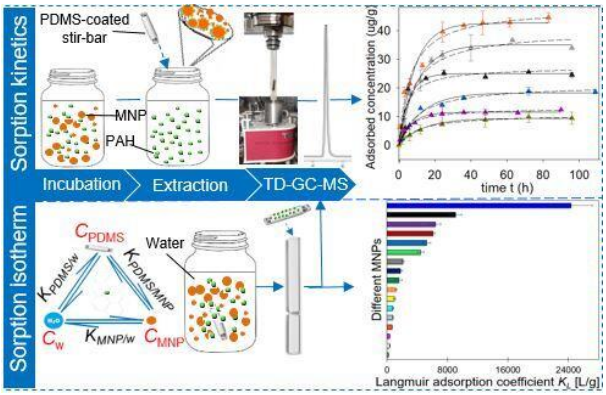

ABSTRACT

Evidence for direct adverse effects of micro- and nanoplastic particles (MNPs) on human health is scarce, but it has been hypothesized that MNPs act as carriers for environmental pollutants such as polycyclic aromatic hydrocarbons (PAHs). Many studies have already investigated the sorption of PAHs to microplastics, typically using the batch-equilibrium method. Here we established a novel third-phase partition (TPP) method utilizing thermo-extractable polydimethylsiloxane-coated stir-bars as re-usable passive samplers to compare the sorption of PAHs to 17 different MNPs. This method facilitates the quantification of MNP-sorbed pollutants, including those with poor water-solubility without requiring laborious filtration and solvent-extraction steps. Using benzo[*a*]pyrene (B[*a*]P) as a representative PAH, sorption kinetics and isotherms for MNPs were evaluated. B[*a*]P sorption was generally strong but

differed by over two-orders of magnitude, clustering according to polymer types in the order of polyamides > polyethylenes ≫ Tire Rubber > polyurethanes > polymethyl methacrylate. B[*a*]P sorption was diminished for photo-aged MNPs. Within given polymer types, properties including particle size, polarity/hydrophobicity and chain mobility notably influenced B[*a*]P sorption. When comparing different PAHs, their sorption to selected MNPs increased over five-orders of magnitude with hydrophobicity: anthracene < B[*a*]P < dibenzo[*a,l*]pyrene. Our data is an important contribution to the understanding of the sorption behaviors of MNPs. The novel TPP-method represents a universally-applicable approach for the reliable evaluation of sorption characteristics of contaminants and MNPs, and can be easily adapted to desorption studies.

Keywords: sorption isotherms, sorption kinetics, microplastics, nanoplastics, PAHs, passive sampling, polymer aging

1. INTRODUCTION

Over the last decades, the demand for plastics has continued to rise with global production reaching 368 million tonnes in 2019 [1]. As a result of mainly mismanaged waste, plastic pollution has similarly grown and became a global health and environmental concern. Microplastics are either intentionally manufactured [2] or result from the fragmentation of bulk plastics into small-scale plastic debris [3-5]. Microplastics are ubiquitous [6]. They can be found in deep seas, soil, air and also in house dust [7-10]. Hence, ingestion and inhalation are plausible exposure routes to microplastics for humans [11-13]. Specific adverse effects have not yet been confirmed but uncertainties remain. For instance, the degradation of microplastics may yield even smaller nanoscaled particles that might differ with respect to uptake and biodistribution [14]. Clearly, the risk assessment of micro- and nanoplastic particles (MNPs) is hampered by analytical challenges and insufficient data [15]. In particular, the ability of MNPs to efficiently sorb hydrophobic toxic environmental pollutants may represent a potential hazard via a transport that may or may not be significant compared to the transport via other vectors such as natural black carbon [16-19]. Environmental pollutants such as polycyclic aromatic hydrocarbons (PAHs) [20-22], heavy metals [23-26], polychlorinated biphenyls (PCBs) [27-29] and polybrominated diphenyl ethers (PBDEs) [30, 31] have been demonstrated to bind to microplastics. However, most studies used research-engineered polymer particles with a low degree of polydispersity, spherical shape and artificially high sorbate concentrations [20, 21, 32-35] that are unlikely to be found in the environment.

In contrast, we investigated MNPs with polydisperse and environmentally relevant size distributions. MNPs were obtained by cryomilling of polymer granules and separating the resulting particles applying different sieve sizes. In one specific case we also extracted particles from the fine fractions which are routinely removed from polymer powders being commercialized. These particles, though not present in the commercial products, feature realistic polymer compositions, polydispersities and non-spherical shapes and are representative of secondary microplastics from environmental fragmentation, but lack aging. Therefore, selected MNPs were aged artificially using standardized methods and included in this investigation.

During their intended use in applications such as additive manufacturing (AM, better known as 3D-printing) [36-38], the polymer powders lose their particle shape by the selective local sintering with a laser (SLS process), but still intermediate materials may enter the environment via spills during production, transport or disposal and subsequently may sorb environmental pollutants (**Figure 1a**). Understanding the sorption behaviors of these materials and persistent organic pollutants (POPs) may be helpful to establish grouping criteria for MNPs that could be useful in the context of plastics regulation [39] (**Figure 1b**), that is, if the fluxes of organic chemicals leaching from natural particles do not overwhelm the leaching from plastics, as it may be the case in many habitats [40].

Here we investigated the sorption kinetics and isotherms of MNPs being relevant for AM (polyamides – PAs, and thermoplastic polyurethanes – TPUs) and PAHs at environmentally relevant sorbate concentrations (ng/L). For comparison, recycled truck tire tread, polyurethanes (PUs) for outdoor applications as well as polydisperse (low-density) polyethylene ((LD)PE) and polymethyl methacrylate (PMMA) were also evaluated (**Table S1**). Benzo[*a*]pyrene (B[*a*]P), a widespread environmental pollutant [41-43] and a mutagenic [44] and genotoxic [45] potential human carcinogen [46], was selected as a lead substance. In addition, anthracene (Anth) [47] and dibenzo[*a,l*]pyrene (DB[*a,l*]P) were included as structurally related PAHs with variable toxicities [47].

Sorption isotherms of particles are commonly investigated according to the batch-equilibrium method [30, 32, 35, 48]. This involves isothermal incubation of the target sorbent in a (typically aqueous) solution of the sorbate, followed by separation of the particles via filtration or centrifugation and quantification of the remaining solubilized sorbate fraction at equilibrium. Challenges arise from the incomplete removal of submicron-/nano-sized and/or low-density particles through filtration or centrifugation. Furthermore, hydrophobic sorbates with low water-solubilities might result in equilibrium concentrations too small to be accurately measured.

Moreover, the batch-equilibrium method is time-consuming, labor-intensive and requires large amounts of organic solvent for sample extraction.

To bypass these challenges, we developed a novel and sensitive third-phase partition (TPP) method for evaluating the sorption of PAHs by polydisperse real-life-type MNPs (**Figure 1c**). The TPP method covers PAH concentrations in the ng/L-range that can be adequately measured [49-51] with minimal sample preparation and without the consumption of significant amounts of organic solvents. Thus, error-prone filtration, centrifugation and extraction steps are omitted, increasing the reliability of results. Inspired by previous work on passive sampling [52], the method relies on partitioning of PAHs in a three-phase system comprised of water, MNPs and a re-usable polydimethylsiloxane (PDMS) coated stir-bar. Quantification of the PAHs partitioned to the PDMS-phase is achieved via automated online-coupled thermal desorption gas chromatography mass spectrometry (TD-GC-MS), from which sorption isotherms can be derived (see method section and the supplementary information (SI) for details). Compared to the batch-equilibrium method and to previously reported TPP approaches [20, 28, 52, 53], the need for laborious solvent extraction is eliminated and the analysis time is significantly reduced. Importantly, this approach also allows to study very hydrophobic pollutants featuring strong binding to MNPs, such as e.g. DB[*a,l*]P, if their PDMS-water partition coefficients ($K_{PDMS,w}$) are known. To the best of our knowledge, this is the first study utilizing a passive sampling approach combined with automated online-coupled TD-GC-MS to evaluate the sorption kinetics and isotherms of microplastics that also contain submicron fractions.

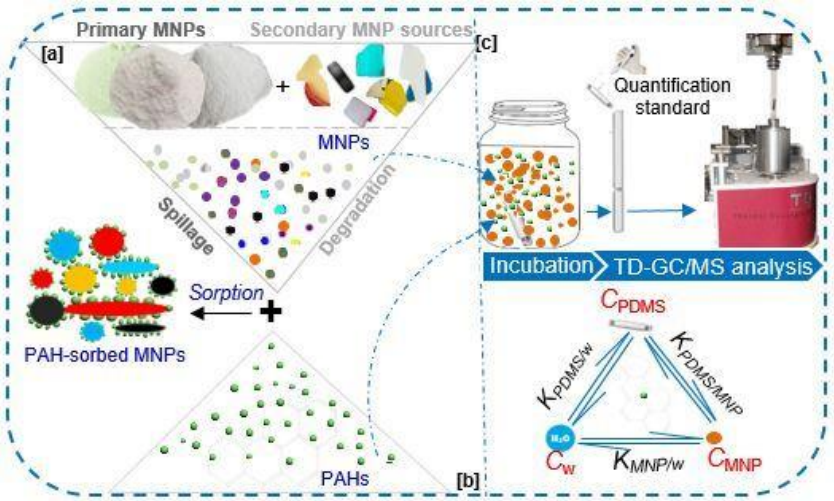

Figure 1. *[a] Release and exposure sources of micro- and nanoplastic particles (MNPs). [b] Released MNPs may sorb ubiquitous pollutants such as polycyclic aromatic hydrocarbons (PAHs). [c] Novel third phase partition (TPP) method reported in this work for evaluating sorption of PAHs to polydisperse real-life-type MNPs.*

2. MATERIALS AND METHODS

2.1. CHEMICALS

B[*a*]P (purity ≥ 99.5 %) was purchased as a standard solution in cyclohexane from Sigma-Aldrich (Steinheim, Germany). Benzo[*a*]pyrene-d_{12} (B[*a*]P-d_{12}), Anth, anthracene-d_{10} (Anth-d_{10}), DB[*a,l*]P and dibenzo[*a,i*]pyrene (DB[*a,i*]P) were purchased as analytical standards in acetonitrile (purity ≥ 98.5 %) from Neochema (Bodenheim, Germany). Acetonitrile, hexane, methanol and dichloromethane in analytical grade were purchased from Merck (Darmstadt, Germany) and used as solvents. Nitrogen and helium of ≥ 99.999 % purity were purchased from Linde (Pullach, Germany). Ultrapure water from a Millipore Q-POD® dispenser connected to a Millipore milli-Q system (Darmstadt, Germany) was used.

2.2. MATERIALS AND DEVICES

250 mL amber glass vials (Duran group, Mainz, Germany) were utilized for all experiments. Transparent 250 mL vials were wrapped with aluminum foil where amber vials were unavailable. All vials were sealed air-tight during experiments with polytetrafluoroethylene (PTFE)-coated screw caps (Duran group, Mainz, Germany). Cimarec multipoint stirring plates (ThermoFisher Scientific, Germany) operating at 600 rotations per minute (rpm) were used for all incubations inside a light-protected and temperature-controlled chamber (Binder GmbH, Tuttlingen, Germany) which was operated at 21°C. Temperature stability inside the incubation chamber was characterized by continuous temperature monitoring using a temperature sensor which was placed inside the 250 mL glass vial and connected to an automated data logger system (ELPRO, Schorndorf, Germany). All filtrations were performed with 1.2 µm GF/C Whatman glass microfiber filters. PDMS-coated magnetic stir-bars (Twister®) with a PDMS film thickness of 0.5 mm, lengths of 10 and 20 mm, PDMS phase volumes of 24 and 126 µL and densities of 965 kg/m^3 were purchased from Gerstel (Mühlheim, Germany) and used as passive samplers. Thermal desorption (TD) glass tubes (length: 60 mm), transport adapters as well as the thermal conditioner 2 (TC 2) connected to an AUX 163 controller were all from Gerstel. Kimtech Science white precision wipes (Kimberly-Clark Professional, Germany) and Solingen tweezers (Kiehl Solingen, Germany) were used for handling the PDMS-coated stir-bars in order to avoid contamination. Details about quality control, cleaning and conditioning procedures for the PDMS-coated stir-bars and glassware are detailed in **Section S1** in the SI.

2.3. MICRO- AND NANOPLASTIC PARTICLES INVESTIGATED IN THIS STUDY

Sorption kinetics and isotherms for PAHs and MNPs were investigated for 17 different particle types. Names and median size distributions of MNPs are listed in **Table 1**. (LD)PE particles were obtained from LyondellBasell (Ludwigshafen, Germany) and Cospheric (Santa Barbara, USA). PMMA particles were purchased from Polysciences (Warrington, USA), and micronized Tire Rubber was obtained from MRH (Mülsener Rohstoff- und Handelsgesellschaft mbH, Mülsen, Germany). Non-crosslinked TPU (elastomer), crosslinked PU (duromer) and PA particles were supplied by BASF SE (Frankfurt, Germany). The MNPs were obtained by cryo-miFlling of polymer granules and sieving the resulting material with different sieve sizes to obtain smaller particle fractions. The particles are generally polydisperse; therefore, additional sieving was introduced to produce a cut-off for the particles within a given distribution. Details about the particles and their physio-chemical properties are presented in **Table S1**. Melting temperatures (T_m) and glass transition temperatures (T_g) were obtained using differential scanning calorimetry (DSC) on a Q2000 instrument (TA Instruments, Eschborn, Germany). Samples were heated from -50 to 300°C at 10°C/min. Brunauer-Emmett-Teller (BET) surface areas of the particles were analyzed with a micromeritics instrument (Norcross, USA). Nitrogen adsorption isotherms were obtained at a temperature of 77 K, an equilibrium time of 5 s and a saturation pressure of 770 mmHg. Sample masses of 0.17–2.5 g were used. Particle size distributions of MNPs were measured via laser diffraction utilizing a Malvern Mastersizer 3000 (Kassel, Germany). Particles were measured in 10 replicates in dispersions containing water plus two drops of Nekanil 910 as a surfactant to stabilize the dispersions (BASF SE, Ludwigshafen, Germany). The average size distributions of the particles are presented as 10^{th} (D×10), 50^{th} (D×50) and 90^{th} percentiles (D×90).

To evaluate the effect of MNP aging on PAH sorption, three selected MNPs (LDPE_215, PA-6_42 and Tire Rubber) were artificially aged via ultraviolet (UV) light exposure. About 0.5–0.7 g of the sample were placed inside a petri dish to form a monolayer powder. The samples were aged without mixing for 1000 and 2000 h inside a Suntest XLS+ chamber (Atlas, Illinois, USA) according to the DIN EN ISO 4892 guideline (Sunlight spectrum, UV intensity of 60 W/m^2 in the wavelength range of 300–400 nm, Black Standard Temperature of 65°C, no rain events) [54]. Fourier transform infrared spectroscopy (FTIR, ThermoFisher IS50 FT-IR spectrometer with a diamond Attenuated Total Reflectance (ATR) accessory (IS50-ATR)) was utilized to evaluate the aged MNPs and their non-aged versions for changes in their functional groups. As described in earlier studies [55], the FT-IR spectra were recorded in the region of 4000–400 cm^{-1} with 32 scans at a resolution of 4 cm^{-1}.

Name	Dx10 (µm)	Dx50 (µm)	Dx90 (µm)
LDPE_215	96.2	215.0	380.0
LDPE_84	19.1	84.0	188.0
PE_0.6	0.3	0.6	1.9
TPU_ester_arom	142.0	254.0	418.0
TPU_ester_alip	143.0	262.0	440.0
TPU_ether_arom	128.0	246.0	413.0
TPU_ether_alip	152.0	267.0	442.0
TPU_melt_arom	272.0	864.0	1560.0
PU_foam	33.1	92.8	211.0
PU_arom_1C	82.8	200.0	354.0
PU_arom_2C	77.2	201.0	368.0
PA-6_7	2.3	6.9	13.5
PA-6_42	13.7	42.2	75.3
PA-12_44	34.4	44.3	57.0
PMMA_0.3	0.3	0.3	0.4
PMMA_6	2.2	6.2	11.6
Tire Rubber	61.7	130.0	233.0

Dx10, Dx50 and Dx90 are 10 th, 50 th and 90 th percentile size distribution, respectively.

Table 1. *MNPs and their size distributions investigated in this study. Detailed physical-chemical properties of all MNPs are summarized in Table S1.*

2.4. QUANTIFICATION OF POLYCYCLIC AROMATIC HYDROCARBONS VIA ONLINE-COUPLED THERMAL DESORPTION GAS CHROMATOGRAPHY MASS SPECTROMETRY

TD-GC-MS is a three-stage process involving TD of substances loaded onto the PDMS-coated stir-bar, followed by separation of the desorbed substances via GC and MS detection. TD was performed with a thermal desorption unit (TDU 2; Gerstel) connected to a 6890 series gas chromatograph that was coupled with a 5975 series mass selective detector (both Agilent, Waldbronn, Germany). The TDU was operated with a helium gas flow of 290 mL/min and a temperature program of 60°C for 0.1 min, then increased to 290°C at 40°C /min and then held for 5 min. During TD, which was performed in split mode with a split ratio of 35:1 in the TDU, analytes were cryo-focused with liquid nitrogen at -100°C in the cold injection system (CIS 4; Gerstel). The CIS, which was directly connected to the TDU, was equipped with a liner packed with deactivated glass wool (Gerstel). The CIS was operated in split mode of 35:1 ratio (combined split of 1:1225 from TDU and CIS), a split flow of 35 mL/min and an inlet pressure

of 149 kPa. After desorption and cryo-focusing, the CIS inlet was rapidly heated to 320°C at 12°C/s and then held for 5 min. The TDU to CIS transfer temperature was 350°C.

The GC was equipped with a DB-EUPAH column of 20 m length, an inner diameter of 0.18 mm and film thickness of 0.14 µm (J & W Scientific, Folsom, U.S.). Helium gas was used as a carrier gas at a constant flow of 1.0 mL/min. The GC oven was operated with a temperature program starting at 60°C for 0.5 min, followed by heating to 180°C at 15°C /min and finally to 320°C at 12°C/min, where the temperature was held for 8 min.

The temperatures of the quadrupole, ion source, and MS transfer line were 150, 230 and 320°C, respectively. The MS detector was operated in combined selective ion monitoring (SIM) and scan mode with a scan rate of 15.99/s. A range of 50–500 m/z was monitored for data acquisition. During SIM data acquisition, two ions were monitored for each analyte: 178 and 176 m/z for Anth, 188 and 187 m/z for Anth-d_{10}, 252 and 250 m/z for B[*a*]P, 264 and 260 for B[*a*]P-d_{12}, 302 and 300 m/z for DB[*a,l*]P, and 302 and 300 m/z for DB[*a,i*]P as quantifier and qualifier ions, respectively. Each ion was monitored with a dwell time of 10 milliseconds.

Quantification of target PAHs were achieved via calibration. A known amount of PAHs and 100 ng of the correlated internal standards (Anth-d_{10} for Anth, B[*a*]P-d_{12} for B[*a*]P and DB[*a,i*]P for DB[*a,l*]P) were spiked on the surface of pre-cleaned PDMS-coated stir-bars. The stir-bars were held with tweezers until the solvent was fully evaporated and then introduced into TD glass tubes and capped with a transport adapter. The calibrations were linear for concentration ranges of 2.5–500 ng for Anth and B[*a*]P and 5–250 ng for DB[*a,l*]P. Exemplary calibration curves are shown in **Figure S1**. In between every sample and calibration run, the system was purged by performing a blank run (**Section S1**).

2.5. DETERMINATION OF KINETIC AND SORPTION ISOTHERMS OF PAHS AND MNPS IN WATER VIA A THIRD-PHASE PARTITION METHOD

Before measuring sorption isotherms of the MNPs, kinetics experiments were firstly conducted to establish the time required for the PAHs to partition to the PDMS (**Section S2**). Secondly, to establish the time required for the PAHs to reach equilibrium with the MNPs in water, kinetics experiments were performed as described in **Section S2** with slight modifications. 5 mg of target MNPs were incubated in 240 mL water spiked with 1 µg/L target PAH in replicate vials. A regular magnetic stir-bar (without PDMS coating) was utilized to stir the dispersions at 600 rpm inside the incubation chamber at 21°C. At specified time intervals up to 132 h, duplicate

vials were withdrawn from the stirring plate and the sample mixture was filtered to separate the MNPs from the aqueous phase. The filtrate was analyzed via stir-bar sorptive extraction (SBSE). To account for losses due to filtration and possible photo-degradation of PAHs, control samples containing 1 µg/L of the target PAH but no MNPs were incubated under identical conditions. For each time point, recovery-corrected concentrations of the control samples were used as initial concentration, C_0 (µg/L). After incubation, the PDMS-coated stir-bars were analyzed via TD-GC-MS. The concentration of PAH sorbed to the MNPs at each time point, $C_{MNP,t}$ (µg/kg), was calculated as follows:

$$C_{MNP,t} = \frac{C_0 - C_{w,t}}{M_{MNP}} V_w \quad \text{(Equation 1)},$$

where $C_{w,t}$ *(µg/L),* V_w (L) and M_{MNP} (kg) are the aqueous PAH concentration at time point *t*, the volume of water and the mass of MNPs, respectively.

Sorption isotherms characterizing the sorption behavior of PAHs and MNPs were obtained using the TPP method (see **Figure 1c**). PAHs will distribute between water, MNPs and the PDMS coating on the stir-bar according to their respective partition coefficients *K* (L/kg). These are defined as the PAH concentration ratios between two phases at chemical equilibrium, e.g.

$$K_{MNP/w} = \frac{C_{MNP}}{C_w} \quad \text{(Equation 2)}.$$

The PAH concentration in the aqueous phase, C_w (µg/L), was derived from

$$C_w = \frac{C_{PDMS}}{K_{PDMS/w}} \quad \text{(Equation 3)},$$

where C_{PDMS} (µg/kg) is the measured concentrations of PAHs in the PDMS phase, and $K_{PDMS/w}$ (L/kg) are the partition coefficients of PAHs for PDMS and water, which was determined experimentally (Anth, B[*a*]P) or calculated (DB[*a*,*l*]P, see **Section S2** for details).

The PAH concentration in the MNP phase, C_{MNP} (µg/kg), was calculated from the total amount of PAH in the system m_{total} (µg), C_w, C_{PDMS} and other characteristic parameters of the system assuming mass balance.

$$C_{MNP} = \frac{1}{M_{MNP}} \left(m_{total} - \frac{C_{PDMS}}{K_{PDMS/w}} V_W - C_{PDMS} M_{PDMS} \right) \quad \text{(Equation 4)},$$

where M_{PDMS} (kg), M_{MNP} (kg) and V_w (L) are the mass of the PDMS phase, the mass of MNPs and the volume of water in the system, respectively.

All isotherms were derived from 5–7 different PAH equilibrium concentrations in duplicate or triplicate to obtain between 10–21 data points per individual isotherm. Sorption experiments

were performed in 240 mL water using stir-bars with 24 µL PDMS-phase volume. Details are summarized in **Table S2**. In brief, aqueous mixtures containing MNPs, PAHs of various initial concentrations and a PDMS-coated stir-bar were incubated by continuous stirring until chemical equilibrium of all components of the system was approached. Organic solvents from PAH stock solutions were kept ≤ 0.03% (*v*/*v*), which has previously been demonstrated to yield negligible co-solvent effects [52, 56, 57]. The stir-bar was removed from the vial with clean tweezers, briefly washed with distilled water and gently wiped with a lint-free tissue to remove water and polymer residues. Subsequently, the stir-bar was spiked with 100 ng of the appropriate internal standards, held with tweezers until the solvent was fully evaporated, inserted into TD glass tubes and finally analyzed via TD-GC-MS for C_{PDMS}.

Quality control measures undertaken to mitigate the loss of the PAH sorbate during incubation and control experiments to verify the conservation of PAH mass are outlined in **Section S1** and **S2**, respectively. The combined measurement uncertainties of $K_{MNP/w}$ determined via the TPP-method were calculated according to the international standard organization (ISO) Guide to the Expression of Uncertainty in Measurement (GUM) [58]. Additionally, the contribution of each component used to calculate of $K_{MNP/w}$ to the combined uncertainties was calculated (see **Section S6** for details).

2.6. DATA ANALYSIS

TD-GC-MS data were acquired and processed with MassHunter software (Agilent, versions B.06.00 and B.05.00). Microsoft Excel 2016 was used for additional data processing. Model fittings were performed by non-linear regression methods using SigmaPlot 14 software application (Systat Software Inc, USA) while two-tailed t-test analysis of the data was performed with GraphPad Prism 9 (GraphPad Software, USA).

Experimentally derived kinetics for the sorption of PAHs to MNPs (**Section S3**) were fitted by applying pseudo-first (**Equation 5**) and pseudo-second (**Equation 6**) order models, respectively [21, 32]:

$$C_{MNP,t} = q_e(1 - e^{-k_a t}) \quad \text{(Equation 5)},$$

$$C_{MNP,t} = \frac{q_e^2 k_b t}{(1 + k_b q_e t)} \quad \text{(Equation 6)},$$

where k_a (h^{-1}) and k_b (g μg^{-1} h^{-1}) are rate constants from both models while q_e is the calculated equilibrium sorption capacity.

The goodness of the model fittings was evaluated using the coefficient of determination (R^2) and chi-square (χ^2) parameters. Better fittings result in R^2 values approaching unity and smaller values for χ^2 (**Section S3**, **Table S3**).

Experimental sorption isotherm data were fitted to eight different isotherm models and compared for their goodness of fit and plausibility of parameters. Exemplary isotherm fittings and corresponding model-parameters for PAH sorption to PA-6_42 are shown in **Figure S4**. The Langmuir model (**Equation 7**) was found most suitable to compare the sorption of the PAHs to MNPs across the tested concentration ranges, and can be utilized to compare different sorbents by means of their Langmuir adsorption coefficients K_L (L/kg) and theoretical maximum monolayer adsorption capacities q_{max} (µg/kg) [59], where $K_L = \alpha_L * q_{max}$ (α_L (L/µg) is the Langmuir isotherm constant).

$$C_{MNP} = \frac{K_L * C_w}{1 + \alpha_L * C_w} \quad \text{(Equation 7)}.$$

We note that the Langmuir model assumes that PAHs bind to MNPs via monolayer surface adsorption, which will most likely not be the case for each of the investigated polymers. Rubbery polymers, in particular, will probably take up PAHs by true partitioning in addition to surface adsorption. Still, the Langmuir model allows to extract comparable (and concentration-independent) physico-chemical parameters for a wide range of MNPs and PAHs, which justified its use in this study.

3. RESULTS AND DISCUSSION

3.1. THE POLYMER TYPE MAINLY DETERMINES SORPTION OF BENZO[*A*]PYRENE TO MICRO- AND NANOPLASTIC PARTICLES

Initially, the kinetics and isotherms for partitioning of PAHs between water and PDMS in the passive samplers were determined (**Figure S2**, see **Section S2** for details). The slopes of the linear isotherms represent the partition coefficients $K_{PDMS/w}$, which are required to calculate PAH concentrations on MNPs (C_{MNP}) from measured concentrations in PDMS (C_{PDMS}) according to **Equation 4**. Values for log $K_{PDMS/w}$ were increasing from 4.05 ± 0.09 for Anth to 5.10 ± 0.10 for B[*a*]P. This is in line with values reported previously for the same polymer [60]. Due to the very low water solubility of DB[*a*,*l*]P, log $K_{PDMS/w}$ for this PAH was calculated to be 6.88 according to **Equation S2** [61], which correlates log $K_{PDMS/w}$ with the logarithmic octanol/water partition coefficient log $K_{o/w}$. Notably, the same correlation yielded a value for log $K_{PDMS/w}$ of 5.0 for B[*a*]P. This is in good agreement with the experiment, supporting the validity of **Equation S2** for substances with log $K_{o/w} > 4$.

First, kinetics experiments for PAH sorption to selected MNPs were conducted according to the batch-equilibrium method, revealing equilibration times of 48 h for the sorption of B[*a*]P, Anth and DB[*a*,*l*]P under the conditions applied (**Figure 2** and **Section S3**). Two of the most common kinetics models for sorption processes, the pseudo-first and pseudo-second-order models [62, 63], were both suitable to describe the observed sorption kinetics process, with no significant difference ($p < 0.01$) between them (see also **Figure S3** and **Table S3**). This further suggests that diffusion-driven mass transfer of the sorbate to the sorbent or sorption onto the active sites of the sorbent or both phenomena may be the rate-limiting steps of the sorption process [32, 64].

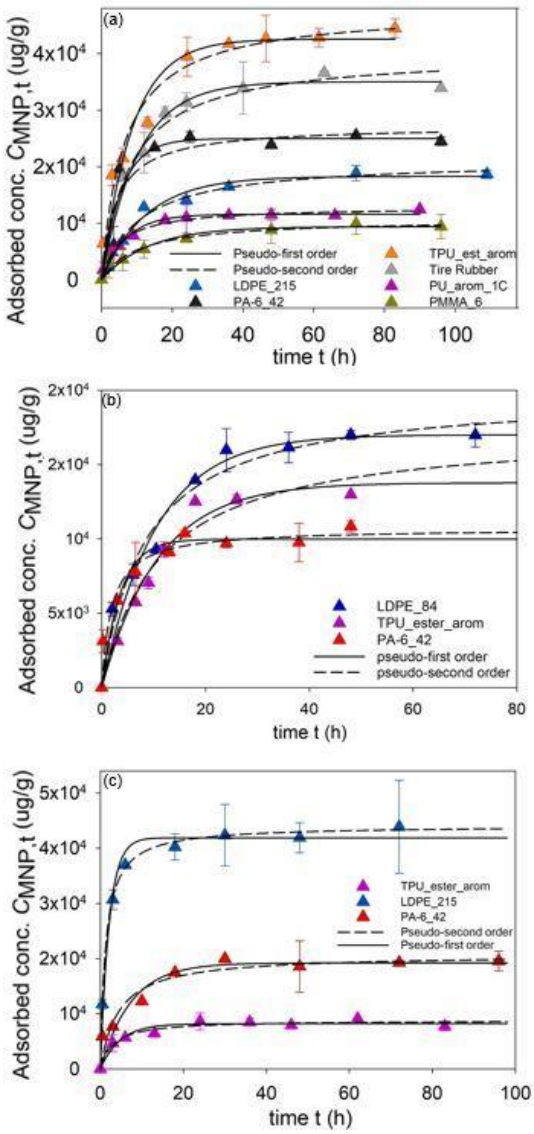

Figure 2. *Sorption kinetics of (a) B[a]P, (b) Anth and (c) DB[a,l]P and selected MNPs (n = 2 ± SD) fitted to pseudo-first and pseudo-second order kinetics models. See Table S3 for model parameters and calculated rate constants.*

We went on to compare the sorption isotherms of various MNPs utilizing B[*a*]P as a representative PAH sorbate. Sorption isotherms were obtained by means of the novel TPP method. Accordingly, MNPs were incubated together with a PDMS-coated stir-bar in aqueous solutions of varying initial B[*a*]P concentrations until equilibrium of the system was approached. C_{PDMS} was then determined via TD-GC-MS, which revealed C_{MNP} (**Equation 4**) and C_w (**Equation 3**). Plots of C_{MNP} as a function of C_w representing sorption isotherms were then fitted to the Langmuir model (**Figure 3a**, see **Section S4** for details). For Anth, B[*a*]P and selected MNPs, the sorption isotherms and corresponding Langmuir adsorption coefficients K_L acquired with the TPP-method were validated using the batch-equilibrium method (**Section S5**). This

confirmed the TPP-method presented herein as an easy, fast and reliable alternative for evaluating the sorption properties of organic pollutants and MNPs.

As illustrated in **Table 2**, K_L differed by more than two orders of magnitude for B[*a*]P, ranging from 150 L/g for PMMA_6 to 25000 L/g for PA-6_7. In addition, the values of the Langmuir separation factor R_L were < 1, suggesting a favorable and reversible sorption process for all investigated MNPs [65]. As shown in **Figure 3b**, K_L values for the different MNPs cluster according to the 'polymer type', decreasing in the order of PA-6 > PA-12 > (LD)PE ≫ Tire Rubber > (T)PUs > PMMA. This ranking suggests that the polymer type which governs the essential chemical and some physical characteristics of the MNPs is a key factor influencing the sorption of B[*a*]P. For example, the exceptionally high sorption of B[*a*]P by PA-6 MNPs is possibly related to the high water absorption capacity of this polymer (up to 9.5%) [66], which is significantly higher than for some of the other investigated materials (0.2–1.5% for PA-12, PE, and TPUs) [66, 67]. This could facilitate the transport of dissolved B[*a*]P to the bulk of the material.

In contrast, PA-12 MNPs yielded strong sorption of B[*a*]P despite this polymer's notably lower water absorption capacity [67]. However, PA-12 MNPs had a relatively high specific surface area (0.73 m^2/g, see **Table S1**), which may favor surface-pore adsorption typical for glassy polymers [68, 69]. Additionally, PA-12 is characterized by a reduced polarity due to longer alkyl chains and lower surface amide densities, which is reflected in higher water contact angles compared to PA-6 [67]. This may render the displacement of water molecules from potential sorption sites on this polymers' surface by B[*a*]P energetically more favorable.

Similarly, strong B[*a*]P sorption was observed for (LD)PE particles. (LD)PE is a rubbery polymer with a glass transition temperature T_g well below room temperature (**Table S1**) and consists of flexible amorphous regions [70], which facilitate the mobility of sorbates within the polymer network. Therefore, it is likely that the observed strong sorption is due to the migration of B[*a*]P into the bulk of the polymer (true partitioning) in addition to surface adsorption [71-73]. On the other hand, PMMA and PU_arom_1C, being glassy polymers at room temperature ($T_{g\,(PMMA)}$ = 41°C, $T_{g\,(PU\_arom\_2C)}$ = 31°C, **Table S1**), exhibited the lowest sorption of B[*a*]P compared to other polymers possibly due to their rigid and condensed structure [74, 75] resulting in slow diffusion that is typical for glassy polymers [76]. Further investigations may reveal the extent to which each individual property of the polymer types affects sorption, and to which extent adsorption to the surface and absorption to the bulk play a role for individual polymer types.

In general, K_L values for all investigated MNPs are well above 10^5 L/kg, which points to efficient sorption of B[*a*]P to the investigated polymer particles in aqueous systems.

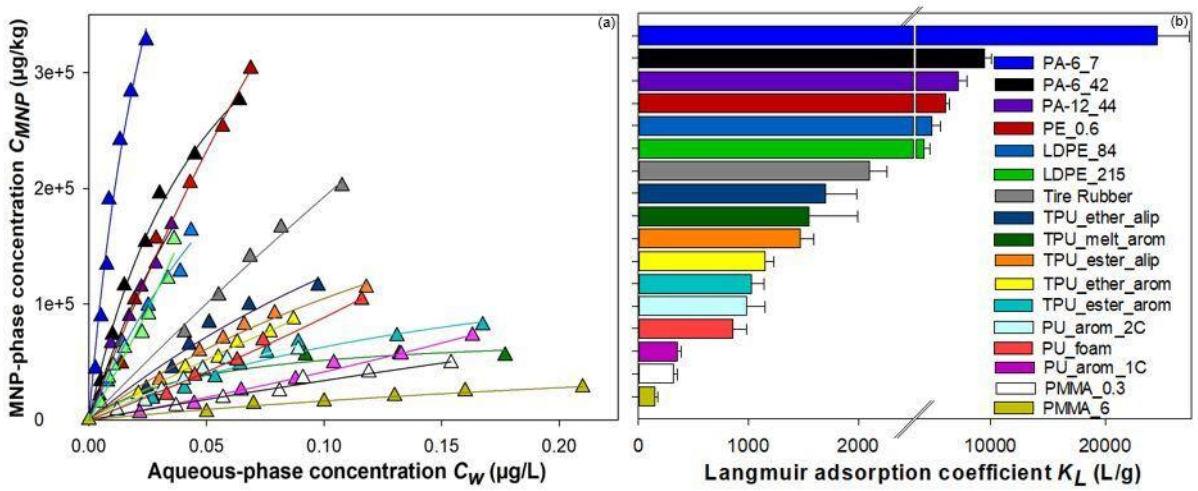

Figure 3. *(a): Experimental sorption isotherms for B[a]P and MNPs fitted to the Langmuir model. (b): Ranking of B[a]P sorption to MNPs based on the Langmuir adsorption coefficients K_L (error bars represent standard errors of K_L).*

3.2 ADDITIONAL FACTORS INFLUENCING SORPTION OF BENZO[*A*]PYRENE TO MICRO- AND NANOPLASTIC PARTICLES

For selected polymer types, the effects of different physico-chemical properties on B[a]P sorption to MNPs were investigated.

Initially, the effect of particle size and surface area was evaluated for PMMA, (LD)PE, and PA-6. As expected, a significant increase in K_L was observed with decreasing mean particle size (**Figure 4a**) for all studied sub-sets. The smaller PA-6_7 MNPs were characterized by a 2.7-fold higher K_L compared to the larger PA-6_42 variants. Regarding (LD)PE, a steady increase in K_L was observed with decreasing particle size. Similarly, K_L for PMMA_0.3 was over 2-fold higher compared to PMMA_6. However, the measured BET surface area for the same MNPs decreased by 10-fold from 15.0 to 1.6 m^2/g, suggesting a limited dependence of sorption on the surface area. The plot in **Figure 4b** indicates that the dependency of the adsorption coefficients of B[*a*]P on the measured BET surface area is particularly relevant within a given polymer type, but not so much between them. The size distribution of the MNPs usually determines the specific surface area and, thus, the number of available adsorption sites on the particle surface [77]. Consequently, smaller particles usually display increased surface adsorption capacities [21, 78]. However, the strength of individual binding interactions will be governed by chemical properties reflected by the polymer type, which could explain the

observed differences. In addition, it should be emphasized that the partitioning into the bulk will likely play a significant role for many of the studied MNPs, which will be reflected in a dependency on particle volume rather than surface area. However, since MNPs in this work are polydisperse, a reliable determination of average particle volumes is challenging.

Among the investigated TPUs, log K_L ranged from 6.01 to 6.23 (**Table 2**). These materials have very similar physical-chemical properties, including similar glass transition temperatures T_g below room temperature. Such polymers are typically classified as rubbery polymers and are characterized by larger free volume and higher flexibility and mobility of their molecular chains [73, 79]. However, the TPUs differ in their chain segments, which were polymerized from aromatic or aliphatic isocyanates in the 'hard' segment and included polyester or polyether chains in the 'soft' segment. TPUs with aliphatic (rather flexible) hard-segments were characterized with significantly higher K_L values compared to their aromatic (rather rigid) counterparts, potentially as a result of the better accessibility for PAHs to the polymer bulk provided by the more flexible polymer chains (**Figure 4c**). We also observed that polyether-based TPUs sorbed slightly higher concentrations of B[*a*]P than polyester-based TPUs, irrespective of the composition of their hard segments. Aliphatic residues and ether moieties are supposed to reduce the polarity of TPU MNPs, thereby favoring the displacement of water molecules from their hydration shells with B[*a*]P. In addition, the influence of the soft and hard segments of TPU polymers were compared. TPU_melt_arom is mainly composed of the polyester soft segment and contains only a minute fraction of the rather rigid aromatic hard segment, while TPU_ester_arom contains almost equal proportions of hard and soft segments. B[*a*]P sorption by TPU_melt_arom was slightly higher (ca. 1.5-fold) compared to TPU_ester_arom (**Figure 4c**). This is despite the larger median particle size of the former (**Table S1**). Notably, TPU_melt arom has a low T_m of 52°C as well as a low T_g of -49°C. This implies amorphous behavior and high mobility of the molecular chains which could have favored partitioning of B[*a*]P to the polymer bulk. Overall, the aforementioned effects are indicative of sorption significantly influenced by bulk partitioning of B[*a*]P.

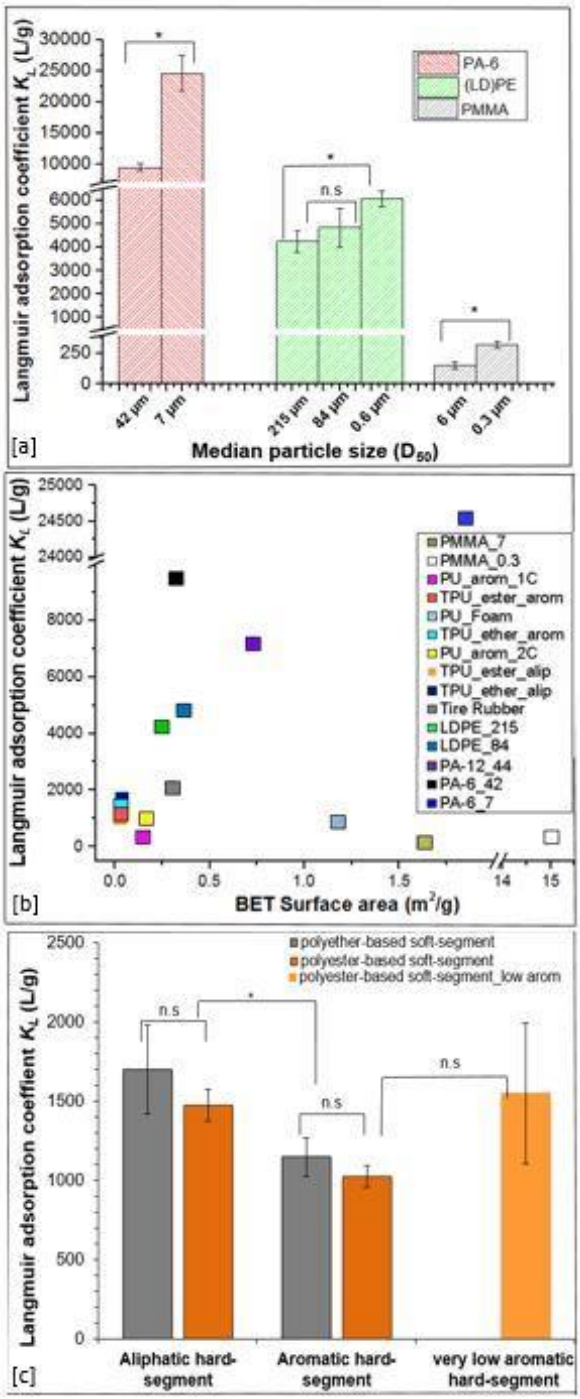

Figure 4. *[a] Effect of particle size on the Langmuir adsorption coefficient K_L for adsorption of B[a]P to MNPs of the same polymer type. [b] Plot of the dependency of K_L on BET surface areas of MNPs. [c] Effect of TPU's hard (aliphatic and aromatic) and soft (polyester or polyether) segments on K_L. Error bars represent the standard error of K_L (*: significantly different ($p < 0.05$), n.s. = not significant at *).*

3.3 PHOTO-AGING OF MICRO- AND NANOPLASTICS REDUCES SORPTION OF BENZO[*A*]PYRENE

Prolonged exposure of MNPs to environmental weathering conditions may cause changes in their (surface) properties during the lifecycle, which can alter the sorption behavior of organic pollutants. In this work, we investigated how accelerated photo-aging of selected MNPs affects the sorption of B[*a*]P. MNPs were exposed to prolonged UV light irradiation (60 W/m^2, 300–400 nm) for 1000–2000 h which is supposed to simulate roughly one year of exposure to sunlight in Europe. Photo-aging significantly reduced B[*a*]P sorption to LDPE_215 and Tire Rubber (**Figure 5a**/**b**). For example, the K_L for LDPE_215 MNPs decreased 3.2-fold after 1000 h of UV light exposure, which did not further change after 2000 h. Similarly, B[*a*]P sorption to Tire Rubber particles decreased by over 2.1-fold after 2000 h. No significant difference was observed for sorption of B[*a*]P to PA-6 after photo-aging, despite the notable effect that photo-aging had on the IR spectrum of these particles (**Figure 5c**). We hypothesize that photo-aging of PA-6 MNPs did not significantly affect their water absorption capacity and, therefore, their ability to transport dissolved B[*a*]P into the bulk.

The decreased K_L values for aged LDPE_215 and Tire Rubber might reflect alterations in surface functional groups, most likely caused by reactions with oxygen following photo-excitation. The incorporation of hydroxyl, carbonyl or carboxyl groups render the surface of the aged MNPs more hydrophilic. This was confirmed by FTIR-spectroscopy, were typical bands for oxygen-containing functional groups were observed at wavenumbers of 3600–3000 and 1780–1700 cm^{-1} [80, 81] after photo-aging (**Figure 5d**/**e**). Water will sorb more strongly to those altered interfaces and thereby diminish the sorption of B[*a*]P by making it energetically more difficult to displace molecules from the hydration shell and, subsequently, to partition into the bulk [82-84]. While we observed a decreased sorption of hydrophobic organic pollutants such as B[*a*]P after photo-aging of non-polar MNPs [68], hydrophilic pollutants may sorb more strongly [33, 85].

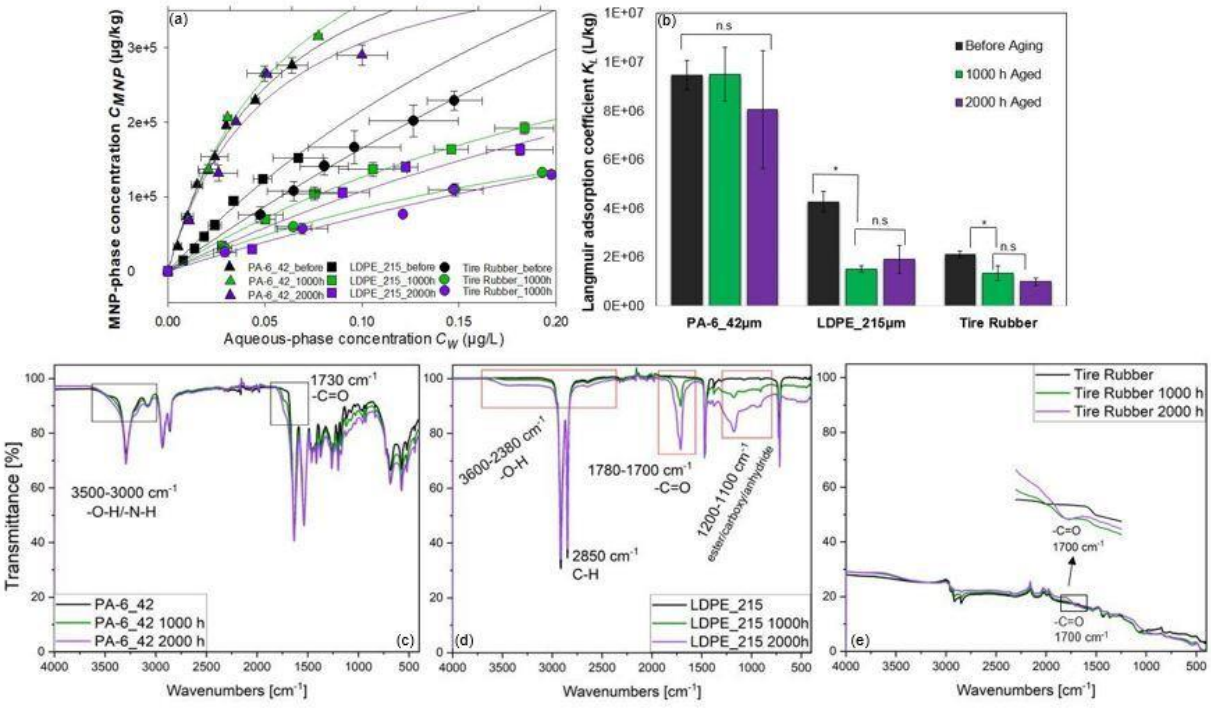

Figure 5. *(a) Sorption isotherms for B[a]P and UV-aged and non-aged MNPs (n = 2, mean ± standard deviation) fitted to the Langmuir model. (b) C orresponding Langmuir adsorption coefficients K_L (error bars represent the standard errors of K_L). FT-IR spectra of aged and non-aged (c) PA-6_42, (d) LDPE_215 and (e) Tire Rubber (*: significantly different ($p < 0.05$), n.s. = not significant at *).*

3.4 STRONGER SORPTION TO MICRO- AND NANOPLASTIC PARTICLES BY MORE HYDROPHOBIC POLYCYCLIC AROMATIC HYDROCARBONS

To investigate the influence that the sorbate imposes on K_L, additional sorption isotherms of the PAHs Anth and DB[*a,l*]P with selected MNPs were measured. Anth, B[*a*]P and DB[*a,l*]P consist of 3, 5 and 6 condensed aromatic rings, respectively. Each sorbate/sorbent pair was studied individually in order to avoid competitive sorption, which was indeed observed in multisorbate systems and was found to be most significant for the smallest PAH Anth (see **Section S6**). The obtained K_L for the three investigated MNPs PA-6_42, LDPE_215 and TPU_est_arom followed the order DB[*a,l*]P > B[*a*]P > Anth (**Figure 6a**) and differed by more than five orders of magnitude. For example, log K_L of sorption isotherms for TPU_est_arom increased from 3.9 (Anth) to 5.8 (B[*a*]P) and 7.8 (DB[*a,l*]P). The same trend was observed for LDPE_215 (log K_L for Anth: 4.5, B[*a*]P: 6.7, DB[*a,l*]P: 8.4) and PA-6_42 (5.0, 7.0, 9.0).

Hydrophobicity usually increases with log $K_{o/w}$ of the sorbate [86] and may also correlate with molecular weight, in particular within a substance class [61]. Therefore, sorption coefficients $K_{MNP/w}$ (derived from the slopes of the linear parts of the isotherms, see **Table S6**) were plotted as a function of reported log $K_{o/w}$ values [87, 88] and molecular weights of the PAHs (**Figure 6b–d**). A linear correlation was found for both variables, suggesting that hydrophobicity of the PAHs is indeed a key factor governing their sorption to micro- and nanoplastics. This highlights the potential for a reliable prediction of the sorption coefficients of MNPs and organic pollutants within compound classes, although further experiments are required to confirm this for sorbates other than PAHs.

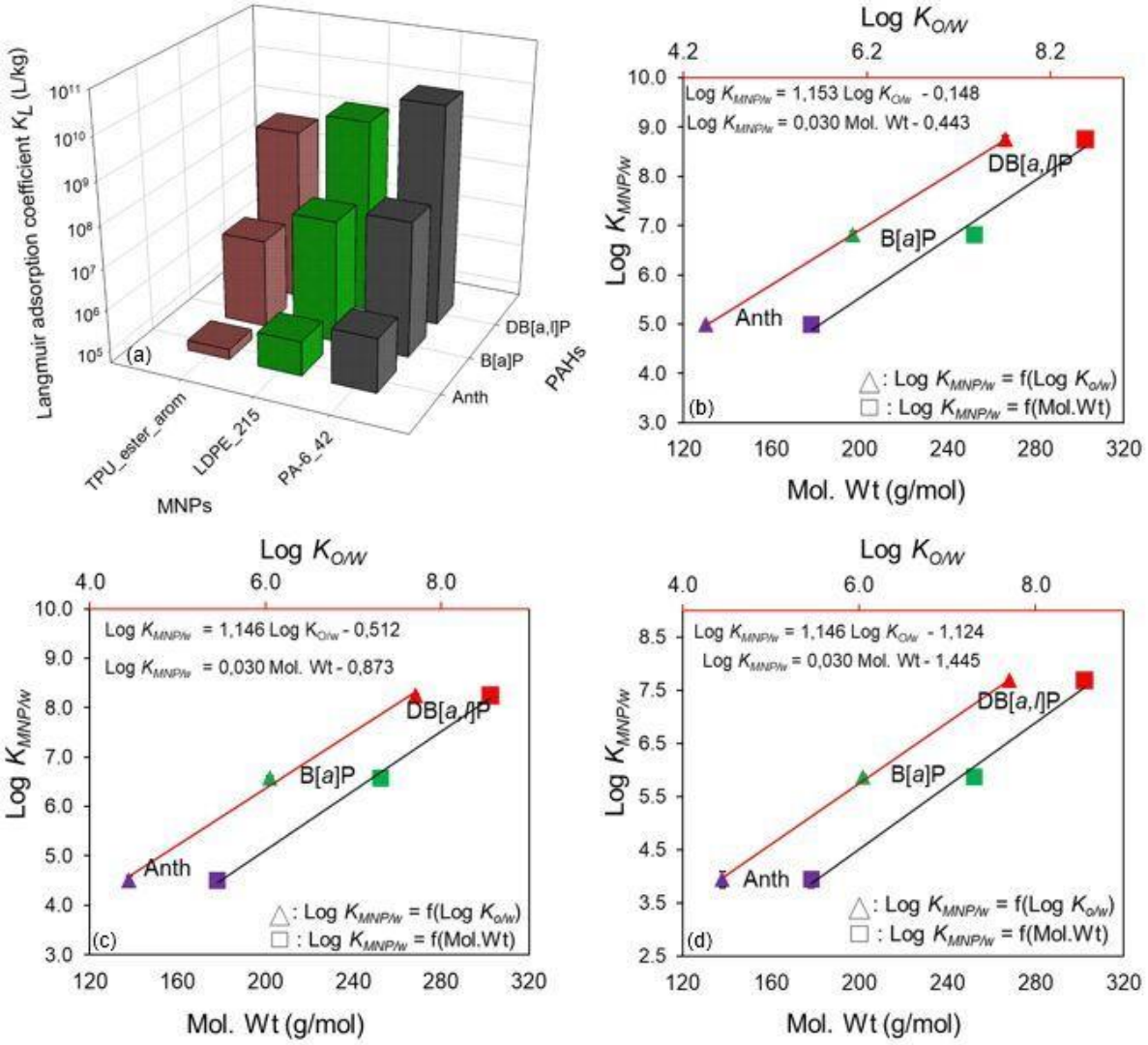

Figure 6. *(a) Comparison of the Langmuir adsorption coefficients K_L for selected MNPs and different PAHs (z-axis is expressed in Log-scale). Plots of log $K_{MNP/w}$ as functions of log $K_{o/w}$ and molecular weight (Mol. Wt) for (b) PA-6_42 (c) LDPE_215 and (d) TPU_ester_arom, illustrating the correlation of adsorption coefficients and hydrophobicity of the studied PAHs (log $K_{O/W}$: 4.45 (Anth), 6.05 (B[a]P), 7.71 (DB[a,l]P)*

		Langmuir model Parameters					Error functions	
Sorbate	**Sorbent**	**K_L ± S.E (L/kg)**	**Log K_L ± S.E**	**α_L (L/µg)**	**q_{max} (µg/g)**	**R_L**	**R^2**	**χ^2 [µg/g]**
DB[a,/]P	PA-6_42	1.0E+09 ± 8.5E+07	9.0 ± 0.1	5370.92	192	0.0001	0.991	1.6
	LDPE_215	2.3E+08 ± 2.5E+07	8.4 ± 0.1	1123.67	207	0.0004	0.988	5.3
	TPU_ester_arom	7.0E+07 ± 1.1E+07	7.8 ± 0.1	706.91	99	0.0007	0.973	2.1
Anth	PA-6_42	1.1E+05 ± 9.3E+03	5.0 ± 0.1	0.10	1136	0.003	0.989	4.5
	LDPE_215	3.1E+04 ± 2.7E+03	4.5 ± 0.1	0.15	205	0.011	0.992	5.8
	TPU_ester_arom	8.7E+03 ± 2.0E+03	3.9 ± 0.2	0.01	694	0.026	0.963	2.0
B[a]P	PA-6_7	2.5E+07 ± 2.8E+06	7.4 ± 0.1	31.0	788	0.009	0.981	15.7
	PA-6_42	9.5E+06 ± 7.9E+05	7.0 ± 0.1	16.84	562	0.016	0.990	14.3
	PA-6_42_1000h	9.5E+06 ± 1.1E+06	7.0 ± 0.1	16.81	565	0.01	0.990	4.3
	PA-6_42_2000h	8.0E+06 ± 2.4E+06	6.9 ± 0.3	16.44	489	0.01	0.927	28.9
	PA-12_44	7.2E+06 ± 7.1E+05	6.9 ± 0.1	17.66	408	0.015	0.989	7.1
	PE_0.6	6.1E+06 ± 3.4E+05	6.8 ± 0.1	5.81	1045	0.033	0.998	0.8
	LDPE_84	4.8E+06 ± 5.2E+05	6.7 ± 0.1	8.66	560	0.030	0.993	1.0
	LDPE_215	4.2E+06 ± 4.5E+05	6.6 ± 0.1	6.16	689	0.051	0.980	5.0
	LDPE_215_1000h	1.5E+06 ± 1.3E+05	6.2 ± 0.1	3.82	391	0.06	0.996	2.1
	LDPE_215_2000h	1.9E+06 ± 5.6E+05	6.3 ± 0.3	3.04	624	0.08	0.961	60.5
	Tire Rubber	2.1E+06 ± 1.6E+05	6.3 ± 0.1	0.88	2380	0.232	0.995	1.2
	Tire Rubber_1000h	1.3E+06 ± 4.8E+04	6.1 ± 0.03	4.02	330	0.06	0.999	0.2
	Tire Rubber_2000h	9.9E+05 ± 1.5E+05	6.0 ± 0.1	1.68	590	0.13	0.984	136.9
	TPU_ether_alip	1.7E+06 ± 2.8E+05	6.2 ± 0.1	3.72	457	0.082	0.968	8.6
	TPU_melt_arom	1.6E+06 ± 3.7E+05	6.2 ± 0.2	20.11	77	0.016	0.980	3.5
	TPU_ester_alip	1.5E+06 ± 1.0E+05	6.2 ± 0.1	4.05	364	0.076	0.992	0.9
	TPU_ether_arom	1.1E+06 ± 1.1E+05	6.1 ± 0.1	1.89	608	0.150	0.996	0.5
	TPU_ester_arom	1.0E+06 ± 4.5E+04	6.0 ± 0.04	6.16	166	0.039	0.972	4.5
	PU_arom_2C	9.9E+05 ± 1.7E+05	6.0 ± 0.1	4.32	229	0.072	0.953	4.1
	PU_foam	8.6E+05 ± 7.0E+04	5.9 ± 0.1	1.07	808	0.238	0.971	11.0
	PU_arom_1C	3.5E+05 ± 3.4E+04	5.5 ± 0.1	-1.38	-255	-0.320	0.984	2.5
	PMMA_0.3.	3.2E+05 ± 5.1E+04	5.5 ± 0.1	-1.33	-241	-0.250	0.989	1.0
	PMMA_6	1.5E+05 ± 2.4E+04	5.2 ± 0.1	-1.62	-91	-0.259	0.951	3.2

K_L, S.E, q_{max}, α_L and R_L are the Langmuir adsorption coefficient, the standard error of K_L, the theoritical maximum adsorption capacity, Langmuir adsorption constant and the dimensionless seperation factor respectively. R^2 and χ^2 are the coefficient of determination and chi-square errors respectively

Table 2. *Langmuir model parameters for the isotherms of the sorption of PAHs to MNPs.*

3.5 CONCLUSIONS

In this work we established a novel analytical TPP method that allows to reliably assess the sorption of contaminants to particulate sorbents in liquids with minimal sample preparation. The method compares favorably with the conventional batch-equilibrium approach, since it lacks laborious solvent extraction and avoids error-prone filtration and centrifugation steps. This makes the TPP method particularly suited to investigate sorption to nano-scale particles. We demonstrated its applicability for evaluating sorption properties of a broad range of MNPs and selected PAHs at environmentally relevant concentrations. The investigated MNPs represent polymer compositions, size distributions, polydispersities and non-spherical shapes that are considered to be realistic for secondary micro- and nanoplastics originating from environmental fragmentation. We demonstrate that the key factor influencing sorption of PAHs to MNPs was the polymer type. Notably, PA-6, a polymer used for example in AM applications, was observed to show exceptionally high sorption of B[*a*]P despite its relatively high polarity, which might be due to the transport of dissolved B[*a*]P to the bulk of the polymer. Furthermore, physico-chemical properties including particle size, polarity/hydrophobicity and polymer chain mobility were important factors modulating sorption within a given polymer type. Of note, photo-aging reduced PAH sorption, whereas more hydrophobic PAHs were sorbed more strongly.

Our data provide valuable insights toward the question whether MNPs play a significant role as carriers for POPs. Current evidence from laboratory studies, field studies and modeling suggest little relevance of MNPs as exposure sources for chemicals, mainly owing to other relevant sources of POP transfer to either marine biota [17] or humans [89]. If this is generally confirmed, our present methodology would not be needed as regulatory criterion in the context of risk assessment of plastics. However, understanding and modeling of the transport properties would still be relevant for targeting remediation activity in hot spots, where the pronounced sorption of contaminants such as PAHs to some plastics is to be considered, and exposure might be more relevant. Importantly, whereas microplastics have been discussed to potentially act as sinks for certain chemicals [90] based on their inertness and inability to enter cells, contaminated sub-micron (nanoplastic) particles may behave completely different. For example, the uptake of some nanoplastics across body barriers and into cells was recently demonstrated [91-93].

In a follow-up study we plan to investigate the *desorption* of MNP-bound pollutants in relevant media for human exposure. Understanding desorption properties constitutes the next puzzle piece towards risk assessment of MNPs, which hinges on the effective contribution of MNPs

to overall POP exposure. Furthermore, we are exploring the possibility to use the sorption characteristics as a grouping criterion for MNPs.

ABBREVIATIONS

Anth: anthracene

ATR: attenuated total reflectance

B[a]P: benzo[*a*]pyrene

B[*a*]P-d_{12}: benzo[*a*]pyrene-d_{12}

BET: Brunauer-Emmett-Teller

CIS: cold injection system

C_{MNP} : concentration of PAHs in the MNP phase

C_{PDMS}: concentration of PAHs in the PDMS phase

C_W: concentration of PAHs in the aqueous phase

DB[*a*,*l*]P: dibenzo[*a*,*l*]pyrene

DB[*a*,*i*]P: dibenzo[*a*,*i*]pyrene

DSC: differential scanning calorimetry

FTIR: Fourier transform infrared

ISO: International Organization for Standardization

K: partition coefficients

K_L: Langmuir adsorption coefficient

$K_{MNP/w}$: MNP/water sorption coefficient for PAHs

$K_{PDMS/w}$: PDMS/water partition coefficient for PAHs

$K_{o/w}$: octanol/water partition coefficient

(LD)PE: (low-density) polyethylene

M_{MNP}: mass of MNPs

MNPs: micro- and nanoplastic particles

Mol. Wt: molecular weight

M_{PDMS}: mass of PDMS

m_{total}: total mass of PAH in the system

n.s.: not significant

p: probability

PA: polyamide

PA-6: polyamide 6

PAHs: polycyclic aromatic hydrocarbons

PBDEs: polybrominated diphenyl ethers

PCBs: polychlorinated biphenyls

PDMS: polydimethylsiloxane

PMMA: polymethyl methacrylate

POPs: persistent organic pollutants

PU: polyurethane

R^2: coefficient of determination

SBSE: stir-bar sorptive extraction

SIM: selective ion monitoring

SLS: selective local sintering

TC: thermal conditioner

TD-GC-MS: thermal desorption gas chromatography mass spectrometry

TDU: thermal desorption unit

T_g: glass transition temperature

T_m: melting temperature

TPP: third-phase partition

TPUs: thermoplastic polyurethanes

UV: ultraviolet

V_w: volume of water

χ^2: Chi-square errors

DECLARATIONS

AVAILABILITY OF DATA AND MATERIALS

Supplementary Information is available in the online version of this article.

COMPETING INTERESTS

The authors declare no competing financial interest. W.W. and P.M.P. are employees of BASF SE, a company producing and marketing polymers, including some of those investigated in this study.

FUNDING

This work was funded by the BMBF (German Federal Ministry of Education and Research) within the InnoMat.Life project (funding no: 03XP0216X).

AUTHORS' CONTRIBUTIONS

A.R. and C.H. conceptualized the study, with contributions from A.H. The experiments for this study were carried out by E.E.E., with contributions from P.M.P. (MNP aging and FT-IR spectroscopy) and D.B.B. (batch-method experiments). W.W. and P.M.P. characterized the MNPs. E.E.E. and A.R. wrote the manuscript with contributions from A.H., C.H., W.W. and P.M.P. The study was supervised by A.R. and A.H.

ACKNOWLEDGEMENTS

This study was supported by the German Federal Institute for Risk Assessment (BfR). We thank Svetlana Kruschinski and Karsten Schön for their excellent technical assistance with TD-GC-MS measurements.

AUTHOR DETAILS

[1]German Federal Institute for Risk Assessment, Department of Chemical and Product Safety, Berlin, Germany.
[2]University of Bayreuth, Bayreuth Center for Ecology and Environmental Research (BayCEER), Bayreuth, Germany.
[3]BASF SE, Carl-Bosch-Str. 38, 67056 Ludwigshafen, Germany.

ETHICS APPROVAL AND CONSENT TO PARTICIPATE

Not applicable.

CONSENT FOR PUBLICATION

All authors read and approved the final version of the manuscript.

REFERENCES

1. PlasticsEurope, *Plastics – the Facts 2020: An analysis of European plastics production, demand and waste data*. 2020: Brussels, Belgium.
2. Environment, A.F.W., *Intentionally added microplastics in products. Final report.* October 2017: London, United Kingdom.
3. Alfaro-Nunez, A., et al., *Microplastic pollution in seawater and marine organisms across the Tropical Eastern Pacific and Galapagos.* Sci Rep, 2021. **11**(1): p. 6424.
4. Kelly, A., et al., *Microplastic contamination in east Antarctic sea ice.* Mar Pollut Bull, 2020. **154**: p. 111130.
5. Tamminga, M. and E.K. Fischer, *Microplastics in a deep, dimictic lake of the North German Plain with special regard to vertical distribution patterns.* Environ Pollut, 2020. **267**: p. 115507.

6. Lim, X., *Microplastics are everywhere - but are they harmful?* Nature, 2021. **593**(7857): p. 22-25.
7. Guzzetti, E., et al., *Microplastic in marine organism: Environmental and toxicological effects.* Environ Toxicol Pharmacol, 2018. **64**: p. 164-171.
8. Jamieson, A.J., et al., *Microplastics and synthetic particles ingested by deep-sea amphipods in six of the deepest marine ecosystems on Earth.* R Soc Open Sci, 2019. **6**(2): p. 180667.
9. Zhang, J., L. Wang, and K. Kannan, *Microplastics in house dust from 12 countries and associated human exposure.* Environ Int, 2020. **134**: p. 105314.
10. Barrett, J., et al., *Microplastic Pollution in Deep-Sea Sediments From the Great Australian Bight.* Frontiers in Marine Science, 2020. **7**.
11. Senathirajah, K., et al., *Estimation of the mass of microplastics ingested - A pivotal first step towards human health risk assessment.* J Hazard Mater, 2021. **404**(Pt B): p. 124004.
12. Cox, K.D., et al., *Human Consumption of Microplastics.* Environ Sci Technol, 2019. **53**(12): p. 7068-7074.
13. Leslie, H.A., et al., *Discovery and quantification of plastic particle pollution in human blood.* Environ Int, 2022. **163**: p. 107199.
14. Gigault, J., et al., *Nanoplastics are neither microplastics nor engineered nanoparticles.* Nat Nanotechnol, 2021. **16**(5): p. 501-507.
15. Koelmans, A.A., et al., *Microplastics in freshwaters and drinking water: Critical review and assessment of data quality.* Water Res, 2019. **155**: p. 410-422.
16. Herzke, D., et al., *Negligible Impact of Ingested Microplastics on Tissue Concentrations of Persistent Organic Pollutants in Northern Fulmars off Coastal Norway.* Environ Sci Technol, 2016. **50**(4): p. 1924-33.
17. Koelmans, A.A., et al., *Microplastic as a Vector for Chemicals in the Aquatic Environment: Critical Review and Model-Supported Reinterpretation of Empirical Studies.* Environ Sci Technol, 2016. **50**(7): p. 3315-26.
18. Gouin, T., *Addressing the importance of microplastic particles as vectors for long-range transport of chemical contaminants: perspective in relation to prioritizing research and regulatory actions.* Microplastics and Nanoplastics, 2021. **1**(1).
19. Kinigopoulou, V., et al., *Microplastics as carriers of inorganic and organic contaminants in the environment: A review of recent progress.* Journal of Molecular Liquids, 2022. **350**.
20. Liu, L., R. Fokkink, and A.A. Koelmans, *Sorption of polycyclic aromatic hydrocarbons to polystyrene nanoplastic.* Environ Toxicol Chem, 2016. **35**(7): p. 1650-5.

21. Wang, W. and J. Wang, *Different partition of polycyclic aromatic hydrocarbon on environmental particulates in freshwater: Microplastics in comparison to natural sediment.* Ecotoxicol Environ Saf, 2018. **147**: p. 648-655.
22. Teuten, E.L., et al., *Potential for plastics to transport hydrophobic contaminants.* Environ Sci Technol, 2007. **41**(22): p. 7759-64.
23. Gao, L., et al., *Microplastics aged in various environmental media exhibited strong sorption to heavy metals in seawater.* Mar Pollut Bull, 2021. **169**: p. 112480.
24. Kedzierski, M., et al., *Threat of plastic ageing in marine environment. Adsorption/desorption of micropollutants.* Mar Pollut Bull, 2018. **127**: p. 684-694.
25. Turner, A. and L.A. Holmes, *Adsorption of trace metals by microplastic pellets in fresh water.* Environmental Chemistry, 2015. **12**(5).
26. Cao, Y., et al., *A critical review on the interactions of microplastics with heavy metals: Mechanism and their combined effect on organisms and humans.* Sci Total Environ, 2021. **788**: p. 147620.
27. Zhan, Z., et al., *Sorption of 3,3',4,4'-tetrachlorobiphenyl by microplastics: A case study of polypropylene.* Mar Pollut Bull, 2016. **110**(1): p. 559-563.
28. Velzeboer, I., C.J. Kwadijk, and A.A. Koelmans, *Strong sorption of PCBs to nanoplastics, microplastics, carbon nanotubes, and fullerenes.* Environ Sci Technol, 2014. **48**(9): p. 4869-76.
29. Syberg, K., et al., *Sorption of PCBs to environmental plastic pollution in the North Atlantic Ocean: Importance of size and polymer type.* Case Studies in Chemical and Environmental Engineering, 2020. **2**.
30. Xu, P., et al., *Sorption of polybrominated diphenyl ethers by microplastics.* Mar Pollut Bull, 2019. **145**: p. 260-269.
31. Wu, J., et al., *Effects of polymer aging on sorption of 2,2',4,4'-tetrabromodiphenyl ether by polystyrene microplastics.* Chemosphere, 2020. **253**: p. 126706.
32. Wang, W. and J. Wang, *Comparative evaluation of sorption kinetics and isotherms of pyrene onto microplastics.* Chemosphere, 2018. **193**: p. 567-573.
33. Liu, G., et al., *Sorption behavior and mechanism of hydrophilic organic chemicals to virgin and aged microplastics in freshwater and seawater.* Environ Pollut, 2019. **246**: p. 26-33.
34. Lee, H., W.J. Shim, and J.H. Kwon, *Sorption capacity of plastic debris for hydrophobic organic chemicals.* Sci Total Environ, 2014. **470-471**: p. 1545-52.
35. Bakir, A., S.J. Rowland, and R.C. Thompson, *Transport of persistent organic pollutants by microplastics in estuarine conditions.* Estuarine, Coastal and Shelf Science, 2014. **140**: p. 14-21.

36. Shahrubudin, N., T.C. Lee, and R. Ramlan, *An Overview on 3D Printing Technology: Technological, Materials, and Applications.* Procedia Manufacturing, 2019. **35**: p. 1286-1296.
37. Fan, D., et al., *Progressive 3D Printing Technology and Its Application in Medical Materials.* Front Pharmacol, 2020. **11**: p. 122.
38. Sigloch, H., et al., *3D Printing - Evaluating Particle Emissions of a 3D Printing Pen.* J Vis Exp, 2020(164).
39. (EU), C.R., *1245 of 2 September 2020 amending and correcting Regulation (EU) No 10/2011 on plastic materials and articles intended to come into contact with food* in *OJ L 288*. 2020. p. 1–17.
40. Koelmans, A.A., et al., *Risk assessment of microplastic particles.* Nature Reviews Materials, 2022. **7**(2): p. 138-152.
41. Mu, Q., et al., *Temperature effect on phase state and reactivity controls atmospheric multiphase chemistry and transport of PAHs.* Sci Adv, 2018. **4**(3): p. eaap7314.
42. Agrawal, S., A.P. Kaur, and K. Taneja, *A Comprehensive Review of Benzo Alpha Pyrene (B[A]P) Toxicology.* Research Journal of Pharmaceutical Biological and Chemical Sciences, 2018. **9**(4): p. 1049-1058.
43. Verma, N., et al., *Review on proteomic analyses of benzo[a]pyrene toxicity.* Proteomics, 2012. **12**(11): p. 1731-55.
44. EEC, *COUNCIL DIRECTIVE 67/548/EEC of 27 June 1967 on the approximation of laws, regulations andadministrative provisions relating to the classification, packaging and labelling of dangerous substances*. 1967. p. 1 - 357.
45. ECHA, *Guidance on information requirements and chemical safety assessment, Chapter R.8: Characterisation of dose [concentration]-response for human health*. 2008. p. 1 - 150.
46. EC, *Regulation (EC) No. 1272/2008 of the European Parlament and of the Council of 16 December 2008 on classification, labelling and packaging of substances and mixtures, amending and repealing Directives 67/548/EEC and 1999/45/EC, and amending Regulation.* Official Journal of the European Union, 2008(L 353-1-L 353/1355): p. .
47. Delistraty, D., *Toxic equivalency factor approach for risk assessment of polycyclic aromatic hydrocarbons.* Toxicological & Environmental Chemistry, 1997. **64**(1-4): p. 81-108.
48. Li, J., K. Zhang, and H. Zhang, *Adsorption of antibiotics on microplastics.* Environ Pollut, 2018. **237**: p. 460-467.

49. Rochman, C.M., et al., *Long-term field measurement of sorption of organic contaminants to five types of plastic pellets: implications for plastic marine debris.* Environ Sci Technol, 2013. **47**(3): p. 1646-54.
50. Gocht, T., O. Klemm, and P. Grathwohl, *Long-term atmospheric bulk deposition of polycyclic aromatic hydrocarbons (PAHs) in rural areas of Southern Germany.* Atmospheric Environment, 2007. **41**(6): p. 1315-1327.
51. Romagnoli, P., et al., *Indoor PAHs at schools, homes and offices in Rome, Italy.* Atmospheric Environment, 2014. **92**: p. 51-59.
52. Jonker, M.T.O. and A.A. Koelmans, *Polyoxymethylene solid phase extraction as a partitioning method for hydrophobic organic chemicals in sediment and soot.* Environmental Science & Technology, 2001. **35**(18): p. 3742-3748.
53. *OECD Guideline for the testing of chemicals: Adsorption - Desorption Using a Batch Equilibrium Method*. 2000.
54. ISO, D.E., *Plastics - Methods of exposure to laboratory light sources - Part 2: Xenon-arc lamps (ISO 4892-2:2013)*. 2013. p. 20.
55. Pfohl, P., et al., *Microplastic extraction protocols can impact the polymer structure.* Microplastics and Nanoplastics, 2021. **1**(1).
56. Kah, M., et al., *Measuring and modeling adsorption of PAHs to carbon nanotubes over a six order of magnitude wide concentration range.* Environ Sci Technol, 2011. **45**(14): p. 6011-7.
57. Cornelissen, G., P.C.M. vanNoort, and H.A.J. Govers, *Desorption kinetics of chlorobenzenes, polycyclic aromatic hydrocarbons, and polychlorinated biphenyls: Sediment extraction with Tenax(R) and effects of contact time and solute hydrophobicity.* Environmental Toxicology and Chemistry, 1997. **16**(7): p. 1351-1357.
58. ISO/IEC, *Uncertainty of measurement — Part 3: Guide to the expression of uncertainty in measurement (GUM:1995)*. 2008. p. 120.
59. Harter, R.D. and D.E. Baker, *Applications and Misapplications of the Langmuir Equation to Soil Adsorption Phenomena.* Soil Science Society of America Journal, 1977. **41**(6): p. 1077-1080.
60. DiFilippo, E.L. and R.P. Eganhouse, *Assessment of PDMS-water partition coefficients: implications for passive environmental sampling of hydrophobic organic compounds.* Environ Sci Technol, 2010. **44**(18): p. 6917-25.
61. Grant, S., et al., *Experimental Solubility Approach to Determine PDMS-Water Partition Constants and PDMS Activity Coefficients.* Environ Sci Technol, 2016. **50**(6): p. 3047-54.

62. Ayawei, N., A.N. Ebelegi, and D. Wankasi, *Modelling and Interpretation of Adsorption Isotherms.* Journal of Chemistry, 2017. **2017**: p. 1-11.
63. Gupta, S. and A. Kumar, *Removal of nickel (II) from aqueous solution by biosorption on A. barbadensis Miller waste leaves powder.* Applied Water Science, 2019. **9**(4).
64. Fu, L., et al., *Adsorption behavior of organic pollutants on microplastics.* Ecotoxicol Environ Saf, 2021. **217**: p. 112207.
65. Belhachemi, M. and F. Addoun, *Comparative adsorption isotherms and modeling of methylene blue onto activated carbons.* Applied Water Science, 2011. **1**(3-4): p. 111-117.
66. www.ultramid.de, *Ultramid® (PA): Product Brochure*, BASF, 2013.
67. Extrand, C.W., *Water contact angles and hysteresis of polyamide surfaces.* J Colloid Interface Sci, 2002. **248**(1): p. 136-42.
68. Huffer, T. and T. Hofmann, *Sorption of non-polar organic compounds by micro-sized plastic particles in aqueous solution.* Environ Pollut, 2016. **214**: p. 194-201.
69. Wright, S.L., R.C. Thompson, and T.S. Galloway, *The physical impacts of microplastics on marine organisms: a review.* Environ Pollut, 2013. **178**: p. 483-92.
70. Agboola, O.D. and N.U. Benson, *Physisorption and Chemisorption Mechanisms Influencing Micro (Nano) Plastics-Organic Chemical Contaminants Interactions: A Review.* Frontiers in Environmental Science, 2021. **9**.
71. Pascall, M.A., et al., *Uptake of polychlorinated biphenyls (PCBs) from an aqueous medium by polyethylene, polyvinyl chloride, and polystyrene films.* J Agric Food Chem, 2005. **53**(1): p. 164-9.
72. Gilbert, D., et al., *Polymers as Reference Partitioning Phase: Polymer Calibration for an Analytically Operational Approach To Quantify Multimedia Phase Partitioning.* Anal Chem, 2016. **88**(11): p. 5818-26.
73. Lohmann, R., *Critical review of low-density polyethylene's partitioning and diffusion coefficients for trace organic contaminants and implications for its use as a passive sampler.* Environ Sci Technol, 2012. **46**(2): p. 606-18.
74. Guo, X., et al., *Sorption of four hydrophobic organic compounds by three chemically distinct polymers: role of chemical and physical composition.* Environ Sci Technol, 2012. **46**(13): p. 7252-9.
75. Liu, X., et al., *Microplastics as Both a Sink and a Source of Bisphenol A in the Marine Environment.* Environ Sci Technol, 2019. **53**(17): p. 10188-10196.
76. Mohamed Nor, N.H. and A.A. Koelmans, *Transfer of PCBs from Microplastics under Simulated Gut Fluid Conditions Is Biphasic and Reversible.* Environ Sci Technol, 2019. **53**(4): p. 1874-1883.

77. Holmes, L.A., A. Turner, and R.C. Thompson, *Adsorption of trace metals to plastic resin pellets in the marine environment.* Environ Pollut, 2012. **160**(1): p. 42-8.
78. Wang, J., et al., *Size effect of polystyrene microplastics on sorption of phenanthrene and nitrobenzene.* Ecotoxicol Environ Saf, 2019. **173**: p. 331-338.
79. Berens, A.R., *Analysis of transport behavior in polymer powders.* Journal of Membrane Science, 1978. **3**(2): p. 247-264.
80. Beachell, H.C. and I.L. Chang, *Photodegradation of urethane model systems.* Journal of Polymer Science Part A-1: Polymer Chemistry, 1972. **10**(2): p. 503-520.
81. Roger, A., D. Sallet, and J. Lemaire, *Photochemistry of aliphatic polyamides. 4. Mechanisms of photooxidation of polyamides 6, 11, and 12 at long wavelengths.* Macromolecules, 2002. **19**(3): p. 579-584.
82. Pan, B. and B. Xing, *Adsorption mechanisms of organic chemicals on carbon nanotubes.* Environ Sci Technol, 2008. **42**(24): p. 9005-13.
83. Ania, C.O., et al., *Effects of activated carbon properties on the adsorption of naphthalene from aqueous solutions.* Applied Surface Science, 2007. **253**(13): p. 5741-5746.
84. Huffer, T., A.K. Weniger, and T. Hofmann, *Sorption of organic compounds by aged polystyrene microplastic particles.* Environ Pollut, 2018. **236**: p. 218-225.
85. Holmes, L.A., A. Turner, and R.C. Thompson, *Interactions between trace metals and plastic production pellets under estuarine conditions.* Marine Chemistry, 2014. **167**: p. 25-32.
86. Zhao, L., et al., *Sorption of five organic compounds by polar and nonpolar microplastics.* Chemosphere, 2020. **257**: p. 127206.
87. National center for biotechnology information, *PubChem Compound Summary for CID 9119, Dibenzo[a,l]pyrene.* 2022.
88. Hansch, C.L., A; Hoekman, D, *Exploring QSAR: Hydrophobic, Electronic, and Steric Constants* C.L. Hansch, A; Hoekman, DH Editor. 1995 American Chemical Society.
89. Mohamed Nor, N.H., et al., *Lifetime Accumulation of Microplastic in Children and Adults.* Environ Sci Technol, 2021. **55**(8): p. 5084-5096.
90. Gouin, T., et al., *A thermodynamic approach for assessing the environmental exposure of chemicals absorbed to microplastic.* Environ Sci Technol, 2011. **45**(4): p. 1466-72.
91. Domenech, J., et al., *Interactions of polystyrene nanoplastics with in vitro models of the human intestinal barrier.* Arch Toxicol, 2020. **94**(9): p. 2997-3012.
92. Lehner, R., et al., *Emergence of Nanoplastic in the Environment and Possible Impact on Human Health.* Environ Sci Technol, 2019. **53**(4): p. 1748-1765.

93. Paul, M.B., et al., *Beyond microplastics - investigation on health impacts of submicron and nanoplastic particles after oral uptake in vitro.* Microplastics and Nanoplastics, 2022. **2**(1).

6.4. SUPPLEMENTARY INFORMATION FOR MANUSCRIPT 1

A Comparative Investigation of the Sorption of Polycyclic Aromatic Hydrocarbons to Various Polydisperse Micro- and Nanoplastics using a Novel Third-Phase Partition Method

Emeka Ephraim Emecheta[1,2], Diana Borda Borda[1], Patrizia Marie Pfohl[3], Wendel Wohlleben[3], Christoph Hutzler[1], Andrea Haase[1*], Alexander Roloff[1*]

[1]German Federal Institute for Risk Assessment, Department of Chemical and Product Safety, Berlin, Germany

[2]University of Bayreuth, Bayreuth Center for Ecology and Environmental Research (BayCEER), Bayreuth, Germany

[3]BASF SE, Carl-Bosch-Str. 38, 67056 Ludwigshafen, Germany

Corresponding authors:

Alexander Roloff, alexander.roloff@bfr.bund.de

Andrea Haase, andrea.haase@bfr.bund.de

Number of pages 30

Number of figures 7

Number of tables 7

Table of Content

SECTION S1: QUALITY CONTROL / QUALITY ASSURANCE

Desorption efficiencies of the PDMS-coated stir-bars were evaluated by performing a carryover test. Desorbed stir-bars were desorbed a second time after purging the TD-GC-MS system via a blank run with empty thermal desorption (TD) tubes. Desorption efficiencies were calculated as the peak areas of the respective PAH signal from the first desorption divided by the peak areas of the first and second desorption multiplied with 100. For Anth and B[*a*]P as well as their respective internal standards, the obtained desorption efficiencies were > 99%. DB[*a,l*]P and DB[*a,i*]P yielded similar desorption efficiency in the range of 85–90%.

To minimize variability and cross-contamination, the TD-GC-MS system was always cleaned by running pre-conditioned empty TD tubes in between every sample. The optimized TDU method utilized for the purging was 720°C/min; held for 5 min. The cold injection system (CIS) was operated in split mode at a high flow of 700 mL/min and a split ratio of 700:1 and held for 5 min at 320°C. The transfer temperature from TDU to CIS was 350°C. The GC oven was operated at a temperature of 60°C for 0.5 min; heated to 300°C at 40°C/min; and then to 320°C at 35°C/min and held for 5 min.

The PDMS-coated magnetic stir-bars were conditioned for re-use by drenching them in acetonitrile overnight or methylene chloride/methanol (50:50, *v*/*v*) for 2 h. Afterwards, the stir-bars were removed from the solvent and baked out under nitrogen flow (100 mL/min) at 300°C for at least 2 h in a TDU conditioner from Gerstel. Used TD glass

tubes were also heated out alongside the stir-bars to recondition them for re-use. After the TDU conditioner was turned off, the stir-bars and TD glass tubes were allowed to cool to at least 50°C, and stored inside a clean beaker that was covered with aluminum foil before further use.

Glass vials utilized for incubation were prepared for re-use by washing them in a dishwasher, followed by rinsing with milli-Q water and heating out in an oven at 150°C for 30 mins.

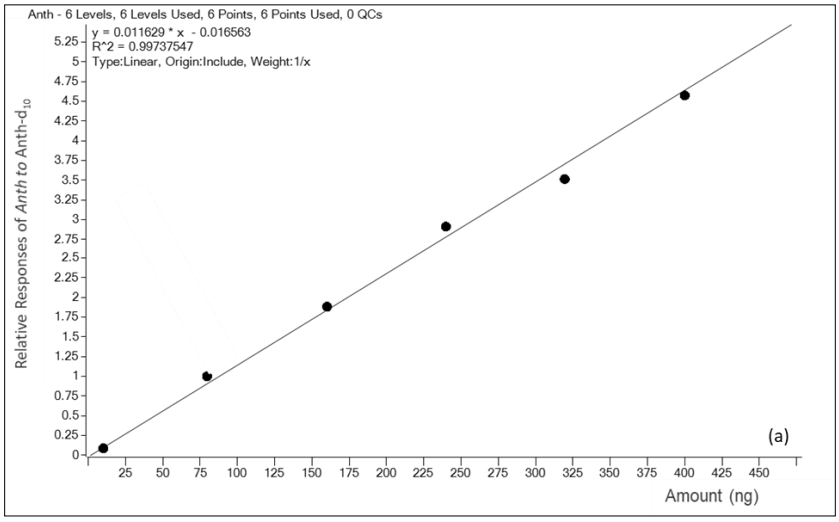

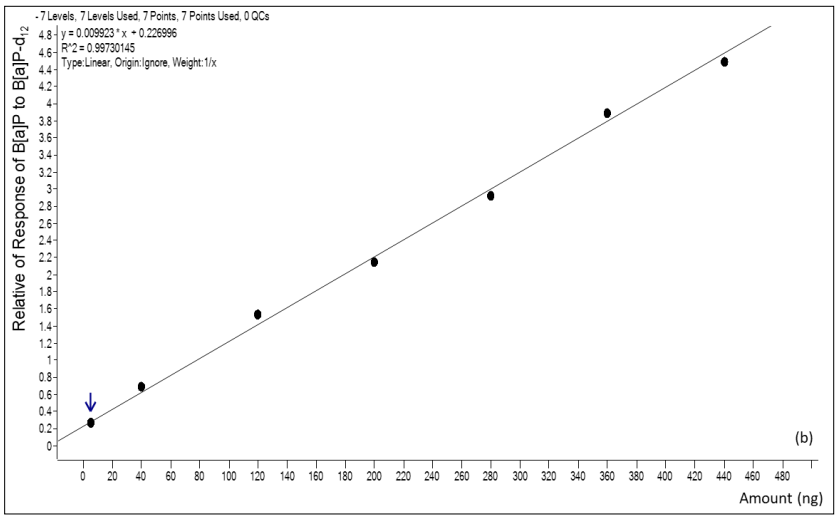

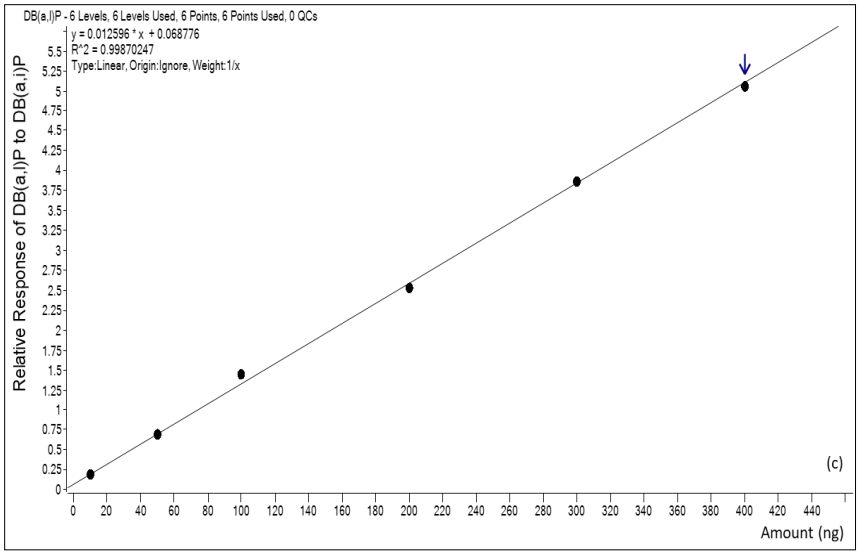

FIGURE S1: EXAMPLES OF TD-GC-MS CALIBRATION CURVES FOR PAHS: (a) Anth, (b) B[a]P and (c) DB[a,l]P. The limit of detection (LOD) was estimated with the MassHunter software as the concentration corresponding to 3 × signal to noise ratio. The limit of quantification (LOQ) was calculated as 3×LOD. The mean LOD (n=6) for Anth, B[a]P and DB[a,l]P was 0.5, 0.8 and 1.2 ng, respectively.

TABLE S1: PHYSICAL-CHEMICAL PROPERTIES OF POLYMERS INVESTIGATED IN THIS STUDY.

Name	Variants	Size Distribution (µm)			T_m (°C)	BET S.A (m^2/g)	T_g (°C)	Crystallinity	Density (g/ml)	Supplier
		Dx10	Dx50	Dx90						
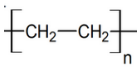 **LDPE**	LDPE_215	96,2	215,5	380,0	104	0,243	-27	Semicrystalline	0.917	BASF SE
	LDPE_84	19,1	84,4	188,0	104	0,326	-27	Semicrystalline	0.917	BASF SE
	PE_0.6	0,3	0,6	1,9	n.a.	n.a.	-80, -120 [b]	Semicrystalline	0.95 - 0.98	BASF SE
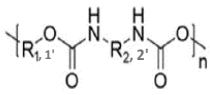 **TPUs**	ester_arom	142,0	254,0	418,0	169	0,027	-40	Amorphous	1.12	BASF SE
	ester_alip	143,0	262,0	440,0	159	0,035	-50	Amorphous	~ 1.2	BASF SE
	ether_arom	128,0	246,0	413,0	169	0,030	-37	Amorphous	-1.12	BASF SE
	ether_alip	152,0	267,0	442,0	159	0,033	-10	Amorphous	~ 1.2	BASF SE
	melt_arom	272,0	864,0	1560,0	52	n.a.	-49	Amorphous	1.12-1.2	BASF SE
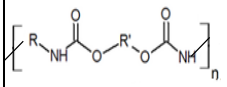 **PUs**	PU_foam	33,1	92,8	211,0	n.a.	1,183	n.a.	Amorphous	1 - 1.2	BASF SE
	arom_1C	82,8	200,0	354,0	n.a.	0,145	n.a.	Amorphous (cross-linked)	~ 1.2	BASF SE
	arom_2C	77,2	201,0	368,0	n.a.	0,159	31	Amorphous (cross-linked)	~ 1.2	BASF SE
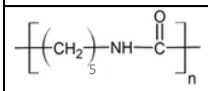 **PA-6**	PA-6_7	2,3	6,9	13,5	220	1,850	53	Semicrystalline	1 -1.2	BASF SE
	PA-6_42	13,7	42,2	75,3	220	0,366	53	Semicrystalline	1 -1.2	BASF SE
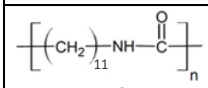 **PA-12**	PA-12_44	34,4	44,3	57,0	177	0,726	38	n.a.	n.a.	BASF SE
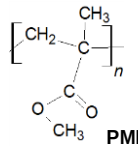 **PMMA**	PMMA_0.3	0,3	0,3	0,4	>160	15,000	44, 105[b]	n.a.	~ 1	BASF SE
	PMMA_6	2,2	6,2	11,6	>160	1,619	44, 105[b]	n.a.	~ 1	BASF SE
Tire Rubber 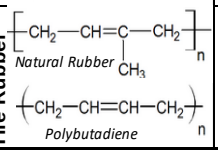 *Natural Rubber* *Polybutadiene*	Tire Rubber	61,7	130,0	233,0	n.a.	0,298	-60 °C		1,19	BASF SE

Data from suppliers unless otherwise stated.
[b] Chemical Retrieval on the Web (CROW), 2021, polymerdatabase.com.
T_m = Melting point temperature. T_g = Glass transition temperature. BET S.A = Brunauer–Emmett–Teller surface area.
n. a. = not available

TABLE S2: EXPERIMENTAL CONDITIONS FOR THE SORPTION ISOTHERM EXPERIMENTS OF PAHS AND MNPS. A VOLUME OF 240 ML WATER WAS USED FOR ALL SORPTION EXPERIMENTS.

Isotherm experiments	Conc. range (ng/L)	Mass of MNPs (mg)	Incubation time (h)	Isotherm points	Replicate per isotherm point
LDPE_215 + 3-PAH Mix	0 - 2500	5,0	104	7	3
PA-6_42 + 3-PAH Mix	0 - 3000	2,5	72	7	3
LDPE_215 + DB*[a,L]*P	0 - 2000	5,0	110	7	2
PA-6_42 + DB*[a,L]*P	0 - 2000	2,5	62	7	2
TPU_ester_arom + DB*[a,L]*P	0 - 2000	5,0	100	7	3
LDPE_215 + ANT	0 - 2000	5,0	62	7	3
PA-6_42 + ANT	0 - 3000	2,5	15	7	3
TPU_ester_arom + ANT	0 - 3000	10,0	34	5	3
LDPE_215 + B*[a]*P	0 - 3750	5,0	108	7	2
PA-6_42 + B*[a]*P	0 - 3750	2,5	36	7	3
TPU_ester_arom + B*[a]*P	0 - 4000	5,0	64	7	3
TPU_ester_alip + B*[a]*P	0 - 4000	5,0	66	7	3
TPU_ether_arom + B*[a]*P	0 - 4000	5,0	117	7	3
TPU_ether_alip + B*[a]*P	0 - 4000	5,0	66	6	2
TPU_ melt_ arom + B*[a]*P	0 - 4000	5,0	106	6	2
PU foam + B*[a]*P	0 - 3750	5,0	108	7	3
PU_arom_1C + B*[a]*P	0 - 3750	5,0	92	7	3
PMMA_0.3 + B*[a]*P	0 - 3750	8,0	92,5	7	3
PMMA_6 + B*[a]*P	0 - 3750	8,0	95,5	7	3
PU_arom_2C + B*[a]*P	0 - 3750	10,0	88	7	3
Tire Rubber + B*[a]*P	0 - 4500	3,0	72	6	3
PA-6_7 + B*[a]*P	0 - 3750	2,5	70	7	2
PA-12_44 + B*[a]*P	0 - 4000	5,0	86	6	3
LDPE_84 + B*[a]*P	0 - 3750	5,0	72	5	2
PE_0.6 + B*[a]*P	0 - 5000	4,0	72	6	2
Tire Rubber_1000h aged + B[a]P	0 - 5000	5,0	76	6	2
PA-6_42_1000h aged + B[a]P	0 - 5000	3,0	68	6	2
LDPE_215_1000h aged + B[a]P	0 - 5000	5,0	96	6	2
Tire Rubber_2000h aged + B[a]P	0 - 5000	5,0	68	5	3
PA-6_42_2000h aged + B[a]P	0 - 5000	3,0	72	5	3
LDPE_215_2000h aged + B[a]P	0 - 5000	5,0	76	5	3

SECTION S2: DETERMINATION OF SORPTION KINETICS AND PARTITION COEFFICIENTS OF PAHS FOR POLYDIMETHYLSILOXANE AND WATER ($K_{PDMS/W}$)

Prior to the kinetics experiments, the stability and recovery of the PAHs were determined via control experiments in 6 replicates. 1 µg/L PAHs were incubated in 240 mL water (without MNPs and PDMS) for 48 h, extracted and quantified following the conditions described below. Average recoveries of 95–120% for Anth, 80–130% for B[*a*]P and 64–67% for DB[*a,l*]P were obtained.

In order to obtain $K_{PDMS/w}$, the equilibrium time for the sorption of the PAHs onto the PDMS passive samplers was determined via kinetics experiments. For all experiments, PDMS-coated stir-bars of 24 µL PDMS phase volume were incubated in 240 mL water spiked with 1 µg/L of target PAHs. Multipoint stirring plates operating at 600 rotations per minute (rpm) were used for all incubations inside a temperature-controlled chamber which was operated at 21°C. The sorption kinetics of Anth and B[*a*]P were evaluated in duplicate. At specified time intervals, replicate vials were withdrawn from the stirring plate, the PDMS-coated stir-bars inside the vials were removed with clean tweezers and wiped gently on a lint-free tissue. 100 ng of the respective internal standard (Anth-d_{10} for Anth, B[*a*]P-d_{12} for B[*a*]P) were spiked on the surface of the PDMS-coated stir-bars, which were held with tweezers until the solvent was fully evaporated. The loaded stir bars were inserted inside pre-conditioned empty TD glass tubes, which were subsequently capped with transport adapters. The amount of PAHs sorbed to the passive samplers at each time point were quantified via TD-GC-MS as described in the method section of the manuscript.

As shown in **Figure S2a**, the experimentally determined sorption kinetics of the PAHs were fitted to the first-order one-compartment model using **Equation S1** [1]:

$$C_{PDMS}(t) = C_{W,O}\ \frac{k_1}{k_2}\ (1 - e^{-k_2 t}) \qquad \textbf{Equation S1},$$

where k_1 and k_2 are the uptake and release rate constants, respectively. $C_{PDMS}(t)$ (µg/kg) and $C_{w,0}$ (µg/L) are the sorbed analyte concentration at time t and the initial analyte concentration in the aqueous phase, respectively.

Using the release rate constants k_2 from the above equation, the time required to reach 90% of equilibrium t_{90} can be estimated by ln (10/k_2) [2]. This resulted in t_{90} values of 32 and 76 h for

Anth and B[a]P, respectively. Notably, the obtained equilibrium times are similar to the findings of Prieto et al. [3] who utilized similar PDMS-coated stir-bars. Thus, the values of $K_{PDMS/w}$ for Anth and B[*a*]P were determined after 66 and 136 h of incubation respectively, which were beyond the t_{90} equilibration time.

With knowledge of the equilibration time, $K_{PDMS/w}$ of the PAHs were determined for five concentration levels. Each concentration level was evaluated in duplicate. PDMS-coated stir-bars of 24 µL PDMS-phase volume were utilized for all $K_{PDMS/w}$ experiments. The samples were stirred on a stirring plate inside an incubation chamber until t_{90} was reached. Experiments were conducted at concentrations below the solubility limit of the respective PAHs but sufficiently high to quantify the aqueous phase concentration at t_{90} [4]. For Anth (water solubility: 44 µg/L) [5, 6], $K_{PDMS/w}$ was determined at different initial concentrations up to 1750 ng/L in 240 mL water. Regarding the more hydrophobic B[*a*]P (water solubility: 2–4 µg/L) [5, 6], initial concentrations up to 1700 ng/L in 3.5 L water were used. This ensured that up to two-thirds of the total amount of B[*a*]P in the system remained in the aqueous phase after 136 h of incubation, which was well beyond t_{90}. The concentration of PAHs that partitioned to the PDMS phase (C_{PDMS}) were quantified via TD-GC-MS whereas the PAH concentration remaining in the aqueous phase (C_w) was determined via a stir-bar sorptive extraction (SBSE) process [3, 7, 8]. Therefore, 100 ng of the respective internal standard was spike into the solution, which was subsequently extracted with a PDMS-coated stir-bar (126 µL PDMS phase volume) for 48 h. Following SBSE, the PAH-load on the PDMS-coated stir-bar was analyzed via TD-GC-MS.

Mass balance for the super-hydrophobic DB[*a,l*]P could not be achieved. This is presumably due to its extremely low water solubility, which can cause losses of analyte through precipitation and/or adsorption of significant fractions to surfaces. The log of $K_{PDMS/w}$ was calculated using a linear relation of log $K_{PDMS/w}$ and the logarithmic octanol/water partition coefficient log $K_{o/w}$ derived for super-hydrophobic (log $K_{o/w}$ > 4) pollutants according to **Equation S2** [9]:

$$K_{PDMS/w} = 1.16 \log K_{o/w} - 2.06 \qquad \textbf{Equation S2}.$$

Mass balance of Anth and B[*a*]P were successfully evaluated across the investigated concentration ranges by comparing the sum of PAHs extracted from the aqueous and PDMS phases with the initial amount of PAHs. This revealed a good recovery of 102 ± 10% and 92 ± 12% for Anth and B[*a*]P, respectively. $K_{PDMS/w}$ (L/kg) for Anth and B[*a*]P was subsequently calculated as the ratio of PAH concentrations partitioned onto the PDMS-coated stir-bar and water (**Equation S3**):

$$K_{PDMS/w} = \frac{C_{PDMS}}{C_w}$$ **Equation S3**,

where C_{PDMS} (µg/kg) and C_w (µg/L) are the concentrations of PAHs in the PDMS and water phases, respectively.

As shown in **Figure S2b**, the values for $K_{PDMS/w}$ for Anth and B[*a*]P were 11421 ± 2255 L/kg and 141244 ± 37444 L/kg respectively; or 4.05 ± 0.09, and 5.13 ± 0.10 in log scale for Anth and B[*a*]P, respectively. The PDMS-water partition coefficients determined herein for Anth and B[*a*]P were consistent with previous values as reviewed by DiFilippo et al [10].

It is noteworthy that to qualify as a third-phase polymer, it is favorable that sorption of POPs (PAHs) to the polymer, in this case the PDMS coating of the stir bar, occurs via 'true-partitioning' [11, 12]. True partitioning is often confirmed by (1) microscopy [12], (2) by a linear relationship between the partition coefficient $K_{\text{third-phase/water}}$ of the POP bewteen the third-phase polymer and water and $K_{o/w}$ [9], (3) by sorption kinetics following a first-order one-compartment model and (4) by linear sorption isotherms over a wide concentration range [11].

Mayer et al. [12] have demonstrated PAH partitioning into PDMS coatings. Notably, an important reason for adopting PDMS as a third-phase polymer in this study is the wide linear range of the dependency of $K_{\text{PDMS/w}}$ on $K_{o/w}$ for POPs (with a slope close to unity stretching up to log $K_{o/w}$ = 7.51 [12]), which compares favorably to other third-phase polymers such as polyoxymethylene (POM) [11]. The log $K_{o/w}$ of PAHs studied herein ranged from 4.45 to 7.71. Furthermore, the linearity of the sorption isotherms for partitioning to PDMS (**Figure S2b**) as well as a good fit of the first-order one-compartment model to the partitioning kinetics data (**Figure S2a**), together with the above-mentioned points informed our choice of PDMS as passive sampler in this study.

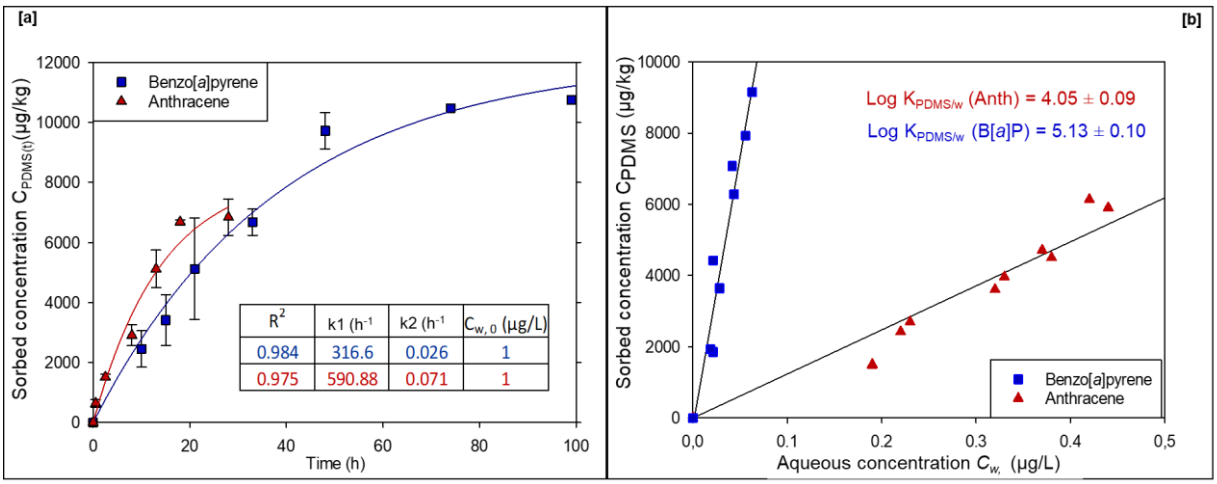

FIGURE S2: [A] FIRST-ORDER ONE-COMPARTMENT MODEL FIT OF EXPERIMENTAL DATA (N = 2, MEAN ± SD) OF PDMS SORPTION KINETICS AND [B] SORPTION ISOTHERMS AND CORRESPONDING PARTITION COEFFICIENTS (DERIVED FROM THE SLOPES OF LINEAR REGRESSIONS) OF PAHS AND PDMS IN WATER.

SECTION S3: DETERMINATION OF KINETICS OF PAH SORPTION ON MNPS IN WATER.

The parameters of pseudo-first and -second order models are shown in **Table S3**. As indicated, both models were compared utilizing their respective coefficients of determination (R^2) and the chi-square errors (χ^2) to evaluate their performance. For the three PAHs, R^2 of the pseudo-second order fittings were generally slightly better than for the pseudo-first order model (**Table S3**). However, a two-tailed student t-test analysis ($p \leq 0.05$) of the calculated $C_{MNP,t}$ from both models as well as their goodness of fit values (R^2, χ^2) indicated no significant difference. Also, the initial adsorption rates *h* which are equal to $k_b q_e^2$ show that the sorption of the PAHs onto the MNPs are relatively high in the beginning.

For B[*a*]P, pivot kinetics experiments were performed for three MNPs: PA-6, LDPE and Tire Rubber that were aged under UV-exposure for 1000 h, as well as variants of (T)PU MNPs. As shown in **Figure S3**, equilibrium was verified by a comparison of B[*a*]P adsorption onto the MNPs in the near-equilibrium region of the sorption processes using a fixed concentration of 1 µg/L. Equilibrium verification was indirectly obtained via a comparison of the PAH concentrations of the resulting aqueous phases following the separation of MNPs via filtration after incubation at two time intervals within the equilibrium region. There were no significant differences for various different MNPs, suggesting that sorption equilibrium has been reached.

TABLE S3: PARAMETERS OF PSEUDO-FIRST AND PSEUDO-SECOND ORDER KINETICS MODELS.

Adsorbate	Adsorbent	Pseudo-first order				Pseudo-second order			
		k_a (h^{-1})	q_e (µg/g)	R^2	χ^2 (µg/g)	k_b (g µg^{-1}h^{-1})	h (µg g^{-1}h^{-1})	R^2	χ^2 (µg/g)
Anth	PA-6_42µm	0,281	10,0	0,929	2,11	0,048	5,51	0,950	1,39
	LDPE_215µm	0,096	17,0	0,973	1,30	0,006	2,34	0,973	0,94
	TPU_ester_arom	0,092	13,8	0,981	0,31	0,005	1,56	0,963	0,63
B[a]P	PA-6_42µm	0,178	25,0	0,920	5,98	0,009	6,57	0,893	8,06
	LDPE_215µm	0,079	18,3	0,983	0,54	0,004	1,98	0,986	0,93
	PMMA_6µm	0,076	9,4	0,961	1,00	0,009	1,03	0,976	0,60
	Tire Rubber	0,098	35,01	0,988	1,50	0,003	4,92	0,977	3,81
	PU_arom_1C	0,145	11,59	0,985	0,77	0,015	2,5	0,992	0,35
	TPU_ester_arom	0,114	42,58	0,965	5,56	0,003	7,44	0,982	2,82
DB[*a,L*]P	PA-6_42µm	0,135	19,24	0,933	4,29	0,011	4,70	0,944	3,12
	LDPE_215µm	0,272	38,85	0,936	8,91	0,018	34,86	0,998	0,09
	TPU_ester_arom	0,211	8,22	0,945	0,54	0,037	2,93	0,960	0,34

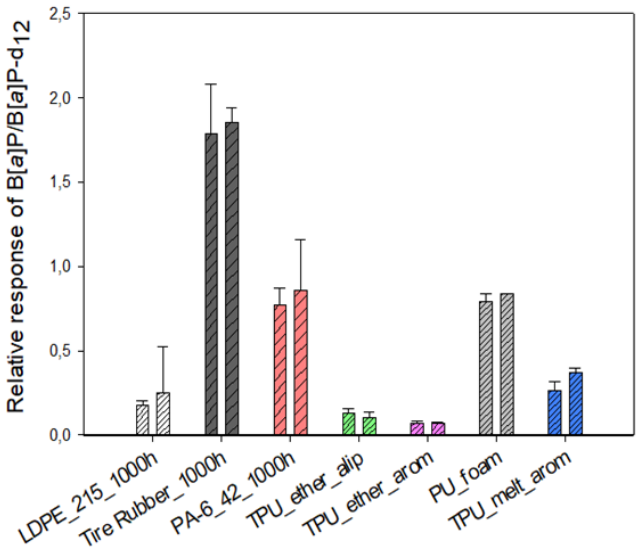

FIGURE S3: Verification of B[a]P sorption equilibrium for selected MNP variants (LDPE_215_1000h, PA-6_42_1000h and Tire Rubber_1000h MNPs were compared at 72 and 100 h, TPU_ether_alip and TPU_ether_arom MNPs were both evaluated at 62 and 106 h, TPU_melt_arom and PU_foam MNPs were assessed at 108 and 132 h, bars represent the average of duplicate measurement at the specified time intervals, error bars indicate ±SD).

SECTION S4: SORPTION ISOTHERMS AND MODEL FITTINGS.

In order to obtain some mechanistic insight into the sorption of PAHs onto MNPs, sorption isotherms were evaluated by applying eight different isotherm models (**Figure S4**). In addition to the parameter of the models, R^2 and χ^2 were utilized to compare the models. R^2 values close to 1 and low values of χ^2 indicate good fits. The parameters and error functions of the isotherm model fittings of B[*a*]P sorption to PA-6_42 MNPs are exemplified in **Table S4.**

If the isotherm is linear across the tested concentration range, it typically fits to the Henry model [13], a one-parameter model which describes the sorption behavior of the sorbent at low concentration of the sorbate (**Equation S4**). K_H (L/kg) is the Henry isotherm constant.

$$C_{MNP} = K_H C_w \qquad \textbf{Equation S4}.$$

The Dubinin-Radushkevich (Dub-Rad) model [14] which assumes a pore filling sorption mechanism with a Gaussian energy distribution onto heterogonous surfaces is commonly applied to distinguish between chemisorption and physisorption using its mean free energy *E* which is equal to $1/\sqrt{(2K_{ad})}$. K_{ad} (mol^2/kJ^2) is the isotherm constant while ε and q_s (µg/g) are the Dub-Rad constant and the theoretical maximum sorption capacity, respectively (**Equation S5**).

The calculated mean free energy values for the sorption of PAHs to MNPs in water from this study range from 41–75 kJ/mol. A number of studies [15-17] investigating sorption isotherms of pollutants have suggested that mean free energy values > 8 kJ/mol imply that sorption involves partitioning into the bulk. Consequently, we conclude that partitioning is significantly contributing to the sorption of PAHs to MNPs studied herein.

$$C_{MNP} = q_S * (e^{-K_{ad}*\varepsilon^2}) \qquad \textbf{Equation S5}.$$

Unlike other models, the Tempkin model contains a factor which describes sorbent/sorbate interactions b_T (**Equation S6**). It assumes that the heat of adsorption of moleules decreases linearly rather than logarithmically with an increase in surface coverage [18]. However, it ignores extremely low and large concentration values (**see Figure S4**). A_T (L/kg) is the Tempkin adsorption constant.

$$C_{MNP} = \frac{RT}{b_T} * \ln A_T C_w \qquad \textbf{Equation S6}.$$

The Freundlich model includes possible heterogeneities between the adsorption sites at the adsorbent surface [19]. K_F (L/kg) and n are the Freundlich isotherm coefficient and exponent respectively (**Equation S7**).

$$C_{MNP} = K_F * C_w \text{^} n \qquad \textbf{Equation S7}.$$

The Brunauer-Emmett-Teller (BET) model (**Equation S8**) theoretically describes multilayer adsorption systems in the gas phase [20, 21], but it has also been modified and widely applied for liquid-solid adsorptions [21]. K_s (L/µg) is the isotherm constant which corresponds to α_L (L/µg) for a single layer adsorption. q_m (µg/g) is the monolayer adsorption capacity while K_l (L/µg) is the equilibrium constant for adsorption at upper layers. The poor fit of this model to our isotherms suggest monolayer adsorption.

$$C_{MNP} = q_m \frac{Ks * C_w}{(1 - K_l * C_w)(1 - K_l * C_w + Ks * Cw)} \qquad \textbf{Equation S8}.$$

Sips (**Equation S9**) and Redlich-Peterson (Red-Pet, **Equation S10**) models are 3-parameter empirical models. The former aims to circumvent the limitation of the Freundlich isotherm, according to which the concentration of the adsorbate increases infinitely for surfaces with finite adsorption sites. The latter is widely used as a compromise between Langmuir and Freundlich systems. The goodness of fit parameters for both models were better than those for the two-parameter models. This is unsurprising because both models contain three adjustable parameters. However, the parameters obtained from these models were inconsistent with those obtained from

the Freundlich and Langmuir models. This is probably due to the additional errors induced by additional parameterization of the models. K_R (L/kg) and K_{sip} (L/kg) are the Red-Pet and Sips isotherm constants, respectively. n is the dimensionless exponent while α_R (L/µg) and α_L (L/µg) are constants related to the activation energy for Red-Pet and Sips, respectively.

$$C_{MNP} = \frac{\mathrm{K_{sip}}\, {C_W}^{n}}{1+ \alpha_S\, {C_W}^{n}} \qquad \textbf{Equation S9},$$

$$C_{MNP} = \frac{\mathrm{K_R}\, C_W}{1+ \alpha_R\, {C_W}^{n}} \qquad \textbf{Equation S10}.$$

The Langmuir model describes monolayer adsorption. It assumes that adsorption can only occur at a finite number of definite localized sites and is characterized by a plateau – an equilibrium saturation point, where once a molecule occupies a site, no further adsorption can occur [22]. It is most commonly used to quantify and contrast different bio-sorbents [19]. From all tested 2-parameter models, the Langmuir model resulted in the best fitting across the tested concentration ranges and thus was chosen to compare the adsorption of PAHs to all investigated MNPs (**Table 2**). K_L (L/kg) is the Langmuir adsorption coefficient and equals $\alpha_L * q_{max}$. α_L (L/µg) is the Langmuir isotherm constant which is related to the free energy of adsorption [23], while q_{max} (µg/kg) is the theoretical maximum monolayer adsorption capacity (**Equation S11**). In addition to the Langmuir parameters, the Langmuir equilibrium factor $R_L = 1 / (1+ \alpha_L\, q_o)$ [23] was utilized to compare the adsorption isotherms. Here, α_L is the Langmuir constant (L/mg), and q_o is the initial concentration of adsorbent (mg/L).

$$C_{MNP} = \frac{K_L * C_w}{1+ \alpha_L * C_w} \qquad \textbf{Equation S11}.$$

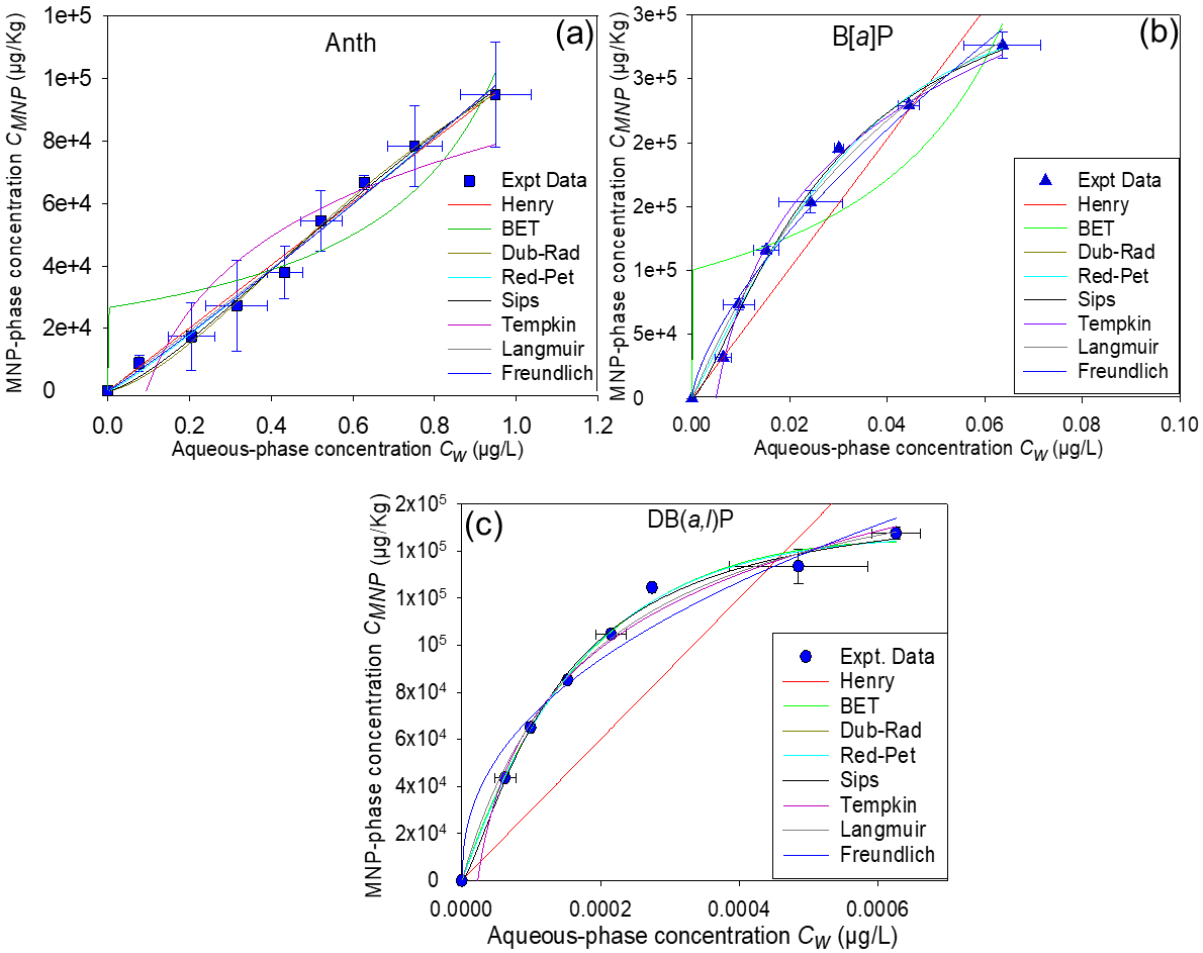

Figure S4: Exemplary experimental isotherms (n = 3, mean ± standard deviation) of PAHs: (a) Anth, (b) B[a]P and (c) DB[a,l]P adsorptions to PA-6_42 fitted to different adsorption isotherm models.

TABLE S4: ISOTHERM MODEL FIT PARAMETERS FOR PAH ADSORPTION TO PA-6_42.

Models	PAHs	Model parameters			Error functions	
		K_L (Log)	**q_{max} (µg/g)**		**R^2**	**χ^2 [µg/g]**
Langmuir	Anth	5.04	1136		0.989	4.5
	B[*a*]P	6.96	540		0.990	14.3
	DB[*a,l*]P	9.01	192		0.991	1.6
		K_F (Log)	**n_F**		**R^2**	**χ^2 [µg/g]**
Freundlich	Anth	5.00	0.95		0.989	4.03
	B[*a*]P	6.28	0.68		0.976	28.75
	DB[*a,l*]P	6.57	0.43		0.966	7.56
		A_T (L kg^{-1})	**b_T**		**R^2**	**χ^2 [µg/g]**
Tempkin	Anth	12.05	0.07		0.904	56.11
	B[*a*]P	204	0.02		0.995	2.56
	DB[*a,l*]P	44231	0.05		0.989	1.60
		K_{ad} (mol^2/ kJ^2)	**q_s (µg/g)**	**E (kJ/mol)**	**R^2**	**χ^2 [µg/g]**
Dub-Rad	Anth	0.0003	149	41	0.993	4.32
	B[*a*]P	0.0001	1897	71	0.976	1437.53
	DB[*a,l*]P	0.0001	3735	75	0.966	7.56
		K_H (Log)			**R^2**	**χ^2 [µg/g]**
Henry	Anth	5.01			0.990	12.92
	B[*a*]P	6.71			0.891	44.76
	DB[*a,l*]P	8.48			0.509	93.43
		K_s (L/µg)	**K_l (L/µg)**	**q_m (µg/g)**	**R^2**	**χ^2 [µg/g]**
BET	Anth	813790891	0.76	28227	0.871	63.70
	B[*a*]P	9741894726	10	100546	0.815	222
	DB[*a,l*]P	417	-1286	2059729	0.994	0.79
		K_{sip} (Log)	**n**	**α_s (L/µg)**	**R^2**	**χ^2 [µg/g]**
Sips	Anth	5.01	0.96	0.03	0.989	5.25
	B[*a*]P	7.65	1.35	123.4	0.994	5.10
	DB[*a,l*]P	10.39	1.34	149662	0.995	0.76
		K_R (Log)	**n**	**α_R (L/µg)**	**R^2**	**χ^2 [µg/g]**
Red-Pet	Anth	5.02	8.02	0.08	0.991	4.22
	B[*a*]P	6.88	1.59	63.03	0.992	9.36
	DB[*a,l*]P	8.90	1.30	36358	0.995	0.73

SECTION S5: VALIDATION OF THE MODIFIED THIRD-PHASE PARTITION METHOD: BATCH-EQUILIBRIUM METHOD FOR DETERMINATION OF ADSORPTION ISOTHERMS FOR PAHS AND MNPS IN WATER.

The novel third-phase partition method was verified using the batch-equilibrium method commonly applied to determine sorption isotherms [24]. For two sorbates (Anth and B[a]P) and two MNP sorbents (LDPE_215 and PA-6_42) sorption isotherms were acquired using the two methods and the obtained adsorption coefficients were compared.

Regarding the batch-equilibrium experiment, B[*a*]P sorption kinetic and isotherm experiments were performed in 500 mL Duran glass vials while those of Anth were conducted in 250 mL Duran glass vials. 5 mg of the target MNPs were utilized for all experiments except for characterizing B[*a*]P sorption onto PA-6_42, where 2.5 mg was used. Shaking of the sample vials were conducted in a two-dimensional IKA® HS 250 compact orbital shaker operated at 200 rpm and positioned inside a temperature-controlled incubation chamber (Binder GmbH, Tuttlingen, Germany). The samples were incubated at 21 ± 1^{o}C until the predetermined minimum equilibrium time was reached. After shaking, the sample vials were filtrated. Owing to the high initial rate of Anth sorption by PA-6_42, internal standard was spiked into the supernatant after filtration in order to circumvent sorption of Anth-d_{10} by the PA-6_42 particles. For B[*a*]P and LDPE_215, internal standard was spiked into the sample mixtures right before filtration. This corrects for the significant losses of B[*a*]P due to binding of this analyte to the filter material. Filtration was performed quickly (< 10 mins) without vacuum. After filtrations, the filtrates were extracted with 2×60 mL (Anth) or 2×100 mL (B[*a*]P) hexane. The combined organic extracts where dried over 3–6 g of anhydrous sodium sulfate, and subsequently concentrated to < 0.1 mL using a BUCHI R-215 Rotavapor System at a vacuum pump pressure of 260 mbar and a water bath temperature of 50^{o}C. Final volumes of 100 µL (B[*a*]P) and 500 µL for (Anth) were constituted with hexane and transferred to GC-vials. For quantification, 1 µL of the sample extracts were injected into a GC-MS system operated in splitless mode of the cold injection system (CIS). The method for GC-MS and data analysis were the same as described for the TPP method.

The minimum equilibrium times for sorption were predetermined by incubating the respective MNPs using a fixed B[*a*]P concentration of 1.0 µg/L in duplicate for different time intervals ranging from 36–336 h. Equilibrium was assumed when the difference between the average

aqueous phase sorbate concentration for two consecutive time points are within the respective standard deviations.

The isotherm experiments were conducted at five different initial PAH concentrations, and were measured at least in duplicate. Initial Anth concentrations of 0.75, 1.50, 2.25, 3.00, 3.50 µg/L in 240 mL water and initial B[*a*]P concentrations of 0.5, 1.0, 1.5, 2.0, 2.5 µg/L in 500 mL water were utilized.

For quality control, triplicates of two concentration points (lowest and highest) were used as control samples (PAH + water) and blank samples (water + MNPs) and were subjected to same conditions as the test samples.

Like the TPP method, an isotherm plot of the aqueous phase concentration of the analyte C_W (µg/L) vs the concentration of analyte sorbed to the MNP phase C_{MNP} (µg/kg) was fitted to the Langmuir model. C_W and C_{MNP} were calculated from **Equation S12** and **S13**, respectively. The sorption coefficient $K_{MNP/w}$ (L/kg) was calculated as the ratio of C_{MNP} and $C_{w.}$

$$C_W = \frac{n}{V_W} \qquad \textbf{Equation S12},$$

$$\mathrm{C_{MNP}} = \mathrm{C_0} - \mathrm{C_W} \qquad \textbf{Equation S13},$$

where V_w (L), C_0 (µg/L) and n (µg) are the volume of water, the initial adsorbate concentration and the measured amount of the sorbate, respectively.

Under the experimental conditions utilized, minimum equilibrium times for the sorption of B[*a*]P onto PA-6_42 and LDPE_215 ranged from 168–336 h and 120–168 h, respectively. For Anth sorption onto PA-6_42 and LDPE_215, the minimum equilibrium time ranged from 72–168 h (**Figure S5**). The recovery of the control samples ranged from 80– 120% for Anth across low and high tested concentrations. Regarding B[*a*]P, the obtained recovery ranged from 86–97% across low and high tested concentrations. The analyte concentrations in the blank were below the limit of quantification of 2.5 µg/L.

The logarithmic sorption coefficients log $K_{MNP/w}$ derived by the batch-equilibrium and the TPP methods for the sorption of Anth and B[*a*]P to PA-6_42 and LDPE_215 are summarized in **Table S5.** The obtained log $K_{MNP/w}$ values are in good agreement. Also, according to Lee *et al.* [25], the reported log $K_{MNP/w}$ values of 4.77 and 7.17 for the sorption of Anth and B[*a*]P, respectively, to PE microplastics (median size: 420 µm) are within the same order of magnitude with the values obtained in this work using the TPP method.

TABLE S5: COMPARISON OF THE LOGARITHMIC SORPTION COEFFICIENT $K_{MNP/W}$ (L/KG) ACQUIRED APPLYING THE BATCH-EQUILIBRIUM AND TPP METHODS (N = 5 ISOTHERM POINTS IN DUPLICATE OR TRIPLICATE, MEAN ± SD).

Sorbate	Sorbent	Batch	TPP
Anth	LDPE_215	4,57 ± 0,04	4,51 ± 0,09
	PA-6_42	4,93 ± 0,19	5,03 ± 0,06
B[a]P	LDPE_215	6,61 ± 0,04	6,58 ± 0,07
	PA-6_42	6,63 ± 0,05	6,82 ± 0,07

Similar to the TPP method, experimental sorption isotherms obtained using the batch-equilibrium method were fitted with the Langmuir model. The log of the Langmuir adsorption coefficient K_L (L/kg) describing the sorption of Anth to PA-6_42 and LDPE_215 were 4.96 and 4.73, respectively, while the obtained log of K_L for the sorption of B[*a*]P onto PA-6_42 and LDPE_215 were 6.65 and 6.60, respectively (**Figure S6**).

In comparison with the TPP method (**Table 2**), the difference between log K_L of the two methods for LDPE adsorption of Anth and B[*a*]P was within the standard error of the Langmuir model parameter K_L. Similarly, the difference between the K_L of the batch and TPP methods for PA-6_42 adsorption of Anth was well within the standard error of K_L. Of note, internal standard was spiked into the sample mixtures containing B[a]P and PA-6_42 after sorption equilibrium was reached in order to correct for nearly 50 % adsorption of B[a]P to the filter paper material. We attribute the slight deviation of the values for K_L to the sorption of fractions of the internal standard (B[*a*]P-d_{12}) to the PA-6 particles (potentially accompanied by displacement of some B[a]P) during the ca. 10 min filtration period. Overall, it can be concluded that the TPP method offers an easy, fast and reliable alternative for evaluating the adsorption properties of organic pollutants onto MNPs, circumventing these issues due to the lack of a filtration step.

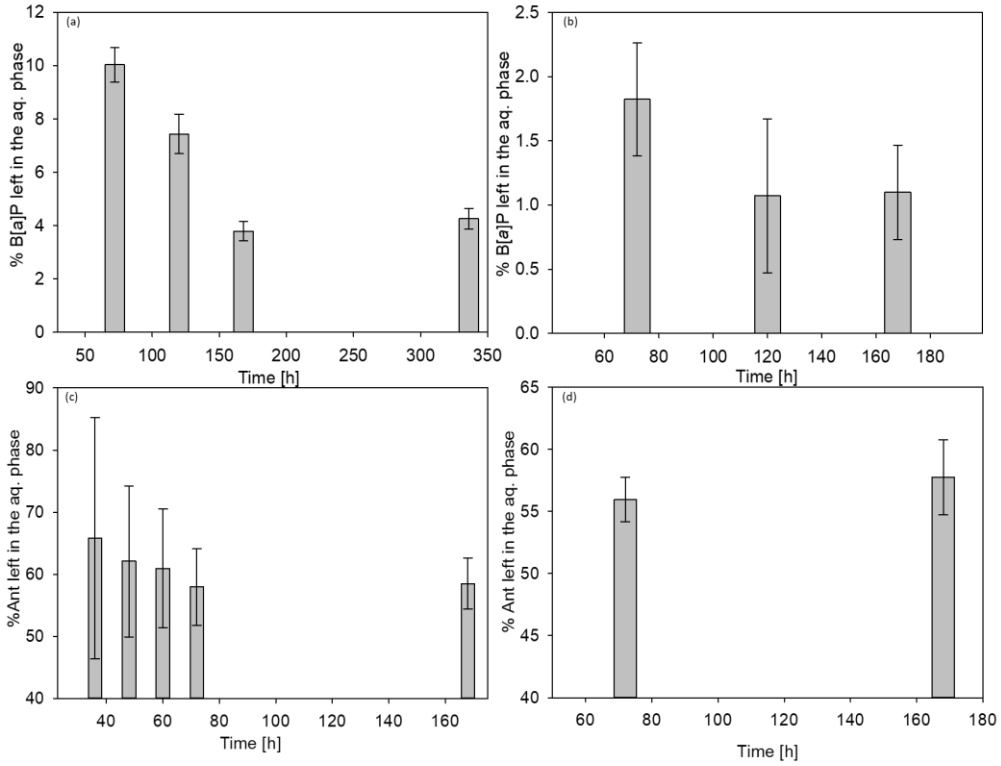

FIGURE S5: VERIFICATION OF EQUILIBRIUM FOR THE SORPTION OF B[A]P ON (A) PA-6, (B) LDPE, AND ANTH ON (C) PA-6 AND (D) LDPE MNPS.

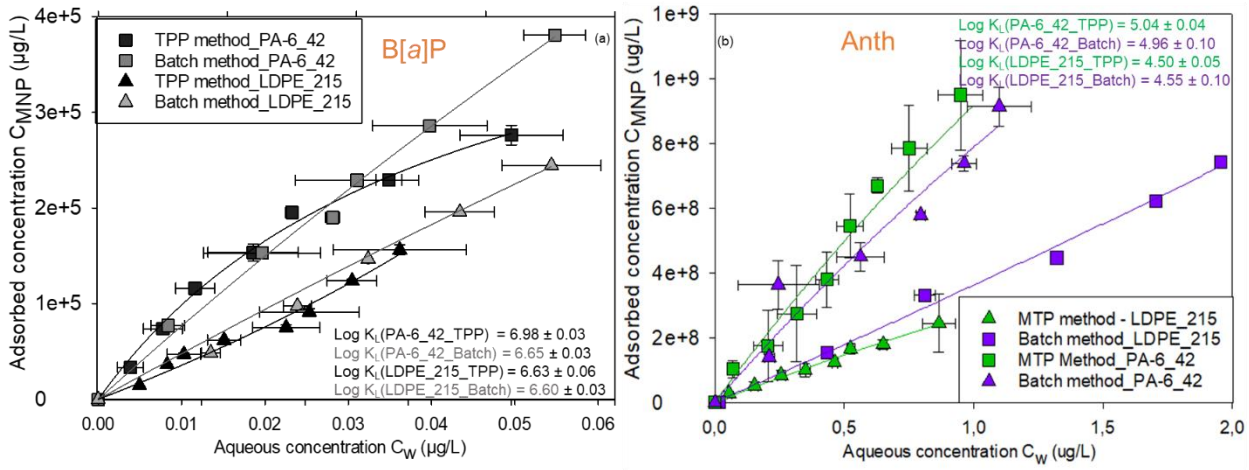

Figure S6: Comparison of the Langmuir adsorption isotherms of (a) B[a]P and (b) Anth sorption to LDPE_215 and PA-6_42 MNPs acquired with the TPP method and the batch-equilibrium method.

SECTION S6: EXPERIMENTALLY DETERMINED PAH SORPTION COEFFICIENTS $K_{MNP/W}$ AND ASSOCIATED COMBINED MEASUREMENT UNCERTAINTIES

$K_{MNP/w}$ of PAH/MNP pairs and their respective combined measurement uncertainties u_c ($K_{MNP/w}$) are shown in **Table 6.** $K_{MNP/w}$ was calculated from the slopes within the linear range of each isotherm. The combined measurement uncertainty u_c ($K_{MNP/W}$) was calculated according to the ISO/IEC Guide to the Expression of Uncertainty in Measurement (GUM) [26]. Initially, the standard uncertainty of each component used to calculate $K_{MNP/w}$ (**Equation S14**) was determined.

$$K_{MNP/w} = \frac{1}{M_{MNP}} \left(\frac{K_{PDMS/w}}{C_{PDMS}} m_{total} - K_{PDMS} M_{PDMS} - V_w \right) \qquad \textbf{Equation S14 [11]}$$

u_c ($K_{MNP/W}$) was then calculated according to **Equation S15**,

$$u_{c=} \sqrt{\left[\frac{\partial y}{\partial M_{MNP}} * u(M_{MNP})\right]^2 + \left[\frac{\partial y}{\partial K_{PDMS/W}} * u\left(K_{PDMS/W}\right)\right]^2 + \left[\frac{\partial y}{\partial C_{PDMS}} * u(C_{PDMS})\right]^2 + \left[\frac{\partial y}{\partial m_{total}} * u(m_{total})\right]^2 + \left[\frac{\partial y}{\partial M_{PDMS}} * u(M_{PDMS})\right]^2 + \left[\frac{\partial y}{\partial V_W} * u(V_W)\right]^2} \qquad \textbf{Equation S15 [31]}$$

where y is the output quantity $K_{MNP/w.}$

The standard deviation of the measured $K_{PDMS/w}$ and C_{PDMS} were utilized as standard uncertainties u ($K_{PDMS/w}$) and u (C_{PDMS}), respectively. The relative standard uncertainty of the total amount of PAH spiked into the system u (m_{total}) was estimated as 5% (with 3.5% being the relative uncertainty of the analytical standard solution according to the manufacturers, and 1.5% being the relative uncertainty due to pipetting). The difference between the actual mass of MNPs M_{MNP} intended and the average mass weighted was utilized as the standard uncertainty of M_{MNP}. The systematic error due to the weighing balance was ignored as negligible. The relative standard uncertainty resulting from measuring the volume of the aqueous phase was assigned to 1%. The uncertainty of the mass of PDMS in the coating of the stir bars, M_{PDMS}, was not declared by the producer and was therefore assigned to 1%.

The contribution of each component of $K_{MNP/w}$ to the combined uncertainty u_c was calculated according to **Equation S16**,

$$contribution\ (x_1) = \frac{\left[\frac{\partial y}{\partial x_1} * u(x_1)\right]^2}{\left[\frac{\partial y}{\partial x_1} * u(x_1)\right]^2 + \left[\frac{\partial y}{\partial x_2} * u(x_2)\right]^2 \ldots . + \left[\frac{\partial y}{\partial x_n} * u(x_n)\right]^2}$$

Equation S16 [26]

where *x* denote any of the six input components of $K_{MNP/w}$.

As shown in **Table S7**, u_c ($K_{MNP/w}$) was dominated by the standard uncertainties from $K_{PDMS/w}$, followed by m_{total}, and C_{PDMS}. For future applicability of this method, the contributions of the components to u_c ($K_{MNP/w}$) identify parameters that can be further optimized to reduce the uncertainty. Remarkably, the u_c ($K_{MNP/w}$) shown in **Table S6** are in the same order of magnitude as the model-generated standard error of K_L (**Table 2**).

TABLE S6: EXPERIMENTALLY DETERMINED SORPTION COEFFICIENTS OF PAHS ONTO MNPS OBTAINED USING THE TPP METHOD.

Polymer class	Polymer variants	Benzo[*a*]pyrene			Anthracene			Dibenzo[*a,l*]pyrene		
		$^{*}K_{MNP/w}$	$^{**}u_{c\,(k\,=\,1)}$	$^{'}$n	$^{*}K_{MNP/w}$	$^{**}u_{c\,(k\,=\,1)}$	$^{'}$n	$^{*}K_{MNP/w}$	$^{**}u_{c\,(k\,=\,1)}$	$^{'}$n
PMMA	PMMA_6	1.7E+05	6.3E+04	5						
	PMMA_0.3	3.6E+05	1.1E+05	5						
PU	PU_arom_1C	8.7E+05	3.0E+05	5						
	PU_arom_2C	3.5E+06	9.9E+05	5						
	PU_foam	1.6E+06	5.3E+05	5						
TPU	TPU_ester_Arom	1.4E+06	3.7E+05	5	1.7E+04	1.6E+04	3	9.7E+07	2.8E+07	5
	TPU_ether_Arom	2.0E+06	5.7E+05	5						
	TPU_ester_Alip	2.3E+06	6.1E+05	5						
	TPU_ether_Alip	2.5E+06	7.8E+05	5						
	TPU_ melt_arom	2.2E+06	7.0E+05	5						
PE	LDPE_215	2.5E+06	9.1E+05	5	3.62E+04	2.47E+04	5	5.4E+08	2.3E+08	5
	LDPE_84	8.0E+06	2.3E+06	5						
	PE_0.6	7.6E+06	1.9E+06	5						
PA	PA-6_42	3.3E+06	9.0E+05	5	1.0E+05	5.3E+04	8	5.7E+08	1.4E+08	5
	PA-12_44	5.3E+06	1.6E+06	5						
	PA-6_7	1.8E+07	5.3E+06	5						
Natural Rubber	Tire Rubber	2.0E+06	6.7E+05	5						
Aged polymers	Tire Rubber_1000h aged	2.0E+06	5.5E+05	4						
	Tire Rubber_2000h aged	1.9E+06	4.6E+05	4						
	PA-6_42_1000h aged	8.0E+06	2.1E+06	4						
	PA-6_42_2000h aged	5.0E+06	1.48E+06	4						
	LDPE_215_1000h aged	3.3E+06	9.3E+05	5						
	LDPE_215_2000h aged	3.2E+06	7.8E+05	4						

* Adsorption coefficient in (L/kg)

** Combined measurement uncertainty of $K_{MNP/w}$

' number of isotherms points used in duplicate or triplicate, and only points within the linear range of each isotherm were utilized to minimize bias.

TABLE S7: CONTRIBUTIONS OF THE UNCERTAINTY COMPONENTS OF $K_{MNP/W}$ FOR THE PAHS

		Contributions (Indexes) of the uncertainty components					
PAH	MNP	$K_{PDMS/W}$ (L/kg)	M_{mp} (kg)	M_{PDMS} (kg)	V_w (L)	C_{PDMS} (µg/kg)	m_{total} (ug)
B[*a*]P	PA-6_7	49.0%	3.2%	3.2%	3.2%	5.2%	36.2%
	PA-6_42	69.8%	0.0%	0.0%	0.0%	5.4%	24.9%
	PA-6_42_1000h	67.0%	0.0%	0.0%	0.0%	4.8%	28.1%
	PA-6_42_2000h	57.8%	0.0%	0.0%	0.0%	4.9%	37.2%
	PA-12_44	62.1%	0.0%	0.0%	0.0%	4.2%	33.7%
	PE_0.6	73.4%	0.0%	0.0%	0.0%	5.4%	21.2%
	LDPE_84	66.0%	0.0%	0.0%	0.0%	4.8%	29.1%
	LDPE_215	49.9%	0.0%	0.0%	0.0%	4.3%	45.7%
	LDPE_215_1000h	64.4%	0.0%	0.0%	0.0%	6.6%	29.0%
	LDPE_215_2000h	80.3%	0.0%	0.0%	0.0%	8.3%	11.4%
	Tire Rubber	50.2%	0.0%	0.0%	0.0%	6.1%	43.7%
	Tire Rubber_1000h	69.7%	0.0%	0.1%	0.0%	9.7%	20.6%
	Tire Rubber_2000h	85.2%	0.0%	0.1%	0.0%	10.6%	4.1%
	TPU_melt_arom	61.7%	0.0%	0.0%	0.0%	8.2%	30.1%
	TPU_ether_alip	57.1%	0.0%	0.0%	0.0%	6.9%	35.9%
	TPU_ether_arom	62.5%	0.0%	0.0%	0.0%	8.5%	28.9%
	TPU_ester_arom	79.7%	0.0%	0.1%	0.0%	13.9%	6.3%
	TPU_ester_alip	72.9%	0.0%	0.0%	0.0%	8.9%	18.1%
	PU_foam	56.3%	0.0%	0.1%	0.0%	9.2%	34.5%
	PU_arom_1C	51.2%	0.0%	0.2%	0.0%	15.5%	33.1%
	PU_arom_2C	65.9%	0.0%	0.0%	0.0%	6.5%	27.6%
	PMMA_0.3	61.3%	0.0%	0.1%	0.0%	13.3%	25.3%
	PMMA_6	52.8%	0.0%	0.5%	0.0%	26.3%	20.4%
Anth	PA-6_42	74.0%	0.0%	0.0%	0.0%	8.0%	17.9%
	LDPE_215	66.1%	0.0%	0.1%	0.1%	9.4%	24.5%
	TPU_ester_arom	81.7%	0.0%	0.1%	0.1%	12.8%	5.2%
DB[*a,l*]P	PA-6_42	76.4%	0.0%	0.0%	0.0%	6.1%	17.4%
	LDPE_215	34.9%	0.0%	0.0%	0.0%	3.1%	62.0%
	TPU_ester_arom	49.4%	0.0%	0.1%	0.0%	9.3%	41.2%

n = mean of at least nine isotherm points

SECTION S7: EVALUATION OF COMPETITIVE SORPTION: SORPTION BEHAVIOR OF MNPS IN SINGLE AND TRI-SORBATE SYSTEMS.

In order to understand possible competitive sorption effects, the sorption behavior of PA-6_42 and LDPE_215 MNPs were studied in mono-sorbate systems (containing a single specific PAH) and tri-sorbate systems (consisting of a mixture of the three PAHs Anth, B[*a*]P and DB[*a*,*l*]P using similar concentration ranges, Error! Reference source not found.**S7**). For both MNP types, a significant reduction in adsorption of Anth in the presence of the higher molecular weight PAHs was observed compared to mono-sorbate systems.

For B[*a*]P and PA-6_42, this effect was much less pronounced. In this case, the obtained K_L values were 17 and 30% lower in single-sorbate systems (B[*a*]P only) compared to tri-sorbate systems containing all three PAHs. The sorption of DB[*a,l*]P was unaffected or even slightly enhanced by the presence of Anth and B[*a*]P. It appears that for a mixture of PAHs, the sorption of the higher molecular weight and more hydrophobic PAHs are more favorable, while the smaller and least hydrophobic PAHs such as Anth suffer from competition for available sorption sites. This suggest a hydrophobicity-driven antagonism and is in line with the findings of Baker *et al*. (2012) [27].

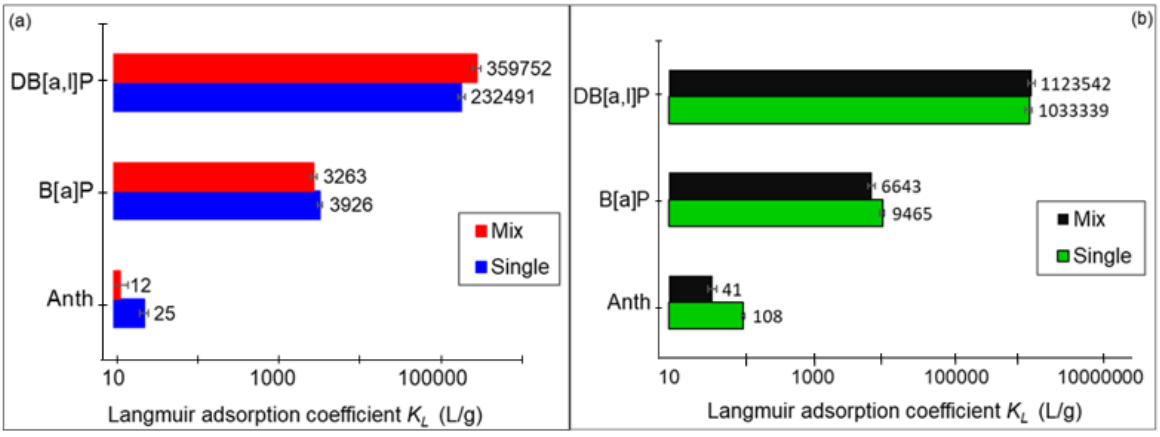

Figure S7: Langmuir adsorption coefficient K_L for Anth, B[a]P and DB[a,l]P sorption on (a) LDPE_215 and (b) PA-6_42 MNPs in single and tri-sorbate systems (error bars represent the standard errors, note that the x-axes are expressed in logarithmic scale).

REFERENCES SI

1. Prieto, A., et al., *Stir-bar sorptive extraction: A view on method optimisation, novel applications, limitations and potential solutions.* J Chromatogr A, 2010. **1217**(16): p. 2642-66.
2. Mayer, P., et al., *Equilibrium sampling devices.* Environ Sci Technol, 2003. **37**(9): p. 184A-191A.
3. Prieto, A., et al., *Development of a stir bar sorptive extraction and thermal desorption-gas chromatography-mass spectrometry method for the simultaneous determination of several persistent organic pollutants in water samples.* J Chromatogr A, 2007. **1174**(1-2): p. 40-9.
4. Gorecki, T. and J. Pawliszyn, *Effect of sample volume on quantitative analysis by solid-phase microextraction. Part 1. Theoretical considerations.* Analyst, 1997. **122**(10): p. 1079-86.
5. Kot-Wasik, A., D. Dąbrowska, and J. Namieśnik, *Photodegradation and biodegradation study of benzo(a)pyrene in different liquid media.* Journal of Photochemistry and Photobiology A: Chemistry, 2004. **168**(1-2): p. 109-115.
6. May, W.E., et al., *Solution thermodynamics of some slightly soluble hydrocarbons in water.* Journal of Chemical & Engineering Data, 2002. **28**(2): p. 197-200.
7. Barco-Bonilla, N., et al., *Comprehensive analysis of polycyclic aromatic hydrocarbons in wastewater using stir bar sorptive extraction and gas chromatography coupled to tandem mass spectrometry.* Anal Chim Acta, 2011. **693**(1-2): p. 62-71.
8. Baltussen, E., et al., *Study into the Equilibrium Mechanism between Water and Poly(dimethylsiloxane) for Very Apolar Solutes: Adsorption or Sorption?* Analytical Chemistry, 1999. **71**(22): p. 5213-5216.
9. Grant, S., et al., *Experimental Solubility Approach to Determine PDMS-Water Partition Constants and PDMS Activity Coefficients.* Environ Sci Technol, 2016. **50**(6): p. 3047-54.
10. DiFilippo, E.L. and R.P. Eganhouse, *Assessment of PDMS-water partition coefficients: implications for passive environmental sampling of hydrophobic organic compounds.* Environ Sci Technol, 2010. **44**(18): p. 6917-25.
11. Jonker, M.T.O. and A.A. Koelmans, *Polyoxymethylene solid phase extraction as a partitioning method for hydrophobic organic chemicals in sediment and soot.* Environmental Science & Technology, 2001. **35**(18): p. 3742-3748.
12. Mayer, P., W.H. Vaes, and J.L. Hermens, *Absorption of hydrophobic compounds into the poly(dimethylsiloxane) coating of solid-phase microextraction fibers: high partition coefficients and fluorescence microscopy images.* Anal Chem, 2000. **72**(3): p. 459-64.

13. Ayawei, N., A.N. Ebelegi, and D. Wankasi, *Modelling and Interpretation of Adsorption Isotherms.* Journal of Chemistry, 2017. **2017**: p. 1-11.
14. Gunay, A., E. Arslankaya, and I. Tosun, *Lead removal from aqueous solution by natural and pretreated clinoptilolite: adsorption equilibrium and kinetics.* J Hazard Mater, 2007. **146**(1-2): p. 362-71.
15. Batool, F., et al., *Study of Isothermal, Kinetic, and Thermodynamic Parameters for Adsorption of Cadmium: An Overview of Linear and Nonlinear Approach and Error Analysis.* Bioinorg Chem Appl, 2018. **2018**: p. 3463724.
16. Gupta, S. and A. Kumar, *Removal of nickel (II) from aqueous solution by biosorption on A. barbadensis Miller waste leaves powder.* Applied Water Science, 2019. **9**(4).
17. Lončarski, M., et al., *Sorption behavior of polycyclic aromatic hydrocarbons on biodegradable polylactic acid and various nondegradable microplastics: Model fitting and mechanism analysis.* Science of The Total Environment, 2021. **785**.
18. Aharoni, C. and M. Ungarish, *Kinetics of activated chemisorption. Part 2.—Theoretical models.* Journal of the Chemical Society, Faraday Transactions 1: Physical Chemistry in Condensed Phases, 1977. **73**(0).
19. Foo, K.Y. and B.H. Hameed, *Insights into the modeling of adsorption isotherm systems.* Chemical Engineering Journal, 2010. **156**(1): p. 2-10.
20. Staudt, P.B., et al., *A new method for predicting sorption isotherms at different temperatures using the BET model.* Journal of Food Engineering, 2013. **114**(1): p. 139-145.
21. Ebadi, A., J.S. Soltan Mohammadzadeh, and A. Khudiev, *What is the correct form of BET isotherm for modeling liquid phase adsorption?* Adsorption, 2009. **15**(1): p. 65-73.
22. Demirbas, E., M. Kobya, and A.E.S. Konukman, *Error analysis of equilibrium studies for the almond shell activated carbon adsorption of Cr(VI) from aqueous solutions.* Journal of Hazardous Materials, 2008. **154**(1-3): p. 787-794.
23. Belhachemi, M. and F. Addoun, *Comparative adsorption isotherms and modeling of methylene blue onto activated carbons.* Applied Water Science, 2011. **1**(3-4): p. 111-117.
24. *OECD Guideline for the testing of chemicals: Adsorption - Desorption Using a Batch Equilibrium Method*. 2000.
25. Lee, H., W.J. Shim, and J.H. Kwon, *Sorption capacity of plastic debris for hydrophobic organic chemicals.* Sci Total Environ, 2014. **470-471**: p. 1545-52.
26. ISO/IEC, *Uncertainty of measurement — Part 3: Guide to the expression of uncertainty in measurement (GUM:1995)*. 2008. p. 120.

27. Bakir, A., S.J. Rowland, and R.C. Thompson, *Competitive sorption of persistent organic pollutants onto microplastics in the marine environment.* Mar Pollut Bull, 2012. **64**(12): p. 2782-9.

6.5. MANUSCRIPT 2

Desorption of Polycyclic Aromatic Hydrocarbons from Microplastics in Human Gastrointestinal Fluid Simulants – Implications for Exposure Assessment

Emeka Ephraim Emecheta[1], Patrizia Marie Pfohl[2], Wendel Wohlleben[2], Andrea Haase[3*], Alexander Roloff[3*]

Authors' affiliations

[1]University of Bayreuth, Bayreuth Center for Ecology and Environmental Research (BayCEER), Dr.Hans-Frisch-Str.1-3, 95448 Bayreuth, Germany

[2]BASF SE, Carl-Bosch-Str. 38, 67056 Ludwigshafen, Germany

[3]German Federal Institute for Risk Assessment, Department of Chemical and Product Safety, Max-Dohrn-Straße 8-10, 10589 Berlin, Germany

Corresponding authors:

Andrea Haase, andrea.haase@bfr.bund.de

Alexander Roloff, alexander.roloff@bfr.bund.de

For Table of Contents Only

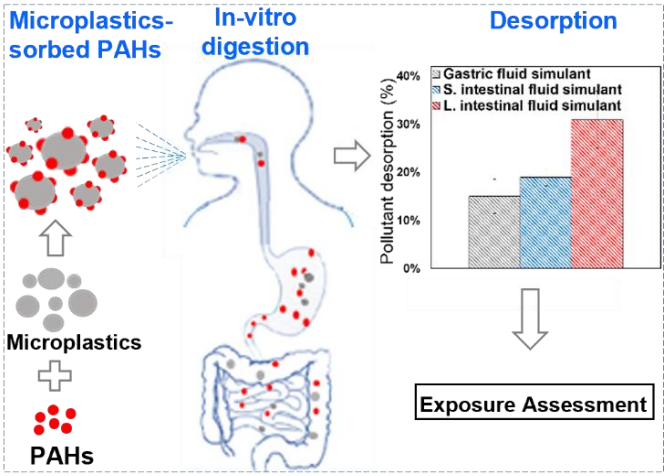

ABSTRACT

Microplastics have been detected in various food types, suggesting inevitable human exposure. A major fraction may originate from aerial deposition and could be contaminated by ubiquitous pollutants such as polycyclic aromatic hydrocarbons (PAHs). While data on the sorption of pollutants to microplastics are abundant, the subsequent desorption in the gastrointestinal tract (GIT) is less understood. This prompted us to systematically investigate the release of microplastics-sorbed PAHs at realistic loadings (44–95 ng/mg) utilizing a physiology-based in-vitro model comprising digestion in simulated saliva, gastric, small, and large intestinal fluids. Using benzo[*a*]pyrene as a representative PAH, desorption from different microplastics based on low density polyethylene (LDPE), thermoplastic polyurethanes (TPUs), and polyamides (PAs) was investigated consecutively in all four GIT fluid simulants. The cumulative relative desorption (CRD) of benzo[*a*]pyrene was negligible in saliva simulant but increased from gastric (4 ± 1 % – 15 ± 4 %) to large intestinal fluid simulant (21 ± 1 % – 29 ± 6 %), depending on the polymer type. CRDs were comparable for ten different microplastics in the small intestinal fluid simulant, except for a polydisperse PA-6 variant (1–10 µm), which showed an exceptionally high release (51 ± 8 %). Nevertheless, the estimated contribution of

microplastics-sorbed PAHs to total human PAH dietary intake was very low (≤ 0.1 %). Our study provides a systematic dataset on the desorption of PAHs from microplastics in GIT fluid simulants.

Keywords: microplastics, PAHs, in-vitro digestion, desorption, bioaccessibility, exposure assessment.

1. INTRODUCTION

As a result of the continuous increase in plastic production, mismanaged plastic waste has commensurably increased to emerge as a global health concern [1, 2]. At the present growth rate in production, plastic waste is projected to triple from the current estimate of 99 metric tonnes per year within the next 40 years [3]. In the environment, larger plastic debris degrades and fragments into smaller particles including micro- and nanoplastics (MNPs), which are already ubiquitous [2, 4].

MNPs also have been frequently detected in several beverages and food products such as tap and bottled water [5], fruits and vegetables [6], milk [7], beer and soft drinks [8, 9], salt [10], and different kinds of fish and fishmeal [11]. These widespread occurrences of MNPs in our ecosystem have made human exposure inevitable. Evidence of MNPs in feces [12, 13] confirms human consumption and subsequent passage through the gastrointestinal tract (GIT). In addition, high concentrations of different MNP particles have been reported in certain indoor and outdoor air settings [14, 15]. In particular, the detection of MNPs in human lung tissues confirms human inhalation exposure [16]. Notably, the majority of directly inhaled MNPs may subsequently be swallowed into the GIT following mucociliary clearance from the respiratory tract [17-19]. Additionally, a significant fraction of the MNPs present in food is estimated to be deposited from indoor air [20, 21]. However, while these reports have generated concerns about

the effects of MNPs on human health [19], a direct adverse health effect remains subject to controversy and uncertainty [22, 23].

It has been speculated that MNP particles might act as carriers for environmental contaminants such as persistent organic pollutants (POPs). Similar to MNPs, many POPs are ubiquitous [24]. For example, sorption of polycyclic aromatic hydrocarbons (PAHs) to MNPs collected from the environment has been demonstrated [25-27]. Therefore, it is conceivable that MNPs entering the GIT via food, water and dust could potentially contain sorbed environmental pollutants [28]. Some of these microplastic-sorbed pollutants are highly toxic and are known for their carcinogenic [29], mutagenic [29], immunotoxic [30], inflammatory, or endocrine-disruptive effects [31]. In the GIT, desorption of POPs, including PAHs, from ingested MNPs could contribute to aggregate human exposure to chemicals.

Several studies have investigated the release of microplastic-sorbed organic pollutants in marine organisms and birds using artificial gut fluids or model simulations [32-35]. Here, we focus on the potential release of MNP-sorbed PAHs in the human GIT as a continuation of our previous work [36], where we systematically investigated the sorption of PAHs to MNPs. Among the studied particles were intentionally-produced MNPs used in additive manufacturing applications. These include variants of polyamide (PA-6) and thermoplastic polyurethane (TPU), as well as crosslinked PU and PA-12, which feature growing utilization in commercial 3D-printing. For comparison, MNPs derived from polymers commonly used for packaging and production materials such as low-density polyethylene (LDPE), polymethyl methacrylate (PMMA), as well as cryomilled end-of-life truck tire tread were also investigated.

To provide realistic insight into the fate of MNP-sorbed PAHs in the human GIT, a physiology-based in-vitro digestion model anchored on the DIN 19738 standard was modified to sequentially simulate the release of PAHs from MNPs in the saliva, gastric, small, and large intestine fluids. Therefore, eleven different MNPs and five photo-aged MNP variants were loaded with benzo[*a*]pyrene (B[*a*]P). As PAHs often occur as variable mixtures, B[*a*]P is

sometimes considered representative for other PAHs owing to its ubiquity and well-characterized toxicity [29]. For comparison, anthracene (Anth) and dibenzo[*a,l*]pyrene (DB[*a,l*]P) were also investigated for selected MNPs. Notably, unlike most studies on the desorption behavior of microplastics [35, 38, 39], our work focuses on polydisperse MNPs with environmentally relevant size distributions, that have been produced from larger particles through cryomilling deploying different sieve sizes. The resulting particles feature polymer compositions, morphologies, and size ranges considered to be realistic for secondary MNPs.

Moreover, efforts were made to estimate the extent to which MNPs contribute to the overall intake of PAHs in the human diet. While it has been suggested that the contribution via marine organisms is negligible [34, 37], the contribution of MNPs to PAH intake in humans has been either estimated through probabilistic modelling or remains undisclosed in the limited studies that have examined PAH desorption from MNPs [38, 39]. Concerned by this paucity of data, the Food and Agriculture Organization of the United Nations (FAO) and the World Health Organization (WHO) recently estimated the significance of microplastics to human PAH exposure using contaminated fish and drinking water as models, albeit assuming complete desorption of PAHs in the GIT [23, 40].

To the best of our knowledge, this is the first systematic study on the in-vitro release of MNP-sorbed PAHs in all four human gastrointestinal compartments, which also provides an estimate on the exposure to bioaccessible PAHs via MNP intakes based on measured release rates.

2. MATERIALS AND METHODS

2.1. MATERIALS AND CHEMICALS

The MNPs from different suppliers (see **Table S1** for details) were cryomilled as described in our previous study [41], and therefore varied in size and shape as confirmed by scanning electron microscopy (SEM) imaging (see the Supporting Information (SI), **Figure S1**). In total, eleven MNP variants from six polymer classes were investigated. Among them are additive

manufacturing-relevant polymers such as polyamides (PA-12_44, PA-6_42, PA-6_7), polyurethane (PU_1C_arom), and thermoplastic polyurethanes (TPUs). The TPUs [42] consist of soft and hard segments. The soft segments comprise polyester or polyether polyols (termed 'ester' or 'ether'), while the hard segments are built from aromatic or aliphatic diisocyanates (termed 'arom' or 'alip'). For comparison, low-density polyethylene (LDPE), polymethyl methacrylate (PMMA), and Tire Rubber particles were also studied.

The size distributions of the investigated MNPs are reported in the SI (**Section S1**). Other physicochemical properties of the MNP materials have been described in our previous study [36]. To investigate the effect of photo-aging on the desorption behavior of the additive manufacturing-relevant MNPs, selected MNP variants (PA-6_42, TPU_ester_arom and TPU_ether_arom) were artificially aged via ultraviolet (UV)-light exposure for 1000 h and 2000 h following a procedure described previously [43].

Anth, B[*a*]P, DB[*a,l*]P (**Table S2**), anthracene-d_{10} (Anth-d_{10}), benzo[*a*]pyrene-d_{12} (B[*a*]P-d_{12}), and dibenzo[*a,i*]pyrene (DB[*a,i*]P) were purchased as analytical standards in acetonitrile (purity ≥ 98.5 %) from Neochema (Bodenheim, Germany). Hexane (≥ 99 % pure), hydrochloric acid (30% *w*/*v*), and sodium hydroxide pellets (reagent grade) were purchased from Merck (Darmstadt, Germany). Anhydrous magnesium sulfate (99.5 %), xylenes (99.0 %) and formic acid (≥ 88 % *w*/*v*) were purchased from Sigma-Aldrich (Steinheim, Germany). All components of the gastrointestinal fluid simulants were purchased from Sigma Aldrich (Steinheim, Germany) in the highest available purity. Ultrapure water was obtained from a Millipore Q-POD dispenser connected to a Millipore milli-Q system (Darmstadt, Germany). All filtrations were performed using 0.7 µm Whatman GF/F Glass Microfiber filters.

2.2. LOADING OF PAHS ONTO MNPS

Before in-vitro digestion experiments, the MNPs were loaded with Anth, B[*a*]P or DB[*a,l*]P using a batch-equilibrium method similar to that described in our previous work [36]. Briefly, 25 mg

MNPs were introduced into a Duran glass vial of 1 L approximate volume (Mainz, Germany). Thereafter, 1.1 L water were introduced into the vial using a Duran glass measuring cylinder (Mainz, Germany) followed by the addition of either 2 µg Anth, B[*a*]P or DB[*a,l*]P from the stock solutions. To achieve a high loading of DB[*a,l*]P on PA-6_42 particles, 25 mg of the polymer was weighted into a glass vial containing 50 mL water and 10 µg DB[*a,l*]P. The mixtures were then incubated on a magnetic stirring plate operated at 600 rotations per minute (rpm) for six days at room temperature. After incubation, the PAH-loaded MNPs were separated by filtration and dried overnight inside a gas chromatography oven (Agilent, Waldbronn, Germany) operated at 40 °C. The amount of PAH loaded onto the MNPs, n_{MNP}, was determined indirectly from the amount in the aqueous phase, n_w, by assuming mass balance of the system (**Equation 1**) according to

$$n_{MNP}\,(ng) = n_{tot}\,(ng) - n_w\,(ng) \qquad (1)$$

where n_{tot} is the initial total amount of PAH spiked into the vial. n_w was determined by solvent extraction of the filtrate with 2×100 mL hexane (see **Section S2**), and subsequent analysis of the resulting extract by gas chromatography coupled to mass spectrometry (GC-MS, see **Section S4**).

For verification, the equilibrium distribution coefficients $K_{MNP/w}$ (**Equation 2**) obtained from previously measured sorption isotherms for PAHs and MNPs [36] were utilized to calculate the expected value for n_{MNP}:

$$K_{MNP/W}(\mathrm{L/kg}) = \frac{n_{MNP}(\mu g)/M_{MNP}(kg)}{n_w(\mu g)/\,V_w(L)} \qquad (2)$$

where M_{MNP} and V_w are the mass of MNPs and volume of water, respectively. As shown in **Table 1**, both methods yield comparable values for n_{MNP}.

Unlike for Anth and B[*a*]P, which partition mainly between the water and MNP phases upon equilibration, for super-hydrophobic compounds such as DB[*a,l*]P, sorption to the glass vessels can be significant, whereby **Equation 1** would have resulted in erroneous n_{MNP} values. To

circumvent this, the amount of DB[*a,l*]P on LDPE_84 and PA-6_42 was determined by dissolving the loaded MNPs in hot xylenes (70°C) and formic acid, respectively, followed by quantification of the released DB[*a,l*]P by GC-MS (see **Section S2** for details). The results are presented in **Table 1**. The B[*a*]P loadings of selected polymers determined with this method confirm the values obtained with the other two approaches.

		PAH concentrations on MNPs (ng/mg)		
PAHs	**MNPs**	**by mass balance (extraction of the aqueous phase)**	**calculated from $K_{MNP/w}$**	**by MNP dissolution and solvent-extraction**
B[*a*]P	PA-6_7	79.1 ± 1.4	79.8 ± 0.2	82.8 ± 3.4
	PA-6_42	79.5 ± 1.0	79.5 ± 0.2	81.2 ± 0.2
	PA-12_44	79.4 ± 0.2	79.4 ± 0.2	–
	LDPE_84	79.1 ± 0.4	79.1 ± 0.2	75.8 ± 44.4
	Tire Rubber	78.8 ± 0.4	78.2 ± 0.4	–
	PMMA_6	61.3 ± 0.6	63.8 ± 6.8	–
	PU_1C_arom	70.3 ± 0.6	71.4 ± 4.8	–
	TPU_est arom	79.0 ± 0.2	75.8 ± 0.6	75.4 ± 8.0
	TPU_est alip	79.3 ± 0.2	77.2 ± 0.6	75.4 ± 8.2
	TPU_eth arom	79.3 ± 0.2	76.7 ± 0.8	84.2 ± 22.4
	TPU_eth alip	79.3 ± 0.4	77.4 ± 1.0	77.3 ± 2.0
Anth	LDPE_84	46.0 ± 16.4	50.2 ± 13.0	–
	PA-6_42	43.5 ± 2.6	55.7 ± 10.2	–
DB[*a,l*]P	LDPE_84	–	–	52.4 ± 13.8
	PA-6_42	–	–	95.1 ± 7.2

Table 1*: PAH loads of MNPs investigated in this study (n = 2, mean ± 2 SD) Anth and B[a]P concentrations on MNPs were calculated by mass balance using the measured aqueous*

concentrations after loading. DB[a,l]P loads were determined by direct extraction of the loaded MNPs. The loadings are comparable to values determined via pre-determined partition coefficients $K_{MNP/w}$ [36] *as well as direct extraction of selected MNPs. PAH loads on MNPs are within the* range of total PAH concentrations in the environment [44]. Reprinted in part with permission from Emecheta, E. E., Borda, D. B., Pfohl, P. M., Wohlleben, W., Hutzler, C., Haase, A. & Roloff, A., *A comparative investigation of the sorption of polycyclic aromatic hydrocarbons to various polydisperse micro- and nanoplastics using a novel third-phase partition method.* Microplastics and Nanoplastics, 2022. **2**(1)[36]. Copyright 2022 (the authors; see http://creativecommons.org/licenses/by/4.0/).

2.3. SEQUENTIAL DIGESTION OF PAH-SORBED MNPS IN GI FLUID SIMULANTS

The in-vitro digestion procedure in saliva, gastric, small and large intestine fluid simulants was based on the *Deutsches Institut fur Normung* (DIN) 19738 standard [45] and a previous publication [46], but modified for the digestion of PAH-loaded MNPs rather than soil or nanoparticles. Importantly, the incubation times in different fluid simulants (5 minutes in artificial saliva, 2 h in gastric, 4 h in small intestinal and 18 h in large intestinal fluid simulants) represent average digestion times in the human GIT, and therefore are considered to reflect realistic desorption conditions, as opposed to equilibration conditions relevant for characterizing desorption in different environmental compartments. Of note, the volumes of the fluid simulants applied for artificial digestion (i.e., 40 mL for the gastric phase, 40 mL for the small intestinal phase) are comparable to the average GI liquid volumes of fasted humans [76]. Increased volumes as a result of food and beverage intake as well as lower particle concentrations may shift desorption rates to higher values.

100 mL Duran glass vials and PAH-loaded MNPs in the mass range of 25–75 mg were used in the in-vitro digestion experiments as specified below. The fluid simulant (**Section S3**, **Table S3**) for each GI phase was freshly prepared for every experiment, and the pH was adjusted with 1 M HCl or NaOH to the values shown in **Figure 1**, using a Knick 765 Calimatic pH meter

(Berlin, Germany). In-vitro digestions were performed by incubating samples in a Burgwedel shaker (Gesellschaft für Labortechnik GmbH, Germany) operated at 250 rpm and positioned inside an incubation chamber (Binder GmbH, Tuttlingen, Germany) operated at 37°C. All digested samples were centrifuged using a 1S-R centrifuge (ThermoFisher Scientific, Germany) and filtered using 0.7 µm Whatman GF/F glass microfiber filters.

In-vitro digestion in artificial saliva was performed by transferring 15 mL of saliva fluid simulant to the digestion vial and adjusting the pH to 6.5 ± 0.1. To start the digestion procedure, a specific mass (25–75 mg) of PAH-loaded MNPs was added to the vial, followed by 5 min incubation. For gastric phase digestion, 40 mL gastric fluid simulant was subsequently added to the mixture, and the pH was adjusted to 1.75 ± 0.1, followed by 2 h incubation. For small intestine phase digestion, 40 mL small intestine fluid simulant were subsequently added to the mixture, the pH was adjusted to 6.5 ± 0.1 and samples were incubated for 4 h. Finally, digestion in the large intestine phase was assessed by adding 15 mL large intestine fluid simulant to the resulting mixture, the pH was adjusted to 8.3 ± 0.1, followed by 18 h incubation. Likewise, the untreated MNPs (without prior loading with PAHs) also underwent sequential digestion as described above and the resulting fluid simulants were analyzed for their PAH contents as negative controls.

For each digestive phase, the desorbed PAHs were analyzed by subjecting the samples to 15 minutes of centrifugation, followed by filtration and the addition of internal standard to the filtrates. 1000 ng of B[*a*]P-d_{12} and DB[*a,i*]P were used as internal standards for B[*a*]P and DB[*a,l*]P, respectively, while 500 ng of Anth-d_{10} were used for experiments involving Anth. To extract the desorbed PAHs, the filtrates were transferred into a 250 mL separatory funnel and extracted with 2×5 and 2×25 mL hexane for saliva and gastric fluid simulant filtrates, respectively. Small and large intestinal phase filtrates were extracted using 2×30 mL hexane. For calibration, different concentrations of the target PAHs were spiked into control samples consisting of GI fluid simulants without PAH-loaded MNPs. The calibration mixtures and

samples were incubated and processed identically. The resulting matrix- and method-matched calibrations (**Figure S3**, **Table S4**) were performed sequentially for each GI phase. The hexane extracts were concentrated to < 1 mL in a Buchi R-215 Rotavapor system (Flawil, Switzerland) and analyzed by GC-MS. The cumulative relative desorption (CRD) of the PAHs in each GI phase was calculated according to **Equation 3**, where n_{des} is the amount of PAH desorbed in the fluid simulant.

$$CRD\ (\%) = \frac{n_{des}\ (ng)}{n_{MNP}\ (ng)} \text{ x } 100\ (\%) \qquad (3)$$

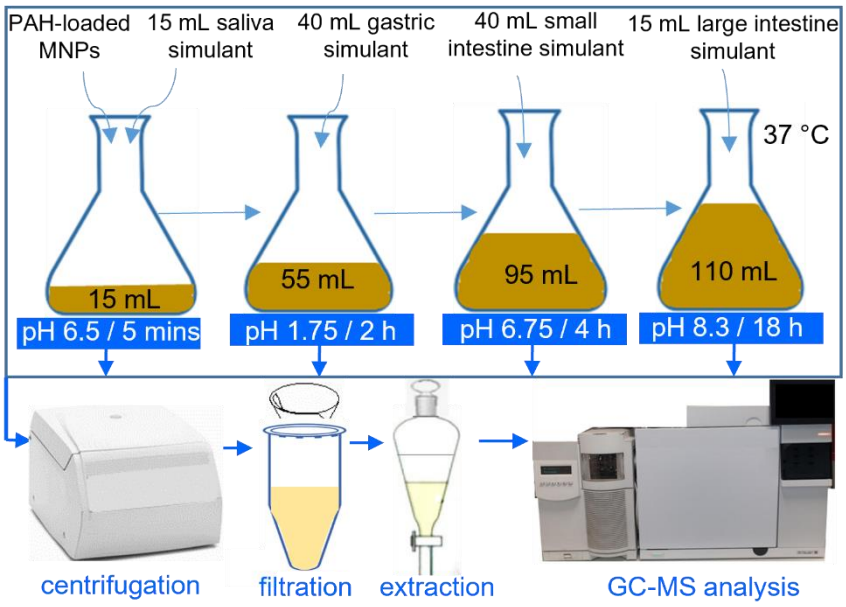

Figure 1: Workflow for the in-vitro digestion of PAH-sorbed MNPs. Each digestive phase was either analyzed for the amount of desorbed PAH (↓) or transferred to the next stage (→) for sequential digestion.

2.4. DATA ANALYSIS

GC-MS data were processed with MassHunter software (Agilent, versions B.06.00 and B.05.00). Microsoft Excel 2016 was used for additional data processing. Two-tailed t-test analysis of the data was performed with GraphPad Prism 9 (GraphPad Software, USA).

3. RESULTS AND DISCUSSION

We aimed to investigate the desorption of PAHs from eleven different MNPs (**Table S1**, **Figures S1**/ **S2**). Initially, the MNPs were loaded with PAHs to yield environmentally relevant sorbate concentrations [44] (**Table 1**, ~44–95 ng/mg). The PAH-loaded MNPs were then sequentially digested in different GI fluid simulants as schematically depicted in **Figure 1**. Thereafter, the digested mixtures were separated from MNPs by centrifugation and filtration, and the resulting filtrates containing the released PAHs were quantified via online-coupled GC-MS using matrix and method-matched calibrations (**Figure S3**, **Table S4**). From the obtained data we finally assessed the potential human exposure to PAHs through the ingestion of contaminated MNPs.

3.1. DESORPTION OF BENZO[*A*]PYRENE FROM MNPS DURING SEQUENTIAL DIGESTION IN GASTROINTESTINAL FLUID SIMULANTS

We initially determined to which extent desorption of PAHs from MNPs would occur in the different compartments of the GIT. To this end, we utilized B[*a*]P as a representative PAH and examined the desorption from three different MNPs (PA-6_42, TPU_est_arom and LDPE_84) in specific GI fluid simulants (see **Table S3** for compositions) applying incubation times that correspond to typical retention times during digestion.

The desorbed amount of B[*a*]P in the saliva simulant after five minutes of incubation was below the limit of detection (LOD, see **Table S4**) and was therefore considered negligible for the three studied MNPs. An increase in the cumulative relative desorption (CRD, the sum of the released amount of PAH during sequential digestion relative to the sorbed amount on the MNPs) along the gastric and both intestinal fluid simulants was observed in the order of LDPE_84 < TPU_est_arom < PA-6_42 (**Figure 2a**).

Specifically, the CRD for B[*a*]P ranged from 4.0 ± 1.1 % to 15.0 ± 3.5 % for the three MNPs after 2 h incubation in the gastric fluid simulant. A further 2.6 ± 1.7 % to 9.8 % ± 1.7 % of B[*a*]P desorbed upon transfer of the gastric chyme into the small intestine fluid simulant and incubating the mixture for 4 h, resulting in CRDs of 13.8 ± 2.8 % to 19.0 ± 1.8 %. Lastly, when the mixture was transferred to the large intestine fluid simulant and digested for 18 h, an additional 4.9 ± 0.6 % to 10.3 ± 4.1 % of B[*a*]P desorbed from the MNPs. This resulted in CRD values of 20.9 % ± 1.3 % to 29.3 ± 5.9 % along the four tested fluids simulating the passage through the whole digestive tract (**Figure 2a**).

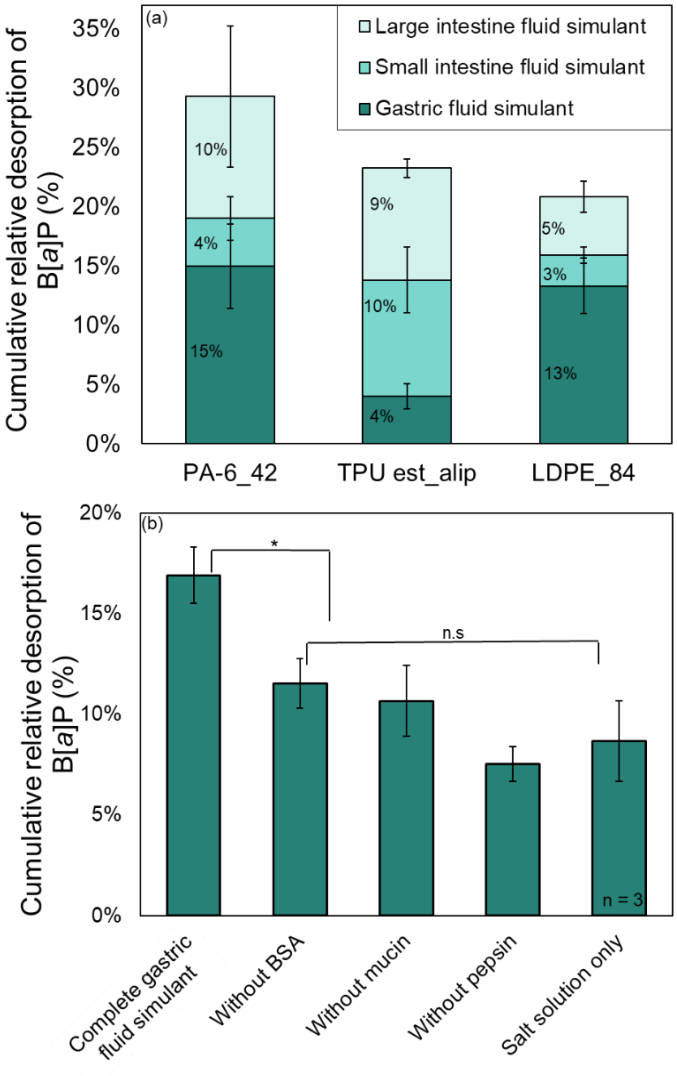

Figure *2 (a): Cumulative relative desorption (CRD) of microplastics-sorbed B[a]P during sequential in-vitro digestion in different human GI fluid simulants (n = 3, mean ± SD). (b): Effect of gastric fluid simulant components on the CRD of B[a]P from PA-6_42 MNPs (n = 2, mean ± SD, * significantly different (p < 0.05), n.s. = not significant at *).*

It has been suggested that proteins and enzymes present in the gastric fluid simulant enhance the solubility of hydrophobic compounds [47-50]. As depicted in **Figure 2b**, mucin, bovine serum albumin (BSA) and pepsin indeed facilitated the release of hydrophobic B[*a*]P from PA-6_42 MNPs in this medium. Specifically, a release of 8 ± 1 % of the loaded B[*a*]P was observed in the gastric fluid simulant in the absence of pepsin, which increased to 17 ± 1 % and 20 ± 5 % when a physiologically relevant pepsin concentration of 1.4 mg/mL or a three-fold higher concentration (4.2 mg/mL) was applied (**Figure S4**). In addition, amphipathic bile acids in the small intestine fluid simulants have been reported to promote the solubilization of hydrophobic organic compounds, including B[*a*]P [47, 51, 52], which may explain the observed relatively high CRDs for this compartment. These results suggest that the desorption of organic compounds from MNPs is dependent on the GI fluid composition and the concentrations of individual constituents. This underscores the need for a standardized method to investigate the in-vitro digestion of MNPs in order to ensure data comparability.

Absorption of nutrients occurs mainly in the small intestine, while in the large intestine, indigestible food components are further processed by bacteria of the microbiome [53]. Across the three MNPs, approximately 5 to 10 % of the total amount of desorbed B[*a*]P were released into the large intestine fluid simulant (**Figure 2a**). Thus, the contribution to the overall CRD is comparable to that observed in the previous two fluids despite the much longer in-vitro digestion time (18 h) in relation to gastric (2 h) and small intestine (4 h) fluid simulants. The rate of desorption is presumably slowed down in the large intestinal fluid simulant after an initial rather rapid desorption in the gastric/small intestine fluid simulants [54, 55]. In total, the CRD for B[*a*]P did not exceed ~30 % across the three investigated MNPs.

3.2. COMPARISON OF THE CUMULATIVE RELATIVE DESORPTION OF B[*A*]P FROM ELEVEN DIFFERENT MNPS IN THE SMALL INTESTINE FLUID SIMULANT

Digestion and absorption of ingested food and nutrients predominantly occurs in the stomach and small intestine [53]. We therefore decided to compare eleven selected MNP variants for their cumulative desorption of B[*a*]P during sequential digestion up to the small intestine fluid simulant (**Figure 3**).

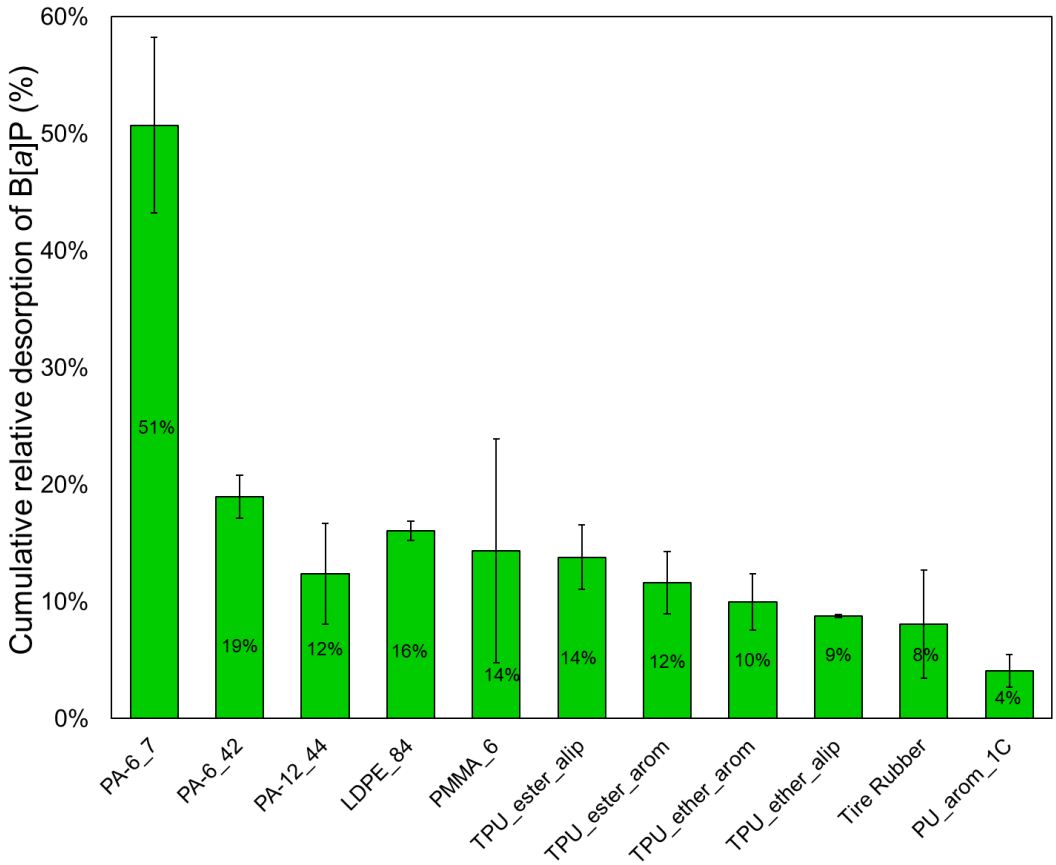

Figure *3: Comparison of the cumulative relative desorption (CRD) of microplastics-sorbed B[a]P during sequential digestion up to the small intestine fluid simulant (containing the preceding saliva and gastric fluid simulants). Each experiment was performed at least in triplicate (n = 3, mean ± SD). The CRD values of PA-6_42, LDPE_84, and TPU_est_alip are replotted from Figure 2a.*

The CRD values for most of the MNPs were rather moderate, typically ranging from 4 % (PU_arom_1C) to 19 % (PA-6_42). Only PA-6_7 showed an exceptionally high CRD (51 %). This could be related to reversible water absorption by PA-6 materials [56-58]. Hydration may result in increased chain segment mobility, thus significantly lowering the glass transition temperature and stiffness of this polymer [59, 60]. This could facilitate diffusion-driven transport of dissolved B[*a*]P from the bulk matrix of the polymer to the aqueous medium. Bulk sorption of estradiol sorbates to PA-6 powders was indeed recently demonstrated by Hummel *et al.* [61].

The overall comparable CRD values can be explained by the non-equilibrium conditions during in-vitro digestion. The cumulative release of B[*a*]P from MNPs in the small intestine fluid was determined after a total incubation time of ca. 6 h. Previous studies demonstrated that equilibrium times for the desorption of POPs from microplastics in GI fluid simulants are in the order of weeks to years [54, 55]. Therefore, unlike for sorption under quasi-equilibrium conditions, where B[*a*]P distribution coefficients for the same MNPs differed by over 100-fold [36], the desorption of B[*a*]P within typical time frames for digestion in humans differed only by 10-fold.

The sorption mechanism presumably also has an influence on the desorption rate. Apart from PMMA_6 and PU_arom_1C, all other MNPs are derived from rubbery polymers, where partitioning of B[*a*]P molecules into the bulk of the particles, in addition to surface adsorption, is considered to significantly contribute to the overall B[*a*]P load [36]. Indeed, the crosslinked PU_1C_arom MNPs desorbed the least B[*a*]P (**Figure 3**), possibly due to restricted B[*a*]P diffusion through the bulk polymer network [54].

Particle size and surface area seem to have an influence on the CRD, but other factors such as the chemical nature of the polymers might be more important. Specifically, PA-6_7 and PMMA_6 have similar size distributions (**Section S1**, **Figure S2**) but the CRD of B[*a*]P from PA-6_7 was 3.5-fold higher than from PMMA_6. When comparing the same polymer type in two different size ranges, we found that the B[*a*]P release was enhanced by 2.7-fold for the smaller-sized PA-6_7 particles compared to PA-6_42. However, this can be only partially

explained by the larger surface area to volume ratio [25, 62, 63]. The specific surface area, determined by the Brunauer-Emmett-Teller (BET) method, is 6-fold higher for PA-6_7 (2.16 m^2/g) compared to PA-6_42 (0.37 m^2/g). These examples point to diffusion from the bulk of the MNP particles also playing a role in the desorption process.

To investigate the influence of polymer aging on desorption, PA-6 and TPU MNPs were photo-aged via UV-light exposure for 1000 or 2000 h, respectively, and subsequently loaded with B[*a*]P. In contrast to sorption which was studied under quasi-equilibrium conditions in water [36], photo-aging had a negligible effect on the CRD of B[*a*]P in the small intestine fluid simulant (**Figure S5**). Interestingly, Fourier transform infrared (FTIR) spectroscopy of the aged and non-aged MNPs indicated an increase in the carbonyl, hydroxyl and amine functional group content on the MNP surfaces (**Section S5**, **Figure S6**). This implies that increased surface functionalization of the aged rubbery MNPs had no significant effect on desorption, further suggesting that diffusion from the bulk of these polymers is rate-limiting for desorption.

Considering the various influences of polymer type as well as morphology, including pore volumes, [38] and of the compositions of the different GI fluid simulants on the desorption process, it can be inferred that the release of PAHs from MNPs in the GIT is a complex phenomenon. Further research is needed to fully elucidate how individual factors specifically modulate desorption of different POPs from MNPs.

3.4 COMPARISON OF THE DESORPTION OF DIFFERENT PAHS FROM MNPS

To ascertain the cumulative relative desorption of PAHs other than B[*a*]P from MNPs in the small intestine fluid simulant, PA and LDPE particles were chosen as examples as these polymer classes showed the highest sorption [36] and desorption of B[*a*]P (**Figure 3**). PA-6_42 and LDPE_84 MNPs were loaded individually with Anth and DB[*a,l*]P. The PAHs differ in their physicochemical properties (**Table S2**) and sorption behaviors [36]. As shown in **Figure 4a**, the

CRD of PAHs sorbed to LDPE_84 differed by over an order of magnitude and increased according to Anth (6 ± 1 %) < B[*a*]P (16 ± 1 %) < DB[*a,l*]P (61 ± 13 %), while for PA-6_42 CRDs of 36 ± 2 % (Anth), 19 ± 2 % (B[*a*]P), and 46 ± 2 % (DB[*a,l*]P) were quantified (**Figure 4b**).

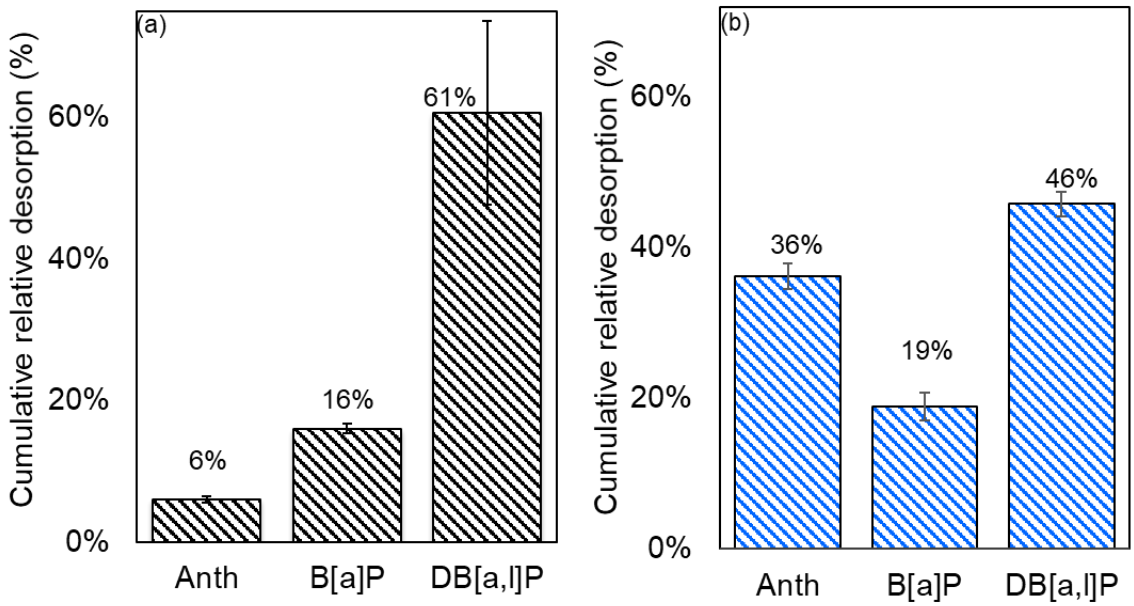

Figure *4: Cumulative relative desorption of PAHs from (a): LDPE_84, (b): PA-6_42 during sequential digestion up to the small intestine fluid simulant (containing the preceding saliva and gastric fluid simulants). Each experiment was performed at least in duplicate (n ≥ 2, mean ± SD).*

Sorption of organic pollutants, including PAHs, to sorbents such as LDPE and PA-6 can principally occur via both surface adsorption [64, 65] and absorption into the bulk [61, 66]. Depending on the specific contribution of each sorption mode, the relative concentrations of the PAHs at the surface versus the bulk will differ. In the case of DB[*a,l*]P in this study, surface adsorption rather than bulk absorption may have dominated the sorption process given its larger molar volume and very low water solubility compared to Anth and B[*a*]P (**Table S2**). This would explain the observed rapid and comparable desorption of DB[*a,l*]P from the surfaces of LDPE_84 and PA-6_42 MNPs, which also have similar surface areas of 0.33 m^2/g and 0.37 m^2/g, respectively [36].

For LDPE, B[*a*]P and particularly Anth are increasingly distributed to the bulk due to their decreasing molar volumes and thus enhanced diffusion during loading of the MNPs. Within the limited time frame of the desorption experiment, the release of Anth is therefore slowest since diffusion to the particle water interface is restricted.

Surprisingly, in the case of PA-6, a higher degree of desorption was observed for Anth compared to B[*a*]P. This behavior can be explained by the dynamics of (de-)sorption in PA-6 materials compared to LDPE. PA-6 is a polymer well known for its high-water absorption capacity [56-58]. We hypothesize that due to the higher water solubility of Anth, this PAH is better solubilized from the bulk of the PA-6 MNPs during swelling with the GI fluid simulants, thereby facilitating its transport into the bulk of the liquid phase.

Analysis of both the small and large intestine fluid simulants following sequential digestion of six selected pristine MNP variants (without prior loading with PAHs) indicated that none of the three investigated PAHs were released (**Section S6** and **Figure S7**). However, for Tire Rubber particles, pyrene was detected in both fluid simulants. It is noteworthy that Tire Rubber is the only polymer investigated in this study that has been exposed to the environment for extended periods. All other MNPs are therefore unlikely to have accumulated POPs including PAHs [27, 67].

4. ASSESSMENT OF THE CONTRIBUTION OF MICROPLASTICS TO TOTAL HUMAN DIETARY PAH EXPOSURE

Understanding the contribution of MNPs as carriers of POPs such as PAHs is vital to assessing the potential health risk posed by human exposure to MNPs. Released PAHs could become translocated across the GI barriers via the gut epithelial cells, among other pathways [23, 68], and might become distributed across the body or accumulate in specific tissues [19]. To provide some insights into the contribution of microplastics to the overall human PAH intake, we estimated the maximum daily intake (MDI) of PAHs from MNPs using **Equation 4** [23, 69].

$$MDI\ (\mu g/kg\ bw) = \frac{C_{PAH}\ (\mu g/g)\ x\ M_{ingest}\ (g)\ x\ Bioac_{SI}\ (\%)}{BW\ (kg\ bw)\quad 140} \qquad (4)$$

Regarding the concentration of PAHs sorbed to MNPs, C_{PAH}, the values shown in **Table 1** were utilized, which represent the equilibrium sorption achieved in our previous study with realistic aqueous PAH concentrations in the ng/L range [36]. Notably, the resulting PAH loads (44–95 µg/g) are within the range of total PAH concentrations (3.4–120 µg/g) quantified from MNPs collected from the environment [44]. For the mass of ingested MNPs, M_{ingest}, a real-life scenario estimate of $4.1 \cdot 10^{-6}$ g/capita/day [70] was used. This was calculated as the 97.5th percentile of MNP intake from air, eight widely consumed food types, two widely consumed fruits and four popular vegetables [70] (see **Section S7** for a detailed analysis). $Bioac_{SI}$ is the bioaccessible fraction of PAHs released from MNPs into the small intestine, where absorption of nutrients but also of contaminants predominantly takes place. This corresponds to the experimentally determined cumulative PAH release in the small intestine fluid simulant (also containing the preceeding saliva and gastric fluid simulants, see **Figure 3** for B[*a*]P and **Figure 4** for Anth and DB[*a,l*]P). Previous assessments of the contribution of MNPs to human chemical exposure either assumed 100 % bioaccessibility of sorbed chemicals [23, 40] or utilized probabilistically modeled values [70]. We applied an average body weight *BW* of 70 kg in our exposure assessment.

As depicted in **Table 2**, the estimated MDI values of the three PAHs from the different MNP variants investigated in this study range from 0.2–2.4 pg/kg bw/day. These results allowed to estimate the individual contributions to the total human dietary PAH intake TI_{cont} (%) according to **Equation 5**,

$$TI_{cont}\ (\%) = \frac{MDI\ (pg/kg\ bw/day)}{TI\ (pg/capita/day)} \text{x}\ BW\ (kg\ bw) \text{x}\ 100\ (\%) \qquad (5)$$

where *TI* is the median dietary intake of PAHs by European adults [71]. *TI* values of 0.34, 0.17, and 0.63 µg/capita/day [71] were utilized for Anth, B[*a*]P, and DB[*a,l*]P, respectively (see **Section S7** for details).

PAH	MNPs	estimated maximum daily human PAH intake (MDI) from ingested MNPs (pg/kg bw/day)	contribution of MNP intake to total daily human dietary PAH exposure (TI_{cont})
B[*a*]P	PA-6_7	2.36	0.10 %
	PA-6_42	0.87	0.04 %
	PA-12	0.57	0.02 %
	LDPE_84	0.74	0.03 %
	PMMA_7	0.51	0.02 %
	TPU est_alip	0.63	0.03 %
	TPU est arom	0.53	0.02 %
	TPU eth_arom	0.46	0.02 %
	TPU eth_alip	0.40	0.02 %
	Tire Rubber	0.37	0.02 %
	PU_binder 1C	0.17	0.01 %
DB[*a,l*]P	PA-6_42	1.40	0.02 %
	LDPE_84	1.85	0.02 %
Anth	PA-6_42	0.92	0.02 %
	LDPE_84	0.17	< 0.01 %

Table 2: Estimated maximum daily human intake (MDI) of PAHs from ingested PAH-contaminated MNPs and contributions to the total daily dietary PAH exposure (TI_{cont}).

As shown in **Table 2**, the estimated relative contribution of MNPs as PAH carriers to the total dietary PAH exposure under realistic scenarios is very small, with the highest contribution estimated at 0.1 % for PA-6_7. However, uncertainties remain especially related to the magnitude of MNP exposure, which could become significant at local hotspots [72, 73]. Here, environmental MNP concentrations can be several orders of magnitude higher than the general estimate [74]. Although it is unclear to what extent this elevates the MNP uptake via food consumption and inhalation, the contribution of MNPs as carriers of ubiquitous PAHs could be significantly augmented if the exposure scenario involves a local source of PAH

pollution. Depending on the assumed MNP uptake [75] and PAH loadings, the calculated contribution of MNPs as carriers of PAHs can increase to values far exceeding the estimated human PAH uptake. Nevertheless, based on the currently available knowledge on microplastic ingestion, our study suggests that this contribution is very small (~ 0.1 %).

5. CONCLUSIONS

In this study, the desorption of PAHs from a variety of polydisperse MNP variants, including photo-aged materials, was investigated via a physiology-based sequential in-vitro digestion model based on the DIN 19738 standard. Using environmentally-relevant loadings of B[*a*]P as a representative PAH, a cumulative release in the range of 21–29 % was observed for three different MNPs (PA-6_42, TPU_est_arom and LDPE_84) after sequential passage through all four investigated fluid simulants. This emphasizes that the release of these toxicologically relevant POPs from microplastic particles upon ingestion can indeed occur to a significant extent.

When comparing the desorption of B[*a*]P from eleven different microplastic materials down to the small intestinal phase, ten of them showed moderate CRDs in the range of 4–19%, with PA-6_7 being an exception (CRD: 51 %). Presumably, the high-water absorption capacity of this polymer facilitated enhanced transport of bulk-bound B[*a*]P to the particle surface. Photo-aging of MNPs composed of TPU or PA-6 had no significant effect on desorption, despite chemical alteration of the polymer surfaces was observed via FTIR-spectroscopy. This further highlights the predominant contribution of bulk desorption of B[*a*]P for these particles.

In addition to B[*a*]P, the sequential desorption of Anth and DB[*a,l*]P into the small intestinal fluid simulant was studied for PA-6 and LDPE MNPs. The degree of desorption varied based on both the type of PAH and the MNP material employed. DB[*a,l*]P, for example, exhibited the strongest desorption from both MNPs, presumably resulting from its predominant adsorption

to the particle surfaces. B[*a*]P and Anth showed less but varying desorption, possibly due to different modes of transport from the bulk to the particle surface for the two polymers.

Finally, we estimated the contribution of MNPs as PAH carriers to the total human dietary PAH exposure to be very small (≤ 0.1 %). Future studies will therefore investigate the leaching of chemical additives and non-intentionally added substances from real-life MNPs in human gastrointestinal fluid simulants.

FUNDING

This work was funded by the BMBF (German Federal Ministry of Education and Research) project entitled InnoMat.Life – Innovative materials: safety in lifecycle, with funding numbers 03XP0216A (BfR) and 03XP0216X (BASF).

AUTHOR CONTRIBUTIONS

AR and AH conceptualized the study. EEE (FT-IR, PAH loading, in-vitro digestion, data analysis) and PMP (SEM, particle size) performed the experiments for this study. EEE and AR wrote the manuscript with contributions from AH, WW, and PP. AR and AH supervised the study. All authors read and approved the final manuscript.

NOTES

The authors declare no competing financial interest. Some of the authors are employees of BASF, a company producing and marketing polymers, including plastics.

ACKNOWLEDGEMENT

This study was supported by the German Federal Institute for Risk Assessment (BfR). We thank Klaudia Michna for her dedicated technical assistance with the GC-MS instrument.

ABBREVIATIONS

Anth: Anthracene

B[*a*]P: Benzo[*a*]pyrene

BET: Brunauer-Emmett-Teller

CRD: Cumulative relative desorption

DB[*a,l*]P: Dibenzo[*a,l*]pyrene

DIN: Deutsches Institut für Normung

FAO: Food and Agriculture Organization

FTIR: Fourier transform infrared

GIT: Gastrointestinal tract

GI: Gastrointestinal

GC-MS: Gas chromatography-mass spectrometry

HCl: Hydrochloric acid

LOD: Limit of detection

LDPE: Low-density polyethylene

MDI: Maximum daily intake

MNP: Micro- and nanoplastics

PA: Polyamide

PAH: Polycyclic aromatic hydrocarbon

POP: Persistent organic pollutant

PMMA: Polymethyl methacrylate

WHO: World Health Organization

NaOH: Sodium hydroxide

UV: Ultraviolet

SD: Standard deviation

SEM: Scanning electron microscopy.

T_g: glass transition temperature

TI: Total intake

TPU: Thermoplastic polyurethane

SUPPORTING INFORMATION

Size distribution of MNPs investigated in this study (Table S1); Selected physico-chemical properties of PAH sorbates used in this study (Table S2); Scanning electron microscopy (SEM) and particle size characterization (Section S1); Analysis of PAH concentrations in MNPs (Section S2); Preparation of the gastrointestinal fluid simulants (Section S3); Quantification of PAHs via GC-MS (Section S4); Characterization of selected MNPs by Fourier transform infrared (FT-IR) spectroscopy (Section S5); Quality control and release of PAHs from unloaded MNPs (Section S6); Estimates of the daily intakes of MNPs and PAHs (Section S7).

REFERENCES

1. Lim, X., *Microplastics are everywhere - but are they harmful?* Nature, 2021. **593**(7857): p. 22-25.

2. Ageel, H.K., S. Harrad, and M.A. Abdallah, *Occurrence, human exposure, and risk of microplastics in the indoor environment.* Environ Sci Process Impacts, 2022. **24**(1): p. 17-31.
3. Lebreton, L. and A. Andrady, *Future scenarios of global plastic waste generation and disposal.* Palgrave Communications, 2019. **5**(1).
4. Kieran D. Cox, Garth A. Covernton, Hailey L. Davies, John F. Dower, Francis Juanes, and Sarah E. Dudas, *Human Consumption of Microplastics.* Environ Sci Technol, 2019. **53**(12): p. 7068-7074.
5. Albert A. Koelmans, Nur Hazimah Mohamed Nor, Enya Hermsen, Merel Kooi, Svenja M. Mintenig, Jennifer De France, *Microplastics in freshwaters and drinking water: Critical review and assessment of data quality.* Water Res, 2019. **155**: p. 410-422.
6. Gea Oliveri Conti, Margherita Ferrante, Mohamed Banni, Claudia Favara, Ilenia Nicolosi, Antonio Cristaldi, Maria Fiore, Pietro Zuccarello, *Micro- and nano-plastics in edible fruit and vegetables. The first diet risks assessment for the general population.* Environ Res, 2020. **187**: p. 109677.
7. Gurusamy Kutralam-Muniasamy, Fermín Pérez-Guevara, I. Elizalde-Martínez, V.C. Shruti, *Branded milks - Are they immune from microplastics contamination?* Sci Total Environ, 2020. **714**: p. 136823.
8. V.C. Shruti, Fermín Pérez-Guevara, I. Elizalde-Martínez, Gurusamy Kutralam-Muniasamy, *First study of its kind on the microplastic contamination of soft drinks, cold tea and energy drinks - Future research and environmental considerations.* Sci Total Environ, 2020. **726**: p. 138580.
9. Yinan Li, Lin Peng, Jianxin Fu, Xueli Dai and Guoqing Wang, *A microscopic survey on microplastics in beverages: the case of beer, mineral water and tea.* Analyst, 2022. **147**(6): p. 1099-1105.
10. Karami A, Golieskardi A, Keong Choo C, Larat V, Galloway TS, Salamatinia B, *The presence of microplastics in commercial salts from different countries.* Sci Rep, 2017. **7**: p. 46173.
11. Makhdoumi, P., H. Hossini, and M. Pirsaheb, *A review of microplastic pollution in commercial fish for human consumption.* Rev Environ Health, 2022.
12. Schwabl P, Köppel S, Königshofer P, Bucsics T, Trauner M, Reiberger T, Liebmann B., *Detection of Various Microplastics in Human Stool: A Prospective Case Series.* Ann Intern Med, 2019. **171**(7): p. 453-457.
13. Luqman, A.; Nugrahapraja, H.; Wahyuono, R.A.; Islami, I.; Haekal, M.H.; Fardiansyah, Y.; Putri, B.Q.; Amalludin, F.I.; Rofiqa, E.A.; Götz, F. and Wibowo, A.T, *Microplastic*

Contamination in Human Stools, Foods, and Drinking Water Associated with Indonesian Coastal Population. Environments, 2021. **8**(12).

14. Gossmann, I., R. Sussmuth, and B.M. Scholz-Bottcher, *Plastic in the air?! - Spider webs as spatial and temporal mirror for microplastics including tire wear particles in urban air.* Sci Total Environ, 2022. **832**: p. 155008.
15. Rachid Dris, Johnny Gasperi, Cécile Mirande, Corinne Mandin, Mohamed Guerrouache, Valérie Langlois, Bruno Tassin, *A first overview of textile fibers, including microplastics, in indoor and outdoor environments.* Environ Pollut, 2017. **221**: p. 453-458.
16. Amato-Lourenço LF, Carvalho-Oliveira R, Júnior GR, Dos Santos Galvão L, Ando RA, Mauad T, *Presence of airborne microplastics in human lung tissue.* J Hazard Mater, 2021. **416**: p. 126124.
17. Vianello, A., Jensen, R.L., Liu, L and Jes Vollertsen, *Simulating human exposure to indoor airborne microplastics using a Breathing Thermal Manikin.* Sci Rep, 2019. **9**(1): p. 8670.
18. Johnny Gasperi, Stephanie L. Wright, Rachid Dris, France Collard, Corinne Mandin, Mohamed Guerrouache, Valérie Langlois, Frank J. Kelly, Bruno Tassin, *Microplastics in air: Are we breathing it in?* Current Opinion in Environmental Science & Health, 2018. **1**: p. 1-5.
19. Wright, S.L. and F.J. Kelly, *Plastic and Human Health: A Micro Issue?* Environ Sci Technol, 2017. **51**(12): p. 6634-6647.
20. Catarino AI, Macchia V, Sanderson WG, Thompson RC, Henry TB, *Low levels of microplastics (MP) in wild mussels indicate that MP ingestion by humans is minimal compared to exposure via household fibres fallout during a meal.* Environ Pollut, 2018. **237**: p. 675-684.
21. W.H.O, *Dietary and inhalation exposure to nano- and microplastic particles and potential implications for human health*. 2022: Geneva.
22. Lehner R, Weder C, Petri-Fink A, Rothen-Rutishauser B., *Emergence of Nanoplastic in the Environment and Possible Impact on Human Health.* Environ Sci Technol, 2019. **53**(4): p. 1748-1765.
23. Food Agriculture Organization (FAO), *Microplastics in fisheries and aquaculture. Status of knowledge on their occurrence and implications for aquatic organisms and food safety*. 2017.
24. Rostami, I. and A.L. Juhasz, *Assessment of Persistent Organic Pollutant (POP) Bioavailability and Bioaccessibility for Human Health Exposure Assessment: A Critical*

Review. Critical Reviews in Environmental Science and Technology, 2011. **41**(7): p. 623-656.

25. Teuten, E.L., et al., *Transport and release of chemicals from plastics to the environment and to wildlife.* Philos Trans R Soc Lond B Biol Sci, 2009. **364**(1526): p. 2027-45.
26. Chih-Feng Chen, Yun-Ru Ju, Yee Cheng Lim, Ning-Hsing Hsu, Kun-Tu Lu, Shu-Ling Hsieh, Cheng-Di Dong, Chiu-Wen Chen, *Microplastics and their affiliated PAHs in the sea surface connected to the southwest coast of Taiwan.* Chemosphere, 2020. **254**: p. 126818.
27. Chelsea M. Rochman, Eunha Hoh, Brian T. Hentschel, and Shawn Kaye, *Long-term field measurement of sorption of organic contaminants to five types of plastic pellets: implications for plastic marine debris.* Environ Sci Technol, 2013. **47**(3): p. 1646-54.
28. Xiangling Tan, Xubiao Yu, Liqi Cai, Jundong Wang, Jinping Peng, *Microplastics and associated PAHs in surface water from the Feilaixia Reservoir in the Beijiang River, China.* Chemosphere, 2019. **221**: p. 834-840.
29. Varjani, S.J., E. Gnansounou, and A. Pandey, *Comprehensive review on toxicity of persistent organic pollutants from petroleum refinery waste and their degradation by microorganisms.* Chemosphere, 2017. **188**: p. 280-291.
30. Corsini E, Luebke RW, Germolec DR, DeWitt JC., *Perfluorinated compounds: emerging POPs with potential immunotoxicity.* Toxicol Lett, 2014. **230**(2): p. 263-70.
31. Kumar M, Sarma DK, Shubham S, Kumawat M, Verma V, Prakash A, Tiwari R., *Environmental Endocrine-Disrupting Chemical Exposure: Role in Non-Communicable Diseases.* Front Public Health, 2020. **8**: p. 553850.
32. Bang, S.-Y., Y. Ha, and J.-H. Kwon, *Relative Importance of Microplastics as Vectors of Hydrophobic Organic Chemicals to Marine Fish and Seabirds.* Ocean Science Journal, 2021. **56**(4): p. 355-363.
33. Bakir, A., S.J. Rowland, and R.C. Thompson, *Enhanced desorption of persistent organic pollutants from microplastics under simulated physiological conditions.* Environ Pollut, 2014. **185**: p. 16-23.
34. Albert A. Koelmans, Adil Bakir, G. Allen Burton, and Colin R. Janssen, *Microplastic as a Vector for Chemicals in the Aquatic Environment: Critical Review and Model-Supported Reinterpretation of Empirical Studies.* Environ Sci Technol, 2016. **50**(7): p. 3315-26.
35. Huiying Guo, Xiaobo Zheng, Shuling Ru, Xiaojun Luo, Bixian Mai, *The leaching of additive-derived flame retardants (FRs) from plastics in avian digestive fluids: The significant risk of highly lipophilic FRs.* J Environ Sci (China), 2019. **85**: p. 200-207.

36. Emecheta, E. E., Borda, D. B., Pfohl, P. M., Wohlleben, W., Hutzler, C., Haase, A., & Roloff, A., *A comparative investigation of the sorption of polycyclic aromatic hydrocarbons to various polydisperse micro- and nanoplastics using a novel third-phase partition method.* Microplastics and Nanoplastics, 2022. **2**(1).
37. Ziccardi, L.M., et al., *Microplastics as vectors for bioaccumulation of hydrophobic organic chemicals in the marine environment: A state-of-the-science review.* Environ Toxicol Chem, 2016. **35**(7): p. 1667-76.
38. Xinlei Liu, Mehdi Gharasoo, Yu Shi, Gabriel Sigmund, Thorsten Hüffer, Lin Duan, Yongfeng Wang, Rong Ji, Thilo Hofmann, and Wei Chen, *Key Physicochemical Properties Dictating Gastrointestinal Bioaccessibility of Microplastics-Associated Organic Xenobiotics: Insights from a Deep Learning Approach.* Environ Sci Technol, 2020. **54**(19): p. 12051-12062.
39. Xiaojie Hu, Qing Yu, Michael Gatheru Waigi, Wanting Ling, Chao Qin, Jian Wang, Yanzheng Gao, *Microplastics-sorbed phenanthrene and its derivatives are highly bioaccessible and may induce human cancer risks.* Environ Int, 2022. **168**: p. 107459.
40. World Health Organization (W.H.O), *Microplastics in drinking-water*. 2019.
41. Pfohl, P., Roth, C., Meyer, L., Heinemeyer, U., Gruendling, T., Lang, C., Nestle, N., Hofmann, T., Wohlleben, W., & Jessl, S., *Microplastic extraction protocols can impact the polymer structure.* Microplastics and Nanoplastics, 2021. **1**(1).
42. Pfohl P, Bahl D, Rückel M, Wagner M, Meyer L, Bolduan P, Battagliarin G, Hüffer T, Zumstein M, Hofmann T, Wohlleben W, *Effect of Polymer Properties on the Biodegradation of Polyurethane Microplastics.* Environ Sci Technol, 2022. **56**(23): p. 16873-16884.
43. Pfohl P, Wagner M, Meyer L, Domercq P, Praetorius A, Hüffer T, Hofmann T, Wohlleben W, *Environmental Degradation of Microplastics: How to Measure Fragmentation Rates to Secondary Micro- and Nanoplastic Fragments and Dissociation into Dissolved Organics.* Environ Sci Technol, 2022. **56**(16): p. 11323-11334.
44. Lei Mai, Lian-Jun Bao, Lei Shi, Liang-Ying Liu, Eddy Y. Zeng, *Polycyclic aromatic hydrocarbons affiliated with microplastics in surface waters of Bohai and Huanghai Seas, China.* Environ Pollut, 2018. **241**: p. 834-840.
45. DIN 19738, *Soil quality - Bioaccessibility of organic and inorganic pollutants from contaminated soil material* 2017, Deutsches Institut fur Normung E.V. (DIN)
46. Yu, Y.Q. and J.Y. Yang, *Oral bioaccessibility and health risk assessment of vanadium(IV) and vanadium(V) in a vanadium titanomagnetite mining region by a*

whole digestive system in-vitro method (WDSM). Chemosphere, 2019. **215**: p. 294-304.

47. Zhang Y, Pignatello JJ, Tao S, Xing B, *Bioaccessibility of PAHs in Fuel Soot Assessed by an in Vitro Digestive Model with Absorptive Sink: Effect of Food Ingestion.* Environ Sci Technol, 2015. **49**(24): p. 14641-8.
48. Wu, J., J. Lu, and J. Wu, *Effect of gastric fluid on adsorption and desorption of endocrine disrupting chemicals on microplastics.* Frontiers of Environmental Science & Engineering, 2021. **16**(8).
49. Tao S, Li L, Ding J, Zhong J, Zhang D, Lu Y, Yang Y, Wang X, Li X, Cao J, Lu X, Liu W., *Mobilization of soil-bound residue of organochlorine pesticides and polycyclic aromatic hydrocarbons in an in vitro gastrointestinal model.* Environ Sci Technol, 2011. **45**(3): p. 1127-32.
50. Agnes G. Oomen, Adrienne J. A. M. Sips, John P. Groten, Dick T. H. M. Sijm, and Johannes Tolls, *Mobilization of PCBs and lindane from soil during in vitro digestion and their distribution among bile salt micelles and proteins of human digestive fluid and the soil.* Environmental Science & Technology, 2000. **34**(2): p. 297-303.
51. Ahrens, M.J., Hertz, J., Lamoureux, E. M., Lopez, G. R., McElroy, A. E., & Brownawell, B. J., *The role of digestive surfactants in determining bioavailability of sediment-bound hydrophobic organic contaminants to 2 deposit-feeding polychaetes.* Marine Ecology Progress Series, 2001. **212**: p. 145–157.
52. Masset, T., D. Ferrari, B. J., Dudefoi, W., Schirmer, K., Bergmann, A., Vermeirssen, E., Grandjean, D., Harris, L. C., & Breider, F., *Bioaccessibility of Organic Compounds Associated with Tire Particles Using a Fish In Vitro Digestive Model: Solubilization Kinetics and Effects of Food Coingestion.* Environ Sci Technol, 2022. **56**(22): p. 15607-15616.
53. Fonseca, M.R.J., *An Engineering Understanding of the Small Intestine*, in *School of Chemical Engineering*. 2011, The University of Birmingham.
54. Mohamed Nor, N.H. and A.A. Koelmans, *Transfer of PCBs from Microplastics under Simulated Gut Fluid Conditions Is Biphasic and Reversible.* Environ Sci Technol, 2019. **53**(4): p. 1874-1883.
55. Peng Liu, Xiaowei Wu, Haiyong Liu, Hanyu Wang, Kun Lu, Shixiang Gao, *Desorption of pharmaceuticals from pristine and aged polystyrene microplastics under simulated gastrointestinal conditions.* J Hazard Mater, 2020. **392**: p. 122346.
56. Sambale AK, Stanko M, Emde J, Stommel M., *Characterisation and FE Modelling of the Sorption and Swelling Behaviour of Polyamide 6 in Water.* Polymers (Basel), 2021. **13**(9).

57. Puffr, R. and J. Šebenda, *On the Structure and Properties of Polyamides. XXVII. The Mechanism of Water Sorption in Polyamides.* Journal of Polymer Science Part C: Polymer Symposia, 1967. **16**(1): p. 79-93.
58. Monson, L., M. Braunwarth, and C.W. Extrand, *Moisture absorption by various polyamides and their associated dimensional changes.* Journal of Applied Polymer Science, 2008. **107**(1): p. 355-363.
59. Reimschuessel, H.K., *Relationships on the effect of water on glass transition temperature and young's modulus of nylon 6.* Journal of Polymer Science: Polymer Chemistry Edition, 1978. **16**(6): p. 1229-1236.
60. Dlubek, G., F. Redmann, and R. Krause-Rehberg, *Humidity-induced plasticization and antiplasticization of polyamide 6: A positron lifetime study of the local free volume.* Journal of Applied Polymer Science, 2002. **84**(2): p. 244-255.
61. Hummel, Darius; Fath, Andreas; Hofmann, Thilo; Hüffer, Thorsten, *Additives and polymer composition influence the interaction of microplastics with xenobiotics.* Environmental Chemistry, 2021. **18**(3).
62. Rochman, C.M., *The Complex Mixture, Fate and Toxicity of Chemicals Associated with Plastic Debris in the Marine Environment*, in Bergmann, M., Gutow, L., Klages, M. (eds) *Marine Anthropogenic Litter*. 2015. p. 117-140.
63. Jang, M., et al., *Styrofoam Debris as a Source of Hazardous Additives for Marine Organisms.* Environ Sci Technol, 2016. **50**(10): p. 4951-60.
64. Lina Fu, Jing Li, Guoyu Wang, Yaning Luan, Wei Dai, *Adsorption behavior of organic pollutants on microplastics.* Ecotoxicol Environ Saf, 2021. **217**: p. 112207.
65. Satshi Endo, A.K., *Sorption of Hydrophobic Organic Compounds to Plastics in the Marine Environment: Equilibrium*, in *Hazardous Chemicals Associated with Plastics in the Marine Environment,* Takada, H., Karapanagioti, H.K. (eds), 2016, Springer International Publishing: Switzerland.
66. Huffer, T. and T. Hofmann, *Sorption of non-polar organic compounds by micro-sized plastic particles in aqueous solution.* Environ Pollut, 2016. **214**: p. 194-201.
67. Coffin S, Dudley S, Taylor A, Wolf D, Wang J, Lee I, Schlenk D, *Comparisons of analytical chemistry and biological activities of extracts from North Pacific gyre plastics with UV-treated and untreated plastics using in vitro and in vivo models.* Environ Int, 2018. **121**(Pt 1): p. 942-954.
68. Jonathan J Powell, Nuno Faria, Emma Thomas-McKay, Laetitia C Pele, *Origin and fate of dietary nanoparticles and microparticles in the gastrointestinal tract.* J Autoimmun, 2010. **34**(3): p. J226-33.

69. EFSA, *Presence of microplastics and nanoplastics in food, with particular focus on seafood*. 2016.
70. Nur Hazimah Mohamed Nor, Merel Kooi, Noël J. Diepens, and Albert A. Koelmans, *Lifetime Accumulation of Microplastic in Children and Adults.* Environ Sci Technol, 2021. **55**(8): p. 5084-5096.
71. European commision health and consumer protection, *Polycyclic Aromatic Hydrocarbons – Occurrence in foods, dietary exposure and health effects*. 2002.
72. Norén, F., *Small plastic particles in Coastal Swedish waters.* 2007, KIMO Sweden.
73. Bingwen Chai, Qiang Wei, Yingzhe She, Guining Lu, Zhi Dang, Hua Yin, *Soil microplastic pollution in an e-waste dismantling zone of China.* Waste Manag, 2020. **118**: p. 291-301.
74. Nanna B Hartmann, Sinja Rist, Julia Bodin, Louise HS Jensen, Stine N Schmidt, Philipp Mayer, Anders Meibom, Anders Baun, *Microplastics as vectors for environmental contaminants: Exploring sorption, desorption, and transfer to biota.* Integr Environ Assess Manag, 2017. **13**(3): p. 488-493.
75. Kala Senathirajah, Simon Attwood, Geetika Bhagwat, Maddison Carbery, Scott Wilson, Thava Palanisami, *Estimation of the mass of microplastics ingested - A pivotal first step towards human health risk assessment.* J Hazard Mater, 2021. **404**(Pt B): p. 124004.
76. Mudie DM, Murray K, Hoad CL, Pritchard SE, Garnett MC, Amidon GL, Gowland PA, Spiller RC, Amidon GE, Marciani L., Quantification of gastrointestinal liquid volumes and distribution following a 240 mL dose of water in the fasted state. Mol Pharm, 2014 .**11**(9):3039-47.

6.6. SUPPLEMENTARY INFORMATION FOR MANUSCRIPT 2

Desorption of Polycyclic Aromatic Hydrocarbons from Microplastics in Human Gastrointestinal Fluid Simulants – Implications for Exposure Assessment

Emeka Ephraim Emecheta[1], Patrizia Marie Pfohl[2], Wendel Wohlleben[2], Andrea Haase[3*], Alexander Roloff[3*]

Authors' affiliations

[1]University of Bayreuth, Bayreuth Center for Ecology and Environmental Research (BayCEER), Dr.Hans-Frisch-Str.1-3, 95448 Bayreuth, Germany

[2]BASF SE, Carl-Bosch-Str. 38, 67056 Ludwigshafen, Germany

[3]German Federal Institute for Risk Assessment, Department of Chemical and Product Safety, Max-Dohrn-Straße 8-10, 10589 Berlin, Germany

Number of pages 24

Number of figures 7

Number of tables 4

TABLE OF CONTENTS

TABLE S1: SIZE DISTRIBUTION OF MNPS INVESTIGATED IN THIS STUDY, AS REPORTED in our previous work [1].

	size distribution (µm)			
MNPs	**D×10**	**D×50**	**D×90**	**supplier**
PA-6_7	2.3	6.9	13.5	BASF
PA-6_42	13.7	42.2	75.3	BASF
PA-12_44	34.4	44.3	57.0	BASF
PU_1C_arom	82.8	200.0	354.0	BASF
TPU_est arom	142.0	254.0	418.0	BASF
TPU_est alip	143.0	262.0	440.0	BASF
TPU_eth arom	128.0	246.0	413.0	BASF
TPU_eth alip	152.0	267.0	442.0	BASF
LDPE_84	19.1	84.0	188.0	LyondellBasell
Tire Rubber	61.8	130.0	233.0	MRH mbH
PMMA_6	2.2	6.2	11.6	Polysciences

TABLE S2: SELECTED PHYSICO-CHEMICAL PROPERTIES OF PAH SORBATES USED IN THIS STUDY.

compound/chemical structure	molecular weight (g/mol)	aqueous solubility (µg/L) [2]	octonal-water partition coefficient (log $K_{o/w}$) [3]	molar volume (cm^3/mol) [4]
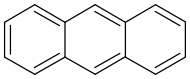 anthracene	178.2	73.0	4.45	158
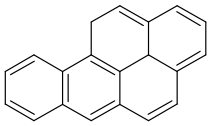 benzo[*a*]pyrene	252.3	3.8	6.05	196
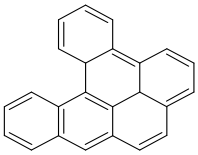 dibenzo[*a,l*]pyrene	302.4	_	7.71	230

SECTION S1: SCANNING ELECTRON MICROSCOPY (SEM) AND PARTICLE SIZE CHARACTERIZATION

A Gemini 500 Scanning Electron Microscopy (Zeiss, Oberkochen, Germany) was utilized to characterize the morphology of the MNPs following a previously described procedure [5]. The SEM instrument was operated at 3 kV, using secondary electrons for improved topography contrast. The MNP particles were fixed onto Leit-C-plast tape on a standard SEM stub and coated with 8 nm platinum.

Particle size distributions of MNPs were measured via laser diffraction using a Malvern Mastersizer 3000 instrument (Kassel, Germany). The instrument was operated at a rotation speed of 2000 rpm. MNP particles were measured in 10 replicates in dispersion medium containing water and two drops of Nekanil surfactants.

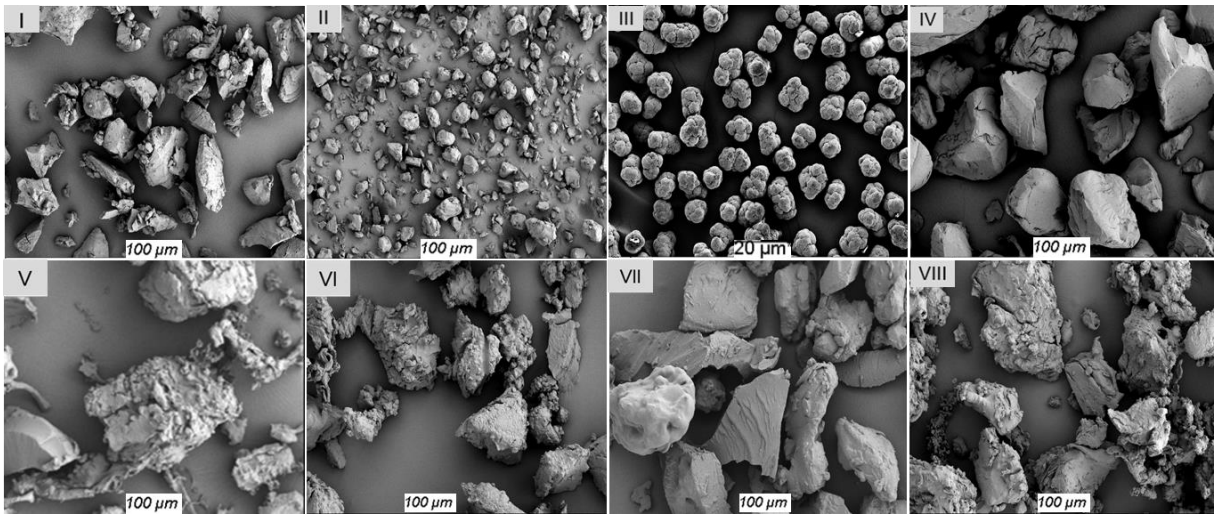

FIGURE S1: SHAPES AND SIZES OF SELECTED MNP MATERIALS USED FOR DESORPTION EXPERIMENTS. Images were acquired using scanning electron microscopy (SEM): (I) Tire Rubber, (II) PA-6_42, (III) PA-12_44, (IV) PU_arom_1C, (V) LDPE_84, (VI) TPU_ester_arom, (VII) TPU_ether_arom, (VIII) TPU_ether_alip. MNPs were cryo-milled and therefore varied in size and shape.

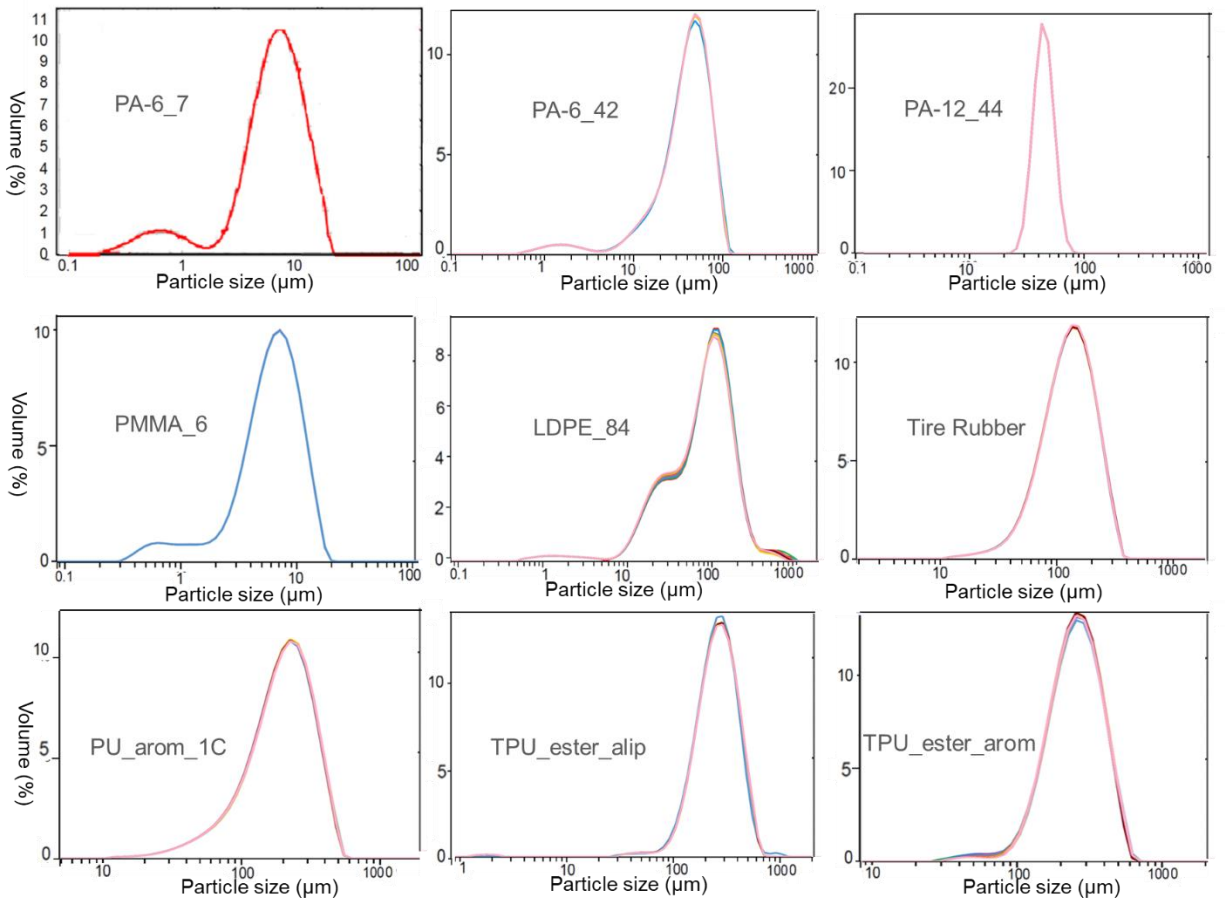

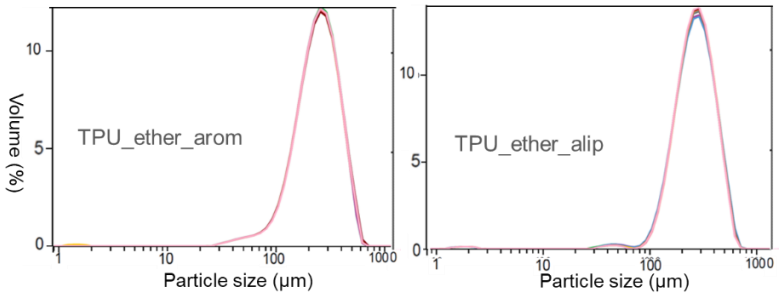

Figure S2: Full size distribution range of the polydisperse MNPs used in this study.

SECTION S2: ANALYSIS OF PAH CONCENTRATIONS IN MNPS

The amount of Anth and B[*a*]P loaded onto the MNPs were calculated via mass balance using the measured aqueous concentrations of the filtrates after loading (duplicate samples). Shortly before filtration, the mixtures were spiked with internal standard (300 ng Anth-d_{10} for Anth, 100 ng B[*a*]P-d_{12} for B[*a*]P) and immediately filtrated. Spiking the deuterated internal standards before filtration corrects for possible losses due to sorption to the microfiber filter [1]. The filtrates were then extracted by five minutes vigorous shaking with 2×100 mL hexane. The hexane extracts were concentrated to < 200 µL using a Rotavapor system. Final volumes of 200 µL (B[*a*]P) and 1000 µL (Anth) were re-constituted with hexane using a calibrated volumetric flask and transferred to GC-vials for GC-MS analysis. Quantification was performed using six-point calibrations of 25, 100, 200, 300, and 400 µg/L.

To directly quantify the amounts of PAHs sorbed to the MNPs, loaded MNPs (1.5 mg) were dissolved in 1 mL of 88% formic acid (PA-6_42, PA-6_7) or xylenes (LDPE_84, TPU_est arom, TPU_eth arom, TPU_est alip, TPU_eth arom) at 70°C. Thereafter, internal standard (500 ng DB[*a,i*]P for DB[*a,l*]P-loaded MNPs, 100 ng B[*a*]P-d_{12} for B[*a*]P-loaded MNPs) was spiked into the vials, the mixtures were sealed and sonicated for 15 minutes (70–80°C). For PA-6 MNPs, DB[*a,l*]P or B[*a*]P in the formic acid solution were extracted with 2×0.5 mL hexane.

For quantification, calibrations with 10, 40, 80, 120, 160 and 200 ng of DB[*a,l*]P or B[*a*]P and internal standard (500 ng DB[*a,i*]P for DB[*a,l*]P-loaded MNPs, 100 ng B[*a*]P-d_{12} for B[*a*]P-

loaded MNPs) were prepared by spiking the respective amounts into 1.5 mL vials containing 1 mL of either hexane or xylenes. The calibration solutions were sealed and sonicated under the same conditions as the samples. 1 µL of each sample was analyzed by liquid injection into the GC-MS system. The results of all quantification experiments are summarized in **Table 1** in the manuscript.

SECTION S3: PREPARATION OF THE GASTROINTESTINAL FLUID SIMULANTS

The digestive fluid simulants were freshly prepared for each experiment. The fluid simulant for each compartment was prepared by weighing an appropriate mass of each component (mg) into 1 L Duran glass vials, followed by the addition of an appropriate volume of water (mL), see **Table S3**. The resulting mixture was simultaneously homogenized and pre-heated to 37 °C by 15 mins incubation on an IKA magnetic stirring plate (Kucera GmbH, Innsbruck, Austria) operated at 750 rpm. The pH of the pre-heated mixture was adjusted to specifications by the additions of a few drops of either 10 M HCl or NaOH. The pH was monitored with a pH-meter (Knick 765 Calimatic, Berlin, Germany).

TABLE S3: COMPOSITION OF THE GASTROINTESTINAL FLUID SIMULANTS USED IN THIS STUDY FOR IN VITRO DIGESTION. CONCENTRATIONS OF INDIVIDUAL COMPOUNDS ARE REPORTED IN MG/ML.

	Composition of the gastrointestinal fluid simulants (mg/mL)			
Components	**Saliva**	**Gastric**	**Small intestine**	**Large intestine**
Sodium chloride	1.5	4.2		-
Calcium chloride dihydrate	0.5	-	0.5	-
Sodium sulfate	1.8	-		-
Potassium chloride	1.5	1.0	0.3	-
Potassium dihydrogen phosphate	2.0	0.4	-	-
Sodium thiocyanate	0.5	-	-	-
Sodium carbonate	0.5	-	1.0	-
Magnesium chloride hexahydrate	-	-	0.2	-
Bile salts	-	-	9.0	-
Urea	0.3	-	0.3	-
Uric acid	0.3	-	-	-
α-Amylase	0.8	-	-	-
Bovine serum albumin (BSA)	-	10.0	-	-
Pepsin	-	1.4	-	-
Mucin	-	4.3	-	-
Lipase	-	-	6.5	-
Pancreatin	-	-	9.0	-
Trypsin	-	-	0.3	-
δ - cellulase	-	-	-	0.2
δ - xylanase	-	-	-	3.5
δ - pectinase	-	-	-	4.7
β-glucanase	-	-		0.08
pH	6.50	1.75	6.75	8.30

SECTION S4: QUANTIFICATION OF PAHS VIA GC-MS

GC-MS analysis was performed with a GC-MS system consisting of a 6890 series gas chromatograph coupled with a 5975 series mass selective detector (both Agilent, Waldbronn, Germany). The GC was equipped with an MPS autosampler (Gerstel, Mühlheim, Germany). The GC oven was equipped with a DB-EUPAH column of 20 m length, an inner diameter of 0.18 mm, and a film thickness of 0.14 µm (J & W Scientific, Folsom, U.S.). Helium, with a purity of 99.999% (Linde, Pullach, Germany), was used as a carrier gas at a constant flow of 1.0 mL/min. The GC oven was operated with a temperature program starting at 60°C for 0.5 min,

followed by heating to 180°C at 25°C /min and finally to 320°C at 15°C/min, where the temperature was held for 10 min. The temperatures of the quadrupole, ion source, and MS transfer line were 150, 230, and 320°C, respectively. The MS detector was operated in combined selective ion monitoring (SIM) and scan mode with a scan rate of 15.99/s. A range of 50–500 m/z was monitored for data acquisition. During SIM data acquisition, two ions were monitored for each analyte: 178 and 176 m/z for Anth, 188 and 187 m/z for Anth-d_{10}, 252 and 250 m/z for B[*a*]P, 264 and 260 for B[*a*]P-d_{12}, 302 and 300 m/z for DB[*a,l*]P and DB[*a,i*]P as quantifier and qualifier ions, respectively. Each ion was monitored with a dwell time of 10 milliseconds. Quantification was performed by liquid injection of 1 µL of the extracts and calibration standards using the splitless mode of the cold injection system (CIS). The CIS inlet was operated at a temperature of 320°C at 12°C/s and held for 3 min.

TABLE S4: PARAMETERS OF METHOD- AND MATRIX-MATCHED CALIBRATIONS. The limit of detection (LOD) was calculated as 3.3 × standard deviation of the response (standard error of the regression coefficient) divided by the slope of the linear regression function, while the limit of quantification (LOQ) was calculated as 3 × LOD. Bioaccessible PAHs were quantified using the matrix- and method matched calibrations.

PAH	**fluid simulant for:**	**tested range (ng)**	**R^2**	**LOD (ng)**	**LOQ (ng)**
B[*a*]P	saliva	5–250	0.981	62	189
B[*a*]P	gastric	50–1000	0.986	81	245
B[*a*]P	small intestine	25–5000	0.987	175	530
B[*a*]P	large intestine	200–5000	0.997	315	954
Anth	small intestine	50–1500	0.997	111	337
DB[*a,l*]P	Small intestine	1000–6000	0.976	1290	3930

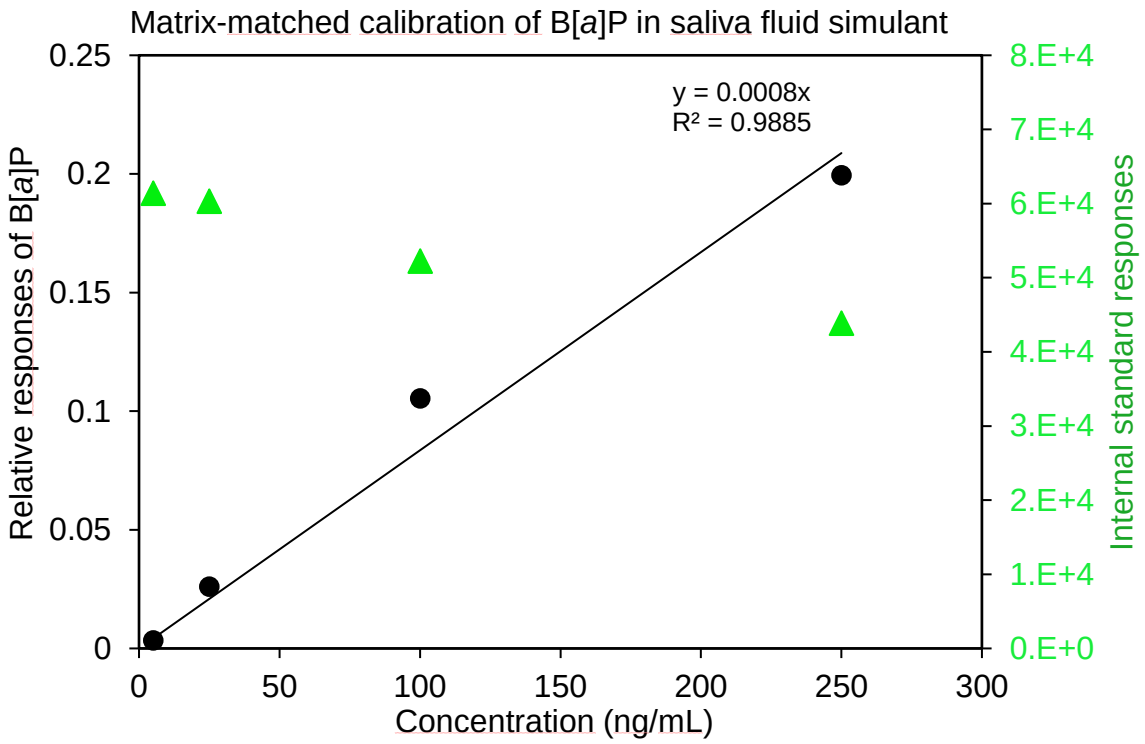
Matrix-matched calibration of B[a]P in saliva fluid simulant
y = 0.0008x
R² = 0.9885
Relative responses of B[a]P
Internal standard responses
Concentration (ng/mL)
0.25
0.2
0.15
0.1
0.05
0
8.E+4
7.E+4
6.E+4
5.E+4
4.E+4
3.E+4
2.E+4
1.E+4
0.E+0
0
50
100
150
200
250
300

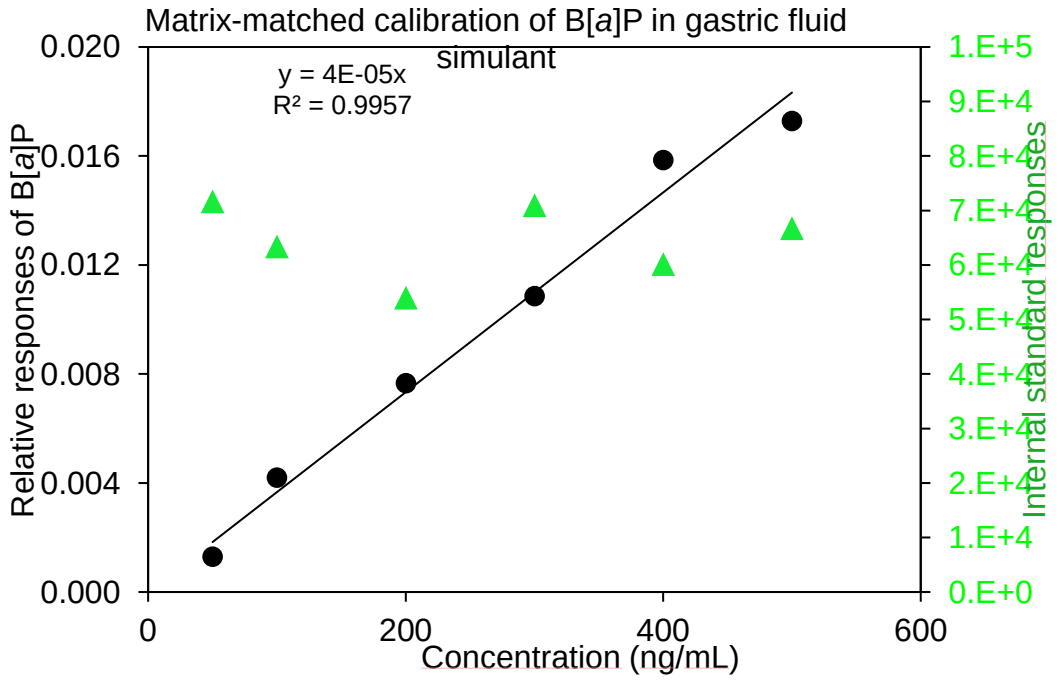
Matrix-matched calibration of B[a]P in gastric fluid simulant
y = 4E-05x
R² = 0.9957
Relative responses of B[a]P
Internal standard responses
Concentration (ng/mL)
0.020
0.016
0.012
0.008
0.004
0.000
1.E+5
9.E+4
8.E+4
7.E+4
6.E+4
5.E+4
4.E+4
3.E+4
2.E+4
1.E+4
0.E+0
0
200
400
600

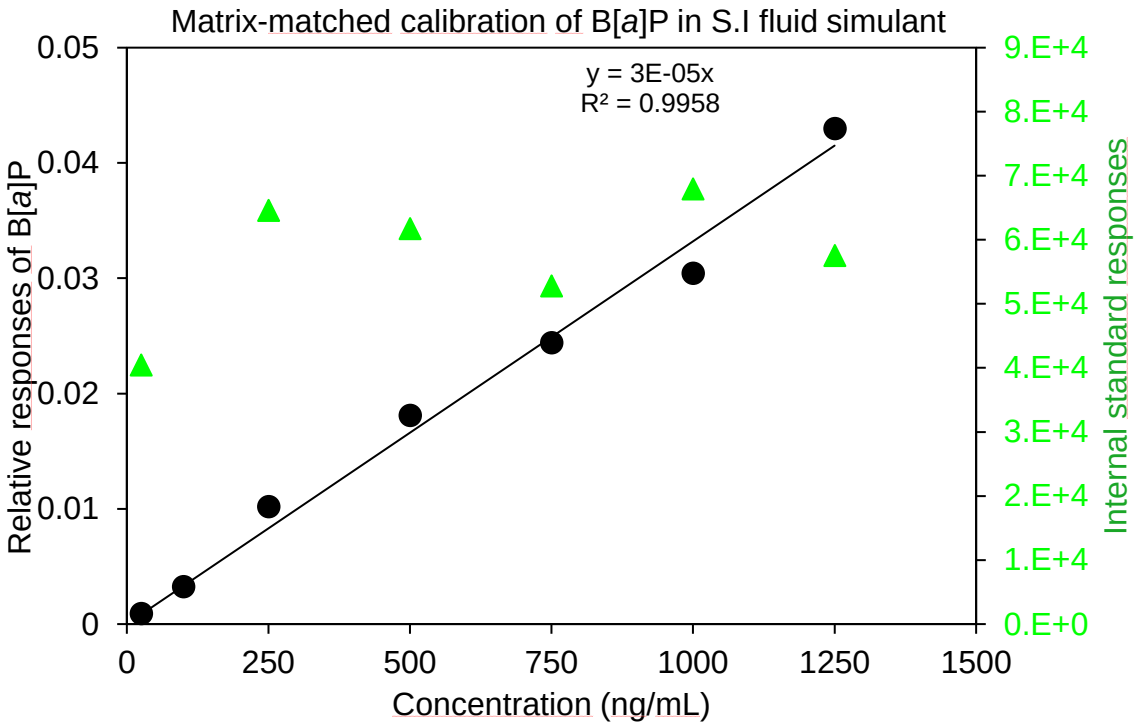
Matrix-matched calibration of B[a]P in S.I fluid simulant
y = 3E-05x
R² = 0.9958
Relative responses of B[a]P
Internal standard responses
Concentration (ng/mL)
0.05
0.04
0.03
0.02
0.01
0
9.E+4
8.E+4
7.E+4
6.E+4
5.E+4
4.E+4
3.E+4
2.E+4
1.E+4
0.E+0
0
250
500
750
1000
1250
1500

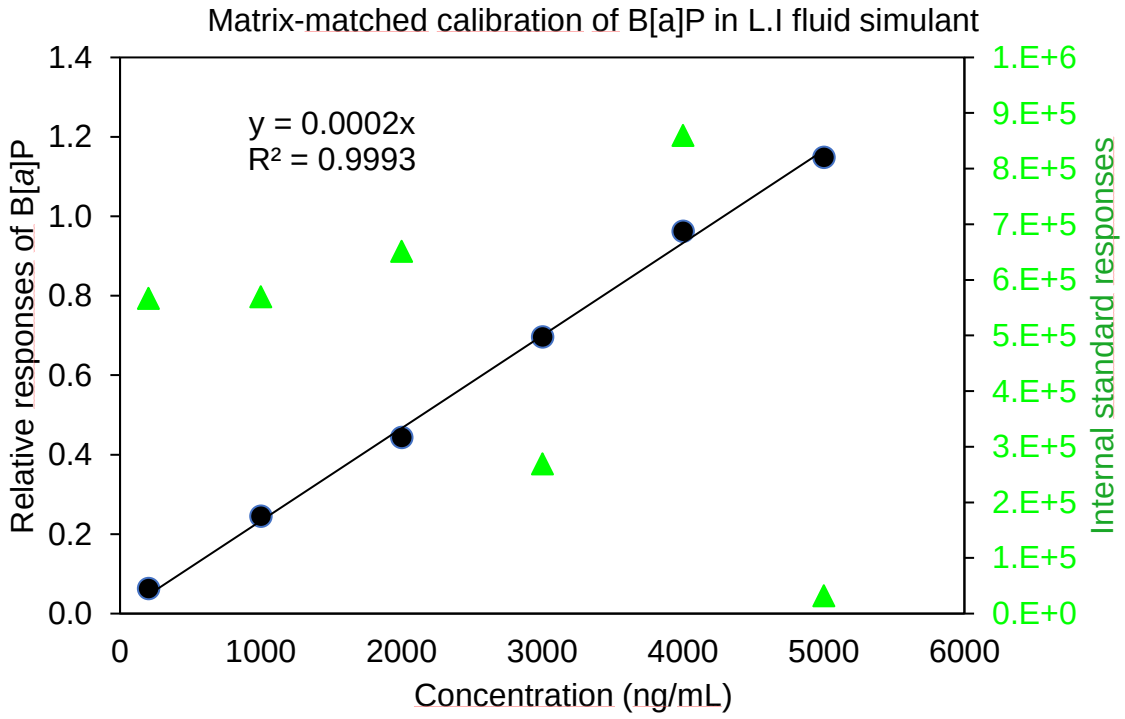
Matrix-matched calibration of B[a]P in L.I fluid simulant
y = 0.0002x
R² = 0.9993
Relative responses of B[a]P
Internal standard responses
Concentration (ng/mL)
1.4
1.2
1.0
0.8
0.6
0.4
0.2
0.0
1.E+6
9.E+5
8.E+5
7.E+5
6.E+5
5.E+5
4.E+5
3.E+5
2.E+5
1.E+5
0.E+0
0
1000
2000
3000
4000
5000
6000

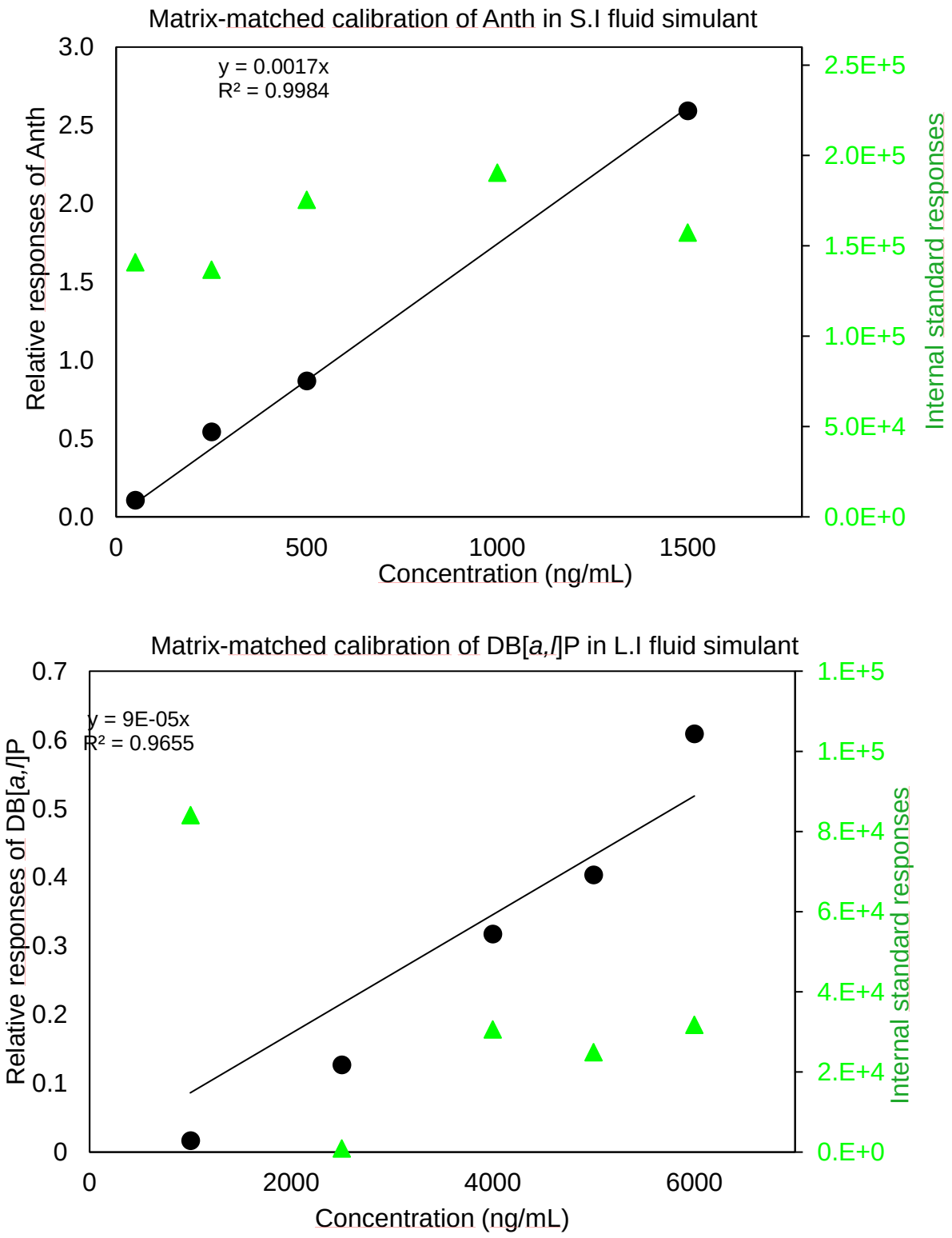

FIGURE S3: EXEMPLARY METHOD- AND MATRIX MATCHED CALIBRATIONS. Black circles correspond to the measured area ratios of the analyte and its corresponding internal standard. Green circles correspond to the measured areas of the corresponding internal standard.

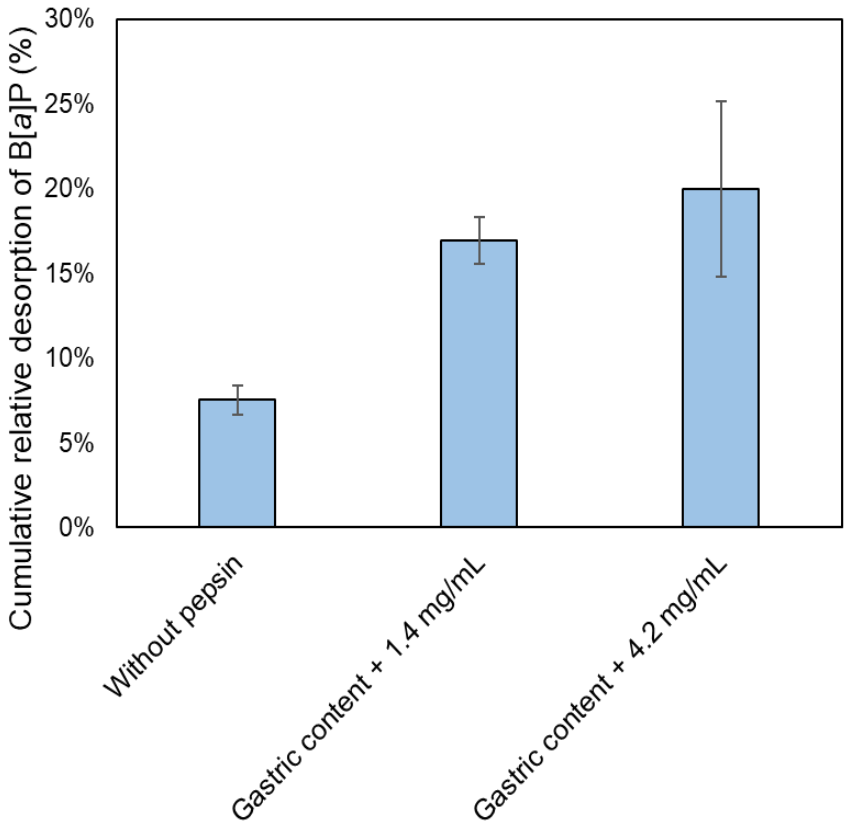

FIGURE S4: DESORPTION OF B[A]P FROM PA-6_42 IN GASTRIC FLUID SIMULANT WITHOUT PEPSIN, WITH 1.4 MG/ML PEPSIN (PHYSIOLOGICAL CONCENTRATION, BOTH REPLICATED FROM FIGURE 2B IN THE MANUSCRIPT) AND WITH 4.2 MG/ML PEPSIN.

SECTION S5: CHARACTERIZATION OF SELECTED MNPS BY FOURIER TRANSFORM INFRARED (FT-IR) SPECTROSCOPY

The photo-aged and non-aged MNP particles were analysed with a ThermoFisher IS50 FT-IR spectrometer (USA) to observe changes in the surface properties of the particles after photo-aging. The FT-IR spectra were recorded in the region of 4000–400 cm^{-1} with 32 scans at a resolution of 4 cm^{-1} and attenuated total reflectance (ATR) correction.

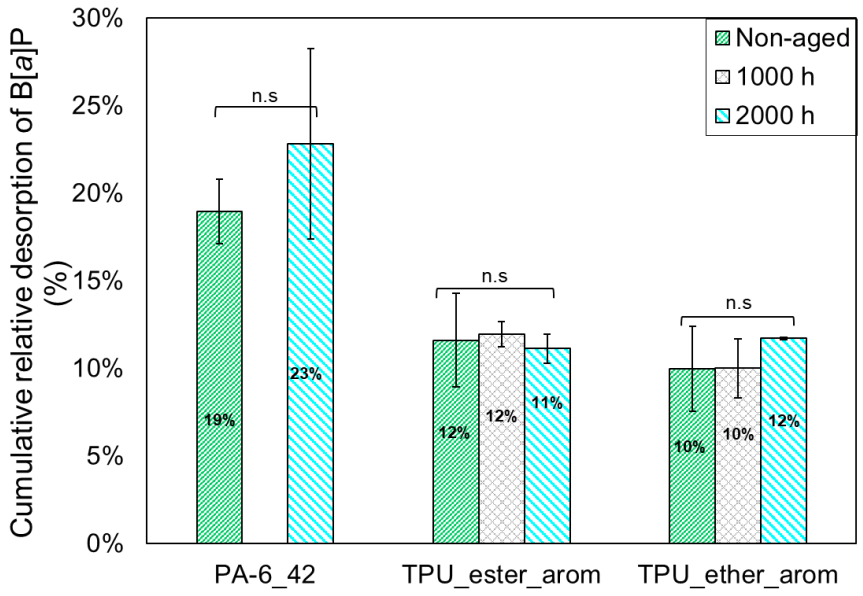

Figure S5: Comparison of CRD Values For B[A]P For aged and non-aged MNPs in the human small intestinal fluid simulants. Photo-aged PA-6_42 was loaded with B[a]P yielding 79.4 ± 0.3 ng/mg, while the aged TPUs were loaded with 78.3 ± 0.1 (TPU_est_arom_1000h), 56.0 ± 0.2 (TPU_est_arom_2000h), 70.5 ± 0.8 (TPU_ether_arom_1000h) and 54.0 ± 0.1 ng/mg, (TPU_ether_arom_2000h), respectively. The loading procedure replicates the method outlined for B[a]P in section 2.2.

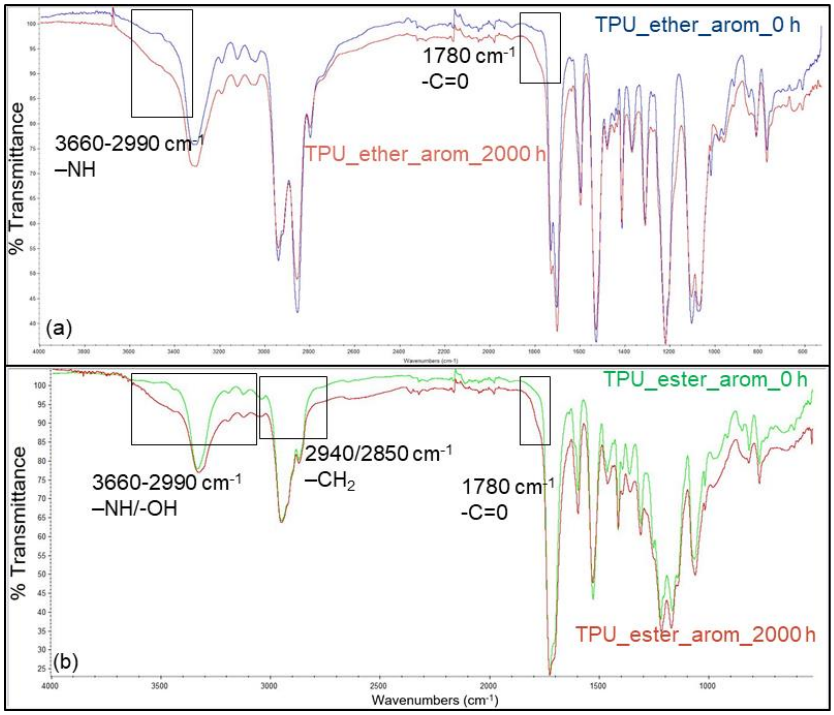

Figure S6: FT-IR spectra of 2000 h aged and non-aged MNPS (A): TPU_Ether_Arom and (B): TPU_Ester_Arom. FT-IR spectra of PA-6_42 have been shown in our previous work [1]

SECTION S6: QUALITY CONTROL AND RELEASE OF PAHS FROM UNLOADED MNPS

In order to monitor possible cross-contamination during handling, in vitro digestion, and solvent extractions, two replicate vials containing the fluid simulants (without MNPs) were incubated for each gastrointestinal phase alongside the samples and the matrix-matched calibration samples. Additionally, selected untreated MNP particles (without prior loading with PAHs) were incubated sequentially in all four fluid simulants. **Figure S7** depicts ion chromatograms of the three studied PAHs (Anth, B[*a*]P, DB[*a,l*]P) extracted from the respective total ion chromatograms obtained from the small and large intestine fluid simulants after sequential digestion of the pristine MNPs. As shown in **Figure S7a**, analytical standards of Anth, B[*a*]P, DB[*a,l*]P, and pyrene were detected at retention times of 24.45 min, 37.65 min, 39.25 min and 29.15 min, respectively, according to the GC-MS method.

For six selected untreated MNP variants digested in the sequential GI fluid simulants, the three PAHs investigated in this study for their desorption behaviors were not detected as shown by the extracted ion chromatograms (**Figure S7c–l**). This outcome was unsurprising as the MNP particles (except tire rubber) were obtained from polymer particles intended for additive manufacturing of plastic products, and not MNP particles collected from the environment.

For the tire rubber MNPs, which were cryomilled from end-of-life truck tire tread, pyrene, a 4-ring PAH, was detected in both fluid simulants (**Figure S7 i/j**). However, the trio of Anth, B[*a*]P, and DB[*a,l*]P was not detected.

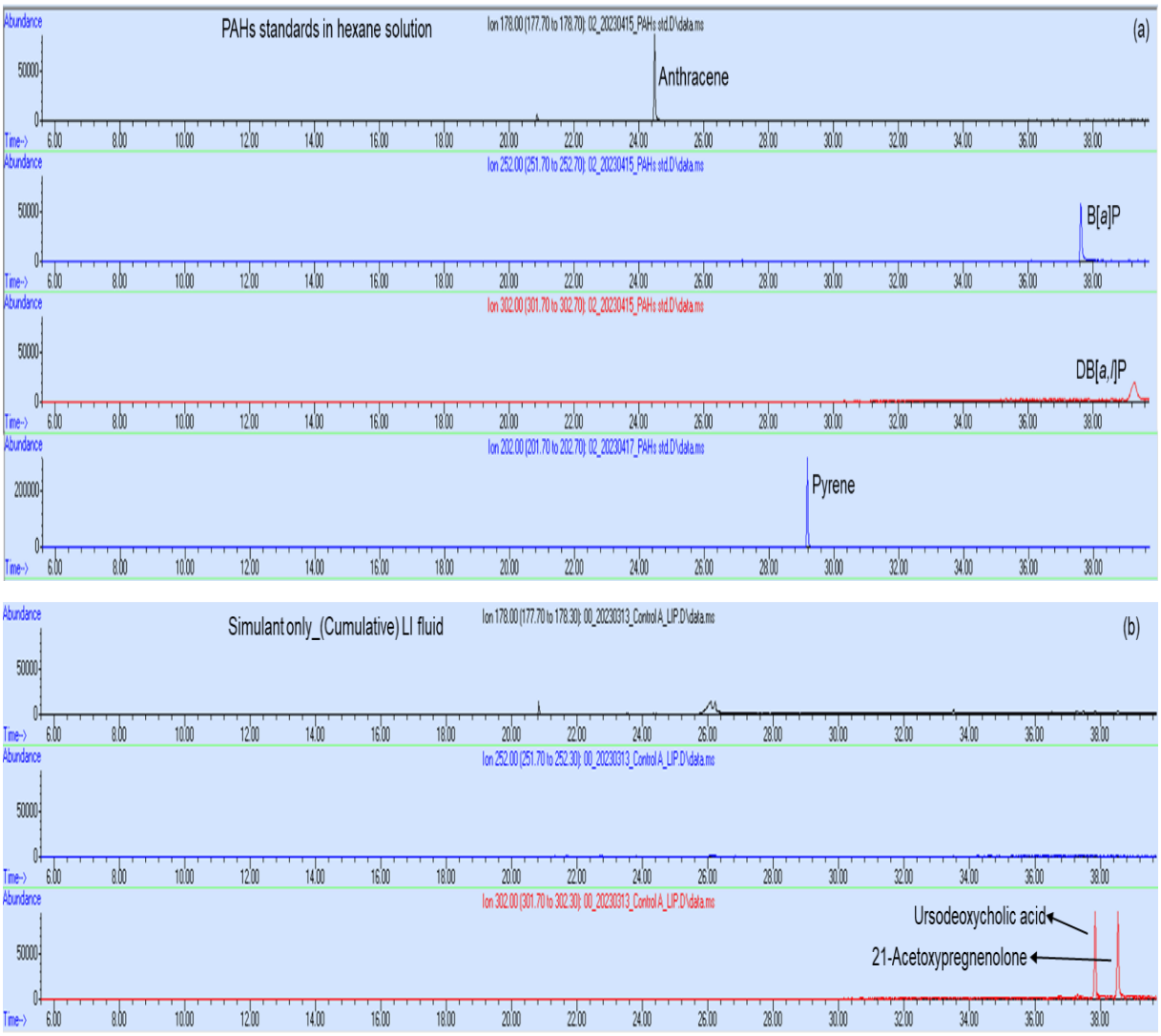

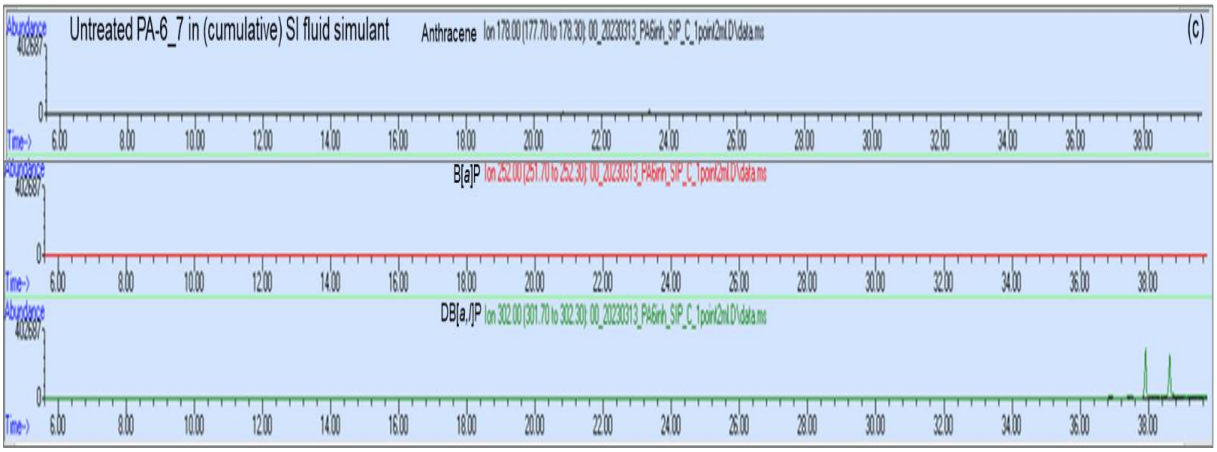
Untreated PA-6_7 in (cumulative) SI fluid simulant
Anthracene
B[a]P
DB[a,l]P
(c)

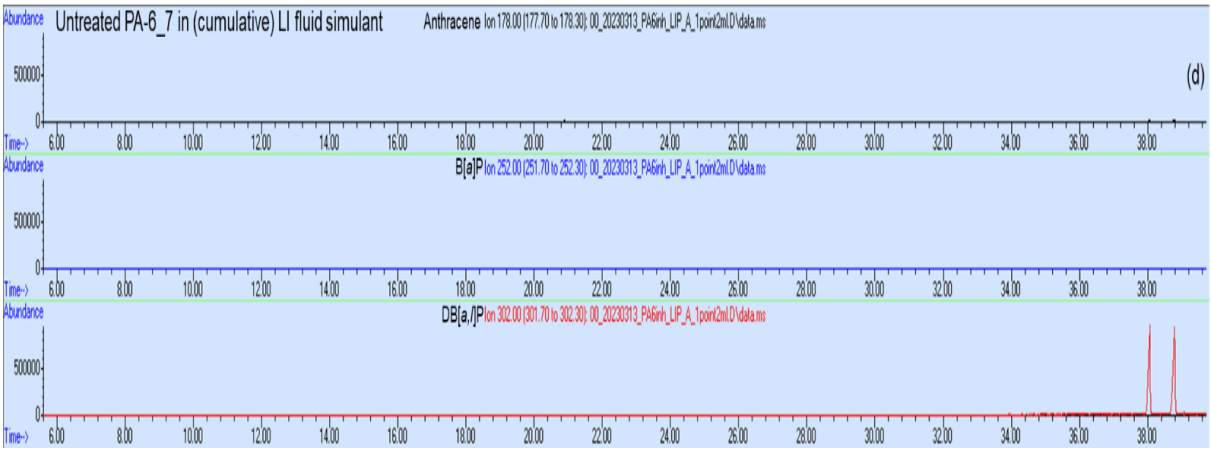
Untreated PA-6_7 in (cumulative) LI fluid simulant
Anthracene
B[a]P
DB[a,l]P
(d)

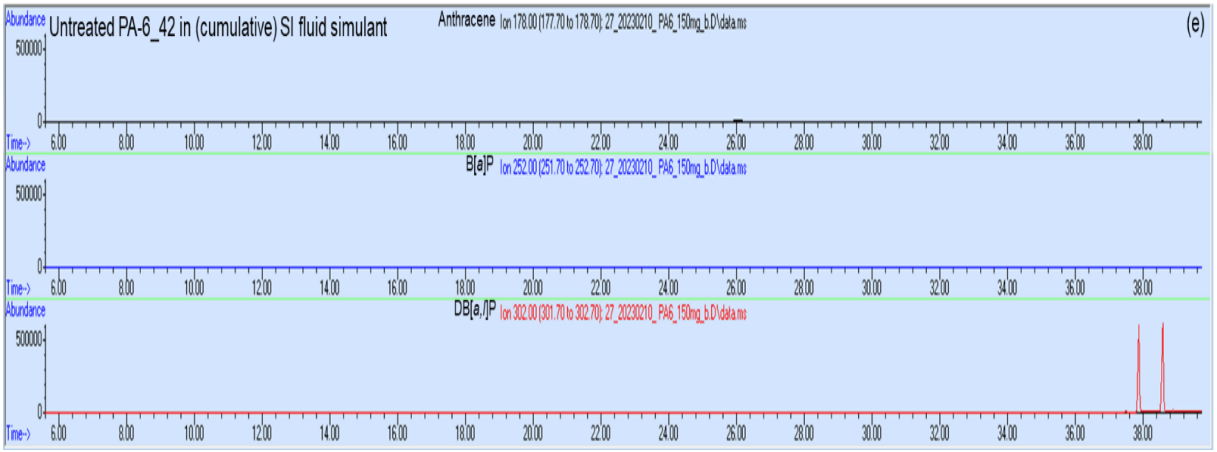
Untreated PA-6_42 in (cumulative) SI fluid simulant
Anthracene
B[a]P
DB[a,l]P
(e)

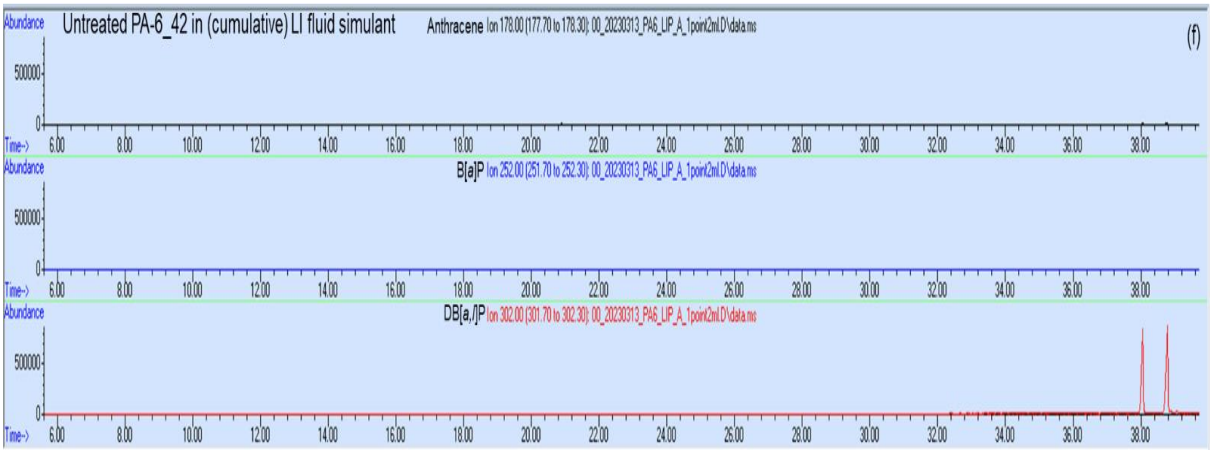
Untreated PA-6_42 in (cumulative) LI fluid simulant
Anthracene
B[a]P
DB[a,/]P
(f)

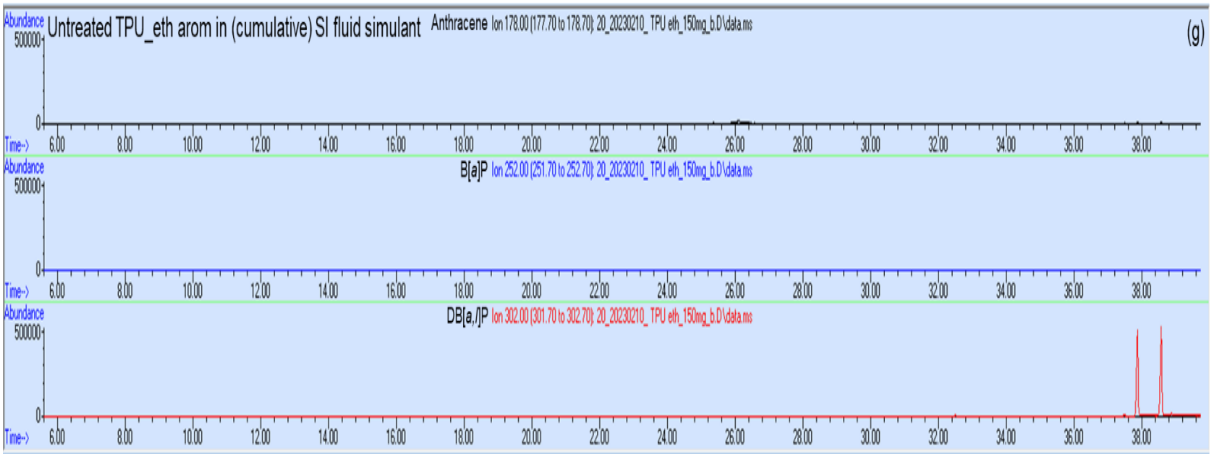
Untreated TPU_eth arom in (cumulative) SI fluid simulant
Anthracene
B[a]P
DB[a,/]P
(g)

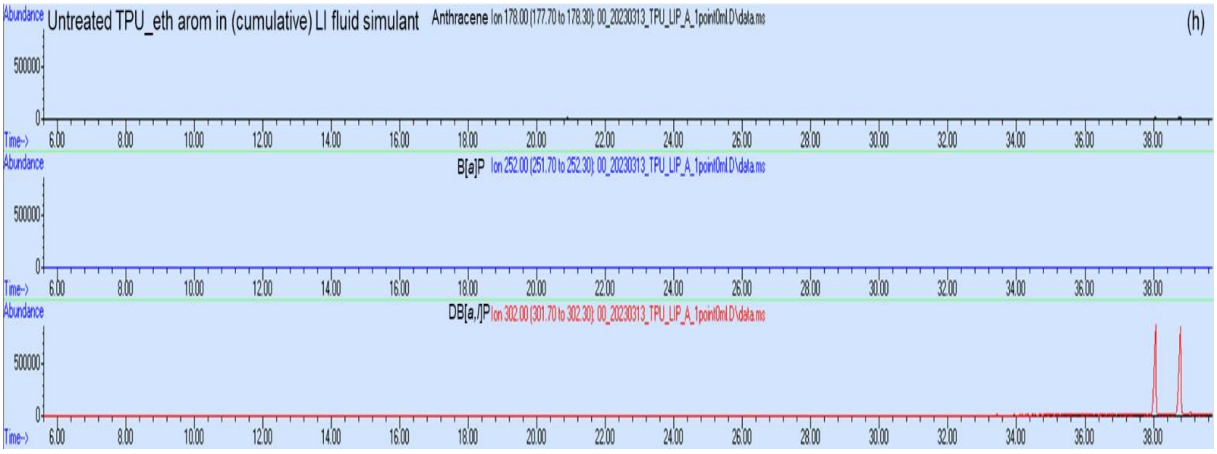
Untreated TPU_eth arom in (cumulative) LI fluid simulant
Anthracene
B[a]P
DB[a,/]P
(h)

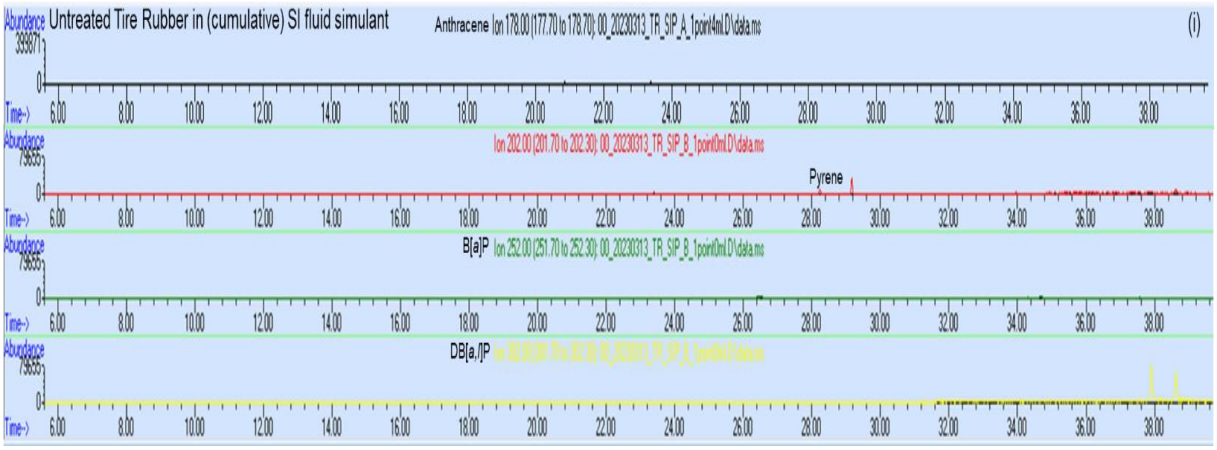
Untreated Tire Rubber in (cumulative) SI fluid simulant
Anthracene
Pyrene
B[a]P
DB[a,l]P
(i)

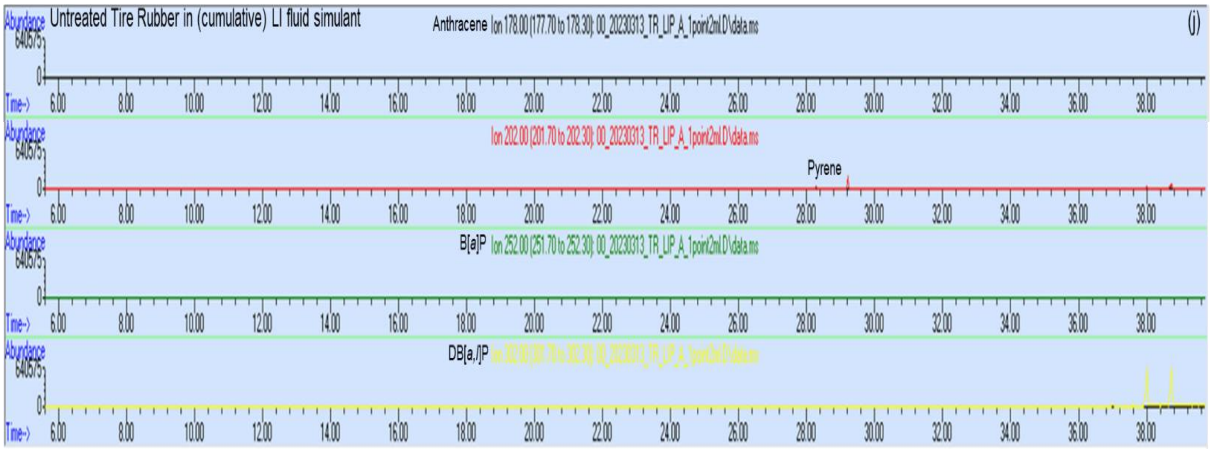
Untreated Tire Rubber in (cumulative) LI fluid simulant
Anthracene
Pyrene
B[a]P
DB[a,l]P
(j)

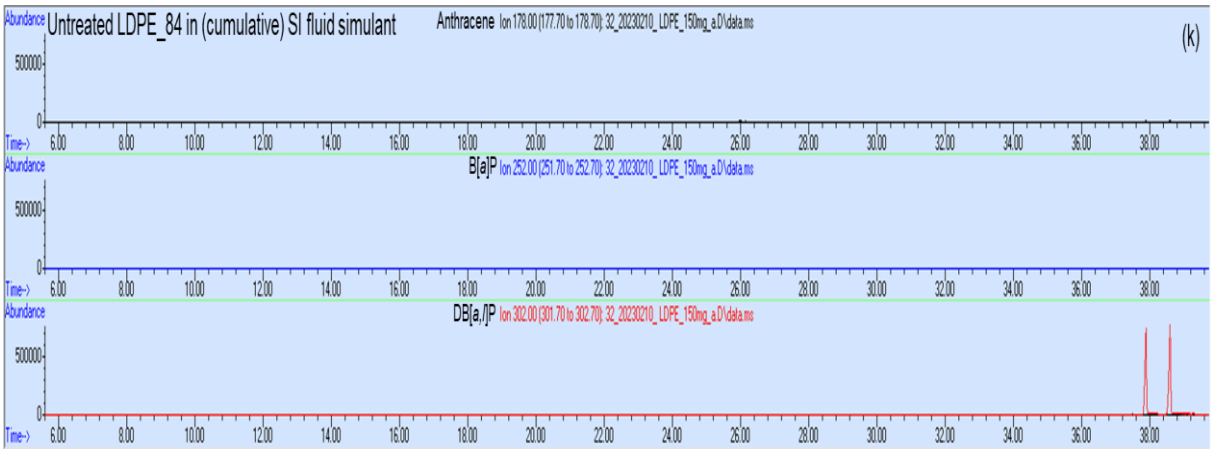
Untreated LDPE_84 in (cumulative) SI fluid simulant
Anthracene
B[a]P
DB[a,l]P
(k)

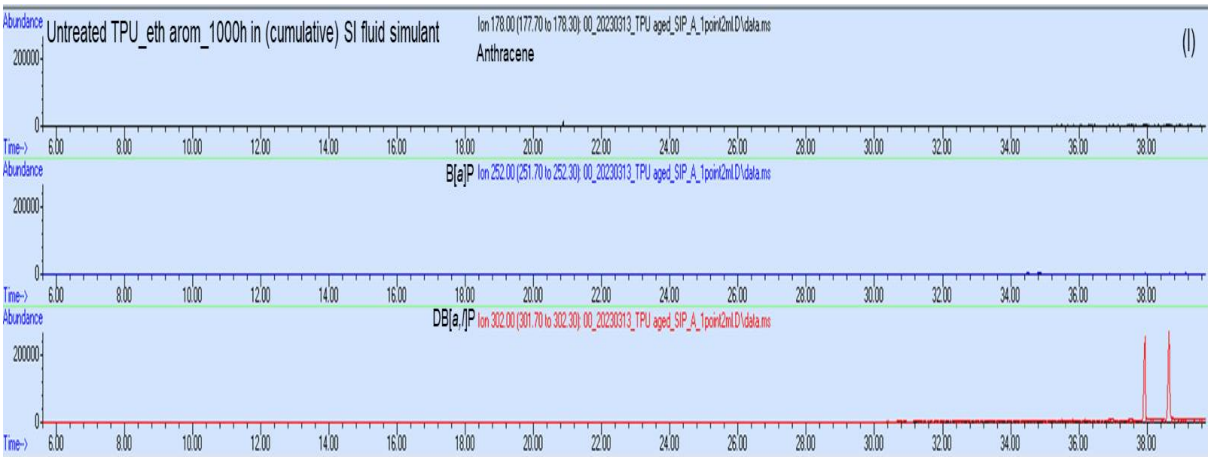
Untreated TPU_eth arom_1000h in (cumulative) SI fluid simulant
Anthracene
(l)
B[a]P
DB[a,l]P
Abundance
Time->

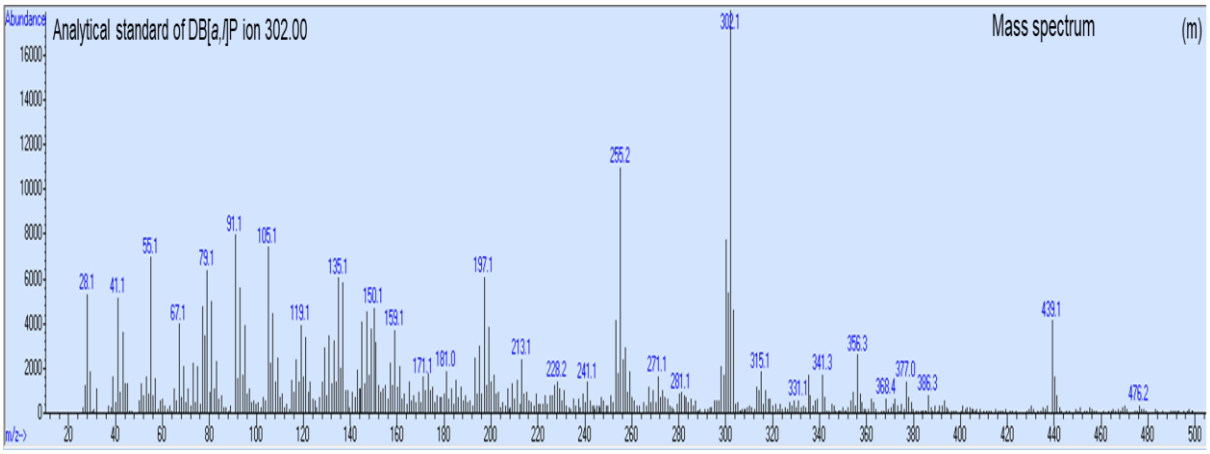
Analytical standard of DB[a,l]P ion 302.00
Mass spectrum
(m)
m/z-->

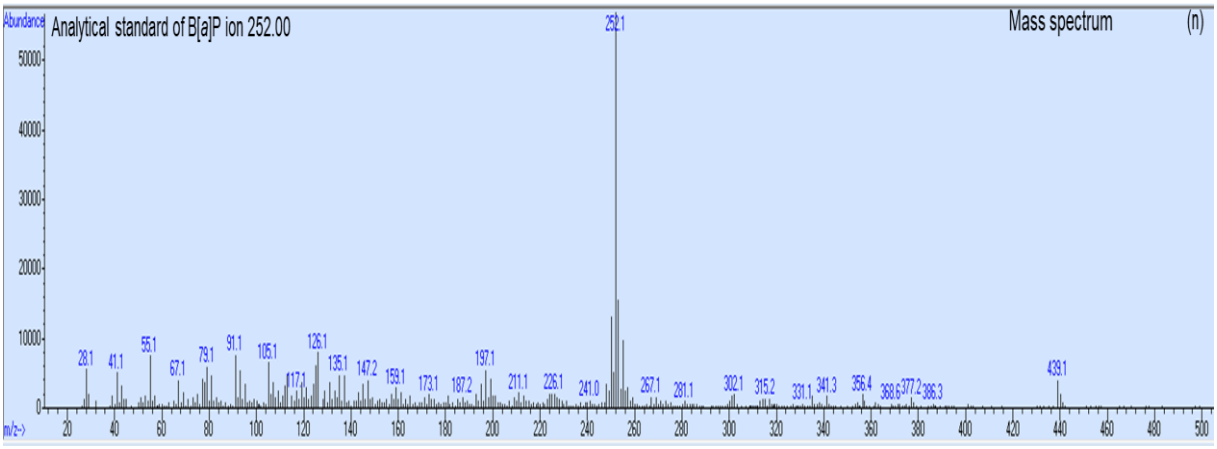
Analytical standard of B[a]P ion 252.00
Mass spectrum
(n)
m/z-->

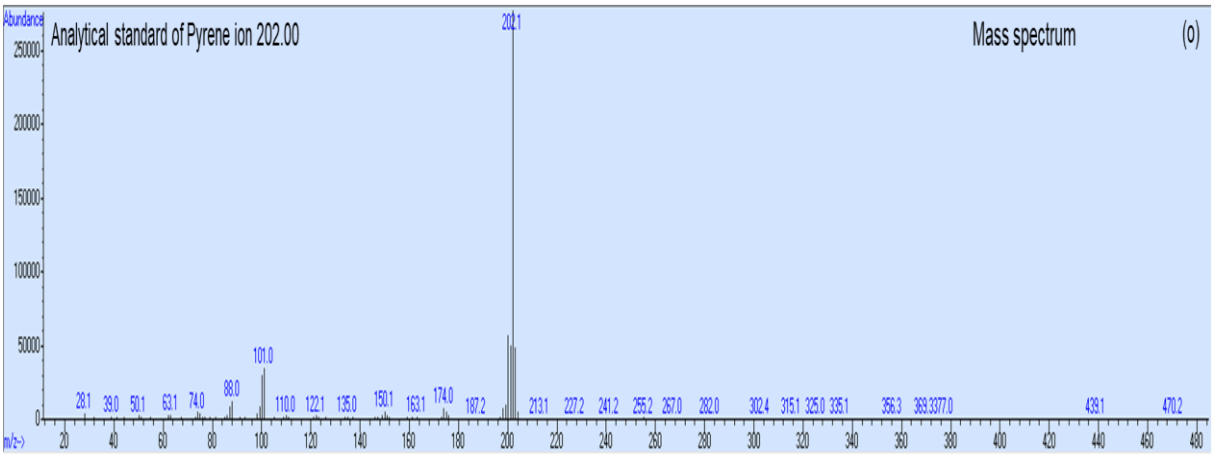
Analytical standard of Pyrene ion 202.00
Mass spectrum
(o)
Abundance
m/z->

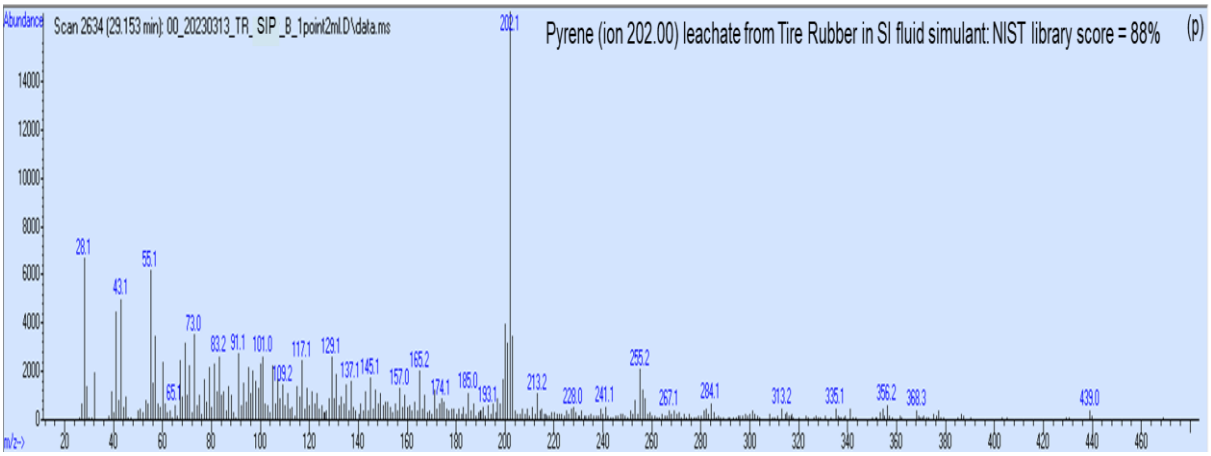
Scan 2634 (29.153 min): 00_20230313_TR_SIP_B_1point2mLD\data.ms
Pyrene (ion 202.00) leachate from Tire Rubber in SI fluid simulant: NIST library score = 88%
(p)
Abundance
m/z->

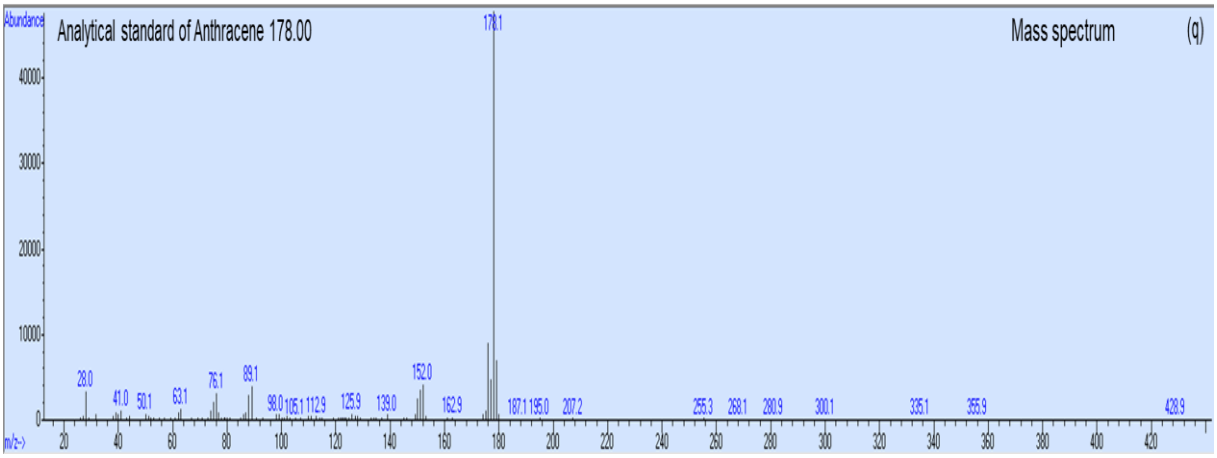
Analytical standard of Anthracene 178.00
Mass spectrum
(q)
Abundance
m/z->

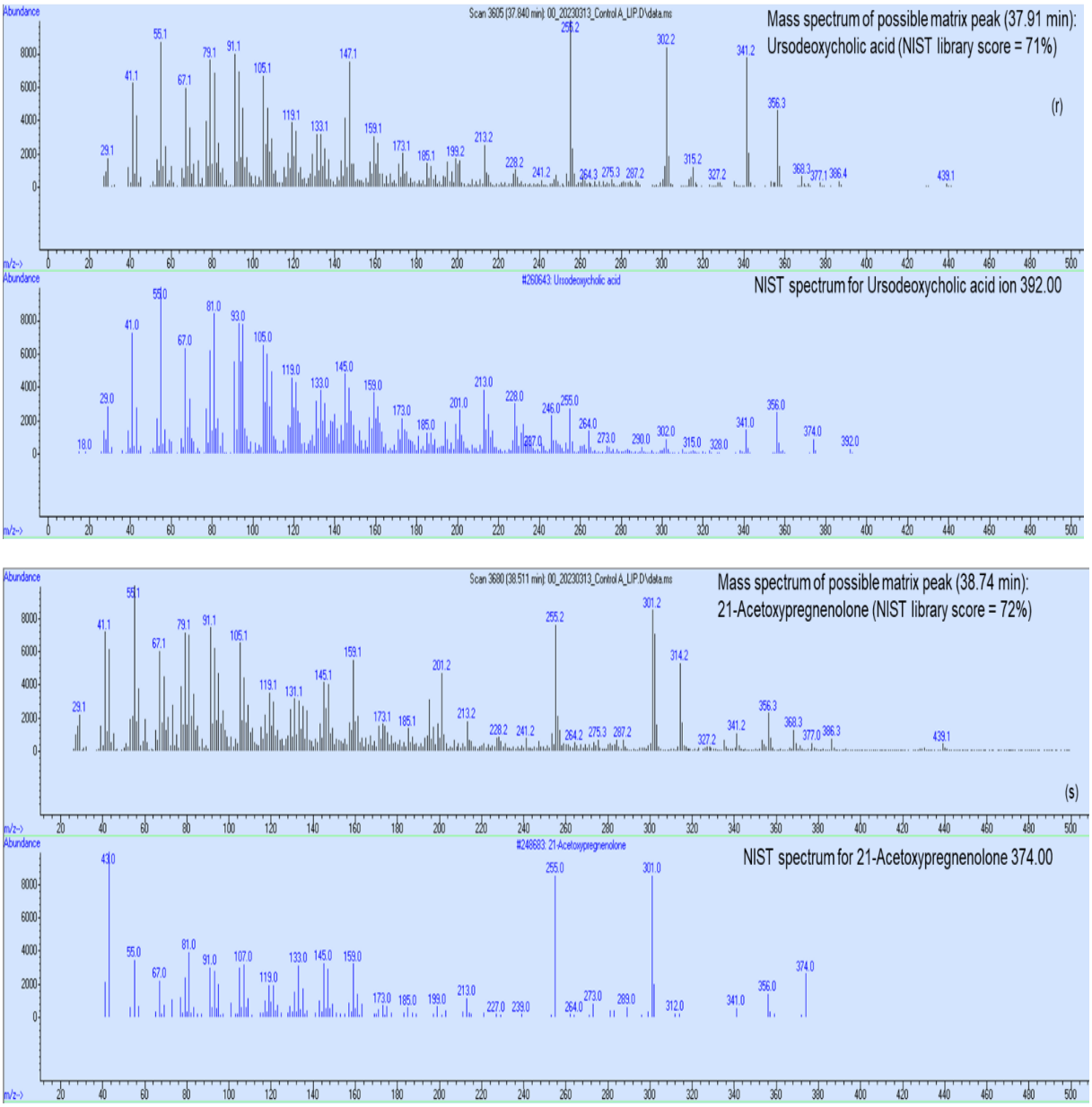

FIGURE S7: Extracted Ions Chromatograms (EIC) of PAH-Selective Ions of (A): PAH standards in Hexane, (B): Sequentially Digested Large Intestine (LI) Fluid Simulant (without microplastics), (C): PA-6_7 In Small Intestine (Si) Fluid Simulant, (D): Pa_7 In Li Fluid Simulant, (E): Pa_42 In Si Fluid Simulant, (F): PA-6_42 In Li Fluid Simulant, (G): TPU_Eth Arom SI Fluid Simulant, (H): Tpu_Eth Arom In LI Fluid Simulant, (I):Tire Rubber in SI Fluid Simulant, (J): Tire Rubber In LI Fluid Simulant, (K): LDPE_84 in SI Fluid Simulant, And (L): Tpu_Eth Arom_1000h In Si Fluid Simulant. M–T: Mass Spectra Of (M): DB[a,l]P, (N): B[A]P And (O): Pyrene Standards In Hexane Solutions. (P): Mass Spectrum of Pyrene Leachate From Tire Rubber In Si Fluid Simulant. Mass Spectra Of (Q): Anthracene Standards in Hexane Solutions. Mass Spectra of (R): Ursodeoxycholic Acid, (S): 21-Acetoxypregnenolone from Si and Li Fluid Simulants.

SECTION S7: ESTIMATES OF THE DAILY INTAKES OF MNPS AND PAHS

Literature data on the daily MNP intake vary widely spanning from microgram to milligram ranges [6-9]. This exposes the wide uncertainty and variability in the estimation of microplastics intake rate for humans. In this study, the intake estimate by Nor *et al.* [9] was utilized for the exposure assessment of MNP-sorbed PAHs. Nor *et al.* identified 135 studies reporting MNP concentrations in nine media relevant for humans. These include fish, mollusc, crustaceans, tap water, bottled water, beer, milk, salt and air. In addition, they also recognized a sole study demonstrating the presence of MNPs in two fruits (apple and common peer) and certain vegetables (broccoli, lettuce, carrot, Irish potato). Remarkably, Nor *et al*. took measures to mitigate inadequacies in MNP occurrence data by eliminating false positives lacking confirmatory spectrometric identification. Also, using mathematical functions, ingestible MNP size ranges were rescaled to the full MNP continuum of 1–5000 µm, while inhalable particles were rescaled to 1–10 µm for comparison. Lastly, the authors converted the particle number concentrations to mass using the MNP continuum which comprises of different shapes, densities, and sizes. Based on their estimated MNP mass distribution in food, the authors estimated average human intake of 1.5 µg/day for the mentioned fruits and vegetables, and a median intake of 0.583 µg/day for air and the food media, resulting to a total daily intake of 2.083 µg MNPs for adults. Considering the unknown contribution from other food types as well as the aforementioned uncertainty in MNP intake rates, the 97.5th percentile value (4.1 µg/day/capita) of Nor et al.'s estimate was utilized for the exposure assessment presented in this study. Of note, in our calculations (**Table 2**) we assumed that the aggregate exposure to MNPs is represented by each individual MNP variant. In reality, different types of MNPs will contribute differently to the total PAH exposure.

Regarding the estimates of the daily dietary intake of PAHs, intake data for European Union (EU) adults obtained as averages of national studies were utilized [10]. For Anth and B[*a*]P, median values of 0.34 and 0.17 µg/capita/day, respectively, were used as total intakes

(TI) for the calculation of the contribution of MNPs to the total human PAH exposure (**Section 4** in the manuscript). The TI values were calculated as the median of the national averages (0.04–0.64 µg/capita/day for Anth and 0.05–0.29 µg/capita/day for B[*a*]P)[10]. No dietary intake data were available for DB[*a,l]*P, therefore, a mean dietary intake value of 0.63 µg/capita/day for the dibenzopyrene isomer DB[*a*,*e*]P [10] was adopted as TI value for DB[*a,l]*P.

REFERENCES

1. Emecheta, E. E., Borda, D. B., Pfohl, P. M., Wohlleben, W., Hutzler, C., Haase, A., & Roloff, A., *A comparative investigation of the sorption of polycyclic aromatic hydrocarbons to various polydisperse micro- and nanoplastics using a novel third-phase partition method.* Microplastics and Nanoplastics, 2022. **2**(1).
2. Lu, N., Dang, Z., Tao, Q., Yang, C., & Yi, Y., *Estimation of Water Solubility of Polycyclic Aromatic Hydrocarbons Using Quantum Chemical Descriptors and Partial Least Squares.* QSAR & Combinatorial Science, 2008. **27**(5): p. 618-626.
3. Hansch, C.L., A; Hoekman, D, *Exploring QSAR: Hydrophobic, Electronic, and Steric Constants* C.L. Hansch, A; Hoekman, DH Editor. 1995 American Chemical Society.
4. EPA, U.S. *ToxCast & compTox chemicals dashboard*. [cited 2023 March]; Available from: https://www.epa.gov/chemical-research/exploring-toxcast-data.
5. Pfohl P, Wagner M, Meyer L, Domercq P, Praetorius A, Hüffer T, Hofmann T, Wohlleben W, *Environmental Degradation of Microplastics: How to Measure Fragmentation Rates to Secondary Micro- and Nanoplastic Fragments and Dissociation into Dissolved Organics.* Environ Sci Technol, 2022. **56**(16): p. 11323-11334.
6. Kala Senathirajah, Simon Attwood, Geetika Bhagwat, Maddison Carbery, Scott Wilson, Thava Palanisami, *Estimation of the mass of microplastics ingested - A pivotal first step towards human health risk assessment.* J Hazard Mater, 2021. **404**(Pt B): p. 124004.
7. Liao, Y.-l. and J.-y. Yang, *Microplastic serves as a potential vector for Cr in an in-vitro human digestive model.* Science of The Total Environment, 2020. **703**.
8. Kieran D. Cox, Garth A. Covernton, Hailey L. Davies, John F. Dower, Francis Juanes, and Sarah E. Dudas, *Human Consumption of Microplastics.* Environ Sci Technol, 2019. **53**(12): p. 7068-7074.

9. Nur Hazimah Mohamed Nor, Merel Kooi, Noël J. Diepens, and Albert A. Koelmans, *Lifetime Accumulation of Microplastic in Children and Adults.* Environ Sci Technol, 2021. **55**(8): p. 5084-5096.
10. European commision health and consumer protection, *Polycyclic Aromatic Hydrocarbons – Occurrence in foods, dietary exposure and health effects*. 2002.

6.7. MANUSCRIPT 3

Leaching of Chemical Additives from Microplastics during *in vitro* Gastrointestinal Digestion and Toxicity Assessment of Leached Compounds

Emeka Ephraim Emecheta[1,2#], Amelie Vogel[1,3#], Antje Begert[1], Roman Schmidt[1], Wendel Wohlleben[4], Andrea Haase[1,5*], Alexander Roloff[1*]

[1]German Federal Institute for Risk Assessment (BfR), Department of Chemical and Product Safety, Berlin, Germany

[2]Bayreuth Center for Ecology and Environmental Research (BayCEER), University of Bayreuth, Bayreuth, Germany

[3]Technische Universität Berlin, Food Chemistry and Toxicology, Berlin, Germany

[4]BASF SE, Ludwigshafen, Germany

[5]Freie Universität Berlin, Institute of Pharmacy, Berlin, Germany

Corresponding authors:

Andrea Haase: andrea.haase@bfr.bund.de

Alexander Roloff: alexander.roloff@bfr.bund.de

# Emeka Ephraim Emecheta and Amelie Vogel contributed equally to this work

* Andrea Haase and Alexander Roloff contributed equally to this work

HIGHLIGHTS

- During *in vitro* digestion, many chemicals were released from tire rubber particles.
- UV-aging of microplastics modulated the composition of leachates.
- Leachates from tire rubber particles induced cytochrome P450 1A1 (CYP1A1) in human CaCo-2 cells.
- Benzothiazole derivatives were found to contribute to CYP1A1 induction.
- 20 leached chemicals were linked to multiple AOPs indicating possible adverse effects.

ABSTRACT ART

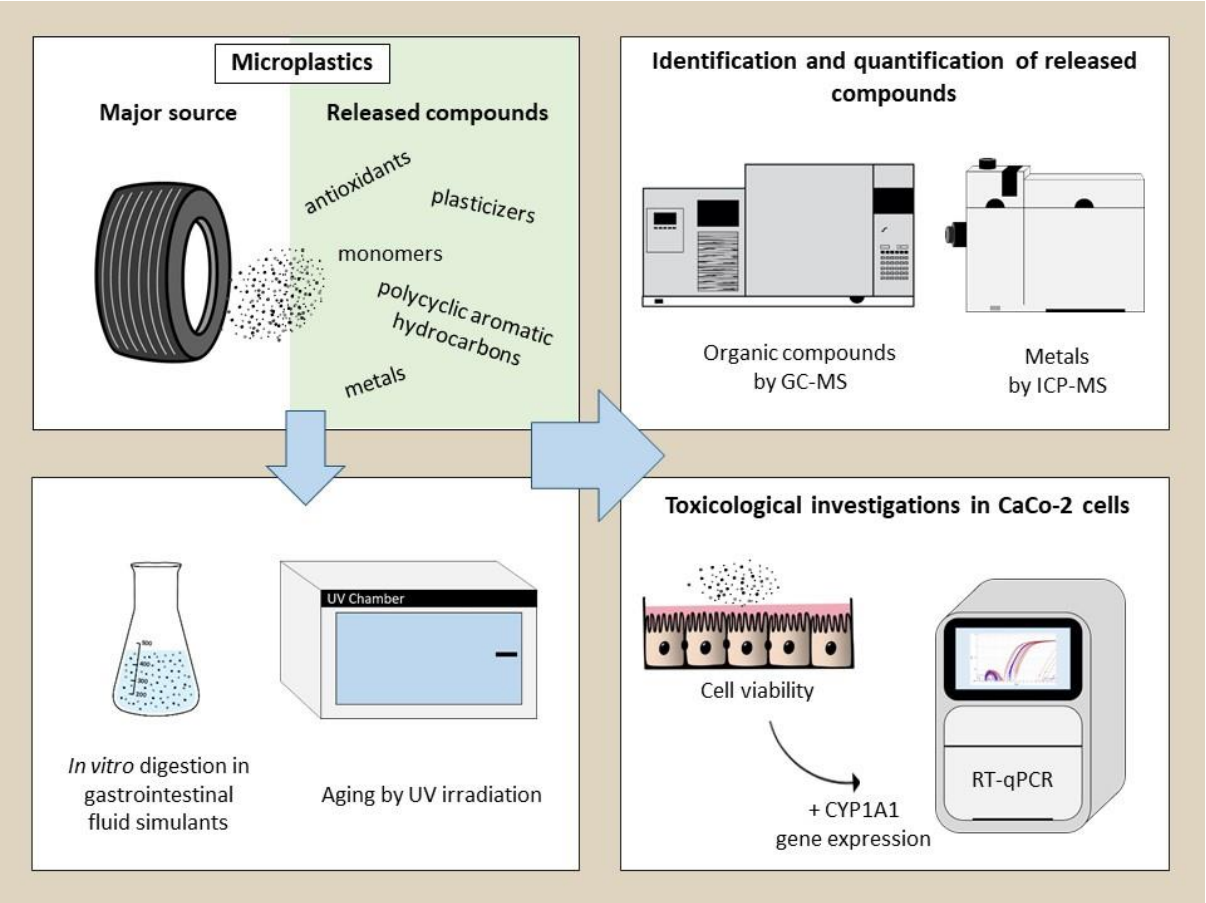

ABSTRACT

Microplastics (MPs) may contain a broad variety of additives, including antioxidants and plasticizers, along with unreacted monomers and sorbed contaminants. Traffic abrasives from tires and crumb granulates from discarded tires have emerged as significant contributors to MP pollution. Concerns have often arisen about the potential for toxic compounds to leach from MPs, yet implications for human health are not well understood.

In this study, we investigated the release of potentially toxic chemicals from three types of MPs: tire rubber (TR), polyamide-6 (PA-6), and thermoplastic polyurethane (TPU) particles during *in vitro* digestion in human gastrointestinal fluid simulants. Furthermore, the effects of UV-aging of the MPs on the leaching of TR compounds was investigated. Leached chemicals and elements were analyzed using gas chromatography-mass spectrometry (GC-MS) and

inductively coupled plasma (ICP)-MS, respectively. All MPs were characterized for selected cellular effects, specifically for cytotoxicity and cytochrome P450 1A1 (CYP1A1) induction in human intestinal CaCo-2 cells.

Most chemicals were leached from TR particles, in particular, benzothiazole (~170 µg/g), (3H)-benzothiazolone (~168 µg/g) and zinc (~1150 µg/g) were quantified in high concentrations in small and large intestine fluid simulants, leaching of the above chemicals decreased following UV-aging of TR particles. All MPs were not cytotoxic within 24 h of exposure. Tire particles induced CYP1A1, but this effect decreased after UV-aging. Benzothiazole derivatives as well as diethyl and dibutyl phthalates were identified as important contributors to CYP1A1 induction. Selected leached additives were further investigated for potential toxic effects by utilizing the EPA ToxCast database, revealing links of 20 leached compounds to specific adverse outcome pathways (AOPs). Our findings indicate that the leaching of specific additives, particularly from TR particles, could pose a risk to human health and that *in vitro* digestion increased the leaching of these additives while UV-aging modulated the composition of leached compounds.

Keywords: Tire wear, Leaching, Chemical additives, Gastrointestinal fluids, CYP1A1, Cytotoxicity, CaCo-2, Adverse outcome pathways.

1. INTRODUCTION

Due to increasing traffic worldwide, the release of tire rubber (TR) particles in the environment has become a major concern. TR particles mainly originate from traffic-related tire abrasion, but also end-of-life tire applications including infill materials for synthetic turf or floorings for playgrounds and athletic tracks may contribute to the aggregate environmental load (Halsband et al., 2020; Ramasamy & Harit, 2023). A fraction of TR particles is classified as microplastics (MPs) due to the high synthetic rubber content and their particle size (ETRMA, 2015). This fraction accounts for the major part of outdoor MP pollution (Kole et al., 2017; UNEP, 2018). Many studies have already demonstrated the presence of TR particles in the environment, especially with a focus on tire wear runoff from rainfall (Rauert et al., 2022), river sediments

(Unice et al., 2013), and water treatment systems (Eisentraut et al., 2018). In addition to tire wear, mismanaged waste of commonly used plastics, such as polyethylene (PE), polystyrene (PS), polyethylene terephthalate (PET), polyurethane (PU) or polyamide (PA) contributes significantly to MP pollution (OECD, 2022). Nowadays, MPs are assumed to be present in every compartment of the ecosystem (Lim, 2021).

As a result of worldwide pollution, human exposure to MPs has been widely reported. Notable exposure routes include oral exposure through seafood (Smith et al., 2018), beverages (Koelmans et al., 2019), vegetables (Oliveri Conti et al., 2020), via direct deposition of airborne MPs on prepared meals (Bai et al., 2022), or via inhalation (Lombardi et al., 2022). Thus, potential human health risks associated with MP uptake need to be considered. In this context, a report by the World Health Organization (WHO) emphasized the need to characterize and quantify the release of chemical additives from MPs (WHO, 2022).

In general, the production of plastics and tires involves plenty of additives to streamline the manufacturing process and obtain certain functionalities in the final product (Groh et al., 2019). Commonly used additives are inorganic fillers, organic stabilizers, and antioxidants; specific uses require flame-retardants, and particularly in the case of polyvinylchloride (PVC) the use of plasticizers, such as phthalates, is frequent (Henkel et al., 2022). The European Chemicals Agency (ECHA) has identified over 400 registered additives commonly used in different plastics, spanning concentration ranges of less than 0.1 to over 50 w/w % (ECHA, 2023a). On the global markets, over 10,000 additives have been associated with plastics (Wiesinger et al., 2021). Other chemicals used specifically in tire manufacturing include metals, carbon black, zinc oxide, and vulcanization additives including benzothiazole (ETRMA, 2015). Moreover, tires can also contain mineral oils, which are used as plasticizers in tire rubber. In addition tires can be contaminated, e.g. by polycyclic aromatic hydrocarbons (PAHs), which are common pollutants in different environmental compartments that can sorb to MPs (Armada et al., 2023; Diekmann et al., 2019; Emecheta et al., 2022; Skoczynska et al., 2021; Stephensen et al., 2003). Finally, unreacted monomer residues and non-intentionally added substances (NIAS)

might be present in MPs depending on the specific polymer, and its synthesis or recycling route (Horodytska et al., 2020; Wiesinger et al., 2021).

Most of these compounds are not chemically bound to the polymers. As a result, human exposure is possible upon MP ingestion. Moreover, additives associated with plastics and TR waste in landfills have been identified in soil and groundwater (Parvin & Tareq, 2021; Wan et al., 2022), from where they can enter the food chain. The release of potentially toxic chemicals from MPs has been intensively studied in the last years. For example, studies have shown the leaching of phthalates and bisphenol A, some of which are potential endocrine disruptors, from MPs in human gastrointestinal (GI) fluid simulants (ECHA, 2023b; Hlisnikova et al., 2020). In addition, the release of many other organic compounds associated with potentially adverse effects from a broad selection of MPs has been detected (Campanale et al., 2020).

For TR particles, the release of benzothiazole, *N*-(1,3-dimethylbutyl)-*N'*-phenyl-1,4-benzenediamine (6PPD) and PAHs has become a major concern. 6PPD is an antioxidant specifically used in tires and has been linked to acute toxicity in different fish species (Brinkmann et al., 2022), whereas benzothiazole can cause respiratory, skin and eye irritation (Fishbein, 1991). In addition, some PAHs including benzo[*a*]pyrene (B[*a*]P) are known to act as genotoxic carcinogen (Lee, 2010). Several PAHs are well known to be aryl hydrocarbon receptor (AhR) agonists and are metabolized by cytochrome P450 (CYP) enzymes, which play an important role in drug and xenobiotic metabolism (Eriksson et al., 2022). Studies have already shown that organic compounds extracted from TR particles act as AhR agonists in mouse and rat hepatoma cell models (He et al., 2011). In addition, TR extracts induced cytochrome P450 1A1 (CYP1A1) in fish (Stephensen et al., 2003). However, it is not fully understood which compounds might be responsible for this induction and how cellular responses might be modulated under more realistic scenarios, including *in vitro* digestion.

This study has three objectives. Firstly, we aimed to identify the chemicals leaching from TR particles during *in vitro* digestion in human GI fluid simulants, also considering the impact of

particle size and the composition of the digestion fluids. Two variants of TR materials were utilized; one cryomilled from recycled truck tire granules (TR_{truck}); and another cryomilled sample obtained from crumb rubber turf being commercially available as infill material (TR_{infill}). For comparison, primary MPs intended for use in additive manufacturing were studied. These includes thermoplastic PU (TPU) and PA-6 particles with broader size distributions. Additionally, variants of the MPs, photo-aged with UV light under ISO-standardized conditions, were also investigated.

Secondly, cellular effects of the MPs in human intestinal CaCo-2 cells were characterized, focusing on cytotoxicity and the induction of CYP1A1, an enzyme commonly induced by many xenobiotics.

Thirdly, we aimed to identify potential adverse outcomes of the leached chemicals by performing a ToxCast database search to elucidate, which effects may arise from human exposure to these MPs.

2. MATERIALS AND METHODS

2.1 CHEMICALS, MEDIA, AND MICROPLASTIC PARTICLES

Except otherwise indicated, all chemicals including analytical standards and the components of the GI fluid simulants were purchased from Sigma-Aldrich in the highest available purity. Solvents and reagents such as hexane (≥ 99 % pure), ethanol (≥ 99 % pure), ethyl acetate (99.8 % pure), propan-2-ol (≥ 99 % pure), nitric acid (70 % w/v), hydrogen peroxide (30 % w/v), hydrochloric acid (30 % w/v), and sodium hydroxide pellets (reagent grade) were purchased from Merck (Darmstadt, Germany). Sulfuric acid (97 % w/v) was acquired from Neolab (Heidelberg, Germany).

The elemental standards for the inductively coupled plasma-mass spectrometry (ICP-MS) analyses were supplied by Thermo Fischer Scientific (Bremen, Germany). Ultrapure distilled

water was obtained from a Millipore Q-POD® dispenser connected to a Millipore milli-Q system (Darmstadt, Germany).

End-of-life truck tires were cryomilled to a median size of 130 µm by Mülsener Rohstoff- und Handelsgesellschaft mbH (Mülsen, Germany) as previously described (Emecheta et al., 2022), and are designated here as TR_{truck} MPs. End-of-life TR_{infill} MPs are commercially available as infill material for artificial turf (Granuflex Sportsfill Eco+) and were purchased from Granuband B.V. (Amsterdam, the Netherlands). For experiments in this study, TR_{infill} was cryomilled. Two PA-6 variants with median particle sizes of 7 µm (PA-$6_{7µm}$) and 42 µm (PA-$6_{42µm}$), respectively, and TPU particles comprised of polyether polyol and aromatic diisocyanates in the hard and soft segments, respectively, were supplied by BASF (Ludwigshafen, Germany). PA-$6_{42µm}$ and TPU MPs were photo-aged for 1000 h following ISO 4892 as described elsewhere (Pfohl et al., 2022) and are referred herein as PA-$6_{42µm,aged}$ and TPU_{aged}, while $TR_{truck,\ aged}$ was irradiated under the same conditions for 2000 h. Media and supplements for cell culture were purchased from Sigma Aldrich (Steinheim, Germany) and Pan Biotech (Aidenbach, Germany) if not stated otherwise. The 3-(4,5-dimethylthiazole-2-yl)-2,5-diphenyltetrazolium bromide (MTT) reagent for cell viability testing was purchased from Carl Roth (Karlsruhe, Germany).

2.2. ANALYSIS OF THE MPS BY PYROLYSIS GAS CHROMATOGRAPHY MASS SPECTROMETRY (PY-GC-MS) AND THERMAL DESORPTION (TD) -GC-MS

To characterize additives or contaminants that could in principle leach from MPs, different MPs were subjected to Pyrolysis and TD-GC-MS. Pyrolysis was performed using the Gerstel thermal desorption unit (TDU 2) pyrolysis-module (Mülheim, Germany). The samples were contained in a double-open pyrolysis glass tube (Gerstel) that were stuffed with quartz wools (Gerstel). The wool was compressed to occupy approximately one-quarter of the tube. Following, the tubes were sterilized over a gas burner for about 5 seconds and allowed to cool. Prior, 3, 6, 9, 12, 15 µL samples were pipetted from 10 mg/mL dispersion in ethanol,

corresponding to 30, 60, 90, 120, 150 µg of the MPs. The dispersion was prepared by weighing 10 mg of target MP into a glass vial containing 1 mL ethanol. The mixture was vigorously shaken to form a dispersion which was quickly pipetted into the pyrolysis tube. The pyrolysis tube was connected to the transport adapter (Gerstel) which was kept under the hood for about an hour until the ethanol was evaporated. Thereafter, the transport adapters were transferred to the autosampler tray for pyrolysis. The samples were pyrolyzed for 0.3 min at 650°C under a constant helium flow of 290 mL/min. Pyrolyzed samples were cryo-focused with liquid nitrogen at -100 °C in the cold injection system (CIS, Gerstel). The transfer temperature from the TDU to the CIS was 350 °C. The gas chromatography-mass spectrometry (GC-MS) analysis was performed as described in **Section 2.4**.

For the TD-GC-MS analysis, 30 µg of the samples (3 µL of 10ng/mL MPs in ethanol suspensions) were loaded into a glass tubes filled with glass wool and subsequently thermally desorbed in a thermal desorption unit (TDU) with a temperature gradient starting at 50 °C (0.5 min), then heated to 320 °C at 50 °C/min, and then held for 1.43 min. The CIS and the GC-MS conditions are identical as described below.

2.3. DETERMINATION OF COMPOUNDS LEACHED FROM MICROPLASTICS DURING DIGESTION IN HUMAN GI FLUID SIMULANTS

To simulate the potential release of additives and contaminants into the GI tract during ingestion, we employed a sequential *in vitro* digestion model, as described in our previous study (Emecheta et al., 2024), albeit with slight modifications. The *in vitro* digestion consists of four sequential steps: digestions in i) saliva, ii) gastric, iii) small intestine (S.I.), and iv) large intestine (L.I.) fluid simulants. Each GI phase contained the preceding digested GI fluid simulant. Fresh GI fluid simulants (**Table S1**) were prepared for every digestion experiment.

To begin the digestion, 50 mg of target MP particles were introduced to a 25 mL Duran glass vial (Mainz, Germany) containing 2 mL saliva fluid simulant. The mixture was adjusted to a pH

of 6.7 ± 0.2, and incubated for five minutes with a three-dimensional shaker (GfL mbH, Germany) operated at 250 rotation per minute (rpm) inside a Binder incubation chamber (Tuttlingen, Germany) operated at 37 °C. Thereafter, 8 mL gastric fluid simulant was added to the mixture, and the pH was adjusted to 1.8 ± 0.3. The mixture was incubated for 2 h as described above. Next, 8 mL S.I. fluid simulant was added to the mixture, and the pH of the mixture was adjusted 6.8 ± 0.3. After 4 h incubation, an aliquot of 1.5 mL was collected for treatment with CaCo-2 cells. The remainder of the mixture was either analyzed for leachates or mixed with 2 mL of artificial L.I. fluid. The pH of the resulting mixture was adjusted to 8.3 ± 0.1 and the mixture was incubated for 18 h. All pH adjustments were performed with 1 M NaOH and 1 M HCl.

For comparative experiments with distilled water and CCM, 50 mg MP was introduced to a mixture containing 2 mL saliva fluid simulant, 8 mL gastric fluid simulant, and 8 mL S.I fluid simulant. The mixture was incubated as described above for 6 h at 250 rpm under a temperature of 37 °C. Similarly, 50 mg identical MP particles were introduced to vials containing 18 mL distilled water and 18mL CCM, the vials were incubated alongside the G.I fluid simulants for 6 h.

To analyze the chemicals released in the S.I. and L.I. fluid simulants, the mixtures were centrifuged (1SR ThermoFischer Scientific, Germany) at 4500 rpm for 20 minutes and filtered using 0.7 µm glass filters. The filtrates were spiked with 2.5 µg anthracene-d10 and naphthalene-d8 as internal standards and extracted with 2×10 mL ethyl acetate and 2×10 mL hexane. In each extraction step, the filtrates were manually shaken for 3 minutes and centrifuged for 20 minutes at 4000 rpm. The extracts were combined, evaporated to 1 mL using a Buchi Syncore evaporation system (Flawil, Switzerland) and analyzed via GC-MS. Quantification of selected leached compounds such as caprolactam, diethyl phthalate, dibutyl phthalate, benzothiazole, and 2(3H)-benzothiazolone were achieved by matrix-matched calibration (**Table S2**) as described previously (Emecheta et al., 2024). To determine leached

metals in the S.I. and L.I. fluid simulants, 1 mL aliquots of the filtrates were diluted to 40 mL with water containing 1 % propan-2-ol, and analyzed with ICP-MS (see **Section 2.4 below**).

2.4. GC- AND ICP-MS METHODS FOR THE ANALYSES OF COMPOUNDS LEACHED FROM MPS DURING *IN VITRO* DIGESTION

GC-MS measurements were performed with a 6890 series GC coupled with a 5975 series mass selective detector (both Agilent, Waldbronn, Germany). The GC oven was equipped with a BPX50 mid polarity (50 % phenyl polysilphenylene-siloxane) capillary column (Forte ACS, New Jersey, USA). The dimensions of the column include a length of 30 m, an inner diameter of 0.25 mm, and a film thickness of 0.25 µm. The oven temperature program consisted of a temperature gradient starting at 60 °C and then heated to 320 °C at 8 °C/min. The starting and final temperatures were held for 1 min and 6 min, respectively. 99.999 % ultrapure helium (Linde, Pullach, Germany) was utilized as a carrier gas at a constant flow of 1.0 mL/min. The MS detector was operated in combined selective ion monitoring (SIM) and scan mode with a scan rate of 15.99/s covering a mass range of 50–500 m/z. The MS quadrupole, ion source, and transfer-line temperatures were operated at 150, 230, and 320 °C, respectively. Each ion was monitored with a dwell time of 10 milliseconds. 1 µL of the extracts was injected into the cold injection system (CIS) in splitless mode at 40 °C, which was heated to a temperature of 320 °C at 12 °C/s and held for 3 min.

The ICP-MS measurements were performed with an iCapQ instrument (Thermofischer scientific, Bremen, Germany) equipped with an electron spray ionization (ESI) SC-4DX prepFast autosampler (Elemental service & instruments, Mainz, Germany). Each sample was subjected to 100 sweeps at a dwell time of 0.01 s and 0.1 u. Data acquisition was performed in collision mode with helium gas applying kinetic energy discrimination (KED) and in standard mode with hydrogen gas. The system was operated at an RF power of 1550 W. The helium gas flow of the nebulizer, auxiliary gas, and cooling gas were set to 1.04, 0.65, and 14 L/min,

respectively. An internal standard solution of rhodium, bismuth, and scandium mix in 10 % propan-2-ol and 3.5 % nitric acid was utilized as injection standard at a concentration of 2 µg/L. Quantification was performed via external calibration. A stock solution of the elemental standards mix was diluted to 8-calibration points by the prepFast autosampler. The concentration of metals in the TR MPs were characterized via microwave-assisted dissolution (**Section S2**).

2.5 DISPERSION OF MPS FOR CELL CULTURE TREATMENT

Prior to cell culture treatment, the pristine particles were prepared according to a published standard operating procedure (SOP) for the dispersion of polydisperse polymers (InnoMat.Life, 2022). In brief, the dispersion medium contains 0.05 % (w/w) bovine serum albumin (BSA) and 0.05 % (w/w) Tween® 40 to facilitate the dispersion of MPs with a low density in an aqueous solution. Subsequently, the dispersion was directly diluted (dilution factor (DF) = 25.0) in cell culture medium (CCM) to achieve a final MP concentration of 100 µg/mL for cell culture experiments. The *in vitro* digested MPs in S.I. fluid simulants were diluted in CCM (DF for TR_{truck} and $TR_{truck,aged}$ = 27.8, for TR_{infill} = 22.2) to the same concentration of 100 µg/mL after 6 h of digestion and were then applied to the cells. As an additional control, the MPs were firstly incubated in CCM at a concentration of 100 µg/mL and after 24 h of incubation, the particles were centrifuged for 10 min at 10,000 g to obtain the supernatants for cell culture treatment. A schematic overview of the whole sample preparation is shown in **Section S3, Fig. S1.**

2.6 CELL CULTIVATION

CaCo-2 cells (ECACC: 86010202) were obtained from the European Collection of Authenticated Cell Cultures (Salisbury, UK). Cells were cultured in Dulbecco's Modified Eagle Medium (DMEM) supplemented with 10 % fetal bovine serum (FBS) superior and 1 % penicillin/streptomycin. CaCo-2 cells were maintained at 37 °C and 5 % CO_2 and passaged every 2–3 days. For differentiation, cells were grown for 21 days and CCM was changed every 2 days. For cell viability testing, CaCo-2 cells were seeded in 96-well plates (5,000 cells per

well). To investigate the induction of CYP1A1 by quantitative reverse transcriptase polymerase chain reaction (RT-qPCR), cells were seeded in 6-well plates (150,000 cells/well). Cells were allowed to attach for 24 h. For the studies involving differentiated CaCo-2 cells, cells were grown in 96-well plates (cell viability) or 6-well plates (CYP1A1 gene expression) for 21 days. CCM was changed every 2 days.

2.7 CELL VIABILITY

Undifferentiated and differentiated CaCo-2 cells were exposed to the different TR MPs in concentrations ranging from 3.125 to 200 µg/mL for 24 h, using three technical triplicates in each experiment. 100 µL of the TR particle dispersion or particle supernatant was added to each well. Triton X-100 was used as a positive control. After 24 h of incubation, the medium was aspirated and each well was washed three times with 100 µL of phosphate buffered saline (PBS). A 5 mg/mL MTT stock solution in PBS was diluted in the corresponding cell culture media to a final concentration of 0.5 mg/mL and the cells were incubated with the dye for 2 h at 37 °C in the dark. The supernatant was aspirated and 150 µL dimethylsulfoxide (DMSO) was added to each well to dissolve the formazan crystals. The 96-well plates were placed on an orbital shaker for 15 min protected from light. The absorption was measured at 570 nm using a multimode microplate reader (BioTek Synergy Neo2, Agilent, Waldbronn, Germany) and the absorption at 630 nm was subtracted to correct for background absorption. Mean values and standard deviations were calculated from three independent biological experiments (using cells with different passage numbers).

2.8 QUANTITATIVE REVERSE TRANSCRIPTASE POLYMERASE CHAIN REACTION (RT-QPCR) FOR ASSESSMENT OF CYP1A1 INDUCTION

Undifferentiated and differentiated CaCo-2 cells were exposed to the different MPs at a concentration of 100 µg/mL and B[*a*]P as positive control at a concentration of 2 µM for 24 h. Additionally, cells were exposed to the following contaminants and additives: pyrene, 6PPD

and 2(3H)-benzothiazolone at a final concentration of 5 µM in CCM and benzothiazole, diethyl phthalate and dibutyl phthalate at a final concentration of 0.5 µM in CCM. All additives were diluted from DMSO stock solutions so that the final DMSO content during cell incubation was less than 0.013 % (v/v). After incubation, cells were washed with PBS, cell pellets were collected by trypsinization and a following centrifugation step at 300×*g* for 5 min. Subsequently, RNA was extracted using the RNeasy Mini Kit (Qiagen, Hilden, Germany) according to the manufacturer's protocol. The RNA concentration was measured with the NanoDrop 1000 spectrophotometer (PeqLab, Erlangen, Germany). 500 ng (undifferentiated CaCo-2 cells) or 1 µg (differentiated CaCo-2 cells) of the RNA was used for cDNA synthesis with reagents from the High-Capacity cDNA Reverse Transcription Kit (Applied Biosystems, California, USA). The synthesis was performed according to the manufacturer's instructions using a T100 Thermal Cycler (Bio-Rad, California, USA).

Quantitative PCR was performed with a QuantStudio™ 3 Real-Time PCR (Thermo Fisher Scientific, Massachusetts, USA) using Fast SYBR™ Green Master Mix (Applied Biosystems, Foster City, CA, USA). The temperature conditions for the qPCR were as following: 95 °C for 20 s, followed by 45 cycles of 95 °C for 3 s and 60 °C for 30 s. Each sample was measured in technical triplicates. The relative gene expression of CYP1A1 (forward primer: 5'-CCA AGA GTC CAC CCT TCC CAG CT-3', reverse primer: 5'-GAG GCC AGA AGA AAC TCC GTG GC-3') was calculated using the $2^{-\Delta\Delta Ct}$ method with hypoxanthine-guanine phosphoribosyl transferase (HPRT) as reference gene (forward primer: 5'-GTT CTG TGG CCA TCT GCT TAG -3', reverse primer: 5'-GCC CAA AGG GAA CTG ATA GTC-3') as referenced elsewhere (Haidar et al., 2021).

2.9 DATA ANALYSIS

GC-MS and ICP-MS data were processed with MassHunter software (Agilent, versions B.06.00 and B.10.00) and Qtegra software (Thermo Fisher Scientific, version 2.14.5122.306), respectively. Total ion chromatograms (TIC) were deconvoluted to obtain spectra of individual

compounds by performing automatic integration and extractions of the peak spectra using the Agilent 10.0 software. The resulting spectrum peaks were identified using the NIST MS program. Further data processing was performed with Microsoft Excel 2016. All figures were prepared with GraphPad Prism 9 (Boston MA, USA). The significance levels were determined by performing one-way ANOVA (* = $p < 0.05$, ** = $p < 0.01$, *** = $p \leq 0.001$). For cell culture experiments, statistical analysis was performed using one-way ANOVA following Dunnet's test (* = $p < 0.05$, ** = $p < 0.01$, *** = $p \leq 0.001$). Untreated cells only exposed to CCM were compared to cells that were treated with the respective MP particles. Statistical analyses were performed for at least 3 independent biological replicates.

3. RESULTS AND DISCUSSION

Firstly, we aimed to screen which chemicals, additives and/ or contaminants can in principle leach from the different MPs using Py-GC-MS and TD-GC-MS. Exemplary chromatograms are shown in **Fig. S2 and Fig. S3**. In addition, **Fig. S3** provides a comparison of thermally extracted chemical compounds that can potentially leach from the MPs and compounds that did in fact leach during *in vitro* GI digestion. A detailed discussion can be found in **Section S4**. In the following, we will focus on chemical additives and contaminants that we have identified and/or quantified in GI fluid simulants and which may have potential toxic effects on human health (**Sections 3.1-3.3**).

3.1. IDENTIFICATION OF CHEMICAL ADDITIVES AND CONTAMINANTS LEACHED INTO GI FLUID SIMULANTS AND WHICH MAY MODULATE CYP1A1 EXPRESSION

Table 1 provides a summary of the organic compounds that leached from the MPs following the sequential digestion in GI fluid simulants as quantified by GC-MS. The selection of chemical compounds is based on their suspected potential to modulate CYP1A1 gene expression, for example, via binding to AhR. CYP1A1 is one of the major enzymes involved in xenometabolism and plays a crucial role in both, the activation and detoxification of

(environmental) organic compounds. Moreover, in our previous study (Emecheta et al., 2024), where we specifically focused on PAHs, we could identify pyrene in the leachates of the TR particles. PAHs in general are well known to be metabolized by CYP1A1. This prompted us to research for other compounds leaching from MPs being metabolized by CYP1A1. In addition, a selection of these compounds where quantified by GC-MS (**Table 2**).

Table 1: Overview of selected leached compounds from microplastics identified as potential AhR agonists or with the potential to modulate CYP1A1 gene expression. These compounds were further investigated in this study.

Compound	Molecular structure	AhR binding and effect on CYP1A1 expression
Pyrene	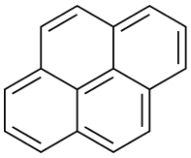	CYP1A1 induction (Lotz et al., 2016)
6PPD	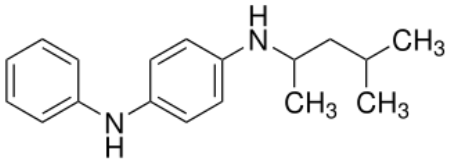	CYP1A1 induction (Zhang et al., 2023)
Benzothiazole derivatives		
Benzothiazole	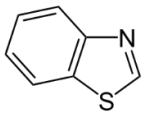	Weak AhR agonist and CYP1A1 induction (He et al., 2011; Kyung Won Seo et al., 2001)
2-Mercaptobenzothiazole	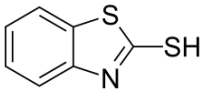	Increased AhR and CYP1A1 gene expression (Zhang et al., 2022)
Plasticizers		
Diethyl phthalate	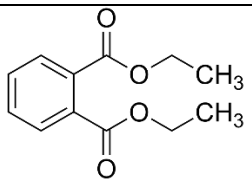	CYP1A1 inhibition (Mukherjee Das et al., 2022; Ozaki et al., 2016)
Dibutyl phthalate	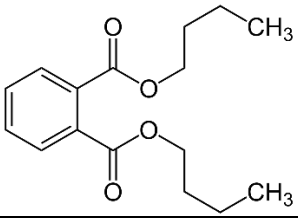	

n.q. = not quantified

Table 2: Quantification of selected compounds that leached from TR particles following sequential digestion in L.I. fluid simulants. The quantification was performed via method- and matrix-matched calibrations (**Table S2**).

	cumulative concentrations of leachates from TR MPs (µg/g) following sequential digestion in L.I. fluid simulants, (n = mean ± SD).		
Compound	**TR_{infill}**	**TR_{truck}**	**$TR_{truck,aged}$**
Benzothiazole derivatives			
Benzothiazole	76 ± 1	170 ± 2	20 ± 3
2(3H)-benzothiazolone	80 ± 7	168 ± 3	39 ± 1
Plasticizers			
Diethyl phthalate	32 ± 1	28 ± 1	21 ± 1
Dibutyl phthalate	6 ± 1	4 ± 1	9 ± 4

In addition to the selected compounds highlighted in **Table 1**, several other leached compounds were identified from TR, TPU and PA-6 particles. Following the deconvolution of mass spectra of the total ion chromatograms (TIC) of the MP leachate samples, TR was observed to leach more substances (see **Table S3** for leached compounds identified with a ≥ 80 % NIST library match score). Furthermore, UV-aging of PA-6 and TPU MPs appeared to trigger the leaching of new chemicals into the GI fluid simulants. For example, additives including 1,4-butanediol, 4-isopropoxybutanol, benzyl oleate, 4-hydroxybutyl acrylate, and diethylene glycol dibutyl ether were detected in leachates of TPU_{aged} but not of TPU (**Table S3**). Similarly, isopropyl linoleate and elaidic acid isopropyl ester were identified from aged PA-6 materials, but not from the non-aged variants. In addition to the vulcanization accelerators and plasticizers which were agonists of AhR (**Table 1**), other classes of additives identified include antioxidants, flame retardants, lubricants, stabilizers, as well as multipurpose additives (**Table S3**). For PA-6 materials, residues of caprolactam monomer and 1,8-diazocyclotetradecane-2,9-dione dimer were detected in the GI fluid simulants. Caprolactam was quantified at a cumulative concentration of 1802 ± 22 µg/g from PA-$6_{7µm}$ following sequential digestion. Lastly, pyrene, a PAH contaminant, was also released from TR particles. µg/L Meanwhile, not all compounds extracted from the MPs via TD-GC-MS were detected by

the GC-MS analyses of the fluid simulants after *in vitro* digestion (**Tables S4 and S5**). This may be related to the sensitivity limitation of the MS analyzer, whereby compounds leachedat low concentrations are indistinguishable from the background noise, unlike the large concentrations extracted via TD-GC-MS method.

3.2. UV-AGING, *IN VITRO* DIGESTION CONDITIONS, AND PARTICLE SIZE AFFECTS THE LEACHING OF CHEMICAL ADDITIVES

For improved understanding of the leaching process, the influences of UV-aging and particle sizes, incubation conditions were studied with selected MPs.

UV-aging of TR_{truck} for 2000 h, as well as PA-$6_{42\mu m}$ and TPU for 1000 h have been previously shown to induce alterations in the functionalization pattern of MP particle surfaces (Emecheta *et al*., 2022; Pfohl *et al*., 2022). As shown in **Fig. 1a**, it was observed that certain substances exhibited enhanced leaching after UV-aging. For instance, the release of diethyl phthalate increased significantly from 0.4 ± 0.1 µg/g to 20.8 ± 0.8 µg/g for PA-$6_{42\mu m}$ and from 0.5 ± 0.4 µg/g to 22 ± 2 µg/g for TPU (**Fig. 1a**). However, the leaching of benzothiazole, and 2(3H)-benzothiazolone from the aged TR_{truck} MPs decreased significantly compared to the non-aged variants. A closer look at the physicochemical properties of the leachates (**Table S2**) showed that benzothiazole and derivatives have lower boiling points and lower molecular weights compared to the phthalates, suggesting possible degradation and loss of the compounds during the 2000 h aging process**.** Similarly, as shown in **Fig. 1a** for caprolactam, the monomer of PA-6 polymer, significantly lower concentration (220 ± 30 µg/g) leached from aged PA-6 material compared to the non-aged variant (699 ± 42 µg/g). The initial caprolactam concentration could not be quantified prior to the leaching experiment; considering the lightweight and low boiling temperature of caprolactam (**Table S2**), it is assumed that non-aged PA-$6_{42\mu m}$ contained significantly higher caprolactam concentration than PA-$6_{42\mu m,\ aged}$ due to possible loss during the 1000 h aging process.

The effect of UV-aging was more pronounced for the phthalates, for which enhanced leaching in the S.I. fluid simulant was confirmed. These findings align with a study by (Luo et al., 2020) who investigated the leaching of additives from aged polyethylene particles and further highlights the significance of weathering for the human exposure to MP-associated chemicals.

As shown in **Fig. 1b**, the leaching of selected TR_{truck} chemicals were compared after incubation for 6 h at 37 °C in distilled water, CCM, and after the sequential digestion in S.I. fluid simulant. Both, the GI fluid simulants and CCM significantly enhanced the leaching of TR_{truck} chemicals compared to distilled water. For example, the leaching of benzothiazole and 2(3H)-benzothiazolone increased from 74 ± 9 µg/g and 45 ± 2 µg/g in distilled water, respectively, to 112 ± 12 µg/g and 83 ± 16 µg/g in S.I. fluid simulant. The release of diethyl and dibutyl phthalates similarly increased from 10 ± 1 µg/g and 1.42 ± 0.3 µg/g to 25 ± 7 µg/g and 3.5 ± 0.5 µg/g, respectively. Remarkably, the leached concentration of 136 ± 16 µg/g for 2(3H)-benzothiazolone in CCM was significantly higher than the cumulative concentration of 83 ± 16 µg/g in S.I. fluid simulant.

Leaching kinetics were studied for TR_{truck} and TR_{infill} variants. The particles were sequentially incubated for 6 h in S.I. fluid simulant and for 24 h in L.I. fluid simulant. As shown in **Fig. 1c**, the leaching of TR chemicals appears to increase upon further digestion in the L.I. fluid simulant. For vulcanization accelerators such as benzothiazole and 2(3H)-benzothiazolone, the kinetic effect was significant. This implies a non-attainment of leaching equilibrium. Lastly, the cumulative concentration of leached caprolactam and diethyl phthalates in the L.I. fluid simulant was significantly enhanced with decreasing median particle size of PA-6 material (**Section S5, Fig. S4**).

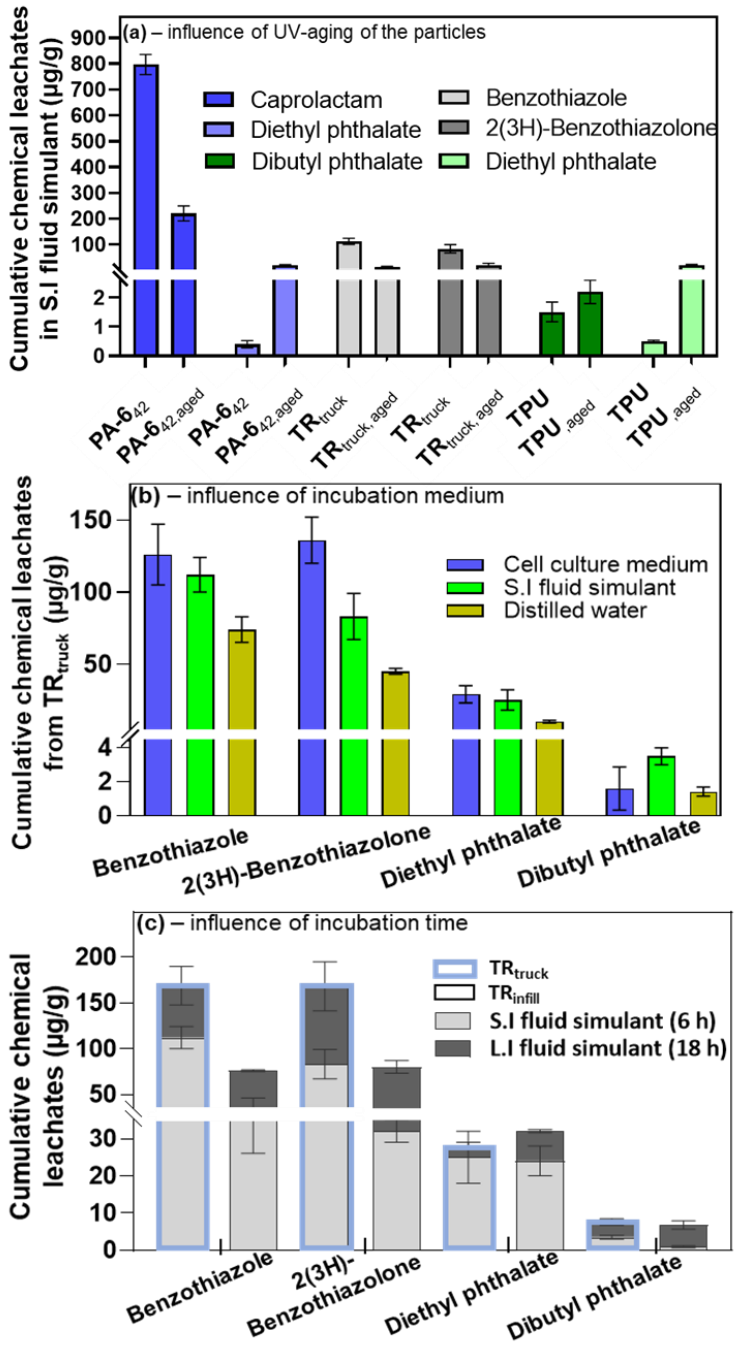

Figure 1: (A) Effect of UV-aging of microplastics on the leaching of chemicals after sequential digestion in S.I fluid simulant, N = 3 ± SD, (B) Effect of different incubation media on the leaching of chemicals from TR truck, (C): Effect of kinetics on the leaching of TR chemicals.

3.3 LEACHING OF METALS FROM TR PARTICLES IN GI FLUID SIMULANTS

A total of 24 elements were quantified at varying concentrations leaching from the TR MPs during sequential digestion in the S.I. simulant. Those include (semi-)metals which have been reported to induce toxicity in humans such as arsenic, silver, lead, cadmium, and copper (Abd Elnabi et al., 2023). As shown in **Table 3**, a high concentration of zinc (1.2 and 1.9 % (w/w) for TR_{infill} and TR_{truck}, respectively) was characterized from both TR variants following microwave-assisted extraction of the pristine particles. This is similar to the range reported in literature. For example, zinc and zinc-containing compounds such as zinc oxide, and cadmium-zinc sulfide yellow which are intentionally added as vulcanization catalysts, typically account for about 2 % (w/w) of TR ingredients (ETRMA, 2015). During *in vitro* sequential digestion for 6 h in S.I. fluid simulant, zinc was released at 1147 µg/g and 464 µg/g from TR_{truck} and TR_{infill}, respectively, representing a cumulative release of 10 % and 2 % (**Table 3**). The observed high leaching of zinc is unsurprising considering the initial high zinc content in TR particles.

Other metals present in TR MPs at mass concentrations of 0.1 – 1.0 % (w/w) such as ruthenium, aluminium, silver, iron, and copper yielded moderately high concentrations in leachates (**Table 3**). For example, silver accumulated at 237 µg/g and 77 µg/g during sequential digestion in the S.I. fluid simulant, accounting for 27 % and 104 % of the total content of TR_{infill} and TR_{truck} materials, respectively. The detected metal leachates observed herein conforms with those observed leaching from crumb TR into marine and fresh waters (Capolupo et al., 2020).

Utilizing an estimated TR ingestion rate of 1.93 µg/day and the measured relative cumulative amount of metals released in the S.I. fluid simulant, the estimated daily metal intake from TR MPs by adults was calculated (**Section S6**). As shown in **Table 3**, for adults this intake ranges from $9.14 \cdot 10^{-11}$ µg/kg/day for mercury to $1.07 \cdot 10^{-5}$ µg/kg/day for zinc. It has been suggested that zinc and other metals like copper, lead, and cadmium may play a role in dose-dependent toxic effects observed in mice and rats. (Baensch-Baltruschat et al., 2020). In this study, however, the estimated daily intake concentrations of metals leached from TR particles are

well below the Reference Dose (RfD) for humans (**Table 3**). The human RfD values presented in **Table 3** have been sourced from the US EPA CompTox Chemicals Dashbord (https://comptox.epa.gov/dashboard). RfD values for human risk assessment have been obtained from different sources, including the Integrated Risk Information System (IRIS, www.epa.gov/iris), Provisional Peer-Revied Toxicity Values (PPRTV, www.epa.gov/pprtv) or Regional Screening Levels (RSL, www.epa.gov/risk/ regional-screening-levels-rsls-generic-tables). All sources are curated by the US EPA.

table 3: overview of the metal contents in TR MPs, the cumulative amounts leached during in vitro digestion in the S.I. fluid simulant, and the estimate of daily metal intake from ingestion of TR MPs and subsequent leaching in the GI tract. *The cumulative absolute (µg/g) and relative (%) conc. of metals released in the small intestine fluid simulant. **estimate of daily metal intake based on the estimated daily MP ingestion rate and measured leaching rates (see section S8 for details). *** the reference dose RFD) values for humans. The RFD values were sourced from the us EPA Comptox chemicals dashboard.

		Total conc. in TR particles (µg/g)		*Leaching in S.I fluid simulant - µg/g (%)		**Estimated daily intake (µg/kg bw-day)		Source	Critical effect	***Reference Dose (RfD)
Metal	**CAS NO**	**TR_{infill}**	**TR_{truck}**	**TR_{infill}**	**TR_{truck}**	**TR_{infill}**	**TR_{truck}**			**(µg/kg bw/day)**
^{7}Lithium	7439-93-2	4.08	1.06	0.17 (4%)	0.06 (6%)	4.71E-09	7.60E-05	PPRTV	adverse effects	2.00E+00
^{9}Beryllium	7440-41-7	0.11	n.a	0.01 (9%)	0.01	2.73E-10	n.a.	IRIS	gastrointestinal	2.00E+00
^{27}Aluminium	7429-90-5	614.85	856.79	64.45 (10%)	27.64 (3%)	1.70E-06	7.09E-07	RSL	-	1.00E+03
^{45}Scandium	7440-20-2	313.78	214.92	236.63 (75%)	117.54 (55%)	6.49E-06	3.26E-06	-	-	n.a
^{51}Vanadium	7440-62-2	2.92	2.04	2.91 (100%)	1.32 (65%)	9.27E-04	8.07E-04	PPRTV	histopathology	7.00E-04
^{52}Chromium	7440-47-3	144.52	5.28	1.03 (1%)	0.40 (8%)	3.98E-08	1.16E-08	IRIS	gastrointestinal	9.00E-04
^{55}Manganese	7439-96-5	15.42	7.27	6.22 (40%)	1.93 (27%)	1.70E-07	5.41E-08	IRIS	nervous	1.40E+02
^{57}Iron	7439-89-6	769.93	926.48	3.89 (1%)	1.93 (0.2%)	2.12E-07	5.11E-08	RSL	-	7.00E+02
^{59}Cobalt	7440-48-4	47.86	335.54	0.22 (0.5%)	0.42 (0.1%)	6.60E-09	9.80E-09	RSL	-	3.00E-01
^{60}Nickel	7440-02-0	123.58	4.17	1.36 (1%)	0.57 (14%)	3.41E-08	1.65E-04	HEAST	decreased body weight	2.00E+01
^{65}Copper	7440-50-8	893.42	154.33	7.64 (1%)	6.63 (4%)	2.46E-07	1.70E-07	RSL	-	4.00E+01
^{66}Zinc	7440-66-6	11854.86	19320.68	1147.30 (10%)	463.46 (2%)	3.27E-05	1.07E-05	IRIS	immune, hematologic	3.00E+02
^{75}Arsenic	7440-38-2	0.63	0.56	1.11 (>100%)	0.57 (101%)	1.74E-08	1.54E-08	IRIS	cardiovascular	3.00E-01
^{95}Molybdenum	7439-98-7	12.68	0.28	0.34 (3%)	0.20 (70%)	1.05E-08	5.40E-09	IRIS	urinary	5.00E+00
^{99}Ruthenium	7440-18-8	1138.25	552.46	29.63 (3%)	23.57 (4%)	9.41E-07	6.09E-07	-	-	n.a
^{103}Rhodium	7440-16-6	332.13	n.a	198.99 (60%)	95.77	5.49E-06	n.a.	-	-	n.a
^{107}Silver	7440-22-4	882.34	73.67	236.81 (27%)	76.61 (104%)	6.57E-06	2.03E-06	IRIS	dermal	5.00E+00
^{111}Cadmium	7440-43-9	0.68	1.04	0.04 (6%)	0.02 (2%)	1.12E-09	2.48E-05	IRIS	proteinuria (water)	5.00E-01
								IRIS	proteinuria (food)	1.00E+00
^{117}Tin	7440-31-5	43.54	1.92	0.01 (0%)	0.03 (2%)	2.40E-10	1.85E-05	RSL	-	6.00E+02
^{121}Antimony	7440-36-0	0.95	0.53	0.09 (10%)	0.05 (9%)	2.62E-09	1.32E-09	IRIS	hematological	4.00E-01
^{202}Mercury	7439-97-6	0.07	0.03	0.00 (5%)	0.002 (8%)	9.65E-11	6.62E-11	OW Drinking Water Standards	-	3.00E-01
^{205}Thallium	7440-32-6	0.09	0.14	0.02 (23%)	0.01 (6%)	5.71E-10	2.32E-10	PPRTV	histopathological	1.00E-02
^{207}Lead	7439-92-1	52.82	22.50	0.53 (1%)	0.21 (1%)	1.46E-08	6.20E-09	-	-	n.a.
^{209}Bismuth	7440-69-9	337.86	n.a	131.77 (39%)	68.16	3.63E-06	n.a.	-	-	n.a.

n.a. = not assessed
PPRTV = Provisonal Peer-Reviewed Toxicity Values
IRIS = Integrated Risk Information System
RSL = Regional Screening Levels

3.4. SOME ADDITIVES RELEASED FROM TR PARTICLES INDUCE CYP1A1 IN CACO-2 CELLS

Before we could investigate whether the MP particles themselves or their leachates actually induce CYP1A1, we firstly had to investigate their potential cytotoxicity on differentiated human intestinal CaCo-2 cells, also considering the variants that were UV-aged or subjected to *in vitro* digestion. Exposure at concentrations ranging from 3-100 µg/mL for 24 h did not result in any significant decrease in cell viability, as measured by means of the MTT assay (**Section S7, Fig. S5**). Similarly, Lehner *et al.* investigated cellular effects of various MPs, including TR, PA-

6 and TPU, in an established 3D CaCo-2/HT29-MTX model. No significant cytotoxic effects were detected via an LDH assay (Lehner et al., 2020).

Next, we assessed the induction of CYP1A1 in undifferentiated and differentiated CaCo-2 cells following exposure to the different MPs. The undifferentiated cell culture model was used for a first screening. Cells were exposed to selected pristine MPs for 24 h at particle concentrations of 100 µg/mL. In addition, cells were exposed to CCM which was pre-incubated with the TR particles for 24 h and then separated from the MPs by centrifugation. The CYP1A1 gene expression was examined by RT-qPCR. Whereas PA-$6_{42µm}$, PA-$6_{7µm}$ and TPU particles did not induce CYP1A1 (**Fig. S6**), all TR materials showed an effect in undifferentiated CaCo-2 cells (**Fig. 2a**). Exposure to TR_{truck} and TR_{infill} led to a significant increase ($p \leq 0.001$) in CYP1A1 expression. For $TR_{truck,\ aged}$, which was UV-aged for 2000 h, the effect was lower and not significant. Furthermore, the exposure to CCM containing the leached compounds but not the TR particles led to comparable results. This indicates that the leached chemicals were indeed responsible for the CYP1A1 induction.

In a next step, we investigated the effects of *in vitro* digestion of the TR particles on CYP1A1 induction in the differentiated CaCo-2 3D model. Cells were exposed for 24 h to the pristine and *in vitro* digested TR particles. The results show a higher variability within the biological replicates compared to the undifferentiated cell culture model (**Fig. 2b**). Therefore, we analysed 4 biological replicates instead of three and depicted the results as box plots. In summary, results are comparable for the pristine particles as shown in **Fig. 2a**. TR_{infill} was the only material that significantly induced CYP1A1 ($p \leq 0.01$) in differentiated CaCo-2 cells compared to the control. TR_{truck} and $TR_{truck,aged}$ showed lower and insignificant effects. *In vitro* digestion in GI fluid simulants resulted in a smaller increase in CYP expression compared to the pristine TR materials. Dilution of the leachates into CCM, which was necessary to achieve comparable MP concentrations and conditions compatible with cell culture, is likely responsible for this effect.

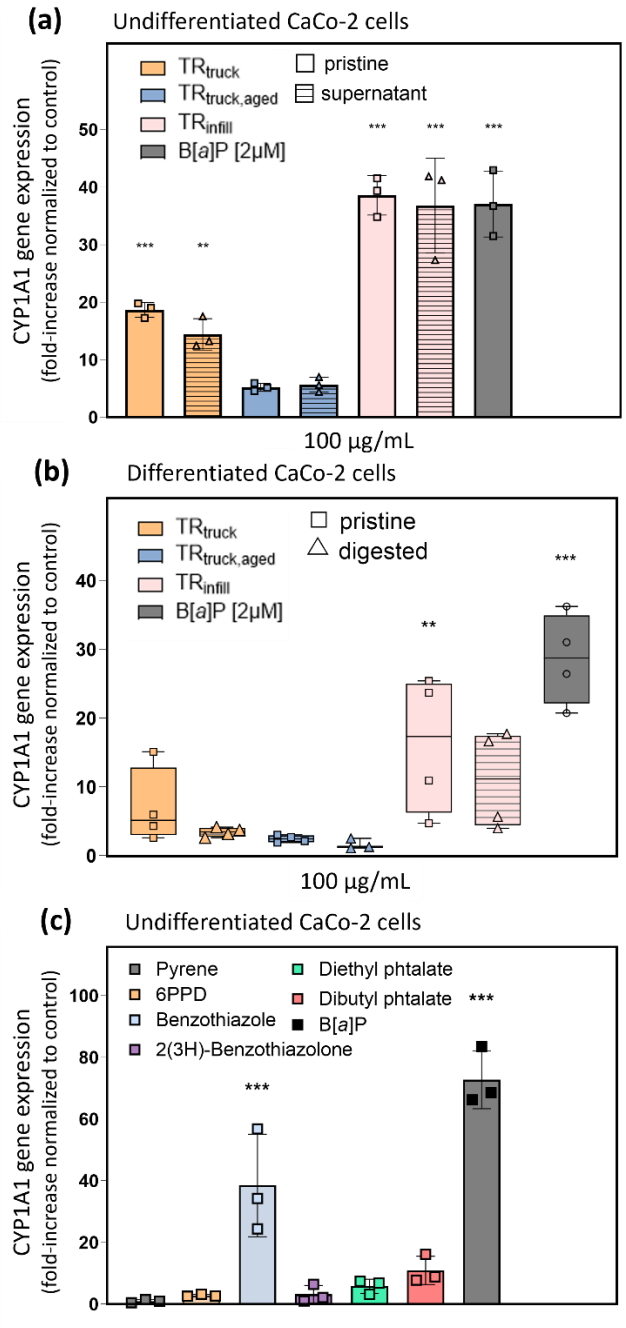

Figure 2: Cytochrome P450 1A1 (CYP1A1) induction in human intestinal CaCo-2 cells. Cells were exposed to different tire wear materials at concentrations of 100 µg/mL in CCM for 24 h. (a) Undifferentiated CaCo-2 cells were exposed to the pristine particles or their corresponding supernatants after incubation for 24 h in CCM. (b) Differentiated cells were exposed to pristine particles and particles that were digestested in gastrointestinal fluid simulants before cell culture treatment. (c) Undifferentiated CaCo-2 cells were exposed for 24 h to selected additives: pyrene, N-(1,3-dimethylbutyl)-N'-phenyl-p-phenylendiamin (6PPD) and 2(3H)-benzothiazolone at concentrations of 5 µM and benzothiazole and diethyl and dibutyl phthalate at concentrations of 0.5 µM. All results were normalized to untreated cells (medium control). For all experiments, benzo[a]pyrene (B[a]P) was used as a positive control at a concetration of 2 µM (a,b) or 5 µM (c). Statistical analysis was performed

by using an one-way ANOVA for at least three (undifferentiated CaCo-2) or four (differentiated CaCo-2) independent biological replicates (* = $p < 0.05$, ** = $p < 0.01$ and *** = $p \leq 0.001$).

We aimed to investigate whether the organic compounds detected in leachates during *in vitro* digestion (**Table 1**) could in principle be responsible for the observed induction of CYP1A1. Thus, undifferentiated CaCo-2 cells were exposed to individual leachates for 24 h. Benzothiazole led to the highest increase of CYP1A1 gene expression with a 38.5-fold induction at a concentration of 0.5 µM (**Fig. 2c**). 2(3H)-benzothiazolone induced CYP1A1 slightly with a 3.2-fold increase. In the context of tire abrasion, benzothiazole derivatives such as 2-methylthiobenzothiazole and 2-mercaptobenzothiazole have already been identified as AhR agonists (He et al., 2011). Benzothiazole itself was only identified as a weak AhR agonist. However, there are other AhR independent pathways for modulating CYP1A1 gene expression (Delescluse et al., 2000; Guigal et al., 2000), which might explain for the high induction after exposure to benzothiazole in our study. The treatment with 0.5 µM diethyl or dibutyl phthalate resulted in 6.1 and 8.7-fold CYP1A1 induction, respectively. Interestingly, other studies have shown that several phthalates can inhibit CYP1A1 gene expression in rat liver microsomes (Barta et al., 2015) or in a virtual screening model (Goh et al., 2021). One potential explanation for these observed discrepancies may be the fact that the specificity of the AhR ligand is highly species-dependent (Murray et al., 2014). Finally, pyrene did not induce CYP1A1 gene expression. However, it is also important to note that other cytochrome P450 enzymes, especially CYP1A2 or CYP1B1, play a significant role in pyrene metabolism in CaCo-2 cells (Hessel et al., 2013).

3.5. PRELIMINARY HAZARD SCREENING OF LEACHATES AND IMPLICATIONS FOR EXPOSURE ASSESSMENT

To provide insight into potential adverse outcomes of the identified leached compounds, they were screened for links to potential AOPs using the ToxCast database (US EPA, 2023). Of all the compounds identified with a NIST library score of ≥ 80 %, 54 were found in the ToxCast database, and 20 of them were linked to relevant AOPs (**Fig. 3**). We screened these AOPs

and identified 32 that apply to humans and have moderate to high evidence of a connection between molecular initiating events, key events, and adverse outcomes (**Section S8**, **Table S6**). Notable AOPs include those associated with the activation of AhR (AOP 41, 57, 131, and 150), estrogen receptors (AOP 167, 200), cyclooxygenase inhibition (AOP 63, 102, 103), and activation of nuclear receptors such as peroxisome proliferator-activated receptors (AOPs 6, 18, 37, 51, 163, and 166). Among the identified compounds, 2-mercaptobenzothiazole and phenolic compounds were associated with the highest number of potential AOPs. In laboratory studies, these compounds have been associated with the disruption of endocrine functions of mammals (Kim et al., 2019; Wang & Qian, 2021), leading to reproductive and neurological disorders (Kim et al., 2019). Recently, exposure to 2-mercaptobenzothiazole was linked to a possible risk of bladder cancer (Zhang et al., 2022).

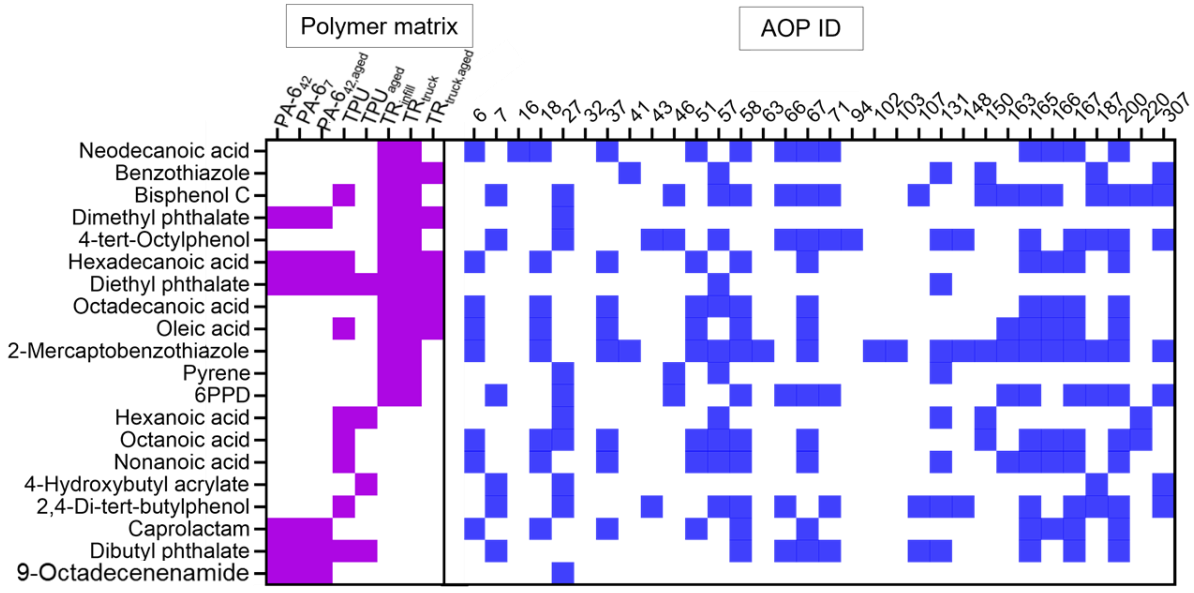

FIGURE 1: OUTLINE OF POTENTIAL ADVERSE OUTCOME PATHWAYS (AOPS) OF CHEMICALS RELEASED FROM MICROPLASTICS DURING SEQUENTIAL DIGESTION IN GASTROINTESTINAL (GI) FLUID SIMULANTS. AOPS WERE SOURCED ONLINE FROM THE EPA TOXCAST DATABASE (US EPA, 2023), AND SCREENED ACCORDINGLY (SEE SECTION S8 FOR DETAILS).

However, a thorough assessment of human exposure to chemical additives from MPs is challenged by several factors. Firstly, there are huge uncertainties related to the mass and type of MP intake. Secondly, the extent to which ingested MP-chemicals become bioavailable

is usually roughly estimated (Mohamed Nor et al., 2021), and remains subject to considerable uncertainty (Ortega-Calvo et al., 2015). Thirdly, the contributions of the bioavailable fraction of additives and contaminants including monomer residues to the body's chemical burden is unknown due to paucity of data (WHO, 2022). Unlike contaminants such as PAHs, for which minimal relative importance has been suggested (Emecheta *et al.*, 2024), human exposure to some high-leaching additives such as benzothiazole, 2(3H)-benzothiazolone, zinc and monomer residues including caprolactam and 1,4-butanediol may become significant, particularly in scenarios involving frequent exposures, such as those encountered in recycling, shredding, or production facilities (Kogevinas et al., 1998; Sorahan, 2009).

4. CONCLUSION

The release of additives from UV-aged and non-aged variants of TR, PA-6, and TPU particles in the human GI tract was simulated *in vitro* by sequential digestion of these materials in intestinal fluid simulants. TR particles released more chemicals compared to MPs derived from PA-6 and TPU. Among quantified leachates, benzothiazole (112 µg/g from TR_{truck} particles), zinc (1147 µg/g from TR_{infill} particles) and caprolactam (1800 µg/g from PA-$6_{7µm}$ MPs) were those with the highest measured concentrations in the S.I. fluid simulant. The leaching behavior was modulated by the composition of the fluid simulants. Compared to the leaching of chemicals in distilled water, there was a significant increase in leaching in the GI fluid simulants and in CCM. After UV-aging, additional chemicals were released from the particles. However, the leaching of other chemicals, including benzothiazole and caprolactam, was reduced.

The cellular effects of the different MPs were investigated in the human intestinal CaCo-2 cell culture model. None of the MP particles showed any cytotoxic effects. However, TR particles induced CYP1A1 gene expression. Specific additives, including benzothiazole and its derivatives and diethyl and dibutyl phthalates were identified as important contributors to the

CYP1A1 induction. UV-aging reduced this effect, which may be linked to the decrease in leaching of benzothiazole detected through GC-MS analysis.

In addition, 20 of the released chemicals from TR were linked to different AOPs, providing indications for other types of toxicities being relevant for humans. Further investigations are required to substantiate these findings, focusing for example on the evaluation of the bioavailability of the leachates across the intestinal barriers, as well as the estimation of the relative contribution of the leached chemicals to total human chemical exposure, and a complete quantitative characterization of the MP leachates in the simulated GI fluids. Only a select number of the identified compounds were quantified in this study.

5. DECLARATION OF COMPETING INTEREST

The authors declare no potential competing interests.

6. ACKNOWLEDGMENT

Dr. Korinna Altmann (Bundesanstalt für Materialforschung, Germany) is acknowledged for providing the cryomilled ELT tire granulates (TR_{infill}). We thank Dr. Benjamin Sachse and Dr. Holger Sieg for providing useful input to this manuscript, specifically on the risk assessment of metals.

7. FUNDING

This work was partially funded by the BMBF (German Federal Ministry of Education and Research) third-party project InnoMat.Life – Innovative materials: safety in lifecycle, (funding no: 03XP0216A (BfR) and the EC Horizon 2020 third-party project POLYRISK (Grant ID 964766)

8. AUTHOR CONTRIBUTIONS

EEE and AV planned the study with support from AH and AR. Experiments were carried out by EEE, AV, AB and RS. The *in vitro* digestion of the different microplastics was conducted by EEE. EEE performed the analytical studies and was supported by RS for the ICP-MS experiments. AV and AB performed the toxicological studies. AV conducted the RT-qPCR experiments. EEE and AV performed the data analysis. EEE and AV wrote the manuscript with contributions from WW, AH and AR. The study was supervised by AH and AR. All authors read and approved the final manuscript.

9. REFERENCES

Abd Elnabi, M. K., Elkaliny, N. E., Elyazied, M. M., Azab, S. H., Elkhalifa, S. A., Elmasry, S., Mouhamed, M. S., Shalamesh, E. M., Alhorieny, N. A., Abd Elaty, A. E., Elgendy, I. M., Etman, A. E., Saad, K. E., Tsigkou, K., Ali, S. S., Kornaros, M., & Mahmoud, Y. A. (2023). Toxicity of Heavy Metals and Recent Advances in Their Removal: A Review. *Toxics, 11*(7). doi:10.3390/toxics11070580

Armada, D., Martinez-Fernandez, A., Celeiro, M., Dagnac, T., & Llompart, M. (2023). Assessment of the bioaccessibility of PAHs and other hazardous compounds present in recycled tire rubber employed in synthetic football fields. *Sci Total Environ, 857*(Pt 2), 159485. doi:10.1016/j.scitotenv.2022.159485

Baensch-Baltruschat, B., Kocher, B., Stock, F., & Reifferscheid, G. (2020). Tyre and road wear particles (TRWP) - A review of generation, properties, emissions, human health risk, ecotoxicity, and fate in the environment. *Sci Total Environ, 733*, 137823. doi:10.1016/j.scitotenv.2020.137823

Bai, C. L., Liu, L. Y., Guo, J. L., Zeng, L. X., & Guo, Y. (2022). Microplastics in take-out food: Are we over taking it? *Environ Res, 215*(Pt 3), 114390. doi:10.1016/j.envres.2022.114390

Barta, F., Levova, K., Hodek P, Schmeiser HH, Arlt VM, & M., S. (2015). The effects of heavy metal ions, phthalates and ochratoxin A on oxidation of carcinogenic aristolochic acid I causing Balkan endemic nephropathy. *Neuro Endocrinol Lett. , 36 Suppl 1:13-21*.

Brinkmann, M., Montgomery, D., Selinger, S., Miller, J. G. P., Stock, E., Alcaraz, A. J., Challis, J. K., Weber, L., Janz, D., Hecker, M., & Wiseman, S. (2022). Acute Toxicity of the Tire

Rubber-Derived Chemical 6PPD-quinone to Four Fishes of Commercial, Cultural, and Ecological Importance. *Environmental Science & Technology Letters, 9*(4), 333-338. doi:10.1021/acs.estlett.2c00050

Campanale, C., Massarelli, C., Savino, I., Locaputo, V., & Uricchio, V. F. (2020). A Detailed Review Study on Potential Effects of Microplastics and Additives of Concern on Human Health. *Int J Environ Res Public Health, 17*(4). doi:10.3390/ijerph17041212

Capolupo, M., Sørensen, L., Jayasena, K. D. R., Booth, A. M., & Fabbri, E. (2020). Chemical composition and ecotoxicity of plastic and car tire rubber leachates to aquatic organisms. *Water Research, 169*. doi:10.1016/j.watres.2019.115270

Delescluse, C., Lemaire, G., de Sousa, G., & Rahmani, R. (2000). Is CYP1A1 induction always related to AHR signaling pathway? *Toxicology, 153*(1-3), 73-82. doi:10.1016/s0300-483x(00)00305-x

Diekmann, A., Giese, U., & Schaumann, I. (2019). Polycyclic aromatic hydrocarbons in consumer goods made from recycled rubber material: A review. *Chemosphere, 220*, 1163-1178. doi:10.1016/j.chemosphere.2018.12.111

ECHA. (2023a). Mapping exercise – Plastic additives initiative. Retrieved from https://echa.europa.eu/mapping-exercise-plastic-additives-initiative

ECHA. (2023b). Endocrine disruptor assessment list. Retrieved from https://echa.europa.eu/ed-assessment

Eisentraut, P., Dümichen, E., Ruhl, A. S., Jekel, M., Albrecht, M., Gehde, M., & Braun, U. (2018). Two Birds with One Stone—Fast and Simultaneous Analysis of Microplastics: Microparticles Derived from Thermoplastics and Tire Wear. *Environmental Science & Technology Letters, 5*(10), 608-613. doi:10.1021/acs.estlett.8b00446

Emecheta, E. E., Borda, D. B., Pfohl, P. M., Wohlleben, W., Hutzler, C., Haase, A., & Roloff, A. (2022). A comparative investigation of the sorption of polycyclic aromatic hydrocarbons to various polydisperse micro- and nanoplastics using a novel third-phase partition method. *Microplastics and Nanoplastics, 2*(1). doi:10.1186/s43591-022-00049-9

Emecheta, E. E., Pfohl, P. M., Wohlleben, W., Haase, A., & Roloff, A. (2024). Desorption of Polycyclic Aromatic Hydrocarbons from Microplastics in Human Gastrointestinal Fluid Simulants─ Implications for Exposure Assessment. *ACS omega*. doi:https://doi.org/10.1021/acsomega.3c09380

Eriksson, U., Titaley, I. A., Engwall, M., & Larsson, M. (2022). Examination of aryl hydrocarbon receptor (AhR), estrogenic and anti-androgenic activities, and levels of polyaromatic compounds (PACs) in tire granulates using in vitro bioassays and chemical analysis. *Chemosphere, 298*, 134362. doi:10.1016/j.chemosphere.2022.134362

ETRMA. (2015). *End-of-life Tyre Report*. Retrieved from Belgium: https://www.etrma.org/wp-content/uploads/2019/09/elt-report-v9a-final.pdf

Fishbein, L. (1991). Municipal and industrial hazardous waste management: an overview. *Toxicol Ind Health, 7*(5-6), 209-220. doi:10.1177/074823379100700524

Goh, J. J. N., Behn, J., Chong, C. S., Zhong, G., Maurer-Stroh, S., Fan, H., & Loo, L. H. (2021). Structure-based virtual screening of CYP1A1 inhibitors: towards rapid tier-one assessment of potential developmental toxicants. *Arch Toxicol, 95*(9), 3031-3048. doi:10.1007/s00204-021-03111-2

Groh, K. J., Backhaus, T., Carney-Almroth, B., Geueke, B., Inostroza, P. A., Lennquist, A., Leslie, H. A., Maffini, M., Slunge, D., Trasande, L., Warhurst, A. M., & Muncke, J. (2019). Overview of known plastic packaging-associated chemicals and their hazards. *Sci Total Environ, 651*(Pt 2), 3253-3268. doi:10.1016/j.scitotenv.2018.10.015

Guigal, N., Seree, E., Bourgarel-Rey, V., & Barra, Y. (2000). Induction of CYP1A1 by serum independent of AhR pathway. *Biochem Biophys Res Commun, 267*(2), 572-576. doi:10.1006/bbrc.1999.1959

Haidar, R., Henkler, F., Kugler, J., Rosin, A., Genkinger, D., Laux, P., & Luch, A. (2021). The role of DNA-binding and ARNT dimerization on the nucleo-cytoplasmic translocation of the aryl hydrocarbon receptor. *Sci Rep, 11*(1), 18194. doi:10.1038/s41598-021-97507-w

Halsband, C., Sørensen, L., Booth, A. M., & Herzke, D. (2020). Car Tire Crumb Rubber: Does Leaching Produce a Toxic Chemical Cocktail in Coastal Marine Systems? *Frontiers in Environmental Science, 8*. doi:10.3389/fenvs.2020.00125

He, G., Zhao, B., & Denison, M. S. (2011). Identification of benzothiazole derivatives and polycyclic aromatic hydrocarbons as aryl hydrocarbon receptor agonists present in tire extracts. *Environ Toxicol Chem, 30*(8), 1915-1925. doi:10.1002/etc.581

Henkel, C., Huffer, T., & Hofmann, T. (2022). Polyvinyl Chloride Microplastics Leach Phthalates into the Aquatic Environment over Decades. *Environ Sci Technol, 56*(20), 14507-14516. doi:10.1021/acs.est.2c05108

Hessel, S., Lampen, A., & Seidel, A. (2013). Polycyclic aromatic hydrocarbons in food--efflux of the conjugated biomarker 1-hydroxypyrene is mediated by Breast Cancer Resistance Protein (ABCG2) in human intestinal Caco-2 cells. *Food Chem Toxicol, 62*, 797-804. doi:10.1016/j.fct.2013.10.007

Hlisnikova, H., Petrovicova, I., Kolena, B., Sidlovska, M., & Sirotkin, A. (2020). Effects and Mechanisms of Phthalates' Action on Reproductive Processes and Reproductive Health: A Literature Review. *Int J Environ Res Public Health, 17*(18). doi:10.3390/ijerph17186811

Horodytska, O., Cabanes, A., & Fullana, A. (2020). Non-intentionally added substances (NIAS) in recycled plastics. *Chemosphere, 251*, 126373. doi:10.1016/j.chemosphere.2020.126373

InnoMat.Life. (2022). *Dispersion of Polydisperse Polymers Particles – SOP – v1.0*. Retrieved from https://nanopartikel.info/wissen/arbeitsanweisungen

Kim, J. J., Kumar, S., Kumar, V., Lee, Y. M., Kim, Y. S., & Kumar, V. (2019). Bisphenols as a Legacy Pollutant, and Their Effects on Organ Vulnerability. *Int J Environ Res Public Health, 17*(1). doi:10.3390/ijerph17010112

Koelmans, A. A., Mohamed Nor, N. H., Hermsen, E., Kooi, M., Mintenig, S. M., & De France, J. (2019). Microplastics in freshwaters and drinking water: Critical review and assessment of data quality. *Water Res, 155*, 410-422. doi:10.1016/j.watres.2019.02.054

Kogevinas, M., Sala, M., Boffetta, P., Kazerouni, N., Kromhout, H., & Hoar-Zahm, S. (1998). Cancer risk in the rubber industry: a review of the recent epidemiological evidence. *Occup Environ Med, 55*(1), 1-12. doi:10.1136/oem.55.1.1

Kole, P. J., Lohr, A. J., Van Belleghem, F., & Ragas, A. M. J. (2017). Wear and Tear of Tyres: A Stealthy Source of Microplastics in the Environment. *Int J Environ Res Public Health, 14*(10). doi:10.3390/ijerph14101265

Kyung Won Seo, Mijung Park, Jun Gyou Kim, Tae Wan Kim, & Kim, H. J. (2001). Effects of benzothiazole on the xenobiotic metabolizing enzymes and metabolism of acetaminophen. *Journal of Applied Toxicology, 20*(6). doi:10.1002/1099-1263(200011/12)20:6<427::AID-JAT707>3.0.CO;2-%23

Lee, B.-K. (2010). *Sources, Distribution and Toxicity of Polyaromatic Hydrocarbons (PAHs) in Particulate Matter*. United Kingdom: IntechOpen.

Lehner, R., Wohlleben, W., Septiadi, D., Landsiedel, R., Petri-Fink, A., & Rothen-Rutishauser, B. (2020). A novel 3D intestine barrier model to study the immune response upon exposure to microplastics. *Arch Toxicol, 94*(7), 2463-2479. doi:10.1007/s00204-020-02750-1

Lim, X. (2021). Microplastics are everywhere - but are they harmful? *Nature, 593*(7857), 22-25. doi:10.1038/d41586-021-01143-3

Lombardi, G., Di Russo, M., Zjalic, D., Lanza, T., Simmons, M., Moscato, U., Ricciardi, W., & Chiara, C. (2022). Microplastics inhalation and their effects on human health: a systematic review. *European Journal of Public Health, 32*(Supplement_3). doi:10.1093/eurpub/ckac131.152

Lotz, A., Pesch, B., Dettbarn, G., Raulf, M., Welge, P., Rihs, H. P., Breuer, D., Gabriel, S., Hahn, J. U., Bruning, T., & Seidel, A. (2016). Metabolites of the PAH diol epoxide

pathway and other urinary biomarkers of phenanthrene and pyrene in workers with and without exposure to bitumen fumes. *Int Arch Occup Environ Health, 89*(8), 1251-1267. doi:10.1007/s00420-016-1160-4

Luo, H., Zhao, Y., Li, Y., Xiang, Y., He, D., & Pan, X. (2020). Aging of microplastics affects their surface properties, thermal decomposition, additives leaching and interactions in simulated fluids. *Sci Total Environ, 714*, 136862. doi:10.1016/j.scitotenv.2020.136862

Mohamed Nor, N. H., Kooi, M., Diepens, N. J., & Koelmans, A. A. (2021). Lifetime Accumulation of Microplastic in Children and Adults. *Environ Sci Technol, 55*(8), 5084-5096. doi:10.1021/acs.est.0c07384

Mukherjee Das, A., Gogia, A., Garg, M., Elaiyaraja, A., Arambam, P., Mathur, S., Babu-Rajendran, R., Deo, S. V. S., Kumar, L., Das, B. C., & Janardhanan, R. (2022). Urinary concentration of endocrine-disrupting phthalates and breast cancer risk in Indian women: A case-control study with a focus on mutations in phthalate-responsive genes. *Cancer Epidemiol, 79*, 102188. doi:10.1016/j.canep.2022.102188

Murray, I. A., Patterson, A. D., & Perdew, G. H. (2014). Aryl hydrocarbon receptor ligands in cancer: friend and foe. *Nat Rev Cancer, 14*(12), 801-814. doi:10.1038/nrc3846

OECD. (2022). Global Plastics Outlook: Economic Drivers, Environmental Impacts and Policy Options, . *OECD publishing, Paris*. doi:10.1787/de747aef-en

Oliveri Conti, G., Ferrante, M., Banni, M., Favara, C., Nicolosi, I., Cristaldi, A., Fiore, M., & Zuccarello, P. (2020). Micro- and nano-plastics in edible fruit and vegetables. The first diet risks assessment for the general population. *Environ Res, 187*, 109677. doi:10.1016/j.envres.2020.109677

Ortega-Calvo, J. J., Harmsen, J., Parsons, J. R., Semple, K. T., Aitken, M. D., Ajao, C., Eadsforth, C., Galay-Burgos, M., Naidu, R., Oliver, R., Peijnenburg, W. J., Rombke, J., Streck, G., & Versonnen, B. (2015). From Bioavailability Science to Regulation of Organic Chemicals. *Environ Sci Technol, 49*(17), 10255-10264. doi:10.1021/acs.est.5b02412

Ozaki, H., Sugihara, K., Watanabe, Y., Ohta, S., & Kitamura, S. (2016). Cytochrome P450-inhibitory activity of parabens and phthalates used in consumer products. *J Toxicol Sci, 41*(4), 551-560. doi:10.2131/jts.41.551

Parvin, F., & Tareq, S. M. (2021). Impact of landfill leachate contamination on surface and groundwater of Bangladesh: a systematic review and possible public health risks assessment. *Appl Water Sci, 11*(6), 100. doi:10.1007/s13201-021-01431-3

Pfohl, P., Wagner, M., Meyer, L., Domercq, P., Praetorius, A., Huffer, T., Hofmann, T., & Wohlleben, W. (2022). Environmental Degradation of Microplastics: How to Measure Fragmentation Rates to Secondary Micro- and Nanoplastic Fragments and

Dissociation into Dissolved Organics. *Environ Sci Technol, 56*(16), 11323-11334. doi:10.1021/acs.est.2c01228

Ramasamy, E. V., & Harit, A. K. (2023). *Microplastics in Human Consumption*. USA: CRC Press.

Rauert, C., Charlton, N., Okoffo, E. D., Stanton, R. S., Agua, A. R., Pirrung, M. C., & Thomas, K. V. (2022). Concentrations of Tire Additive Chemicals and Tire Road Wear Particles in an Australian Urban Tributary. *Environ Sci Technol, 56*(4), 2421-2431. doi:10.1021/acs.est.1c07451

Skoczynska, E., Leonards, P. E. G., Llompart, M., & de Boer, J. (2021). Analysis of recycled rubber: Development of an analytical method and determination of polycyclic aromatic hydrocarbons and heterocyclic aromatic compounds in rubber matrices. *Chemosphere, 276*, 130076. doi:10.1016/j.chemosphere.2021.130076

Smith, M., Love, D. C., Rochman, C. M., & Neff, R. A. (2018). Microplastics in Seafood and the Implications for Human Health. *Curr Environ Health Rep, 5*(3), 375-386. doi:10.1007/s40572-018-0206-z

Sorahan, T. (2009). Cancer risks in chemical production workers exposed to 2-mercaptobenzothiazole. *Occup Environ Med, 66*(4), 269-273. doi:10.1136/oem.2008.041400

Stephensen, E., Adolfsson-Erici, M., Celander, M., Hulander, M., Parkkonen, J., Hegelund, T., Sturve, J., Hasselberg, L., Bengtsson, M., & Forlin, L. (2003). Biomarker responses and chemical analyses in fish indicate leakage of polycyclic aromatic hydrocarbons and other compounds from car tire rubber. *Environ Toxicol Chem, 22*(12), 2926-2931. doi:10.1897/02-444

UNEP. (2018). *Mapping of global plastics value chain and plastics losses to the environment (with a particular focus on marine environment)*. Retrieved from https://www.unep.org/resources/report/mapping-global-plastics-value-chain-and-plastics-losses-environment-particular

Unice, K. M., Kreider, M. L., & Panko, J. M. (2013). Comparison of tire and road wear particle concentrations in sediment for watersheds in France, Japan, and the United States by quantitative pyrolysis GC/MS analysis. *Environ Sci Technol, 47*(15), 8138-8147. doi:10.1021/es400871j

US EPA. (2023). ToxCast & compTox chemicals dashboard. Retrieved from https://www.epa.gov/chemical-research/exploring-toxcast-data

Wan, Y., Chen, X., Liu, Q., Hu, H., Wu, C., & Xue, Q. (2022). Informal landfill contributes to the pollution of microplastics in the surrounding environment. *Environ Pollut, 293*, 118586. doi:10.1016/j.envpol.2021.118586

Wang, Y., & Qian, H. (2021). Phthalates and Their Impacts on Human Health. *Healthcare (Basel), 9*(5). doi:10.3390/healthcare9050603

WHO. (2022). *Dietary and inhalation exposure to nano- and microplastic particles and potential implications for human health*. (978-92-4-005460-8). Geneva

Wiesinger, H., Wang, Z., & Hellweg, S. (2021). Deep Dive into Plastic Monomers, Additives, and Processing Aids. *Environ Sci Technol, 55*(13), 9339-9351. doi:10.1021/acs.est.1c00976

Zhang, Cui, S., Shen, L., Gao, Y., Liu, W., Zhang, C., & Zhuang, S. (2022). Promotion of Bladder Cancer Cell Metastasis by 2-Mercaptobenzothiazole via Its Activation of Aryl Hydrocarbon Receptor Transcription: Molecular Dynamics Simulations, Cell-Based Assays, and Machine Learning-Driven Prediction. *Environ Sci Technol, 56*(18), 13254-13263. doi:10.1021/acs.est.2c05178

Zhang, Gan, X., Shen, B., Jiang, J., Shen, H., Lei, Y., Liang, Q., Bai, C., Huang, C., Wu, W., Guo, Y., Song, Y., & Chen, J. (2023). 6PPD and its metabolite 6PPDQ induce different developmental toxicities and phenotypes in embryonic zebrafish. *J Hazard Mater, 455*, 131601. doi:10.1016/j.jhazmat.2023.131601

6.8. SUPPLEMENTARY INFORMATION FOR MANUSCRIPT 3

Supplementary Information

Leaching of Chemical Additives from Microplastics during *in vitro* Gastrointestinal Digestion and Toxicity Assessment of Leached Compounds

Emeka Ephraim Emecheta[1,2#], Amelie Vogel[1,3#], Antje Begert[1], Roman Schmidt[1], Wendel Wohlleben[4], Andrea Haase[1*], Alexander Roloff[1*]

[1]German Federal Institute for Risk Assessment (BfR), Department of Chemical and Product Safety, Berlin, Germany

[2]Bayreuth Center for Ecology and Environmental Research (BayCEER), University of Bayreuth, Bayreuth, Germany

[3]Technische Universität Berlin, Food Chemistry and Toxicology, Berlin, Germany

[4]BASF SE, Ludwigshafen, Germany

[5]Freie Universität Berlin, Institute of Pharmacy, Berlin, Germany

Corresponding authors:

Andrea Haase: andrea.haase@bfr.bund.de

Alexander Roloff: alexander.roloff@bfr.bund.de

# Emeka Ephraim Emecheta and Amelie Vogel contributed equally to this work
* Andrea Haase and Alexander Roloff contributed equally to this work

TABLE OF CONTENTS

SECTION S1: DETERMINATION OF COMPOUNDS LEACHED FROM MICROPLASTICS DURING DIGESTION IN HUMAN GI FLUID SIMULANTS

Table S1: Composition of the GI fluid simulant adapted from (Emecheta et al., 2024).

	Composition of the gastrointestinal fluid simulants (mg/mL)			
Components	**Saliva**	**Gastric**	**Small intestine**	**Large intestine**
Sodium chloride	1.5	4.2		-
Calcium chloride dihydrate	0.5	-	0.5	-
Sodium sulfate	1.8	-		-
Potassium chloride	1.5	1.0	0.3	-
Potassium dihydrogen phosphate	2.0	0.4	-	-
Sodium thiocyanate	0.5	-	-	-
Sodium carbonate	0.5	-	1.0	-
Magnesium chloride hexahydrate	-	-	0.2	-
Bile salts	-	-	9.0	-
Urea	0.3	-	0.3	-
Uric acid	0.3	-	-	-
α-Amylase	0.8	-	-	-
Bovine serum albumin (BSA)	-	10.0	-	-
Pepsin	-	1.4	-	-
Mucin	-	4.3	-	-
Lipase	-	-	6.5	-
Pancreatin	-	-	9.0	-
Trypsin	-	-	0.3	-
δ - cellulase	-	-	-	0.2
δ - xylanase	-	-	-	3.5
δ - pectinase	-	-	-	4.7
β-glucanase	-	-		0.08
pH	6.50	1.75	6.75	8.30

Table S2: parameters of the method and matrix-matched calibration as described elsewhere (Emecheta et al., 2024). the calibrations were linear in the tested range of 50–5000 ng. a qualifier ion was monitored for each quantifier ion. 2500 ng of internal standards (ISD) were utilized. ǂ, ǂǂ, and * denotes ISD for caprolactam, the benzothiazoles, and the phthalates respectively.

Standards	RT	Qualifier	Quantifier	Tested range (ng)	Log $K_{o/w}$	B.P (° C)
Caprolactam	16.66	85	113	50 - 5000	-0.218	269

Benzothiazole	15.50	108	135	50 - 5000	2.1	230
2(3H)-Benzothiazolone	23.60	146	151	50 - 5000	2.09	262
Diethyl phthalate	20.88	135	222	50 - 5000	2.63	296
Dibutyl phthalate	25.28	136	278	50 - 5000	4.61	340
[f]Naphthalene-d8	13.81	134	136	-	-	-
[#]Anthracene-d10	24.38	187	188	-	-	-
[*]Atrazin-d5	23.32	222	220	-	-	-

SECTION S2: ANALYSIS OF TR MPS METAL CONTENTS BY MICROWAVE-ASSISTED DISSOLUTION

Microwave digestion of TR particles was performed by weighing four replicates of 20 mg particles into 30 mL Teflon digestion tubes and spiked with 5 mL 70 % nitric acid. 40 µL of 5 ppm ruthenium and indium were added as internal standard, and the mixture was allowed to stand overnight. Following, additional 2 mL 70 % nitric acid was added to the mixture and the sample mixtures were digested using a Terminal 640 microwave system (MLS GmbH, Leutkirch im Allgäu). The digestion Teflon bowel inside the microwave system contained a mixture of 2 mL sulfuric acid, 20 mL hydrogen peroxide, and 320 mL water. The digestion was performed for 76 minutes at a temperature of 220 °C, pressure of 224 bar, and electrical energy of 1000 W. The digested samples were allowed to cool, and subsequently diluted further with 2 mL 70 % nitric acid, before being subjected to ICP-MS analysis.

SECTION S3: SCHEMATIC OVERVIEW ON THE SAMPLE PREPARATION FOR CELL CULTURE EXPERIMENTS

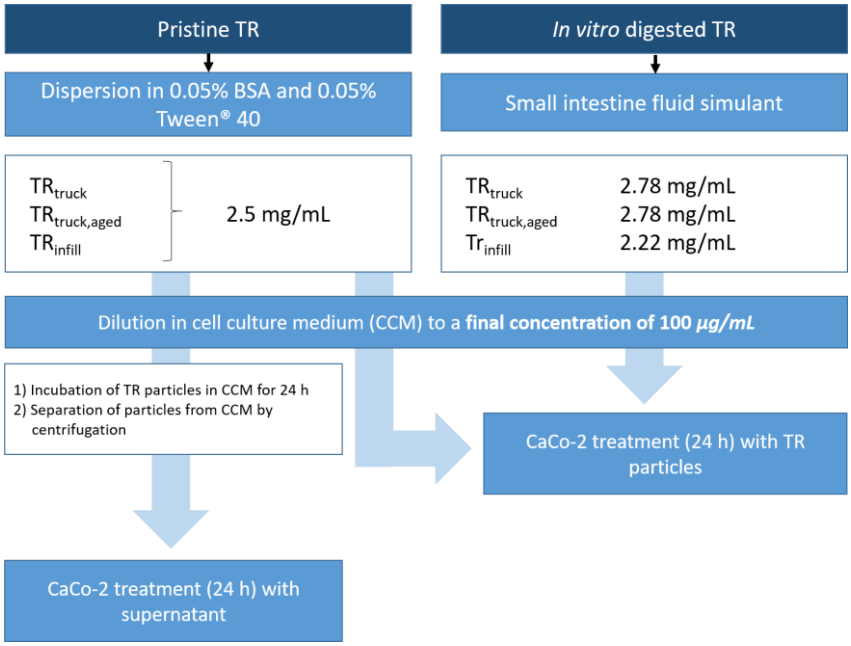

Figure S1: Preparation of TR MPs dispersions for cell culture experiments.

SECTION S4: EXEMPLARY CHROMATOGRAMS AND OVERVIEW OF CHEMICAL LEACHATES FROM MPS

To characterize additives or contaminants that could leach from MPs in principle, different MPs were subjected to Py- and TD-GC-MS analysis as described in **section 2.2**. Exemplary pyrograms for the different MPs are shown in **Fig. S2**. For PA-6 polymer (**Fig. S2a**), it was observed that both the monomer and dimer compounds: caprolactam and 1,8-diazatetracyclodecane-2,9-dione which were detected at retention times of 16.55 and 31.56 minutes respectively leached from the polymer particles during sequential digestion in GI fluid simulants (See **Table S1**). However, for TR particles (**Fig. S2b**), the identified monomer and dimer compounds were not detected after *in vitro* digestion of the particles. Regarding TPU MP in **Fig. S2c**, while the monomer and dimers compounds were not detected after *in vitro* digestion, 1,4-butanediol, a chain extender (co-monomer) in TPU polymerization was detected after sequential digestion of the particles.

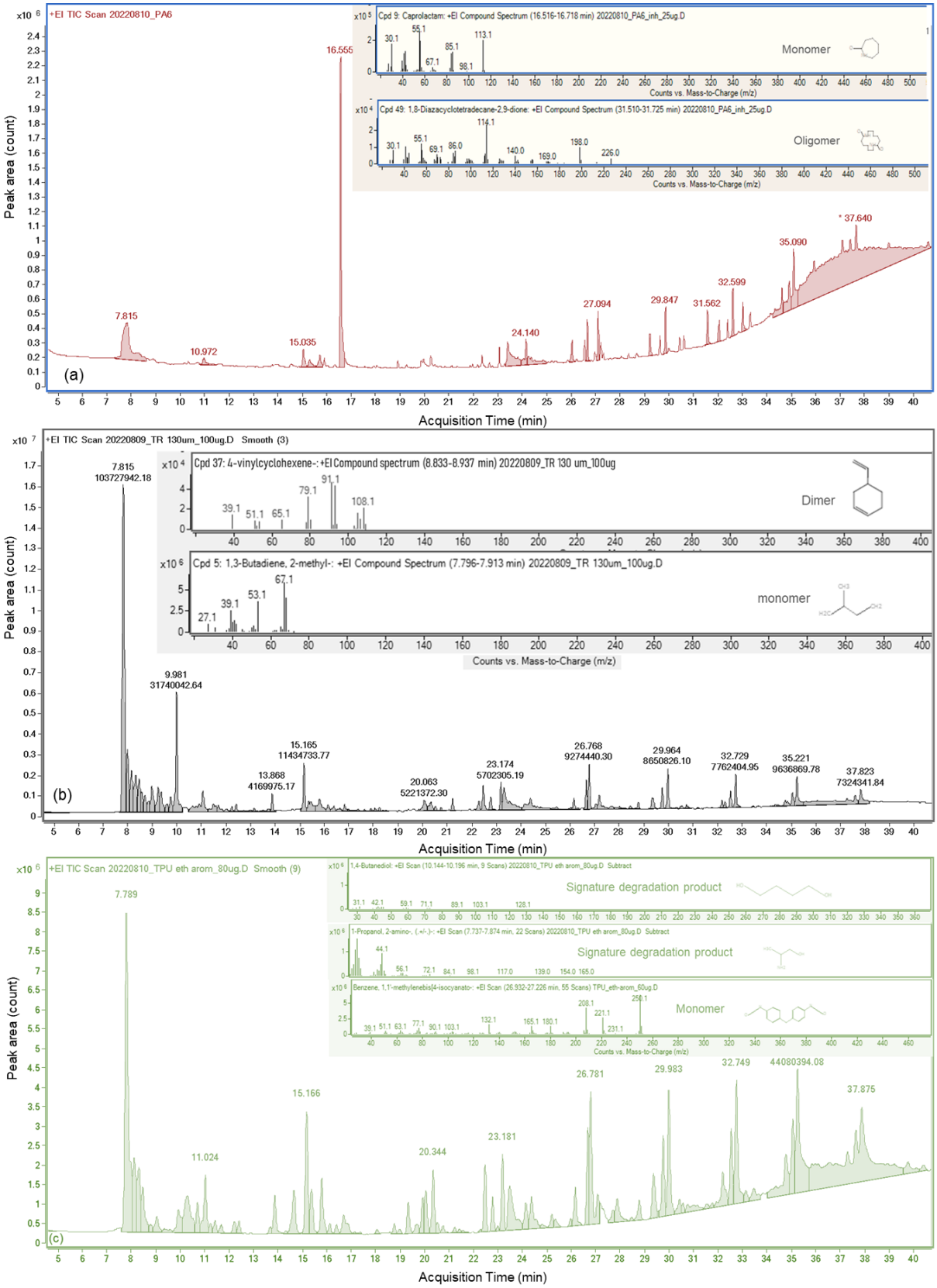

Figure S2: Exemplary Pyrograms of (A): PA-6$_{7\mu m}$, (B): TR$_{truck}$, and (C): TPU_eth_arom. Signature spectra of the monomers and dimers of the polymers are illustrated.

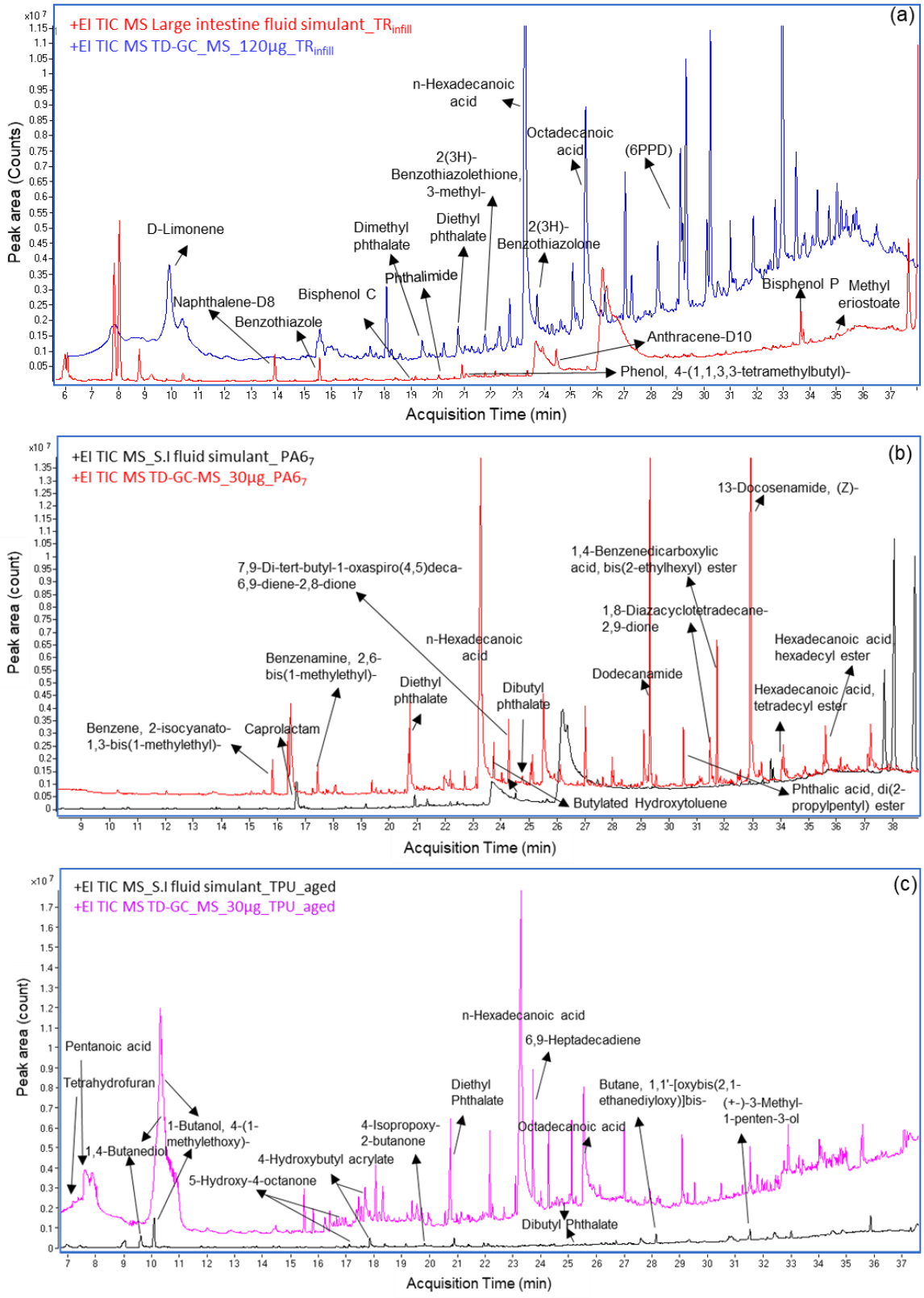

Figure S3: Exemplary GC-MS chromatograms (TIC) of (A): TR_{infill}, (B): $PA\text{-}6_{7\mu m}$, and (C): TPU_{aged} chemicals following thermal desorption or sequential digestion in GI fluid simulant. Chromatograms of the thermally desorbed or leached compounds were acquired with same GC-MS method and therefore overlaid herein for comparison. For each MP, 30 µg and 50 mg were used for thermal desorption and *in vitro* digestion experiments, respectively.

Figure S3 shows an exemplary chromatogram of thermally extracted compounds overlaid with the chromatogram of leached chemicals obtained after sequential digestion in S.I. and L.I. fluid simulants. Both chromatograms were analysed with the same GC-MS method. 58 of the thermally extracted compounds were also identified after sequential digestion of the particles. A detailed list of thermally extracted compounds identified after sequential digestion of the particles are shown in **Table S3**. Only compounds with a NIST-match threshold of 80% and above are shown, along with the functions of the additives in the plastics.

However, some of the thermally extracted compounds were not detected following GC-MS analysis of the fluid simulants. For TR_{infill} particles, examples include D-Limonene; 2(3H)-benzothiazolone, 3-methyl; and styrene.

Other thermally extracted compounds not detected after sequential GI digestion are listed in **Table S4** for TR particles, and **Table S5** for PA-6 and TPU MPs. We suspect that the leached concentrations of some additives may be below the detection limit of the GC-MS method utilized in this study. Furthermore, mid-polar ethyl acetate and non-polar hexane solvents were used for extraction of the leached chemicals. Thus, sufficiently polar compounds soluble in water may not have been extracted.

Table S3: Overview of chemicals leached from MPs in the sequential small intestine fluid simulants following GC-MS analysis**.** **functions of identified additives according to databases (Groh et al., 2019; Knovel, 2023; polymerdatabase.com, 2023). n.f = not found.

RT (min.)	CAS NO	Compound	Polymer matrix	**Function	NIST library Score (%)
7.08	124-07-2	Octanoic acid	TR_{infill}	additive	92
7.10	67160-14-9	Oxime-, methoxy-phenyl-	TR_{truck}, TR_{infil}, $TR_{truck, aged}$	_	89
8.76	n.f	Oxalic acid, cyclohexyl propyl ester	TR_{truck}, TR_{infil}, $TR_{truck, aged}$	_	87
10.16	62-53-3	Aniline	TR_{infill}	Accelerator, antioxidant	88
12.70	26896-20-8	Neodecanoic acid	TR_{truck}, TR_{infill}	Stabilizers, initiators	84
13.51	816-19-3	Hexanoic acid, 2-ethyl-, methyl ester	TR_{truck}	additive	87
15.38	272-16-2	1,2-Benzisothiazole	TR_{truck}, TR_{infill}	additive	92
15.45	95-16-9	Benzothiazole	TR_{truck}, TR_{infil}, $TR_{truck, aged}$	vulcanization additive	87
18.899	79-97-0	Bisphenol C	TR_{truck}, TR_{infill}, TPU	additive	87
19.11	131-11-3	Dimethyl phthalate	TR_{truck}, TR_{infil}, $TR_{truck, aged}$	plasticizer	95
20.01	140-66-9	4-tert-Octylphenol	TR_{truck}, TR_{infill}	antioxidant, additive	90
20.24	85-41-6	Phthalimide	TR_{truck}, TR_{infill}	retardant, additive	94
20.75	84-66-2	Diethyl Phthalate	TR_{truck}, TR_{infil}, $TR_{truck,aged}$, TPU, $TPU_{aged,}$ $PA\text{-}6_{7,}$ $PA\text{-}6_{42,}$ $PA\text{-}6_{42,aged}$	plasticizer	92
21.34	629-80-1	Hexadecanal	TR_{truck}, TR_{infil}, $TR_{truck, aged}$	_	82
23.35	57-10-3	n-Hexadecanoic acid	TR_{truck}, TR_{infil}, $TR_{truck, aged,}$ TPU	Surfactant/additive	87
23.74	934-34-9	2(3H)-Benzothiazolone	TR_{truck}, TR_{infil}, $TR_{truck, aged}$	vulcanization additive	89
25.59	57-11-4	Octadecanoic acid	TR_{truck}, TR_{infil}, $TR_{truck, aged}$	plasticizer/additives	92
25.61	107770-99-0	3,5-Dimethyldodecane	TR_{infill}	_	80
26.20	112-80-1	Oleic acid	TR_{truck}, TR_{infil}, $TR_{truck, aged,}$ TPU	additive	94
27.04	1120-07-6	Nonanamide	TR_{truck}, TR_{infil}, $TR_{truck, aged}$	_	80
28.30	149-30-4	2-Mercaptobenzothiazole	TR_{truck}	vulcanization additive	88
29.02	129-00-0	Pyrene	TR_{truck}, TR_{infill}	Contaminant; PAH	59
26.17	1233691-10-5	3-Undecene, 5-methyl-	TR_{infill}	_	82
30.41	793-24-8	1,4-Benzenediamine, N-(1,3-dimethylbutyl)-N'-phenyl-	TR_{truck}, TR_{infill}	Antioxidant	80
34.69	2167-51-3	Bisphenol P	TR_{infill}	Additive	80
35.33	n.f	2H,8H-Benzo[1,2-b:5,4-b']dipyran-10-propanol, 5-methoxy-2,2,8,8-tetramethyl-	TR_{infill}	_	80
6.59	110-64-5	2-Butene-1,4-diol	TPU, TPU_{aged}	Resins, plasticizer, additive	85
6.56	5371-52-8	Tetrahydro-2-furanol	TPU_{aged}	additive	90
7.41	142-62-1	Hexanoic acid	TPU, TPU_{aged}	contaminant; solvent	95
8.33	41453-56-9	2-Nonen-1-ol	TPU, TPU_{aged}	contaminant	82
11.82	124-07-2	*Octanoic acid*	TPU	lubricant, additive	84
9.61	110-63-4	1,4-Butanediol	TPU_{aged}	co-monomer, additive	90
10.07	31600-69-8	4-Isopropoxybutanol	TPU_{aged}	_	93
8.74	n.f	Benzoic acid, 2-methyl-, 4-acetylphenyl ester	TPU_{aged}	additive	83
9.79	100-52-7	Benzaldehyde	TPU	additive	84
11.38	55130-16-0	Benzyl oleate	TPU_{aged}	additive	83
13.46	112-05-0	Nonanoic acid	TPU	additive	86
12.03	104-67-6	2(3H)-Furanone, 5-heptyldihydro-	TPU, TPU_{aged}	_	81
13.87	1883-13-2	Dodecanoic acid, 3-hydroxy-	TPU, TPU_{aged}	_	81
17.84	2478-1o-6	4-Hydroxybutyl acrylate	TPU_{aged}	adhesive, additive,	83
18.15	96-76-4	2,4-Di-tert-butylphenol	TPU	antioxidant	83
25.29	84-74-2	Dibutyl Phthalate	TPU, TPU_{aged}	plasticizer, additive	88
25.49	40290-32-2	Hexadecanoic acid, 1-(hydroxymethyl)-1,2-ethanediyl ester	TPU	additive residues; lubricants,	82
18.62	863489-15-0	Z-(13,14-Epoxy)tetradec-11-en-1-ol acet	TPU	_	84
28.57	593-39-5	6-Octadecenoic acid, (Z)-	TPU	additive residues; lubricants,	87
29.33	112-73-2	Diethylene glycol dibutyl ether	TPU_{aged}	solvent, additive	80
29.36	2091-29-4	9-Hexadecenoic acid	TPU	additive residues; lubricants,	82
23.98	105794-58-9	1-Heptatriacotanol	TPU_{aged}	additive residues; lubricants,	85
16.55	105-60-2	Caprolactam	$PA\text{-}6_{7}$, $PA\text{-}6_{42}$, $PA\text{-}6_{42,aged}$	PA monomer	94
24.26	82304-66-3	7,9-Di-tert-butyl-1-oxaspiro(4,5)deca-6,9-diene-2,8-dione	$PA\text{-}6_{7}$, $PA\text{-}6_{42}$, $PA\text{-}6_{42,aged}$	antioxidant	94
25.67	22147-34-8	Elaidic acid, isopropyl ester	$PA\text{-}6_{42,aged}$	additive	91
25.97	5654-87-5	hexahydro-	$PA\text{-}6_{7}$, $PA\text{-}6_{42}$, $PA\text{-}6_{42,aged}$	antioxidant	82
25.86	22882-95-7	Isopropyl linoleate	$PA\text{-}6_{42,aged}$	additive	87
29.07	1120-16-7	Dodecanamide	$PA\text{-}6_{7}$, $PA\text{-}6_{42}$, $PA\text{-}6_{42,aged}$	additive	84
29.13	301-02-0	9-Octadecenamide, (Z)-	$PA\text{-}6_{7}$, $PA\text{-}6_{42}$, $PA\text{-}6_{42,aged}$	additive (slip agent)	89
31.56	56403-09-9	1,8-Diazacyclotetradecane-2,9-dione	$PA\text{-}6_{7}$, $PA\text{-}6_{42}$, $PA\text{-}6_{42,aged}$	PA dimer	85
32.15	112-73-2	Diethylene glycol dibutyl ether	$PA\text{-}6_{7}$, $PA\text{-}6_{42}$, $PA\text{-}6_{42,aged}$	solvent, additive	82
33.28	633-31-8	Cholesteryl n-propionate	$PA\text{-}6_{7}$, $PA\text{-}6_{42}$, $PA\text{-}6_{42,aged}$	_	93

Table S4: Overview of TR_{truck} chemicals detected by thermal desorption-GC-MS but not detected by the GC-MS after sequential digestion in the small and large intestine fluid simulants.

RT (min.)	Chemical additives extracted by TD-GC-MS from TR MPs but not detected by GC-MS after digestion experiment	NIST library Score (%)
9.22	Styrene	87
9.92	Limonene	90
10.39	1-Dodecene	87
13.59	Octadecane, 6-methyl-	82
17.47	Benzenamine, 2,6-bis(1-methylethyl)-	85
18.07	Quinoline, 1,2-dihydro-2,2,4-trimethyl-	87
18.17	1H-Indole, 2-(1,1-dimethylethyl)-	80
18.44	Quinoline, 2,4-dimethyl-	90
19.39	Dodecyl acrylate	96
21.71	Benzothiazole, 2-(methylthio)-	82
21.82	Hexestrol	82
22.33	2,6,9,11-Dodecatetraenal, 2,6,10-trimethyl-, (E,E,E)-	87
22.49	Cyclohexane, 1-ethenyl-1-methyl-2-(1-methylethenyl)-4-(1-methylethylidene)-	82
22.21	Hexadecanoic acid, methyl ester	94
22.23	Cyclohexane, 1-ethenyl-1-methyl-2-(1-methylethenyl)-4-(1-methylethylidene)-	86
22.63	Hexadecanenitrile	82
22.80	Bicyclo[5.2.0]nonane, 4-methylene-2,8,8-trimethyl-2-vinyl-	87
22.96	Hexadecanoic acid, ethyl ester	91
23.29	Cyclohexene, 4-(1,5-dimethyl-1,4-hexadienyl)-1-methyl-	87
23.41	Bicyclo[4.3.0]nonane, 7-methylene-2,4,4-trimethyl-2-vinyl-	86
23.68	1,2-Benzenedicarboxylic acid, bis(2-methylpropyl) ester	85
24.11	Dodecane, 2,6,10-trimethyl-	88
24.28	7,9-Di-tert-butyl-1-oxaspiro(4,5)deca-6,9-diene-2,8-dione	95
24.62	Methyl stearate	81
25.07	Octadecanenitrile	88
25.15	Hexadecanoic acid, butyl ester	83
25.43	1-Hexadecanol, acetate	88
26.27	Nonane, 3-methyl-5-propyl-	92
26.53	10-Methyl-octadec-1-ene	81
26.69	Benzoic acid, 2-benzoyl-, methyl ester	82
26.83	1,3-Bis-(2-cyclopropyl,2-methylcyclopropyl)-but-2-en-1-one	85
26.91	Benzothiazole, 2-phenyl-	88
27.98	Hexanedioic acid, bis(2-ethylhexyl) ester	89
28.04	4,8,12-Trimethyltridecan-4-olide	88
28.26	Dodecane, 2,7,10-trimethyl-	89
29.20	Undecane, 3,8-dimethyl-	89
29.25	Nonadecanenitrile	86
28.39	Phosphoric acid, tris(2-ethylhexyl) ester	85
29.85	Quinoline, 2-(2-methylphenyl)-	93
30.25	Oleanitrile	84
30.52	Nonadecane	92
31.55	Phthalic acid, di(2-propylpentyl) ester	90
32.48	1,3-Benzenedicarboxylic acid, bis(2-ethylhexyl) ester	93
32.61	Heneicosane	82
32.96	Tetracosane	80
32.79	Dodecanamide	82
35.27	Hexadecanoic acid, dodecyl ester	86
35.55	13-Docosenamide, (Z)-	88
37.30	Hexadecanoic acid, hexadecyl ester	80

Table S5: Overview of aged and non-aged PA-6 and TPU chemicals extracted by TD-GC-MS but not detected by GC-MS after sequential digestion in the large intestine fluid simulants.

RT (min.)	Compounds extracted by TD-GC-MS from PA-6 and TPU MPs but not detected by GC-MS after digestion experiments	Polymer matrix	NIST library Score (%)
7.56	Nitrous oxide	PA-6_7, PA-6_{42}, PA-$6_{42,aged}$	91
15.49	2,4,7,9-Tetramethyl-5-decyn-4,7-diol	PA-6_7, PA-6_{42}, PA-$6_{42,aged}$	90
15.81	Benzene, 2-isocyanato-1,3-bis(1-methylethyl)-	PA-6_7, PA-6_{42}, PA-$6_{42,aged}$	96
16.24	Triacetin	PA-6_7, PA-6_{42}, PA-$6_{42,aged}$	86
17.43	Benzenamine, 2,6-bis(1-methylethyl)-	PA-6_7, PA-6_{42}, PA-$6_{42,aged}$	95
18.06	Propanoic acid, 2-methyl-, 1-(1,1-dimethylethyl)-2-methyl-1,3-propanediyl ester	PA-6_7, PA-6_{42}, PA-$6_{42,aged}$	93
19.37	Dodecyl acrylate	PA-6_7, PA-6_{42}, PA-$6_{42,aged}$	96
22.25	Hexadecanoic acid, methyl ester	PA-6_7, PA-6_{42}, PA-$6_{42,aged}$	90
22.67	Hexadecanenitrile	PA-6_7, PA-6_{42}, PA-$6_{42,aged}$	97
22.96	Hexadecanoic acid, ethyl ester	PA-6_7, PA-6_{42}, PA-$6_{42,aged}$	89
23.08	Isopropyl palmitate	PA-6_7, PA-6_{42}, PA-$6_{42,aged}$	88
23.71	1,2-Benzenedicarboxylic acid, bis(2-methylpropyl) ester	PA-6_7, PA-6_{42}, PA-$6_{42,aged}$	94
23.88	Heptadecanenitrile	PA-6_7, PA-6_{42}, PA-$6_{42,aged}$	86
23.99	Dodecanoic acid, isooctyl ester	PA-6_7, PA-6_{42}, PA-$6_{42,aged}$	87
24.06	2H-Azepin-2-one, hexahydro-1-(3,4,5,6-tetrahydro-2H-azepin-7-yl)-	PA-6_7, PA-6_{42}, PA-$6_{42,aged}$	93
24.59	Methyl stearate	PA-6_7, PA-6_{42}, PA-$6_{42,aged}$	86
25.04	Octadecanenitrile	PA-6_7, PA-6_{42}, PA-$6_{42,aged}$	98
25.49	Octadecanoic acid	PA-6_7, PA-6_{42}, PA-$6_{42,aged}$	95
26.99	Hexadecanamide	PA-6_7, PA-6_{42}, PA-$6_{42,aged}$	87
27.24	Tetracosane	PA-6_7, PA-6_{42}, PA-$6_{42,aged}$	90
28.22	Hexadecane, 2,6,10,14-tetramethyl-	PA-6_7, PA-6_{42}, PA-$6_{42,aged}$	92
29.29	Oleanitrile	PA-6_7, PA-6_{42}, PA-$6_{42,aged}$	87
29.52	Methyl dehydroabietate	PA-6_7, PA-6_{42}, PA-$6_{42,aged}$	86
30.49	Phthalic acid, di(2-propylpentyl) ester	PA-6_7, PA-6_{42}, PA-$6_{42,aged}$	92
31.51	1,4-Benzenedicarboxylic acid, bis(2-ethylhexyl) ester	PA-6_7, PA-6_{42}, PA-$6_{42,aged}$	83
32.44	Hexadecanoic acid, dodecyl ester	PA-6_7, PA-6_{42}, PA-$6_{42,aged}$	86
32.89	13-Docosenamide, (Z)-	PA-6_7, PA-6_{42}, PA-$6_{42,aged}$	82
34.03	Hexadecanoic acid, tetradecyl ester	PA-6_7, PA-6_{42}, PA-$6_{42,aged}$	86
35.52	Hexadecanoic acid, hexadecyl ester	PA-6_7, PA-6_{42}, PA-$6_{42,aged}$	80
35.59	9-Hexadecenoic acid, octadecyl ester, (Z)-	PA-6_7, PA-6_{42}, PA-$6_{42,aged}$	81
37.18	Oxacycloheptadecan-2-one	PA-6_7, PA-6_{42}, PA-$6_{42,aged}$	80
14.39	2-Oxepanone	TPU, TPU_{aged}	91
17.72	5-Hydroxy-4-octanone	TPU, TPU_{aged}	81
23.42	6,9-Heptadecadiene	TPU, TPU_{aged}	64
23.72	1,2-Benzenedicarboxylic acid, bis(2-methylpropyl) ester	TPU, TPU_{aged}	82
24.26	7,9-Di-tert-butyl-1-oxaspiro(4,5)deca-6,9-diene-2,8-dione	TPU, TPU_{aged}	91
29.08	Nonanamide	TPU, TPU_{aged}	83
29.29	Oleanitrile	TPU, TPU_{aged}	86
31.68	1,5,9-Undecatriene, 2,6,10-trimethyl-, (Z)-	TPU, TPU_{aged}	81
32.91	13-Docosenamide, (Z)-	TPU, TPU_{aged}	83
34.02	Hexadecanoic acid, tetradecyl ester	TPU, TPU_{aged}	85
36.11	Palmitoleic acid	TPU, TPU_{aged}	83
39.21	9-Hexadecenoic acid, octadecyl ester, (Z)-	TPU, TPU_{aged}	82

SECTION S5: EFFECT OF PA-6 PARTICLE SIZES ON LEACHING OF CHEMICALS

The effect of particle sizes on the leaching of contaminants during sequential digestion into S.I. and L.I. fluid simulants was studied for PA-6 material with median size distributions of 7 µm and 42 µm. As shown in **Fig. S6** for three selected leachates, the cumulative release of caprolactam and diethyl phthalates was significantly enhanced with decreasing median particle size. For dibutyl phthalates, the increase in leaching was not statistically significant. (Yan et al., 2021) reported a significant effect of polyvinyl chloride (PVC) particle sizes on the leaching of dibutyl phthalates in water. In PVC, phthalates serve as plasticizers in high concentration (up to 40%), that is, they are intentionally-added substances (IAS), whereas their observation in leachates from PA-6 was unexpected and not explainable by intentional addition, and instead considered as contaminants (non-intentional added substances (NIAS). It is conceivable that owing to reduced distances for diffusive transport in submicro- and nanoplastics, the leaching of chemicals will be higher from smaller particles (Gigault et al., 2021). The significance of this effect on human health requires further investigation.

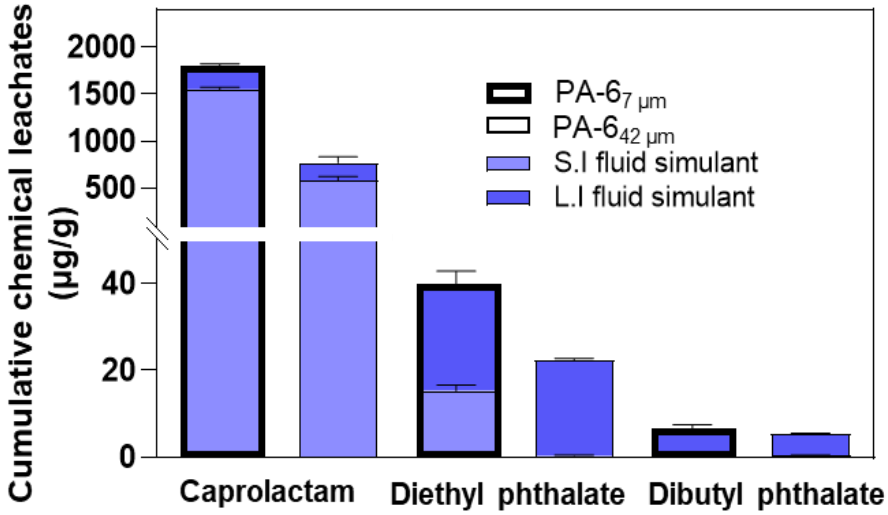

Figure S4: Influence of PA-6 particle size on the leaching of chemicals during sequential digestion in GI fluid simulants.

SECTION S6: ESTIMATE OF HUMAN DAILY METAL INTAKE FROM MICROPLASTICS.

The estimated daily intake of metals by humans through TR particles was calculated according to equation 1 (WHO, 2019). C_{metal} (µg/g) is the concentration of metal in TR particles. M_{ingest} (g) is the estimated daily intake of TR particle. For humans, an estimated MP intake value of 4.1 x 10^{-6} g/capita/day has been previously calculated (Mohamed Nor et al., 2021), of which about 47% has been suggested to be of TR origin (UNEP, 2018). Therefore, M_{ingest} (g) value of 1.93 x 10^{-6} g/capita/day was utilized in this study. $Leach_{S.I.}$ is the fraction of the initial metal content in the particle released in the S.I. fluid simulant. A body weight (*bw*) value of 70 kg was used.

$$EDI = \frac{C_{metal} \times M_{ingest} \times Leach_{SI}}{bw} \qquad (1)$$

SECTION S7: MPS DID NOT REDUCE CELL VIABILITY OF INTESTINAL CACO-2 CELLS

The exposure of differentiated CaCo-2 cells to PA-$6_{42µm}$, PA-$6_{7µm,}$ and TPU_{ether_arom} did not result in a decrease of cell viability (**Fig. S5a**). In addition, we investigated the different tire wear particles more closely. In **Section 3.1**, we identified potentially harmful substances, including benzothiazole derivatives and 6PPD that were released from these materials. Thus, TR_{truck}, $TR_{truck,aged,}$ TR_{infill} as well as their corresponding *in vitro* digested TR particles were investigated for their cytotoxic effects. The concentrations ranged from 3.1 to 100 µg/mL. The pristine TR particles did not decrease the cell viability of differentiated CaCo-2 cells. Neither aging of TR_{truck} by UV light nor *in vitro* digestion induced cytotoxic effects of the tire materials (**Fig. S5b**).

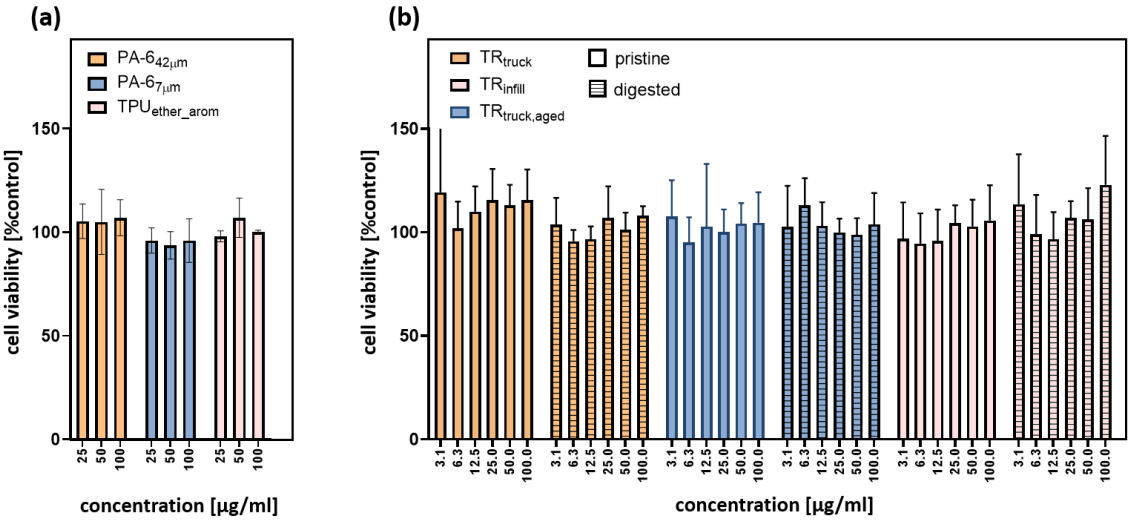

Figure S5: viability of differentiated Caco-2 cells after the treatment with different microplastic particles for 24 h. Cells were exposed to (a) PA-6$_{42µm}$, PA-6$_{7µm}$ and TPU$_{ether_arom}$ and (b) pristine, UV-aged (2000 h) and *in vitro* digested (simulating passage through the gastrointestinal tract) tire wear materials. Results are given as percentage of the viability normalized to untreated cells (medium control). Mean values ± SD of n = 3 independent experiments are presented. Statistical analysis was done by one way ANOVA (*p < 0.05, compared to untreated controls).

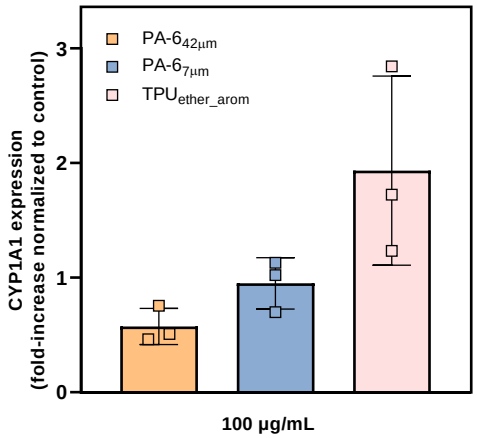

Figure S6: cytochrome p450 1a1 (cyp1a1) induction in undifferentiated Caco-2 cells after exposure with different MPs. Cells were exposed for 24 h to the different MPs at a concentration of 100 µg/ml. Results were normalized to untreated cells (medium control). Statistical analysis was performed by using a one-way Anova for at least three independent biological replicates (*p < 0.05, **p < 0.01, ***p ≤ 0.001).

SECTION S8: SCREENING OF AOPS LINKED TO THE LEACHED CHEMICALS ACCORDING TO THE TOXCAST DATABASE.

Adverse outcome pathways (AOPs) have been recently introduced in human risk assessment as pragmatic tools with several applications (OECD, 2016). In the current study, it intends to

provide a clear-cut presentation of potential toxicological endpoints for human exposure to the leached chemicals at the lowest observed adverse effect level (LOAEL). AOPs are typically composed of a molecular initiating event (MIE), a series of intermediate steps and key events (KE) that lead to an adverse effect (Halappanavar et al., 2020). The AOPs linked to the leached chemicals in the ToxCast database (US EPA, 2023) were screened using the OECD AOP-knowledge base (OECD, 2023). Among the AOPs linked to the chemicals, those with taxonomic applicability to mammals were selected. Also checked was the evidence of the link between the MIE, the KE, and the adverse outcome (AO); as well as the confidence of the evidence assessment which describes the biological plausibility, empirical support, and quantitative understanding of the key event relationships in the AOP. Linked AOPs with undeclared taxonomic applicability, or applicability to amphibians, or fish were rejected. The potential adverse effects obtained with the AOPs listed in **Table S6** provide a clear focus and framework for future risk assessment of the chemicals associated with TR, PA-6, and TPU particles.

Table S6: Overview of 32 relevant AOPs linked to some chemicals leached from the investigated MP particles. Superscripts denote the number of high, moderate, or weak evidence in the events.

AOP ID	AOP title	Evidence of link between MIE, KE and AO	Evidence of taxonomic applicability	Confidence of evidence assessment
6	Antagonist binding to PPARα leading to body-weight loss	^{5}High/^{3}moderate	High (humans)	strong
7	Aromatase (Cyp19a1) reduction leading to impaired fertility in adult female	^{2}High/^{2}moderate	Low (humans)	Moderate/strong
16	Acetylcholinesterase inhibition leading to acute mortality	Moderate/high	Moderate (humans)	strong
18	PPARα activation in utero leading to impaired fertility in males	^{3}High/^{3}moderate/^{2}low	Low (humans)	^{2}Strong/^{4}Moderate/^{4}weak
27	Cholestatic Liver Injury induced by Inhibition of the Bile Salt Export Pump (ABCB11)	^{7}High/^{2}moderate	High (humans)	n.s
32	Inhibition of iNOS, hepatotoxicity, and regenerative proliferation leading to liver tumors	^{5}High	High (mice)	n.s
37	PPARα activation leading to hepatocellular adenomas and carcinomas in rodents	^{7}High	High (mammals)	strong

41	Sustained AhR Activation leading to Rodent Liver Tumours	[4]High	High (mammals)	strong
43	Disruption of VEGFR Signaling Leading to Developmental Defects	[4]High/[1]moderate	Moderate (humans)	strong
46	AFB1: Mutagenic Mode-of-Action leading to Hepatocellular Carcinoma (HCC)	[2]High/[5]moderate	High (humans)	strong
51	PPARα activation leading to impaired fertility in adult male rodents	[1]High/[5]moderate	High (Rat)	n.s
57	AhR activation leading to hepatic steatosis	[10]High/[2]moderate	High (Mouse)	n.s
58	NR1I3 (CAR) suppression leading to hepatic steatosis	[18]High/[2]moderate	Moderate (humans)	n.s
63	Cyclooxygenase inhibition leading to reproductive dysfunction	[1]High/[2]moderate	Low (humans)	n.s
66	Modulation of Adult Leydig Cell Function Subsequent Glucocorticoid Activation in the Fetal Testis	n.s	High (Rat)	n.s
67	Modulation of Adult Leydig Cell Function Subsequent to Estradiaol Activation in the Fetal Testis	n.s	High (Rat)	n.s
71	Modulation of Adult Leydig Cell Function Subsequent to Glucocorticoid Activation	n.s	High (mammals)	n.s
94	Sodium channel inhibition leading to congenital malformations	[1]High/[3]moderate	n.s (mammals)	n.s
102	Cyclooxygenase inhibition leading to reproductive dysfunction via interference with meiotic prophase I /metaphase I transition	[6]High/[3]moderate	Low (humans)	n.s
103	Cyclooxygenase inhibition leading to reproductive dysfunction via interference with spindle assembly checkpoint	[5]High/[3]moderate/[1]low	Low (humans)	n.s
107	Constitutive androstane receptor activation leading to hepatocellular adenomas and carcinomas in the mouse and the rat	[4]High	High (mammals)	n.s
131	Aryl hydrocarbon receptor activation leading to uroporphyria	[2]High/[3]moderate	High (humans)	strong
148	EGFR Activation Leading to Decreased Lung Function	[3]High/[1]moderate	High (humans)	strong
150	Aryl hydrocarbon receptor activation leading to early life stage mortality, via reduced VEGF	[4]High/[3]moderate	Low (mammals)	Moderate/strong
163	PPARgamma activation leading to sarcomas in rats, mice, and hamsters	[7]High/[1]moderate	Moderate/High (mammals)	n.s
165	Antiestrogen activity leading to ovarian adenomas and granular cell tumors in the mouse	[8]High/[2]moderate	Moderate/High (mammals)	n.s

166	PPARalpha activation leading to pancreatic acinar tumors in the rat and mouse	[2]High/[2]moderate/[1]low	Moderate/High (mammals)	n.s
167	Early-life estrogen receptor activity leading to endometrial carcinoma in the mouse	[6]High	High (mouse)	n.s
187	Anticoagulant rodenticide inhibition of vitamin K epoxide reductase resulting coagulopathy and haemorrhage	[5]High/[1]moderate/[1]low	High (mammals)	n.s
200	Estrogen receptor activation leading to breast cancer	[19]High/[5]moderate	High (humans)	strong
220	Cyp2E1 Activation Leading to Liver Cancer	[4]High/[3]moderate	Moderate (humans)	strong/moderate
307	Decreased testosterone synthesis leading to short anogenital distance (AGD) in male (mammalian) offspring	[3]High/[3]moderate	Moderate (humans)	n.s

REFERENCES

Emecheta, E. E., Pfohl, P. M., Wohlleben, W., Haase, A., & Roloff, A. (2024). Desorption of Polycyclic Aromatic Hydrocarbons from Microplastics in Human Gastrointestinal Fluid Simulants─ Implications for Exposure Assessment. *ACS omega*. doi:https://doi.org/10.1021/acsomega.3c09380

Gigault, J., El Hadri, H., Nguyen, B., Grassl, B., Rowenczyk, L., Tufenkji, N., Feng, S., & Wiesner, M. (2021). Nanoplastics are neither microplastics nor engineered nanoparticles. *Nat Nanotechnol, 16*(5), 501-507. doi:10.1038/s41565-021-00886-4

Groh, K. J., Backhaus, T., Carney-Almroth, B., Geueke, B., Inostroza, P. A., Lennquist, A., Leslie, H. A., Maffini, M., Slunge, D., Trasande, L., Warhurst, A. M., & Muncke, J. (2019). Overview of known plastic packaging-associated chemicals and their hazards. *Sci Total Environ, 651*(Pt 2), 3253-3268. doi:10.1016/j.scitotenv.2018.10.015

Halappanavar, S., van den Brule, S., Nymark, P., Gate, L., Seidel, C., Valentino, S., Zhernovkov, V., Hogh Danielsen, P., De Vizcaya, A., Wolff, H., Stoger, T., Boyadziev, A., Poulsen, S. S., Sorli, J. B., & Vogel, U. (2020). Adverse outcome pathways as a tool for the design of testing strategies to support the safety assessment of emerging advanced materials at the nanoscale. *Part Fibre Toxicol, 17*(1), 16. doi:10.1186/s12989-020-00344-4

Knovel. (2023). Plastics Additives Database. Retrieved from https://app.knovel.com/kn/resources/kpPAD00004/toc

Mohamed Nor, N. H., Kooi, M., Diepens, N. J., & Koelmans, A. A. (2021). Lifetime Accumulation of Microplastic in Children and Adults. *Environ Sci Technol, 55*(8), 5084-5096. doi:10.1021/acs.est.0c07384

OECD. (2016). OECD series on adverse outcome pathways number 1: users' handbook supplement to the guidance document for developing and assessing adverse outcome pathways. *OECD Publishing, Paris*.

OECD. (2023). Adverse Outcome Pathway Knowledge Base (AOP-KB). Retrieved from https://aopkb.oecd.org/index.html

Polymerdatabase.com. (2023). Plastics Additives. Retrieved from https://polymerdatabase.com/Additives/Polymer%20Additives.html

UNEP. (2018). *Mapping of global plastics value chain and plastics losses to the environment (with a particular focus on marine environment)*. Retrieved from https://www.unep.org/resources/report/mapping-global-plastics-value-chain-and-plastics-losses-environment-particular

US EPA. (2023). ToxCast & compTox chemicals dashboard. Retrieved from https://www.epa.gov/chemical-research/exploring-toxcast-data

WHO. (2019). *Microplastics in drinking-water*. Retrieved from

Yan, Y., Zhu, F., Zhu, C., Chen, Z., Liu, S., Wang, C., & Gu, C. (2021). Dibutyl phthalate release from polyvinyl chloride microplastics: Influence of plastic properties and environmental factors. *Water Res, 204*, 117597. doi:10.1016/j.watres.2021.117597

ACKNOWLEDGEMENTS

To begin with, I would like to express my profound gratitude to PD Dr. Andrea Haase for her supervision and for availing me the opportunity to carry out this doctoral research at BfR. Thank you, Andrea, for your trust, unflinching support, and guidance.

I wish to also express my deep thanks to Dr. Alexander Roloff for his dedicated and hands-on supervision of my laboratory works. Thank you Dr. Alex for your time, your tutorship, and patience. I benefited immensely from your academic curiosity, meticulosity, and expertise. Your support to this doctoral project is greatly appreciated.

I am thankful to Prof. Dr. Eva Lehndorff for her immense support from the inception of this PhD, and for kindly accepting to supervise this dissertation. I am grateful to my colleagues and members of staff at the BfR. Thank you, Dr. Christoph Hutzler, for your contribution to this thesis, particularly in the first year. I also appreciate members of the InnoMat.Life consortium for their collaborations and enthusiasm. Thanks especially to the BASF team: Dr. Wendel Wohlleben, Dr. Patrizia Marie Pfohl and Dr. Sarah Jessl, thank you all for your close cooperation and commitments. I would also like to extend my gratitude to my master's students: Diana Borda Borda, and Mengya Zhou. Thank you very much for your assistance and contributions.

I would not forget to acknowledge my friends for their encouragement, moral support and motivation. Thanks, Gabriel Onyenso, for your moral support. I am highly indebted to you Humay Rahimova, Ridwan Shittu, and Rev. Fr. Dr. Casmir Nzeh for your assistance and genuine care.

Most importantly, my heartfelt praise goes to my family for their unconditional support and great wishes. Thank you, Prisca Aririguzo, for being always there for me. Special thank also to Rev. Fr. Bona Opara, your contribution to my academic journey is hugely appreciated.

Above all, I am very thankful to God almighty for everything.